Universidade de Aveiro Departamento de Ambiente e Ordenamento
2006

Paulo Gabriel Fernandes de Pinho

Chamber Validation of the Explicit Master Chemical Mechanism (MCM) and Application to Air Pollution Studies

Validação Experimental do Mecanismo Químico Explícito (MCM) e Aplicação a Estudos de Poluição Atmosférica

Dissertação apresentada à Universidade de Aveiro para cumprimento dos requisitos necessários à obtenção do grau de Doutor em Ciências do Ambiente, realizada sob orientação científica do Professor Doutor Casimiro Adrião Pio, Professor Catedrático do Departamento de Ambiente e Ordenamento da Universidade de Aveiro e sob co-orientação do Doutor Michael Jenkin do Imperial College (UK)

Dissertation presented to Aveiro University to obtain PhD in Applied Environmental Sciences, made under scientific orientation of Doctor Casimiro Adrião Pio, Cathedratic Professor of the Department of Environment of Aveiro University and co-supervision of Doctor Michael Jenkin of the Imperial College (UK)

o júri

presidente

Doutor Joaquim Arnaldo Carvalho Martins
Professor Catedrático da Universidade de Aveiro

Doutor Casimiro Adrião Pio
Professor Catedrático da Universidade de Aveiro (Orientador)

Doutor Michael Edwin Jenkin
Principal Research Felow – Centre for Environmental Policy og Imperial College of London (Co-Orientador)

Doutor Sebastião José Formosinho Sanches Simões
Professor Catedrático da Universidade de Coimbra

Doutor Carlos Alberto Diogo Soares Borrego
Professor Catedrático da Universidade de Aveiro

Doutora Teresa Filomena Vieira Nunes
Professora Associada da Universidade de Aveiro

Doutor Luís Eugénio Pinto Teixeira de Lemos
Professor Coordenador de Nomeação Definitiva da Escola Superior de Tecnologia de Viseu, Instituto Politécnico de Viseu

acknowledgments

I wish to express my warm thanks to Professor Casimiro Adrião Pio and Doctor Michael Jenkin for their supervision and support.

I also thank Professor Luís Teixeira de Lemos for the encouragement and Professor William P. L. Carter who kindly provided essential data for this work.

Obrigado à família e amigos.

Obrigado Isabel pela tua paciência.
Desculpa as ausências Gabo.

Em memória do meu Pai

palavras - chave

Oxidação de COV, alcenos, hidrocarbonetos biogénicos, química da troposfera, mecanismos de oxidação, câmaras ambientais, modelação fotoquímica.

resumo

A presente dissertação consiste essencialmente na avaliação de vários mecanismos de oxidação incluídos no mecanismo químico (Master Chemical Mechanism) e a sua capacidade de prever os processos de transformação dos poluentes na atmosfera. Esta avaliação foi realizada por comparação das simulações de um modelo, incluindo o mecanismo químico, com os dados de câmaras ambientais e também por incorporação do mecanismo químico num modelo troposférico, permitindo a comparação das previsões do modelo com dados de observações atmosféricas.

Os mecanismos de degradação do butano, do eteno, do propeno, do 1-buteno, do 1-hexeno, do isopreno, do α-pineno, do β-pineno, do formaldeído, do acetaldeído, da metacroleína, da acetona, da metiletil cetona e da metilvinil cetona, incluídos na versão 3.1 do Master Chemical Mechanism (MCM v3.1) foram avaliados utilizando dados das câmaras ambientais presentes na base de dados do Centro de Investigação da Universidade da Califórnia (Statewide Air Pollution Research Center).

A fotooxidação do butano e dos seus produtos de oxidação, metilvinilcetona acetaldeído e formaldeído foi realizada em conjunto com a avaliação inicial dos mecanismos auxiliares das câmaras. Verificou-se que o mecanismo para o butano contém um conjunto de reacções que descrevem de forma aceitável as experiências de fotooxidação do butano e dos seus produtos de oxidação, tendo no entanto sido proposto um determinado número de modificações que resultaram numa melhoria de desempenho. As alterações propostas estão essencialmente relacionadas com a magnitude dos radicais livres provenientes da fotólise dos carbonilos.

As simulações para os sistemas eteno e propeno permitiram verificar que estes são sensíveis à fracção de radicais livres ou produtos moleculares definidos pela reacção destas espécies com o átomo de oxigénio ($O(^3P)$). Com esta limitação, os mecanismos de oxidação para o eteno e propeno, inseridos no MCM v3.1, de uma forma geral tem um bom desempenho. A avaliação dos mecanismos contidos no MCM v3.1 para o 1-buteno e 1-hexeno foram inconclusivos.

A avaliação do mecanismo de fotooxidação do isopreno foi realizada em simultâneo com os mecanismos de fotooxidação dos seus produtos, metacroleina e metilvinilcetona. Verificou-se que o mecanismo para o isopreno contém um conjunto de reacções que descrevem de forma aceitável as experiências de fotooxidação do isopreno e dos seus produtos de oxidação, tendo no entanto sido proposto um determinado número de modificações que resultaram numa melhoria de desempenho. As alterações propostas estão relacionadas com a magnitude dos radicais livres provenientes dos processos de fotólise dos carbonilos e a taxa de formação de radicais proveniente da reacção do O_3 com os compostos oxigenados

insaturados. Para além das referidas alterações foi necessário incluir a representação das reacções do $O(^3P)$ com o isopreno, metacroleina e metilvinil cetona.

Os mecanismos de degradação do α-pineno and β-pineno incluídos no MCM v3.1 foram avaliados e melhorados. Verificou-se que o mecanismo de degradação do α-pineno sobrestimava o parâmetro $D(O_3\text{-}NO)$ especialmente para baixas razões de COV/NO_x. Verificou-se, também, que a simulação do decaimento do α-pineno estava sobrestimado e a formação de HCHO era subestimada relativamente aos valores observados. Um determinado número de modificações introduzidas resultaram numa melhoria de desempenho. Todas as alterações relacionadas com a magnitude das fontes de radicais livres resultantes do processo químico orgânico. A reacção do $O(^3P)$ com o α-pineno foi incorporada, no entanto verificou-se que o efeito da sua inclusão foi reduzido. As principais alterações propostas para o mecanismo de degradação do α-pineno são o aumento da formação de nitratos orgânicos a partir dos radicais peroxilo (RO2) e o decréscimo da formação de OH da reacção com o O_3. O mecanismo de degradação do β-pineno foi avaliado com os dados de câmara, no entanto, não se conseguiu obter uma melhoria de desempenho para todas as experiências avaliadas.

Como resultado da avaliação do MCM com dados de câmara ambiental, é possível sugerir um número de recomendações para trabalho futuro, relativamente a lacunas e incertezas nas bases de dados cinéticos e de mecanismos e disponibilidade de dados de câmaras ambientais. A confiança nas avaliações com base em dados de câmaras ambientais requer: que a incerteza seja reduzida nos dados cinéticos da reacção do OH com o NO_2; a avaliação de COV requer uma confirmação das suas reacções com $O(^3P)$; mais informação é necessária para quantificar a formação de radicais livres da reacção dos alcenos com O_3 sob condições ambientais

O mecanismo químico MCM v3.1 foi incorporado num modelo fotoquímico de uma camada, Modelo Fotoquímico de Trajectória utilizando uma aproximação Lagrangeana. O Modelo Fotoquímico de Trajectória foi aplicado para avaliação e intercomparação da versão original do mecanismo químico e da versão adaptada (resultante dos desenvolvimentos da avaliação em câmara ambiental), em condições ambientais típicas na camada limite poluída da atmosfera. O Modelo Fotoquímico de Trajectória foi aplicado a uma situação real na costa Oeste portuguesa, durante a ocorrência de um episódio de poluição fotoquímica. O modelo simulou o transporte da massa de ar, por acção da brisa marítima, desde a linha de costa (Aveiro) até uma localidade (Covelo) situada a aproximadamente 65 km da linha de costa. O Modelo Fotoquímico de Trajectória foi aplicado para os dias 29 e 30 de Junho de 2001, utilizando os dados meteorológicos e de qualidade do ar obtidos numa campanha de campo. Os resultados obtidos por aplicação do Modelo, utilizando o mecanismo químico MCM v3.1, são uma boa aproximação dos valores medidos em Sangalhos e Covelo.

Os desenvolvimentos no mecanismo, MCM v3.1, resultantes da avaliação em câmara ambiental apenas resultaram numa pequena variação quando aplicados a estas condições ambientais. Os testes de sensibilidade mostraram que a temperatura tem um efeito significativo nas concentrações de ozono calculadas.

A avaliação do mecanismo químico, inserido num Modelo Fotoquímico de Trajectória, com dados reais da atmosfera indicou que existem demasiadas incertezas no Modelo para permitir uma análise quantitativa para as várias espécies representadas nos mecanismos explícitos.

keywords

VOC oxidation, alkenes, biogenic hydrocarbons, tropospheric chemistry, degradation mechanisms, environmental chamber data, ozone modelling.

abstract

The present dissertation consisted essentially in the evaluation of several schemes included in Master Chemical Mechanism and in its capability of predicting the transformation processes of pollutants in the atmospheric environment. This was achieved by comparison of model simulations with environmental chamber data, and also by incorporation of the chemical mechanism into a tropospheric model, allowing the comparison of model predictions with atmospheric observational data.

Butane, ethene, propene, 1-butene, 1-hexene, isoprene, α–pinene, β–pinene, formaldehyde, acetaldehyde, methacrolein, acetone, methylethyl ketone, and methylvinyl ketone degradation mechanisms included in version 3.1 of Master Chemical Mechanism (MCM v3.1) were evaluated using environmental chamber datasets from the Statewide Air Pollution Research Center at the University of California.

Photo-oxidation of butane, and its degradation products methylethyl ketone, acetaldehyde and formaldehyde, was made in conjunction with an initial evaluation of the chamber-dependent auxiliary mechanisms. The MCM v3.1 mechanism for butane was found to provide an acceptable reaction framework for describing the NO_X-photo-oxidation experiments on the above systems, although a number of parameter modifications and refinements were identified which resulted in an improved performance. These generally relate to the magnitude of sources of free radicals from carbonyl photolysis processes.

The simulations for ethene and propene systems were found to be sensitive to the branching ratios assigned to molecular and free radical forming pathways of the $O(^3P)$ reactions. With this constraint, the MCM v3.1 mechanisms for ethene and propene generally performed well. Evaluation of the MCM v3.1 1-butene and 1-hexene degradation mechanisms was found to be inconclusive.

Photo-oxidation of Isoprene was made simultaneously with its degradation products, methacrolein and methylvinyl ketone. The MCM v3.1 mechanism for isoprene was found to provide an acceptable reaction framework for describing the NO_X-photo-oxidation experiments, although a number of parameter modifications and refinements were identified which resulted on improved performance. These all relate to the magnitude of sources of free radicals from organic chemical process, such as carbonyl photolysis rates and the yields of radicals from the reactions of O_3 with unsaturated oxygenates, and specific recommendations are made for refinements. In addition to this, it was necessary to include a representation of the reactions of $O(^3P)$ with isoprene, methacrolein and methylvinyl ketone.

α-Pinene and β-pinene degradation mechanism included in MCM v3.1 has been evaluated and refined. α-pinene mechanism was found to overestimate D(O_3-NO) specially for low VOC/NO_x ratios. In addition, the simulated decay of α-pinene was in advance and formation of the product HCHO is underpredicted relative to the observations. A number of parameter modifications and refinements were identified which resulted in an improved performance. These all relate to the magnitude of sources of free radicals from organic chemical process. The reaction of O(^{3}P) with α-pinene was incorporated, although the effect of its inclusion was found to be small. The main refinements proposed to α-pinene degradation mechanism are the increasing of nitrate yields from the initially formed RO2 and decreasing the OH yield from the reaction of O_3. β-pinene mechanism was evaluated against the chamber data. However, an improvement of it was not obtained for all the evaluated runs.

As a result of chamber evaluation of MCM, it is possible to make a number of suggestions and recommendations for future work, in relation to gaps and uncertainties in the kinetic and mechanistic database, and the availability of chamber data: confidence in chamber evaluations requires the uncertainty to be reduced on the kinetics of the reaction of OH with NO_2; Chamber evaluation of VOC systems requires confirmatory information on their reactions with O(^{3}P); further information is required to quantify fully free radical formation from reactions of ozone with alkenes under atmospheric conditions.

The MCM v3.1 was incorporated into a Photochemical, one layer, Trajectory box Model (PTM) using a Lagrangian approach. The PTM was used to evaluate and intercompare the original and adapted versions of MCM v3.1, (resulting from refinements provided by chamber evaluation), at normal environmental conditions, in the polluted boundary layer atmosphere. The PTM was applied to a real situation in the Portuguese west coast, during an ozone summer episode, by following the air mass transported by sea breeze, from the coast line (Aveiro) to a location, approximately 65 kilometres inland (Covelo). The PTM was applied during the period of June 29 and 30 (2001), using meteorological and air quality data, obtained from a field campaign. The ozone concentrations obtained by application of PTM, using as chemical mechanism MCM v3.1 are a good approximation to the measured values in Sangalhos and Covelo.

The refinements in MCM v3.1 resulting from chamber evaluation show only a very small change when applied to these field conditions. Sensitivity tests show that temperature has a large effect in calculated ozone concentrations.

The field evaluation of MCM v3.1 inserted in the photochemical trajectory model indicate that there are too many model uncertainties to allow a quantitative analysis for the several species represented on explicit mechanisms.

Contents

1 Introduction

Photochemical ozone formation is very complex, depending on meteorological parameters and concentration of precursors, primarily NO_x and VOCs. Volatile organic compounds (VOC) are emitted in substantial quantities from both biogenic and anthropogenic sources (e.g. Guenther *et al.,* 1995), and have a major influence on the chemistry of the lower atmosphere. It is well established that degradation of emitted volatile organic compounds has a major influence on the chemistry of the lower atmosphere (e.g. Finlayson Pitts and Pitts, 2000; Atkinson, 2000; Jenkin and Clemitshaw, 2000), contributing to the formation of ozone (O_3) and other secondary pollutants. The complete gas phase oxidation of VOC into carbon dioxide and water occurs predominantly (but not exclusively) by sunlight-initiated mechanisms, and produces carbon monoxide and a variety of intermediate oxidised organic products, some nitrogen-containing, which may have detrimental health effects (e.g. PORG, 1997). O_3 is known to have adverse effects on health, vegetation and materials, it is a greenhouse gas, and it promotes the oxidation of trace gases both directly, and as a free radical precursor (e.g. PORG, 1997).

The development and application of mathematical models describing the chemistry, meteorology, and deposition (also designated Airshed models) are critical elements in the development and assessment of effective control strategies (e.g. Carter, 2000; Finlayson-Pitts and Pitts, 2000).

A major component of air quality simulation models is the chemical mechanism that describes how VOCs and NO_x interact to produce O_3 and other oxidants (e.g. Carter, 2000; Dodge, 2000). Chemical mechanisms are an important component for the reason that if the mechanism is incorrect or incomplete in significant respects, then the model's predictions of secondary pollutant formation may also be incorrect, and its use might result in implementation of inappropriate air pollution control strategies (Carter, 2000). Chemical mechanisms were used in air quality simulation models on the last four decades (e.g., Reynolds *et al.,* 1973; McRae *et al.,* 1982; Gery *et al.,* 1988; Carter and Lurmann, 1991).

The essential features of the chemistry of VOC degradation, particularly in relation to O_3 formation, are now well documented (e.g., Atkinson, 2000; Jenkin and Clemitshaw, 2000). However, it is well established that the degradation of each emitted VOC occurs by a specific mechanism (because of differences in reactivity and structure), such that the relative contributions of VOC to the formation of O_3 and other secondary pollutants varies from one compound to another (e.g., Carter and Atkinson, 1987; Derwent and Jenkin, 1991). Over the past two decades, the availability of kinetic and mechanistic data to help elucidate the degradation mechanisms of VOC has increased significantly, and various aspects of the tropospheric chemistry of organic compounds have been reviewed extensively (e.g., Atkinson, 1997b; Calvert *et al.,* 2000). The

individual propensity of VOC to form O_3 was studied and scales of photochemical O_3 creation potentials (e.g., Derwent *et al.,* 2001; Saunders *et al.,* 2003) and incremental reactivities (e.g. Carter, 1994) were established.

Despite that knowledge, there are two fundamental problems in developing chemical mechanisms: how to represent chemical reactions for which kinetic/mechanistic information is lacking (several important processes, such as the oxidation of aromatics and biogenics are incompletely understood (e.g. Carter *et al.,* 1995a; Dodge, 2000; Jenkin *et al.,* 2000; Bloss *et al.,* 2005a)); how to incorporate all the chemistry that is occurring in the lower troposphere into an oxidant mechanism (a major disadvantage of explicit chemical mechanisms is the very large number of reactions potentially generated, if a series of rules is rigorously applied (Jenkin *et al.,* 1997). A mechanism that treated oxidant formation explicitly would easily contain tens of thousands reactions and several thousands of organic reactants and products (e.g. Dodge, 2000))

There are condensed chemical reaction mechanisms to describe and represent atmospheric chemical transformations involving air pollutants: e.g. Carbon Bond Mechanism – Version IV (CB4) (Gery *et al.,* 1988); Regional Acid Deposition Model (RADM) (Stockwell *et al.,* 1990). On other hand exist mechanisms with a detailed description of chemical transformation processes for primary and secondary atmospheric species. The Master Chemical Mechanism (MCM) (Jenkin *et al.,* 1997) and the Statewide Air Pollution Research Center (SAPRC) mechanism (Carter and Lurmann, 1991; Carter, 2000) are two well known examples.

Because the chemistry of ground level O_3 formation is highly complex and nonlinear and has many uncertainties, no chemical mechanism can be relied upon to give even approximately accurate predictions unless it has been evaluated by comparing its predictions with experimental data. Models based on assuming that O_3 reductions are proportional to precursor reductions may result in inappropriate or counter-effective control strategies (Carter *et al.,* 1995a).

There are essentially two ways a photochemical oxidant model can be evaluated. The first is to compare the predictions of the complete model against data taken during an historic O_3 pollution episode from which field data exist for the important precursors and products. The other approach for evaluating models is to evaluate each of the components separately. In the case of gas-phase chemical mechanisms, this means evaluating the predictions of the mechanism against results of environmental chamber experiments (Carter *et al.,* 1995a). Only extensively testing against experimental data ensures that their predictions are appropriately simulating the chemical and physical processes involved and not the result of fortuitous cancellation of errors (Finlayson-Pitts and Pitts, 2000).

The focus of this dissertation is the analysis of one explicit chemical mechanism; the Master Chemical Mechanism (MCM). The mechanism was developed primarily to provide a research tool for investigating the contribution of specific VOC emission sectors (with varying VOC composition) to the production of ozone. This has also led to the development of the Photochemical Ozone Creation Potential (POCP) concept, as a measure of the relative propensities of emitted VOC to generate ozone under representative ambient conditions (e.g. Derwent *et al.,* 1998). The MCM has also been applied in atmospheric chemistry studies where detailed chemistry is required, e.g. to simulate the generation of speciated organic intermediates (e.g. multifunctional carbonyls, hydroperoxides and nitrates) for which field data are becoming available and how the generation of these products is influenced by newly identified or postulated chemical pathways or redetermined kinetic parameters. However the performance of MCM has not been extensively tested and validated (Saunders *et al.,* 2003).

The present work is a contribution to the validation of Master Chemical Mechanism; the work consists essentially in the evaluation of its capability of predicting the transformation processes of pollutants in the atmospheric environment. This is achieved both by comparison of product simulations with environmental chamber data, and by incorporation of the chemical mechanisms into a suitable tropospheric model, allowing the comparison of model predictions with atmospheric observational data.

The photo-oxidation of mixtures of hydrocarbons and NO_x in comparatively large volume chambers has long been used as a method of investigating their potential atmospheric impact, and in recent decades, chamber studies have been used as the experimental basis of defining the relative propensities of a large number of hydrocarbons to generate ozone in urban atmospheres. Corresponding datasets, describing the time dependence of hydrocarbons, NO, NO_2 and ozone are available for large smog chambers. In this study MCM schemes is tested with data from smog chambers of the Statewide Air Pollution Research Center (SAPRC) at the University of California (Carter *et al.,* 1995a).

This work evaluates the alkanes available in the SAPRC environmental chamber datasets. There is a large number of single VOC-NO_x-Air runs for n-butane in the SAPRC database. However, only 2 runs of n-heptane and 4 runs of n-octane exist, which represent the complete database for monoalkanes for which VOC-NO_x-Air are available. The series of butane-NO_X photo-oxidation experiments was used for initial assessment of the auxiliary mechanism parameters. Photo-oxidation of butane, and its degradation products methylethyl ketone, acetaldehyde and formaldehyde, was made in conjunction with an initial evaluation of the chamber-dependent auxiliary mechanisms.

The representation of alkene degradation is evaluated, using environmental chamber data on the photo-oxidation of ethene, propene, 1-butene and 1-hexene, which represent the complete database for monoalkenes (excluding α– and β–pinene) for which multiple runs are available.

A special attention is considered in this work relatively to the biogenic species present in MCM. The photo-oxidation mechanisms of isoprene, α-pinene and β-pinene are evaluated. Photo-oxidation of Isoprene is made simultaneously with its degradation products, methacrolein and methylvinyl ketone.

Several shortcomings in the ability of the MCM to describe the chamber data were detected and investigated, and possible refinements are identified for inclusion in future releases of the MCM.

Throughout the study, the performance of MCM v3 is also compared with that of the SAPRC-99 mechanism, which was developed and optimized in conjunction with the chamber datasets.

The photo-oxidation mechanisms for aromatics (benzene, toluene, *p*-xylene and 1,3,5-trimethylbenzene) were evaluated by Bloss *et al.* (2005a) and some deficiencies were identified in the mechanisms: an over-estimation of the ozone concentration; an under-estimation of the NO oxidation rate and under-estimation of OH. The refinements mechanism improvements provided some agreement but significant discrepancies remain. In this study, the photo-oxidation mechanisms for aromatics were not evaluated taking into consideration the recent evaluation and conclusions of Bloss *et al.* (2005a), together with the fact that the evaluation is extremely time consuming.

One of the aims of the current study was the application of MCM, after applied refinements resulting from chamber evaluation, to a concrete environmental situation where photochemical pollution formation is well established and defined in order to further test the Photochemical Trajectory Model and the modifications introduced in MCM. The field study is the application of a Photochemical Trajectory Model to a real situation in the Portuguese west coast: the air mass transported by the sea breeze, from the coast line (Aveiro) to a location, approximately 65 kilometres inland, (Covelo). The Photochemical Trajectory Model is applied for the days June 29 and 30, 2001.

2 The Master Chemical Mechanism (MCM)

The MCM is a near-explicit chemical mechanism that describes the detailed degradation of a series of emitted VOC, and the resultant generation of O_3 and other secondary pollutants, under conditions appropriate to the planetary boundary layer. It was developed in the United Kingdom by a consortium of groups (Leeds University, Imperial College, AEA Technology, Meterological Office), primarily with the support of the UK Department of the Environment, Food and Rural Affairs, DEFRA (Jenkin *et al.,* 1997; Saunders *et al.,* 2003; Jenkin *et al.,* 2003). The philosophy behind the construction of the MCM is to use the available information on the kinetics and products of elementary reactions relevant to VOC oxidation to build up a near-explicit representation of the degradation mechanisms. A fundamental assumption in the mechanism construction, therefore, is that the kinetics and products of a large number of unstudied chemical reactions can be defined on the basis of the known reactions of a comparatively small number of similar chemical species, by analogy and with the use of structure-reactivity correlations (Jenkin *et al.,* 1997; Saunders *et al.,* 2003; Jenkin *et al.,* 2003; Bloss *et al.,* 2005a).

Jenkin *et al.* (1997) describes the protocol used in mechanism construction, the rules were applied in the treatment of a wide range of non-aromatic hydrocarbons and oxygenated and chlorinated VOCs. The protocol describes the initiation reactions, the reactions of the radical intermediates and the further degradation of first and subsequent generation products. The protocol described in Jenkin *et al.,* 1997 takes into consideration work available in the open literature up to the end of 1994, and some further studies known by the authors, which were under review until that time. New work since the publication of the original protocol paper Jenkin *et al.* (1997) has been taken into consideration in the production of version 2 and 3. The revised protocol for version 3 is detailed in Saunders *et al.* (2003).

Compilation of the individual VOC degradation schemes led to first version of the Master Chemical Mechanism (MCMv1.0) (1996). The MCMv1.0 contains the gas phase tropospheric degradation of 120 volatile organic compounds. The organic component of the MCMv1.0 contains 7500 reactions and 2500 chemical species. Further developments in the understanding of aromatics oxidation and the introduction of oxidation mechanisms of more three organic compounds led to new version of the Master Chemical Mechanism, MCMv2.0 (1999). MCMv2.0 involves the gas phase tropospheric degradation of 123 volatile organic compounds and the organic component contains 10500 reactions and 3480 chemical species. The MCMv3.0 (2002) considers the oxidation mechanisms of 125 volatile organic compounds and the mechanism comprises 12691 reactions of 4351 organic species. The MCMv3.1 (October 2003) considers the oxidation mechanisms of 135 volatile organic compounds and the mechanism comprises 13500 reactions of 5600 organic species

and 46 associated inorganic reactions. MCM v3.1 updates MCM v3, although the chemistry for non-aromatic VOC remains unchanged. The MCM can be accessed at, and downloaded from, the website: http://mcm.leeds.ac.uk/MCM.

The mechanism was developed primarily to provide a research tool for investigating the contribution of specific VOC emission sectors (with varying VOC composition) to the production of O_3. This has also led to the development of the Photochemical Ozone Creation Potential (POCP) concept, as a measure of the relative propensities of emitted VOC to generate O_3 under representative ambient conditions (e.g. Derwent *et al.,* 1998). However, the MCM has also been applied in atmospheric chemistry studies where detailed chemistry is required, e.g. to simulate the generation of speciated organic intermediates (e.g. multifunctional carbonyls, hydroperoxides and nitrates) for which field data are becoming available and how the generation of these products is influenced by newly identified or postulated chemical pathways or redetermined kinetic parameters.

In addition to the application on the examination of detailed chemical processing on local and regional scales (e.g., Derwent *et al.,* 2005; Utembe *et al.,* 2005), the MCM is also increasingly being used as a benchmark mechanism for the development and/or testing of reduced chemical mechanisms for use in local, regional and global scale models requiring more economical representations of chemical processing (e.g., Poschl *et al.,* 2000; Jenkin *et al.,* 2002; Whitehouse *et al.,* 2004a,b; Bonn *et al.,* 2004). It is therefore desirable that the performance of the MCM is evaluated, when possible, using the results of environmental chamber experiments. A number of previous studies have used the results of experiments from the European Photoreactor (EUPHORE) to evaluate the performance of MCM v3 (and MCM v3.1) degradation schemes for α–pinene (Saunders *et al.,* 2003), benzene, toluene, *p*-xylene and 1,3,5-trimethylbenzene (Bloss *et al.,* 2005a) and ethene (Zador *et al.,* 2005). Very recently, Hynes *et al.* (2005) have tested the MCM v3.1 schemes for propene and 1-butene, in conjunction with characterisation of the CSIRO indoor chamber.

3 Environmental Chambers

The photo-oxidation of mixtures of VOC and NO_x in comparatively large volume chambers has long been used as a method of investigating their potential atmospheric impact, and in recent decades, chamber studies have been used as the experimental basis of defining the relative propensities of a large number of VOC to generate O_3 in urban atmospheres. Simulating atmospheric conditions using larger chambers is, perhaps, the most direct experimental mean of examining the relationships between emissions and air quality (e.g. Carter, 2000; Finlayson-Pitts and Pitts, 2000).

Environmental chamber data have been used to test/refine chemical mechanisms, rather than ambient data, because environmental chambers, although they have problems like dilution and wall effects and cannot be characterized as completely controlled environments, at least are "closed systems" (Dodge, 2000) more easily controllable and analysable.

The environmental chambers are irradiated with sunlight, or lamps used to replace the sun, and concentration *vs.* time profiles of the primary (injected) and secondary (produced inside the chamber) species are measured. The initial conditions, namely; primary species concentrations, temperature, relative humidity, radiation (if not natural) can be systematically varied to establish the relationship between emissions and air quality, without the complexity of ambient air data (e.g. Finlayson-Pitts and Pitts, 2000). In the environment, it is difficult to separate the chemistry from meteorology and other processes (Dodge, 2000).

Simulating chamber data, necessarily implies to include in the model appropriate representations of the conditions of the chamber experiments that affect the simulation results. These include initial reactant, physical conditions such as light intensity and spectrum, temperature, humidity and chamber effects (e.g., Carter and Lurmann, 1991; Carter et al., 1995a,b).

Unfortunately, the use of environmental chamber data to evaluate mechanisms has several importante difficulties. To successfully use such data for this purpose, the uncertainties in characterizing the conditions of the experiments, including chamber wall effects as well as light intensity and spectrum, temperature, reactant levels, etc., must be lesser than the uncertainties in the mechanism being evaluated (e.g. Carter *et al.,* 1995a,b).

The errors in the chamber or experimental characterization assumptions could result in a correct mechanism giving predictions which are inconsistent with the chamber data or, worse, an erroneous mechanism appearing to be validated by the data because of compensating errors (e.g. Carter *et al.,* 1995a,b; Finlayson-Pitts and Pitts, 2000).

Despite all this problems, environmental chambers have proven extremely useful in studying the chemistry of photochemical air pollution under controlled conditions. While there are some uncertainties and limitations in quantitatively extrapolating the results to ambient air, it may be that what appear to be chamber-specific complications may apply in ambient air as well (Finlayson-Pitts and Pitts, 2000).

3.1 Chamber Effects

There is some disagreement, about how chamber artifact effects should be represented in the model as characterizing them is extremely difficult (e.g. Dodge, 2000).

Killus and Whitten, (1990) refer to three major groups of heterogeneous processes occurring at the chamber walls which can interfere with the evaluation and interpretation of experiments carried out in environmental chambers (i) the introduction of free radicals through wall reactions, (ii) the adsorption or desorption of oxidised nitrogen species (NO_y), and (iii) off-gassing of organics that can lead into OH (hydroxyl) to HO_2 (hydroperoxyl) conversion and therefore supplement O_3 production in the system.

Walls can serve as both sources and sinks of gaseous species. Species such as O_3, HNO_3, N_2O_5, H_2O_2 and HCHO can adhere to surfaces or be adsorbed into surface water films; these species can be re-emitted into the gas-phase later in the experiment, or in subsequent experiments (Dodge, 2000). Several characteristics of photochemical air pollution are observed, when clean air is irradiated on environmental chambers that have been in use previously (Finlayson-Pitts and Pitts, 2000).

The level of NO_x off-gassing, maybe the most important of the off-gassing species, varies from run to run, making it exceedingly difficult to characterize this heterogeneous process when simulating chamber data (Dodge, 2000). For example, the formation of peroxyacetyl nitrate (PAN), whose formation requires the presence of NO_x, has been observed in NO_x -free acetaldehyde-air runs that are routinely performed in many chambers (Dodge, 2000).

One of the most important chamber effects which can influence mechanism evaluations is the chamber radical source parameter (Carter *et al.,* 1995a). The high reactivity observed in chamber irradiations of NO_x-air and NO_x-CO-air mixtures can only be explained by assuming a continuous OH radical source (Dodge, 2000). Although, the identity and mechanism of formation of OH radical are unknown and there is no consensus among modelers about how best to represent the radical source (Dodge, 2000, Finlayson-Pitts and Pitts, 2000). For example, Gery *et al.* (1988) represent the process by assuming continuous off-gassing of HONO and formaldehyde. Both, HONO and HCHO, photolyze to produce OH radicals; the photolysis of HONO also yields NO. Carter and Lurmann (1990, 1991) represent NO_x independent and NO_x dependent radical source

parameters. Besides, they consider the radical source dependent on light intensity, temperature and humidity. Killus and Whitten (1990) concluded that the chamber radical source can contribute from 10 to 50% of the total radicals in a chamber experiment, having the greatest effect on low-reactivity experiments such as those involving alkanes or those performed at low VOC/NO_x ratios.

Carter *et al.* (1995b) re-evaluated the radical source assignments using butane and CO - NO_x and concluded that the use of the tracer - NO_x -air experiments, used in Carter and Lurmann (1990, 1991), may give inappropriately high radical sources. Carter *et al.* (1995b) shows that if the radical source assignments of Carter and Lurmann (1990, 1991) are employed, the model consistently overpredicts, by 50% to more than a factor of 2, the rate of D(O_3-NO) (see D(O_3-NO) parameter definition in section 5.3) formation in the n-butane runs.

Carter in the SAPRC 99 mechanism (Carter, 2000) considered the HONO from the walls to represent both the chamber radical source and NO_x offgasing.

Because of the sensitivity of simulations of chamber runs to this parameter, an inappropriate radical source assignment is probably the most likely source of compensating errors when evaluating mechanisms using chamber data (Carter *et al.,* 1995a).

The magnitude of these processes differs from chamber to chamber and often from run to run. Chamber radical sources and other chamber artifact effects could easily be uncertain by 50% (Dodge, 2000 and references therein).

3.2 Light Source

The nature of the light source is probably the most important factor when distinguishing different types of chambers, since light provides the energy which drives the entire photochemical smog formation process (Carter *et al.,* 1995b). The light source must approximate both the intensity and spectrum of sunlight if it is to provide an appropriate simulation of atmospheric chemistry (e.g. Carter *et al.,* 1995b; Dodge, 2000; Finlayson-Pitts and Pitts, 2000).

Light characterization for environmental chamber runs requires information about both the intensity and the spectrum of the light, and how they change with time. This is difficult to characterize, being a source of uncertainty in mechanisms tested against chamber data (e.g. Carter *et al.,* 1995b; Dodge, 2000; Finlayson-Pitts and Pitts, 2000).

The use of outdoor chambers and natural sunlight is one way to address this problem, but outdoor chamber experiments are much more difficult to control and characterize for modelling, being also more expensive (Carter *et al.,* 1995b). The light intensity in outdoor chambers is extremely difficult to characterize. Radiometer readings are usually taken outside the chamber and thus do not directly measure light intensity within the chamber. Light is attenuated as it passes through the Teflon film of outdoor chambers; further attenuation of the light can occur if water is condensed on the

chamber walls. Some chambers also have reflective floors which can complicate the determination of light intensity. In addition, the intensity of the sunlight can be altered by passing clouds in a manner that is difficult to measure and describe accurately. The experiments in these outdoor chambers are then limited to days with appropriate meteorology. (e.g. Dodge, 2000; Finlayson-Pitts and Pitts, 2000).

Indoor chambers allow for conditions to be more controlled and better characterized, but require the use of artificial light sources whose spectrum can only approximate that of sunlight. In the case of indoor chamber runs, the intensity and the spectrum is usually assumed to be constant during an experiment; the problem is assigning some measure of light intensity and a spectrum of relative intensities as a function of wavelength for each run (e.g. Carter *et al.,* 1995b; Dodge, 2000).

Various alternatives for indoor chamber lighting are analysed and discussed in detail in Carter *et al.* (1995b). However, a brief description of the black lights and xenon arc lamps is presented below.

A black lamp is a low-pressure mercury lamp covered with a phosphorescent material such as strontium fluorcarbonate or barium disilicate (Finlayson-Pitts and Pitts, 2000). The type of phosphor determines the spectral distribution of the lamp output (Finlayson-Pitts and Pitts, 2000 and references therein). Blacklights spectral distribution is very different from the sun; the output is poor in the UV region of 290 to 340 nm; have a good light intensity in region of 340 to ≈375 nm; the intensity decrease for $\lambda > 375$ nm and much of the intensity resides in the sharp mercury lines. These differences from the sun light spectrum significantly affect the relative rate constants for the photolysis (Carter *et al.,* 1995b; Finlayson-Pitts and Pitts, 2000). Photolysis of acrolein, benzaldehyde, and nitrites are higher than they are under sunlight; the photolysis rates for glyoxal and methyl glyoxal are significantly lower with blacklights than sunlight, and the NO_3 photolysis hardly occurs at all (Carter *et al.,* 1995b). Carter *et al.* (1995b) conclude however that even if blacklight spectra doesn't look much like that of sunlight, they may provide a reasonably good representation of rate constant ratios for chemical systems which are driven by photolysis of simple aldehydes and ketones and they present a complication in using chamber data to test mechanisms for biogenic alkenes, and introduce major uncertainties in using such data to test mechanisms for aromatics.

Xenon arc lights could provide the most faithful artificial simulation of sunlight in the wavelength region 290-700 nm (Carter *et al.,* 1995b; Finlayson-Pitts and Pitts, 2000). Xenon arc lights are much more intense in the UV than sunlight, at ground level, and filters are required to remove the UV below ≈290 nm. Although even after application of filters, xenon arc lights still have some problems; one is the price, but the major one is the fact that their spectra is very variable (Carter *et al.,* 1995b). The spectral distribution and light intensity must be measured periodically since the lamp characteristics change with the time. In most indoor chambers the absolute light intensities

are determined by conducting NO_2 actinometry experiments to measure the NO_2 photolysis rate and relative spectra are measured using spectrometers (e.g. Carter *et al.,* 1995a,b). The photolysis rate for NO_2 might be expected to be a good indicator of the intensity in the region of $\lambda<430$ since it absorbs strongly in this range (Finlayson-Pitts and Pitts, 2000).

A standard procedure in chamber runs is to calculate the actinic flux from the NO_2 photolysis rate (k_1) and the relative spectral distribution ($J_{rel}(\lambda)$) for the experiment with the following equation:

$$J(\lambda) = J_{rel}(\lambda)\frac{k_1}{\sum_{\lambda} J_{rel}(\lambda)\sigma_{NO_2}(\lambda)\Phi_{NO_2}(\lambda)}$$

where σ_{NO2} and Φ_{NO2} are the NO_2 absorption cross sections and photolysis quantum yields for NO_2.

3.3 Measurement Uncertainties

Most of the used environmental chambers employed inadequate analytical equipment. So, most of the current environmental chamber data base is not suitable for evaluating chemical mechanisms under the lower NO_x conditions found in rural and urban areas with lower pollutant burdens (Carter *et al.,* 2002). Because of this, one cannot necessarily be assured that models developed to simulate urban source areas with high NO_x conditions will satisfactorily simulate downwind or cleaner environments where NO_x is low (e.g. Dodge, 2000; Carter *et al.,* 2002).

In most chamber studies, measurement data do not exist for: other aldehydes than HCHO and CH_3CHO; dicarbonyls and other multi-functional products formed during the oxidation of aromatic and biogenic VOC; organic nitrates, organic peroxides and many other carbon-containing products; inorganic species such as HONO and H_2O_2 and free radicals like OH and HO_2 (Dodge, 2000). Also, NO_2 is not measured directly, but is assumed to be the difference between the measured levels of NO_x and NO.

The measured species in chamber studies usually have large uncertainties. Measurements for O_3 and many of the hydrocarbon species should be accurate to ±10%, PAN measurements are uncertain by ±20% and measurements of most oxygenates are uncertain by at least ±30% (Dodge, 2000).

4 Atmospheric chemistry of VOCs and NO_x

Considering that the essential features of the chemistry of VOC degradation, particularly in relation to O_3 formation, are now well documented (e.g., Atkinson, 2000; Jenkin and Clemitshaw, 2000) and attending the goal of this work, this section only tries to describe in a synthesized way (if any simple way exists to explain the extremely complex atmospheric chemistry), the daytime gas-phase photochemical transformations of NO_x and VOCs, and their role in the formation of O_3. Latter, in section 5, a more detailed feature of the chemistry of VOC degradation is presented, in conjunction with description of MCM degradation mechanism of several species evaluated against chamber data.

Under tropospheric conditions O_3 is formed photochemically from the photolysis of NO_2 and reacts rapidly with NO. This three reaction cycle (usually designated by Basic Photochemical Cycle) result in equilibrium between NO, NO_2 and O_3 with no net formation or loss of O_3:

$$NO_2 + h\nu \rightarrow NO + O(^3P) \qquad (\lambda < 420\text{nm}) \tag{1}$$

$$O(^3P) + O_2 + M \rightarrow O_3 + M \tag{2}$$

$$NO + O_3 \rightarrow NO_2 + O_2 \tag{3}$$

However, in the presence of VOCs, the degradation reactions of VOCs lead to the formation of intermediate radicals: RO_2 (peroxyl radical) and HO_2 (e.g. Atkinson, 2000; Calvert *et al.,* 2000; Jenkin and Clemitshaw, 2000). These peroxyl radicals react with NO, converting NO to NO_2:

$$HO_2 + NO \rightarrow OH + NO_2 \tag{4}$$

$$RO_2 + NO \rightarrow RO + NO_2 \tag{5}$$

Since conversion of NO to NO_2, as a result of previous reactions, does not consume O_3 the subsequent photolysis of NO_2 represents a net source of O_3. These reactions assume the major role of photochemical O_3 production in the troposphere where NO_x, VOCs and sunlight are the main ingredients (e.g. Atkinson, 2000; Calvert *et al.,* 2000; Jenkin and Clemitshaw, 2000).

The major recognized oxidants for VOCs in atmosphere are OH and O_3, plus NO_3 at night (e.g. Atkinson, 2000; Calvert *et al.,* 2000; Finlayson-Pitts and Pitts, 2000; Jenkin and Clemitshaw, 2000). The major source of OH is the reaction of electronic excited oxygen atoms (O^1D), produced by photolysis of O_3, with water vapour. Figure 1 shows, in a simplified way, the inter-conversions between OH and HO_2:

It is well established that the degradation of each emitted VOC occurs by a specific mechanism (because of differences in reactivity and structure), such that the relative contributions of VOC to

the formation of O_3 and other secondary pollutants varies from one compound to another (e.g., Carter and Atkinson, 1987; Derwent and Jenkin, 1991).

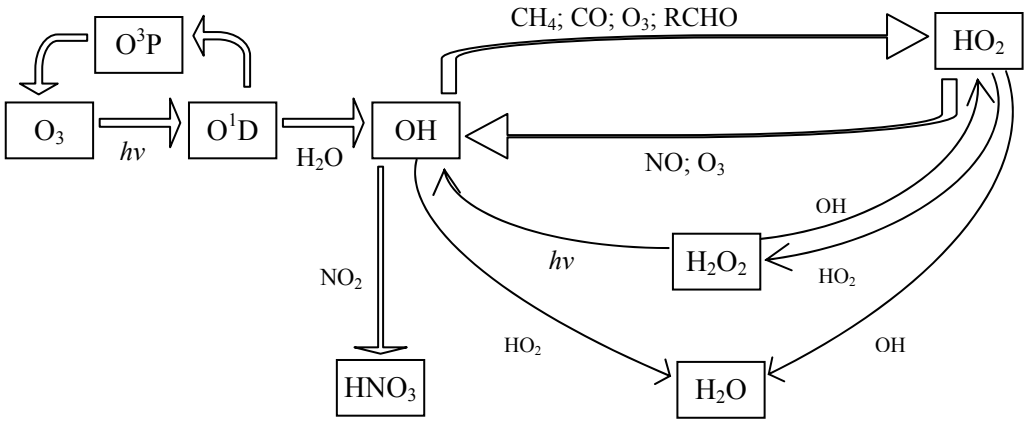

Figure 1: Schematic representation of major tropospheric inter-conversions between OH and HO_2 radicals.

However, the oxidation by OH of a generic saturated hydrocarbon, RH (i.e., an alkane), into its first generation oxidised products has some common features with the tropospheric oxidation of most organic compounds. The oxidation is initiated by reaction with the OH, leading to a rapid sequence of reactions, (see scheme in Figure 2). Since OH is regenerated, this mechanism is a catalytic cycle with OH, R (alkyl radical), RO_2, RO (alkoxy radical) and HO_2 acting as chain propagating radicals. As it is evidenced in scheme, peroxy radicals reactions, reactions 4 and 5, play a key role in O_3 formation by oxidising NO to NO_2.

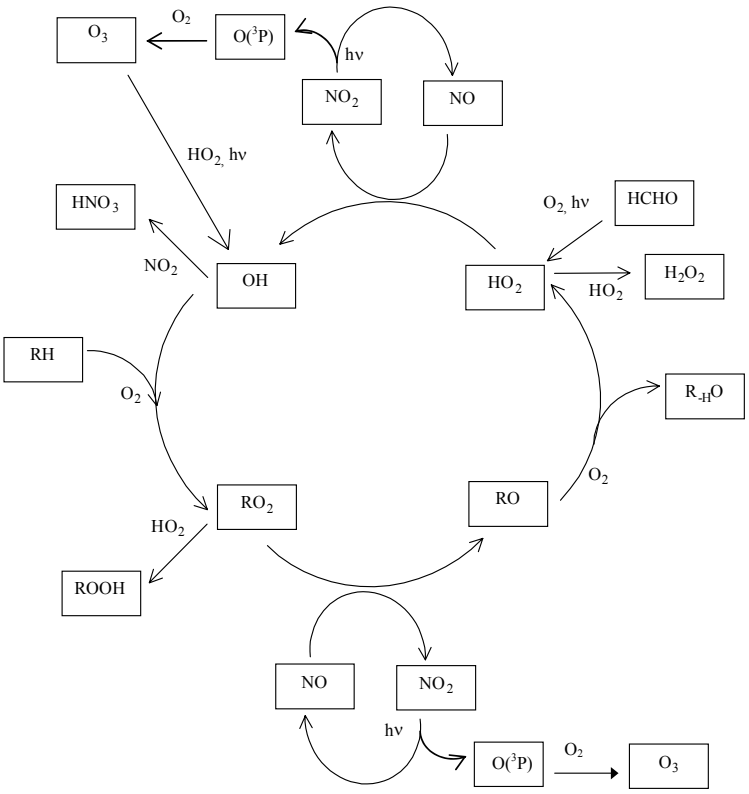

Figure 2: Schematic representation of the free radical-catalysed oxidation of a generic saturated hydrocarbon, RH, to its first generation oxidised product, aldehyde or ketone (R_HO). Adapted from PORG, 1997.

5 Evaluation of MCM v3.1, using environmental chamber data

The major objective defined in PhD program consisted in the evaluation of some degradation schemes from Master Chemical Mechanism and its capability of predicting the transformation processes of pollutants in the atmospheric environment, by comparison of product simulations with environmental chamber data. The MCM schemes evaluated during this work were: Butane, n-heptane, n-octane, ethene, propene, 1-butene, 1-hexene, isoprene, α-pinene and β-pinene, formaldehyde, acetaldehyde, methacrolein, acetone, methylethyl ketone and methylvinyl ketone.

The model was integrated with variable order Gear's method FACSIMILE (Curtis and Sweetenham, 1987) using software FACSIMILE[1].

5.1 Chamber data

5.1.1 Source of data

The mechanistic evaluation was carried out using the database of the indoor chambers of the Statewide Air Pollution Research Center (SAPRC) at the University of California (Carter *et al.,* 1995a). A set of computer data files containing the SAPRC environmental chamber data was obtained on the Internet by anonymous FTP at carterpc.ucr.edu, and a more recent set of data, used in the evaluation of SAPRC-99 mechanism, was kindly provided directly by Prof. William P. L. Carter.

Data from the following environmental chambers were used in the present evaluation: Indoor Teflon Chamber #1 (ITC); Indoor Teflon Chamber #2 (ETC); Dividable Teflon Chamber (DTC); Xenon Arc Teflon Chamber (XTC) and CE-CERT Xenon Arc Teflon Chamber (CTC). The major characteristics of these chambers are summarized in Table 1. The available datasets from these chambers were used previously in the development and evaluation of the SAPRC-99 mechanism (Carter, 2000).

[1] FACSIMILE for Windows, version 3.5.5, ©UES Software 2000.

Table 1: Summary of chambers used for experiments modelled in this work.

Chamber	Volume (dm^3)	Walls	Light Source	Humidity	References (a)
SAPRC ITC	≈6400	Semi-collapsible 2 mil FTP Teflon bag held by frame	Blacklight	≈50%	(Carter and Lurman, 1991) (Carter *et al.,* 1995a)
SAPRC ETC	≈3000	Semi-collapsible 2 mil FTP Teflon bag held by frame	Blacklight	<5%	(Carter *et al.,* 1995a)
SAPRC DTC	≈2x2500	Two Semi-collapsible 2 mil FTP Teflon bags held by frames	Blacklight	<5%	(Carter *et al.,* 1995)
SAPRC XTC	≈5000	Semi-collapsible 2 mil FTP Teflon bag held by frame	4 x 6 KW Xenon Arc	<5%	(Carter and Lurman, 1991) (Carter *et al.,* 1995a)
SAPRC CTC (11-82)	≈5000	Semi-collapsible 2 mil FTP Teflon bag held by frame	4 x 6 KW Xenon Arc	<5%	(b)
SAPRC CTC (83+)	≈2x2500	Two Semi-collapsible 2 mil FTP Teflon bags held by frames	4 x 6 KW Xenon Arc	<5%	(c)

Note:

(a) References where more details can be obtained concerning the chambers and the experimental procedures.

(b) Very similar to XTC.

(c) Very similar to XTC except dual bags.

5.1.2 Characterisation of chamber wall effects

The chamber wall effects can be characterized for a given chamber, through experiments which are designed to be especially sensitive to the wall effects, but for which the gas phase chemistry is reasonably well understood. Such characterization experiments can be used to create a model for chamber wall effects and chamber-dependent parameters (Carter *et al.,* 1995a), which is usually termed the 'auxiliary mechanism' (Jeffries *et al.,* 1992). The auxiliary mechanism may then be applied when conducting model simulations of experiments where less well-established gas-phase chemistry is being evaluated and refined.

A database for mechanism evaluation is therefore not complete without recommendations for appropriate inputs to auxiliary mechanisms. Such chamber effects models have already been developed for the SAPRC chambers as part of the process of evaluating SAPRC-99 and related mechanisms (e.g. Carter, 2000), and these form the basis of the auxiliary mechanisms applied in the present study.

Table 2 lists the corresponding series of pseudo-reactions which provide a description the wall-related processes indicated above, along with the associated recommended parameters characteristic for each of the chambers for which data are considered, (see section 5.4).

Table 2: Pseudo-reactions representing chamber-dependent processes (based on Carter, 2000).

Process	ITC chamber	ETC chamber	DTC chamber		XTC chamber	CTC chamber	
Initial HONO in experiment, assumed to be independent of other reactants.	1.7 (ppb)	-	-		-	-	
Ratio of the initial HONO concentration to the measured initial NO_2. [The initial NO_2 in the experiment is reduced by a factor of 1 - (HONOF)].	-	-	Set (c)		1.2%	0.8%	
			1	0.1%			
			3	0.4%			
			10	0.8%			
			11	0.6%			
Walls + hν → HONO (ppb)x JNO_2 (T – temperature) (a) (b)	0.061	$1.22E^{10}$exp(-9712/T)	Set		$6.3E^{9}$exp(-9712/T)	Set	
			1	0.070		1-8	0.077
			3	$2.59E^{10}$exp(-9712/T)			
			10	$9.77E^{9}$exp(-9712/T)		9	0.116
			11	0.096			
Walls + NO_2 → 0.2 HONO + (1-0.2) Wall-NOx	All $1.6E^{-4}min^{-1}$						
Walls + O_3 → (loss of O_3)	All $1.5E^{-4}min^{-1}$						
N_2O_5 + walls → 2 Wall-NOx	All $2.8E^{-3}$ min^{-1}						
N_2O_5 + H_2O + walls → 2 Wall-NOx	All $1.1E^{-6}$ ($ppm^{-1}min^{-1}$)						
OH → HO_2	All $250min^{-1}$						

Notes:

(a) The formation of HONO from the walls was used to represent both the chamber radical source and NO_x offgasing, because the HONO so formed would photolyze rapidly to produce both OH radicals and NO. The values represent the contribution ratio of the rate of Walls + hν → HONO to the NO_2 photolysis rate.

(b) The values used in this work were obtained by optimization and are related with the values used in the SAPRC-99 evaluation (Carter, 2000), see section 5.4. The values used in this work are bigger by a ratio of 1.35, for the ITC and ETC chambers, and by a ratio of 1.2, for the DTC, CTC and XTC chambers, relatively to the values applied in SAPRC-99 evaluation.

(c) "Set" column on the table indicates the "characterization set", which refers to a group of runs that are all assumed to have the same characterization parameters (Carter *et al.,* 1995a). The characterization set changes if the results of characterization runs indicate that the wall effects parameters have changed. For the CTC, characterization sets are also used to refer to runs that are assumed to have the same spectral distribution.

5.2 Photolysis processes

The rates of photolysis processes depend on the intensity and spectral distribution of the light source, which vary from one chamber to another. Spectral distributions (based on spectrometer measurements) and absolute light intensities (based on NO_2 actinometry experiments) are documented for all the SAPRC chambers (e.g. Carter *et al.,* 1995a,b). The rates of photolysis processes for application in MCM v3.1 were thus determined using this spectral information in conjunction with absorption cross sections and quantum yield data previously used in conjunction with the MCM, mainly based on the sources summarised by Jenkin *et al.* (1997), (see section 6.1.1.1). Furthermore, the rates of a number of photolysis reactions were updated during the course of the present study, as discussed further below.

5.3 Criterion to Evaluate Model Performance

As with previous assessments (e.g. Carter, 2000), the quantity $D(O_3\text{-NO})$ was used as the main criterion of model performance. This quantity is defined as: $D(O_3\text{-NO})_t = [O_3]_t - [NO]_t - ([O_3]_0 - [NO]_0)$, where $[O_3]_0$, $[NO]_0$, and $[O_3]_t$, $[NO]_t$ are the concentrations of O_3 and NO at the beginning of the run, and at time 't', respectively. As described in detail previously (e.g., Carter and Lurmann, 1991, Carter *et al.,* 1995a, Carter, 2000), $D(O_3\text{-NO})$ is an indicator of the ability of the mechanism to simulate the chemical processes that cause O_3 formation, giving a useful measure, even when O_3 is suppressed by the presence of excess NO. In addition, use of this measure allows a direct comparison with the SAPRC-99 published results. The precursor decay rate and formation of the carbonyl products and PAN were also used as criteria of model performance.

5.4 Auxiliary Mechanism Assessment

As with the chamber characterisation studies of Carter (Carter, 2000), the series of butane-NO_X photo-oxidation experiments was used for initial assessment of the auxiliary mechanism parameters. This system is believed to provide a good test for the chamber wall effects because the degradation chemistry of butane is quite well characterized (Carter and Lurmann, 1991; Carter *et al.,* 1995a), and because of the large set of experiments available.

Initial simulations were carried out to compare the SAPRC-99 and MCM v3.1 butane mechanisms for the conditions of the butane-NO_X experiments, using the auxiliary mechanism parameters defined by Carter, (2000), and a consistent set of inorganic reaction rate coefficients. The MCM v3.1 and SAPRC-99 butane mechanisms were found to perform very similarly, suggesting a good level of consistency in the understanding and representation of butane oxidation in these mechanisms.

To allow a full evaluation, however, it is necessary to consider not only the experimental data for the butane-NO_X system, but also the NO_X photo-oxidation runs for intermediate products, MEK, CH_3CHO and HCHO. The aim of the mechanism refinements for butane degradation, therefore, was to provide an adequate, self-consistent description of all these systems, whilst simultaneously identifying any required modifications to the auxiliary mechanism parameters. Mechanism testing and refinement was therefore carried out by an iterative procedure, considering butane photo-oxidation and each of the sub-systems in turn. The adapted version of MCM v3.1, resulting from identified modifications during the optimization of butane and intermediate products of it oxidation, is denoted MCM v3.1a throughout this work. MCM v3.1 is relate to the MCM as available for download in internet, namely with rate coefficient for the reaction of OH with NO_2 with a value (at 298 K and 760 Torr) of 1.19 x 10^{-12} cm^3 $molecule^{-1}$ s^{-1} (based on the value recommended by IUPAC - IUPAC Subcommittee on Gas Kinetic Data Evaluation – Data Sheet NOx13 updated in 16th January 2003).

In conjunction with these tests, the opportunity was taken to revise and update the inorganic chemistry parameters. The most notable change from the reference simulations, as performed for SAPRC-99 by Carter, (2000), was a change in the assigned rate coefficient for the reaction of OH with NO_2 from a value (at 298 K and 760 Torr) of 8.98 x 10^{-12} cm^3 $molecule^{-1}$ s^{-1} (based on value recommended by Jet Propulsion Laboratory (JPL), (DeMore *et al.,* 1997), to a value of 1.05 x 10^{-11} cm^3 $molecule^{-1}$ s^{-1} (based on JPL, Sander *et al.,* 2003). This reaction represents an important radical sink in the system, which was found to have a particularly significant impact under the conditions of some of the butane-NOx photo-oxidation experiments. As described further below, this required small compensating increases to be applied to the chamber radical source parameter. Apart from

this, it was not necessary to make any other changes to the auxiliary mechanism parameters defined by Carter (2000) and shown in Table 2.

A large set of chamber experimental runs were employed in this evaluation. These consisted of 46 butane-NO_X-air, 6 MEK-NO_X-air, 11 CH_3CHO-NO_X-air and 24 HCHO-NO_X-air experiments, in the initial evaluation of the chamber dependent processes and butane degradation chemistry. The ranges of reagent concentrations for the considered experiments are presented in Table 3. Full details of the experimental conditions and reagent concentrations are available elsewhere (Carter *et al.,* 1995a; Carter, 2000), which includes detailed documentation of the measurement uncertainties associated with the analytical methods employed for the reactants and products, and the precision and accuracy of other experimental parameters (e.g. temperature; light intensity and spectrum of the photolysing radiation).

Table 3: Ranges of reagent concentrations for experiments involving the degradation of butane and its degradation products.

	Butane-NOx	MEK-NOx	CH_3CHO-NOx	HCHO-NOx
[VOC] (ppm)	1.47–4.95	7.83–9.49	0.44–1.67	0.29–1.01
[NOx] (ppm)	0.09-0.66	0.09–0.29	0.14–0.28	0.16-0.54
[VOC]/[NOx]	5.22-39.89	26.61–99.44	1.71–11.73	1.00–3.40

5.4.1 Chemistry of butane photo-oxidation

The complete degradation chemistry of butane, as represented in MCM v3.1, consists in 538 reactions of 184 species. It can be viewed and downloaded using the subset mechanism assembling facility, available as part of the MCM website. The methodology of mechanism construction has been described in detail by Jenkin *et al.* (1997) and Saunders *et al.* (2003). The main features of the degradation chemistry of butane when NO_X is present are summarized in Figure 3.

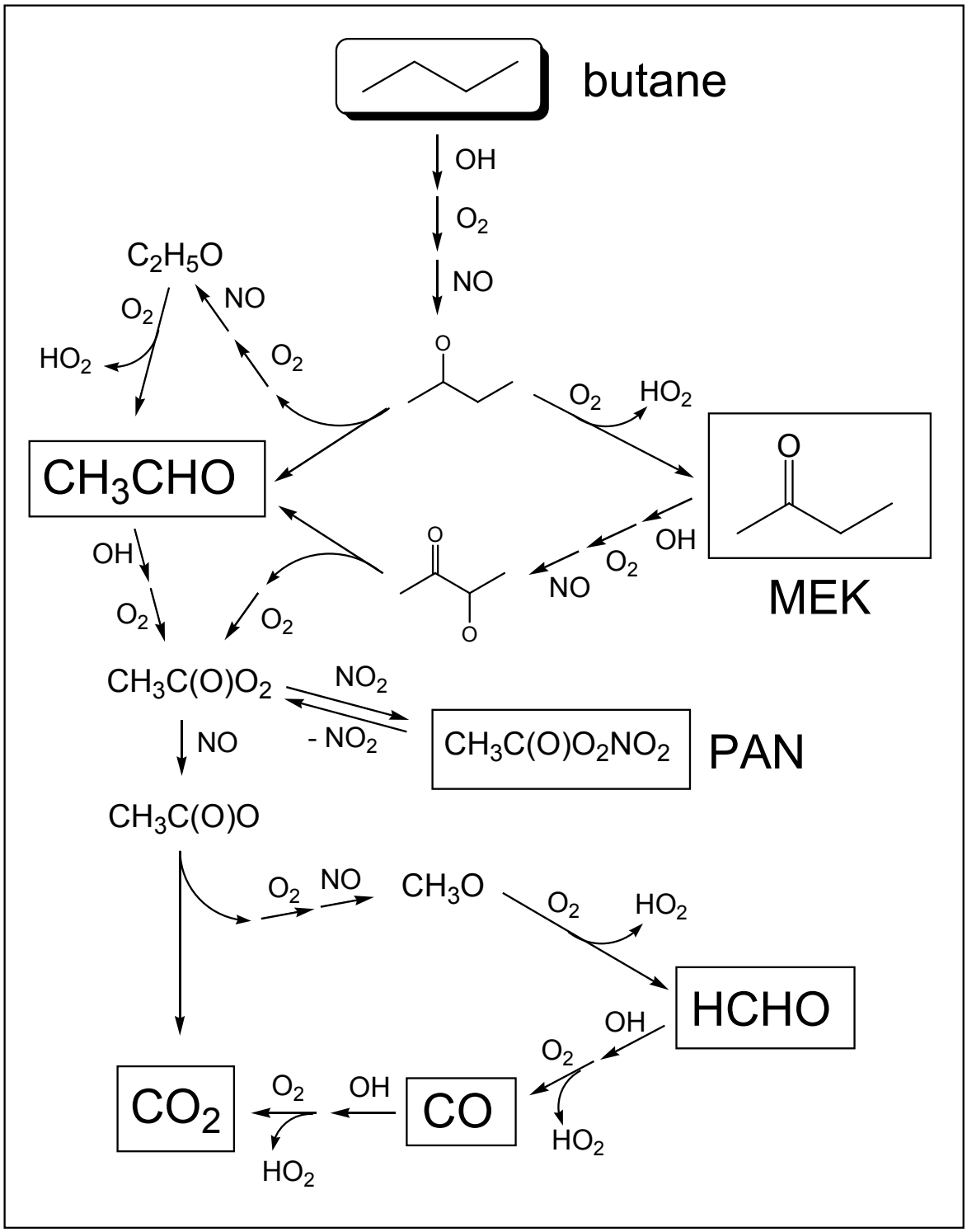

Figure 3: Schematic representation of the major radical propagation pathways of the OH-initiated degradation of butane, also illustrating the sequential formation of the intermediate products MEK, CH_3CHO, HCHO and CO. Reaction steps involving NO are reactions with organic peroxy radical intermediates, which lead to NO-to-NO_2 conversion and O_3 production (see discussion in text). The reactions of OH with butane and MEK possess additional channels which are fully represented in the mechanism, but not shown in the diagram (Figure from Pinho *et al.,* 2005).

This figure shows the complete oxidation of butane to CO and CO_2 proceeding via the formation of the major intermediate carbonyl compounds, MEK, CH_3CHO and HCHO. At each oxidation stage, the chemistry is propagated by reactions of peroxy (RO_2) and oxy (RO) radical intermediates. For example, the initial oxidation of butane (C_4H_{10}) to MEK ($CH_3C(O)C_2H_5$) proceeds via the following catalytic cycle:

$$OH + C_4H_{10} (+O_2) \rightarrow sec\text{-}C_4H_9O_2 + H_2O \quad (6)$$

$$sec\text{-}C_4H_9O_2 + NO \rightarrow sec\text{-}C_4H_9O + NO_2 \quad (7)$$

$$sec\text{-}C_4H_9O + O_2 \rightarrow CH_3C(O)C_2H_5 + HO_2 \quad (8)$$

$$HO_2 + NO \rightarrow OH + NO_2 \quad (4)$$

The peroxy radicals (*sec*-$C_4H_9O_2$ and HO_2) thus provide the coupling with the chemistry of NO_X, which leads to NO-to-NO_2 conversion, and formation of O_3 upon photolysis of NO_2, reaction (1) and (2).

This basic pattern is repeated throughout the degradation mechanisms of organic compounds, and demonstrates how VOC, NO_X and sunlight are able to generate O_3 under tropospheric conditions, through the reactions of peroxy radicals with NO. The subsequently-formed oxy radicals determine the identity or identities of the carbonyl products generated from the degradation. In the case of *sec*-C_4H_9O, the reaction with O_2 forming MEK and HO_2 (reaction (8)) occurs in competition with thermal decomposition, which leads to the ultimate formation of HO_2 and two molecules of CH_3CHO (see Figure 3).

As shown in Figure 3, the further degradation of MEK, CH_3CHO and HCHO, initiated by reaction with OH, leads to further NO-to-NO_2 conversion (and therefore O_3 formation). Consequently, the number of NO-to-NO_2 conversions at each oxidation step, and the lifetimes of butane and the product carbonyl compounds (which are partially determined by their OH reactivity) have an important influence on the rate of NO oxidation and O_3 formation.

However, other factors may also contribute. Reactions (6)-(8), reaction (4), and the reactions illustrated in Figure 3, are all radical propagation reactions which conserve the radical population in the system. The organic degradation chemistry can also influence oxidation rates, and therefore O_3 formation, through either producing or removing radicals. The photolysis of carbonyl compounds is a potential source of free radicals, which may have an important influence in some systems. Of relevance to butane oxidation is the photolysis of MEK, CH_3CHO and HCHO, for which the following radical-forming photolysis channels are represented in MCM v3.1:

$$CH_3C(O)C_2H_5 + h\upsilon (+2O_2) \rightarrow CH_3C(O)O_2 + C_2H_5O_2 \quad (9)$$

$$CH_3CHO + h\upsilon\ (+2O_2) \rightarrow CH_3O_2 + CO + HO_2 \quad (10)$$

$$HCHO + h\upsilon\ (+2O_2) \rightarrow CO + HO_2 + HO_2 \quad (11)$$

In addition, photolysis reactions are generally included for products containing nitrate, hydroperoxide and peracid functionalities, as described by Jenkin *et al.* (1997) and Saunders *et al.* (2003).

At the typical concentrations of NO_X in chamber experiments, the most significant radical removal reactions of organic species tend to involve the reactions of intermediate peroxy radicals with either NO or NO_2. For example, the reaction of *sec*-$C_4H_9O_2$ with NO has a minor (9%), but significant terminating channel generating *sec*-$C_4H_9ONO_2$,

$$sec\text{-}C_4H_9O_2 + NO \rightarrow sec\text{-}C_4H_9ONO_2 \quad (12)$$

and similar nitrate-forming channels exist for most peroxy radicals. The reactions with NO_2 tend to be most significant for acyl peroxy radicals, leading to the formation of peroxyacyl nitrates. In the case of butane degradation, the acetyl peroxy radical ($CH_3C(O)O_2$) is formed from both MEK and CH_3CHO, and the reversible formation of PAN ($CH_3C(O)OONO_2$) from its reaction with NO_2 leads temporary loss of free radicals:

$$CH_3C(O)O_2 + NO_2 \leftrightarrows CH_3C(O)OONO_2 \quad (13)$$

As described in detail elsewhere (Jenkin *et al.,* 1997, Jenkin *et al.,* 2003 and Saunders *et al.,* 2003), MCM v3.1 incorporates all the above types of process explicitly, in addition to competitive reactions which gain in significance at lower concentrations of NO_X.

5.4.1.1 HCHO-NO_X experiments

The MCM v3.1 mechanism was found to under-predict $D(O_3\text{-NO})$ in many (but not all) of the runs, principally for the CTC and DTC chambers. This discrepancy was improved through the implementation of revised absorption cross section and quantum yield data for the photolysis of HCHO. The photolysis parameters were updated in line the latest IUPAC recommendations (Data Sheet P1 updated in 16th May 2002), the preferred cross sections being based on the data of Meller and Moortgat (2000), and the quantum yields based on data from Smith *et al.* (2002). The new cross sections are 5-10% higher than the values previously recommended by IUPAC (and adopted for the MCM by Jenkin *et al.,* 1997). The improved performance of the modified mechanism, MCM v3.1a, in simulating the HCHO-NO_X chamber experiments is summarised in Figure 4 and Figure 5. The improvement is particularly apparent for the large set of CTC and DTC chambers runs, which represent the majority of the dataset for HCHO.

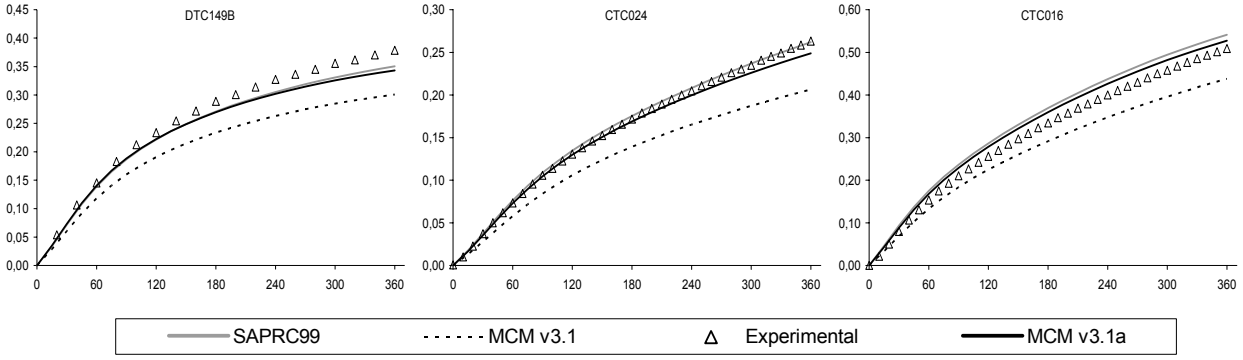

Figure 4: Plots of experimental and calculated D(O_3-NO) (ppm) vs. time (min) for the HCHO – NO_x -air experiments.

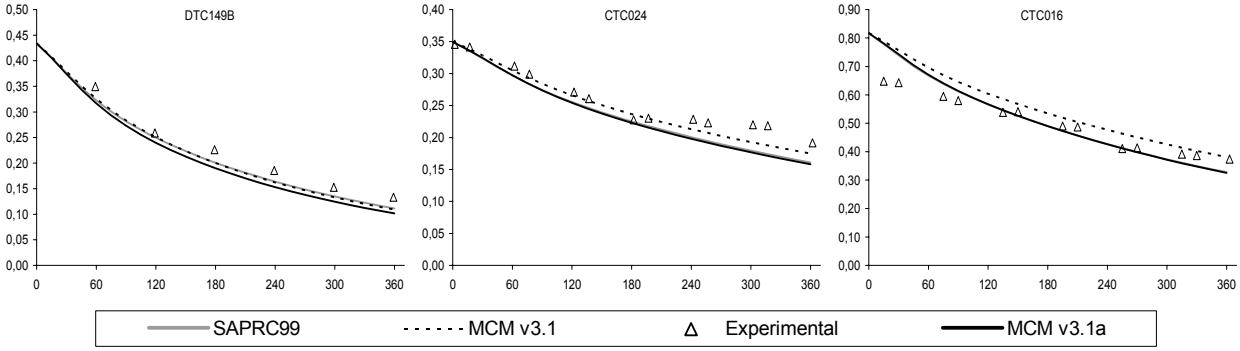

Figure 5: Plots of experimental and calculated HCHO (ppm) vs. time (min) for the HCHO – NO_x -air experiments.

5.4.1.2 CH_3CHO-NO_X experiments

Apart from a small secondary influence of the changes in the HCHO photolysis parameters, no further modifications were required to the acetaldehyde mechanism. As shown in Figure 6 to Figure 9, MCM v3.1 and MCM v3.1a provides a very good description of D(O_3-NO) in the complete set of CH_3CHO-NO_X chamber experiments.

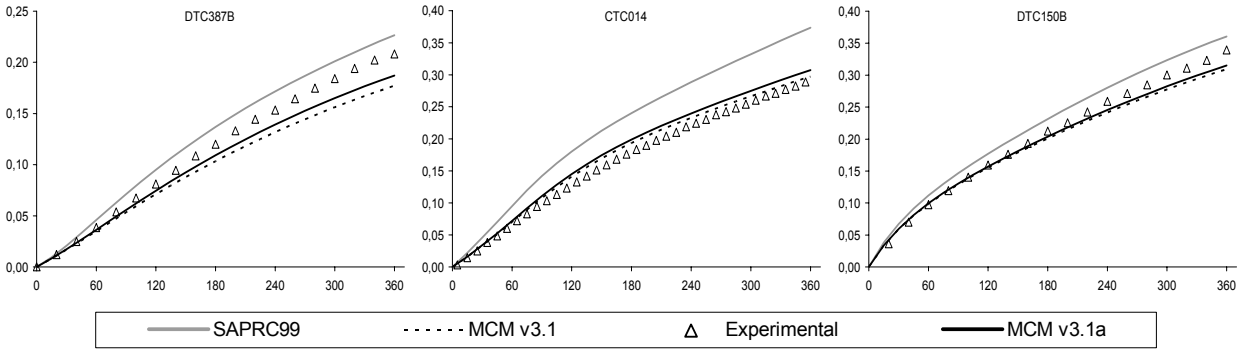

Figure 6: Plots of experimental and calculated D(O_3-NO) (ppm) vs. time (min) for the CH_3CHO – NO_x –air experiments.

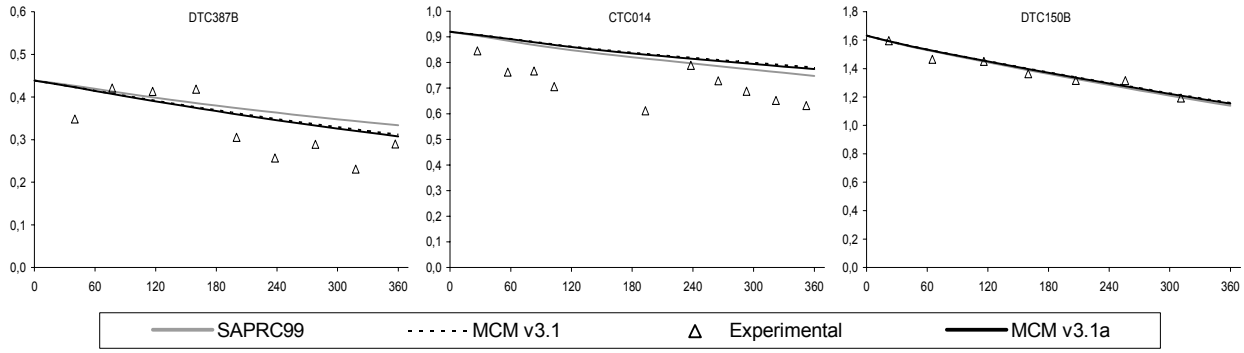

Figure 7: Plots of experimental and calculated CH_3CHO (ppm) vs. time (min) for the CH_3CHO – NO_x –air experiments.

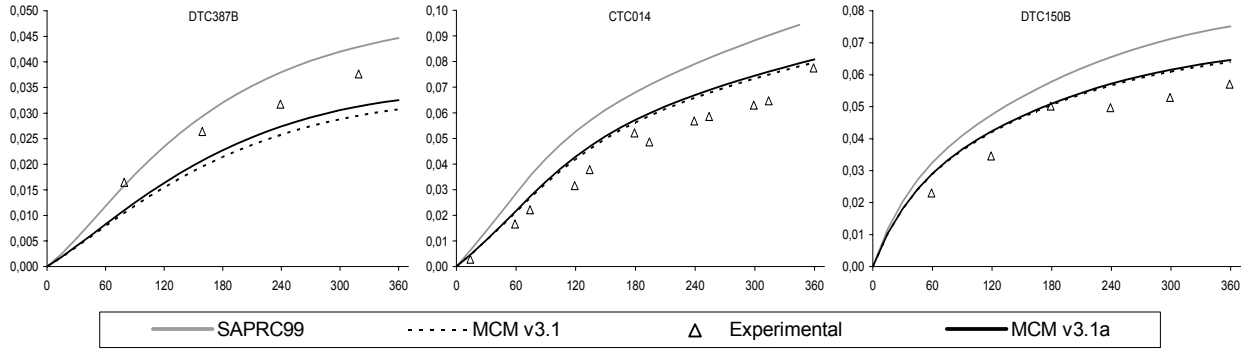

Figure 8: Plots of experimental and calculated HCHO (ppm) vs. time (min) for the CH_3CHO – NO_x –air experiments.

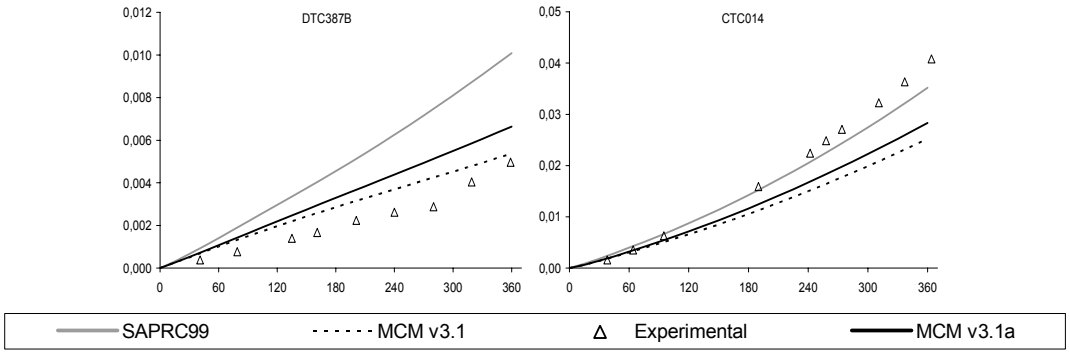

Figure 9: Plots of experimental and calculated PAN (ppm) vs. time (min) for the CH_3CHO – NO_x –air experiments.

5.4.1.3 MEK-NO_X experiments

The MCM v3.1 mechanism was found to over-predict D(O_3-NO) in many of the chamber runs, particularly in the early stages of the experiment. This discrepancy was improved by reducing the quantum yield for the photolysis of MEK (reaction (9)). In MCM v3.1, a wavelength-independent value of 0.34 is applied, based on the atmospheric pressure data from Raber and Moortgat (1996). That study demonstrated that the quantum yield decreases with increasing pressure, but also quoted increasingly wide uncertainty limits on the quantum yield at pressures approaching one atmosphere. The value was therefore optimized within MCM v3.1a, to give the best fit to the MEK-NO_X chamber data (see Figure 10 to Figure 14). This led to a best fit value of 0.17, which is close to the extremity of the uncertainty limit of the determination of Raber and Moortgat (1996). This value is also consistent with the value of 0.15 obtained by Carter (2000) during evaluation and optimization of the SAPRC-99 mechanism.

It was noted, however, that MCM v3.1a systematically overestimates the formation of HCHO in the system (Figure 12), even though it performs adequately in relation to the other criteria. In view of the good description of CH_3CHO formation (Figure 13), it can be inferred that the formation of HCHO from the MEK oxidation pathway illustrated in Figure 3 is well represented. The excess formation of HCHO must therefore derive from attack of OH at the terminal carbon in the C_2H_5-group, which also makes a significant contribution to the overall reaction in MCM v3.1:

$$CH_3C(O)C_2H_5 + OH\ (+O_2) \rightarrow CH_3C(O)CH_2CH_2O_2 \qquad (14)$$

The subsequent NO-propagated reaction sequence mainly generates a complex α-carbonyl oxy radical, which is assumed to decompose on the basis of a generic rule in the MCM protocol (Jenkin *et al.,* 1997):

$$HOCH_2CH_2C(O)CH_2O \rightarrow HCHO + HOCH_2CH_2CO \qquad (15)$$

This generates HCHO both directly, and through the subsequent chemistry of the $HOCH_2CH_2CO$ radical. Because of the activating influence of the δ-hydroxy group, however, it is probable that the 1,5 H shift isomerisation reaction (16), not producing HCHO, can compete with reaction (15) (e.g., Atkinson, 1997a):

$$HOCH_2CH_2C(O)CH_2O \rightarrow HOCH_2C(O)CH_2CHOH \qquad (16)$$

$$HOCH_2C(O)CH_2CHOH + O_2 \rightarrow HOCH_2C(O)CH_2CHO + HO_2 \qquad (17)$$

Additional simulations including reaction (16) (and a provisional representation of the subsequent chemistry) indicated that the production of HCHO in Figure 12 could be well described if reaction (16) accounts for *ca*. 70% of the fate of the oxy radical, but with this change having no major

influence on any of the other profiles in Figure 10, Figure 11 and Figure 13. As a result, it was decided that the MCM v3.1a MEK mechanism optimised as described above could reasonably be applied in the remainder of this evaluation. Furthermore, it is suggested that the generic MCM rule regarding the exclusive decomposition of α-carbonyl oxy radicals may be inappropriate in some cases.

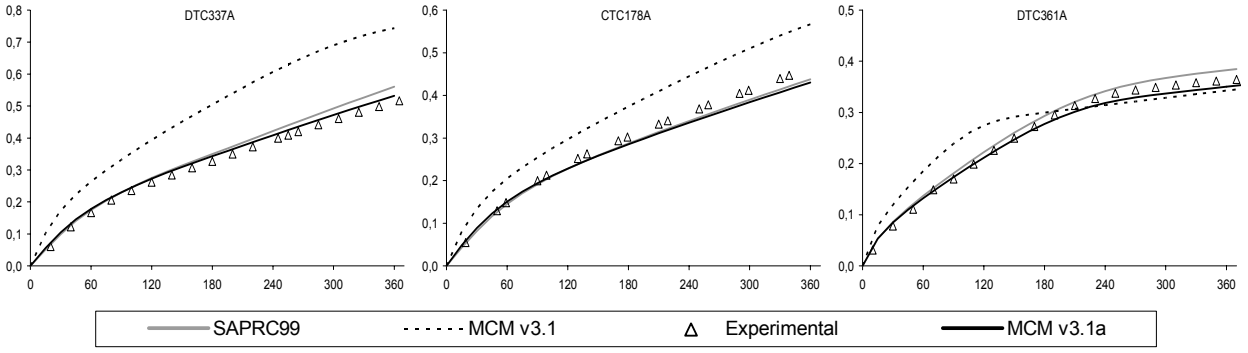

Figure 10: Plots of experimental and calculated D(O_3-NO) (ppm) vs. time (min) for the MEK – NO_x –air experiments.

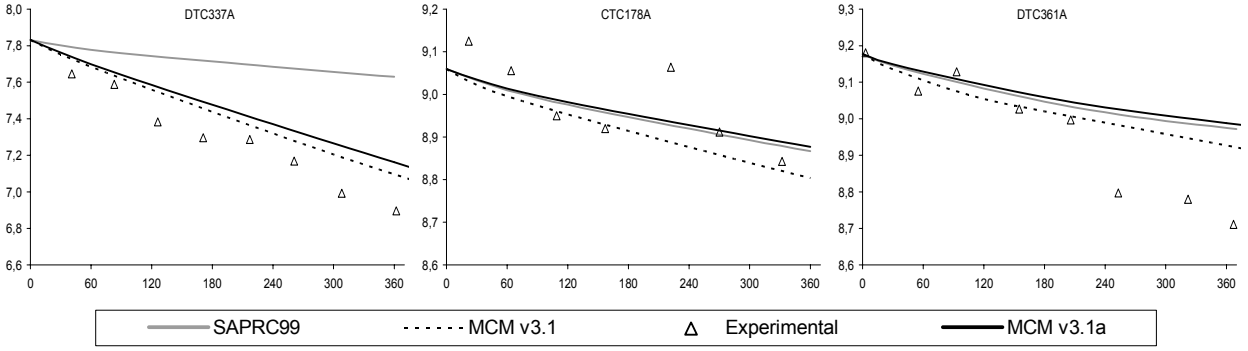

Figure 11: Plots of experimental and calculated MEK (ppm) vs. time (min) for the MEK – NO_x –air experiments.

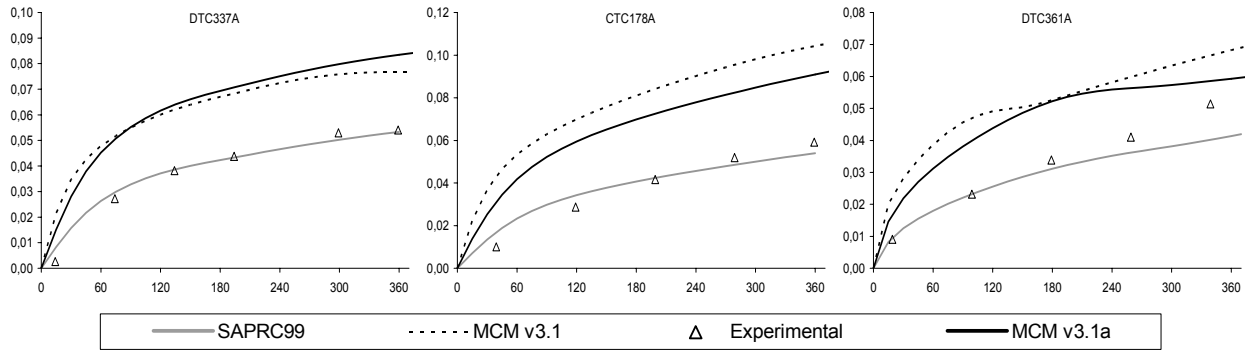

Figure 12: Plots of experimental and calculated HCHO (ppm) vs. time (min) for the MEK – NO_x –air experiments.

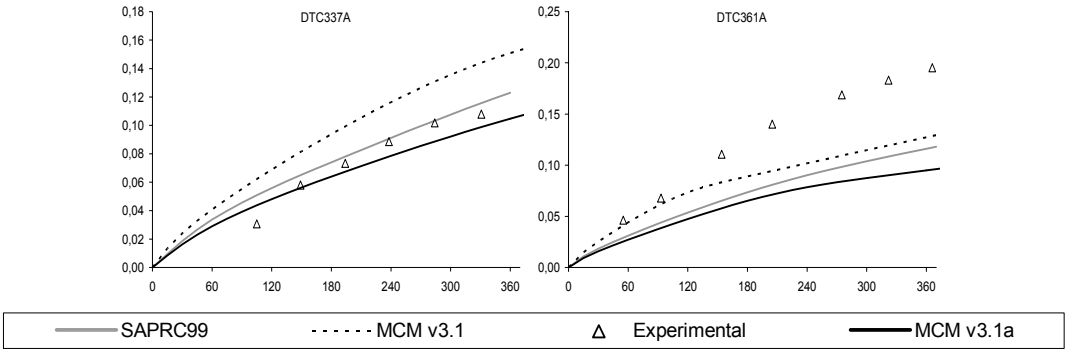

Figure 13: Plots of experimental and calculated CH_3CHO (ppm) vs. time (min) for the MEK – NO_x –air experiments.

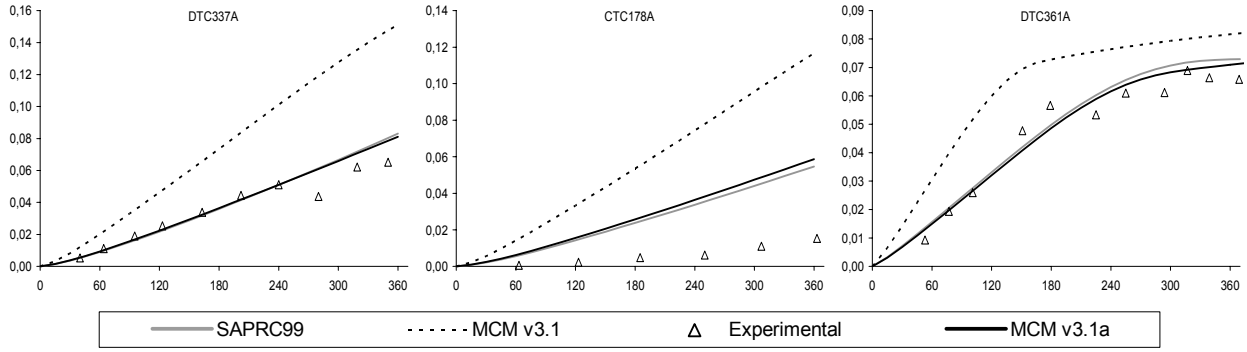

Figure 14: Plots of experimental and calculated PAN (ppm) vs. time (min) for the MEK – NO_x –air experiments. The experimental PAN data in the CTC chamber runs appear anomalous and are not well described by either MCM or SAPRC-99.

5.4.1.4 Butane-NO_X experiments

Because there is no primary radical source during butane photo-oxidation, this parent system was the most sensitive to changes in the chamber radical source parameter. In conjunction with the optimizations described above, it was found that the best fit to the butane-NO_X photo-oxidation data was obtained by multiplying the Carter chamber radical source values used in the SAPRC evaluation (Carter, 2000) by a factor of 1.35 for the ITC chamber, and by a factor of 1.2 for the DTC, CTC and XTC chambers, (see Table 2). The few butane-NO_X experiments performed in the ETC chamber appear to be anomalous (Carter, 2000), so the chamber radical source scaling factor for this chamber was subsequently assumed to be the same as that derived for ITC in the evaluations of other VOC.

With these changes, the adapted MCM v3.1a butane mechanism was found to give generally good fits to D(O_3-NO) data in the complete series of butane–NO_X photo-oxidation experiments. The scatter in the results was indicative of run-to-run variability, with most of the data being fit by the mechanism to within +/- 30%, with no consistent biases. Examples of D(O_3-NO), butane decay rate and formation of CH_3CHO and MEK are presented in Figure 15 to Figure 18.

As indicated above, the butane, HCHO, CH_3CHO and MEK systems were considered iteratively, such that the optimized chamber radical sources and the changes made to the photolysis parameters for HCHO and MEK led to a self-consistent description of all the systems. The auxiliary mechanism presented in Table 2, with the chamber radical sources adjusted as indicated above, was therefore believed to provide an acceptable basis for evaluation of the other VOC degradation mechanisms.

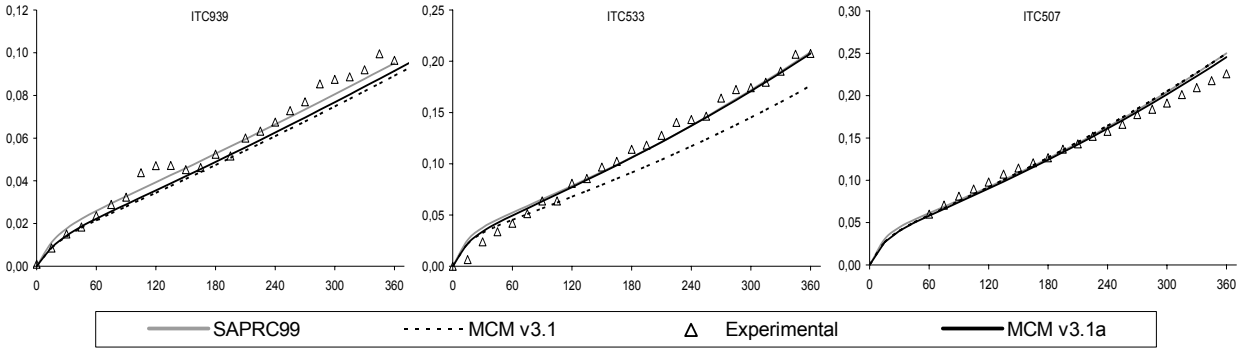

Figure 15: Plots of experimental and calculated $D(O_3\text{-NO})$ (ppm) vs. time (min) for the butane – NO_x -air experiments.

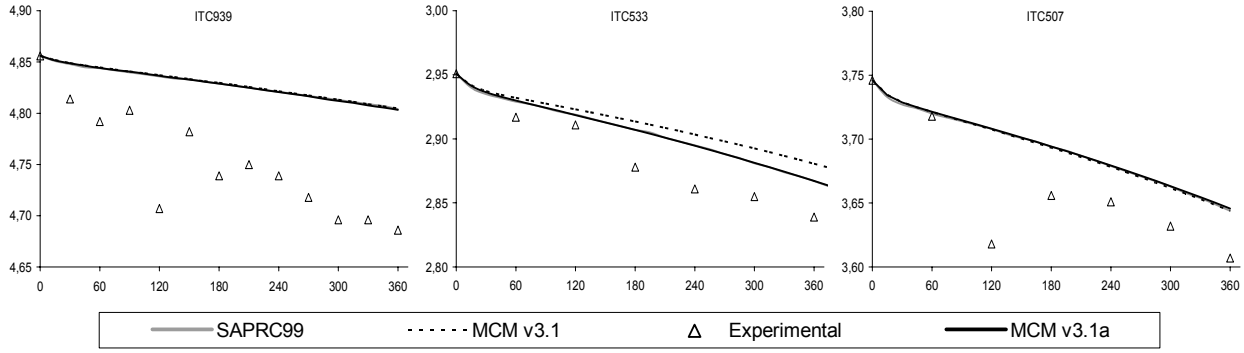

Figure 16: Plots of experimental and calculated butane (ppm) vs. time (min) for the butane – NO_x -air experiments.

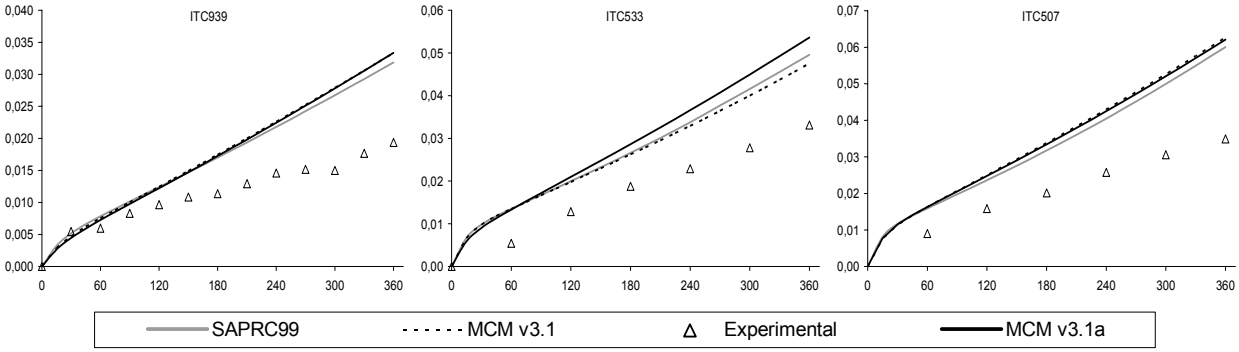

Figure 17: Plots of experimental and calculated CH_3CHO (ppm) vs. time (min) for the butane – NO_x -air experiments.

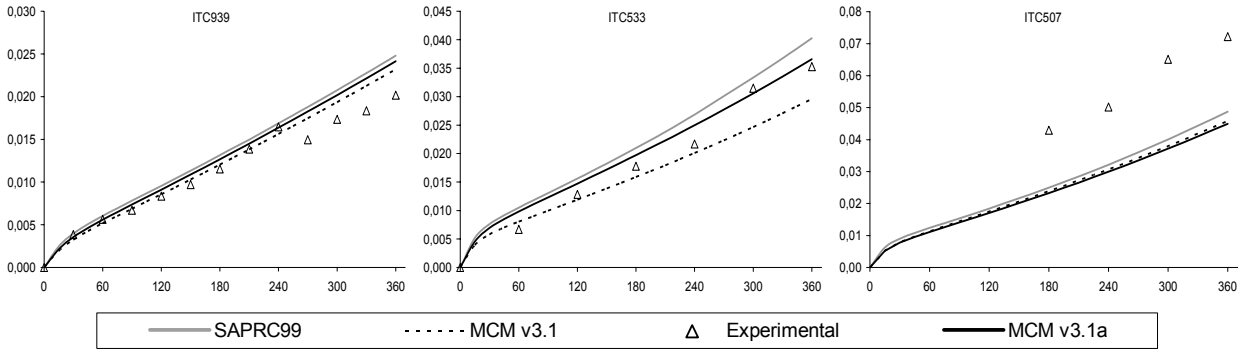

Figure 18: Plots of experimental and calculated MEK (ppm) vs. time (min) for the butane – NO_x -air experiments.

5.5 Alkanes Photo-oxidation Mechanism Assessment

There is a large number of single VOC-NO_x-Air runs for n-butane in the SAPRC database that, as described in above section, were used for mechanism evaluation.

However, only 2 runs of n-heptane and 4 runs of n-octane exist, which represent the complete database for monoalkanes for which VOC-NO_x-Air are available.

MCM v3.1 was found to under-predict significantly the observed D(O_3-NO) in both systems. Some sensitivity tests were made to verify if some refinements in MCM v3.1 degradation mechanism of n-heptane and n-octane could improve the MCM v3.1 prediction.

Sensitivity test to alkyl nitrates and hydroxyalkyl nitrates yield in the reactions of peroxy or hydroperoxy radicals with NO were made. The main factor that needs to be determined when generating reactions of peroxy or hydroperoxy radicals with NO is the branching ratio between formation of NO_2 and the corresponding alkoxy radical, or addition and rearrangement forming the organic nitrate, e.g:

$$RO_2\cdot + NO \rightarrow RO\cdot + NO_2 \quad (18)$$

$$RO_2\cdot + NO + M \rightarrow RONO_2 + M \quad (19)$$

The rate constant ratio $k_{19}/(k_{18}+k_{19})$, defined as nitrate yield or hydroxynitrate yield, is a potentially important factor affecting a VOC's atmospheric impact because nitrate formation (reaction (19)) is a radical termination process and can significantly remove NO_x, and therefore inhibit O_3 formation and parent alkane decay, if it is sufficiently important compared to propagation (reaction (18)).

When the alkanes degradation mechanisms, used in MCM v3.1, were written, contemporary knowledge was consistent with large yields of alkyl nitrates and hydroxyalkyl nitrates. In the case of heptane, the MCM v3.1 considers a nitrate yield and hydroxynitrate yield of 27.8% and 11.1%; for n-octane the considered values are 34.6% and 13.8% respectively.

In 2001 Arey *et al.* remeasured yields in C_5-C_8 alkane systems and came to the conclusion that they should be substantially lower than previous predictions. For heptane the revised yields are 17.8% and 5.7%, respectively for alkyl nitrates; hydroxyalkyl nitrates and for octane the revised yields are 22.6% and 7.0% respectively.

The only two chamber runs of n-heptane-NO_x-Air are high NO_x limited and very sensitive to the nitrate and hydroxynitrate yield in the reactions of peroxy or hydroperoxy radicals with NO. As can be seen in Figure 19, considering the Arey *et al.* (2001) proposed values for nitrate and hydroxynitrate yields in the reactions of peroxy or hydroperoxy radicals with NO isn't enough to fit the experimental data. The scaling factors from the two experiments are not consistent, although the shape of the O_3 plot in run 540 is unusual and therefore may be erroneous in some way.

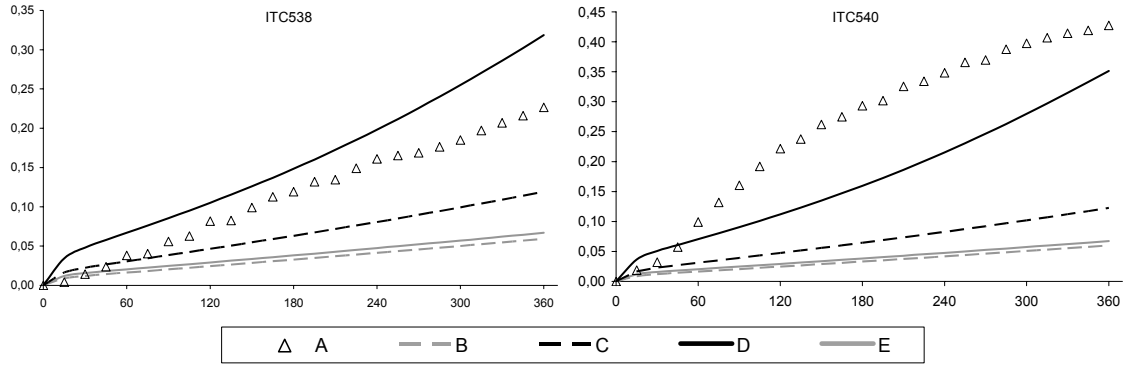

Figure 19: Plots of experimental and calculated D(O_3-NO) (ppm) vs. time (min) for the n-heptane – NO_x –air experiments: A – experimental data; B - MCM v3.1a; C - MCM v3.1a with the nitrate and hydroxynitrate yield of 17.8% and 5.7% based in Arey *et al.* (2001); D - MCM v3.1a with the nitrate and hydroxynitrate yield of 8.9% and 2.85% (see discussion in text); E - SAPRC99. ITC538-VOC/NO_x=87; ITC540-VOC/NO_x=371.

Relatively to the n-octane degradation mechanism, it can be seen in Figure 20 and Figure 21 that, like for n-heptane, considering the Arey *et al.* (2001) proposed values for nitrate and hydroxynitrate yield only have a corrective but insufficient small effect.

The 2 n-octane-NOx-Air runs designated by ITC552 and ITC762 are high NO_x limited and, like in the n-heptane case, very sensitive to the nitrate and hydroxynitrate yield. Consideration of a value equal to 35% of Arey *et al.* (2001) estimatives allow to fit the experimental data, (see Figure 20). For the other existing 2 runs, designated by ITC763 and ITC797, only the consideration of a zero nitrate and hydroxynitrate yield could approximate the modelled and the experimental values.

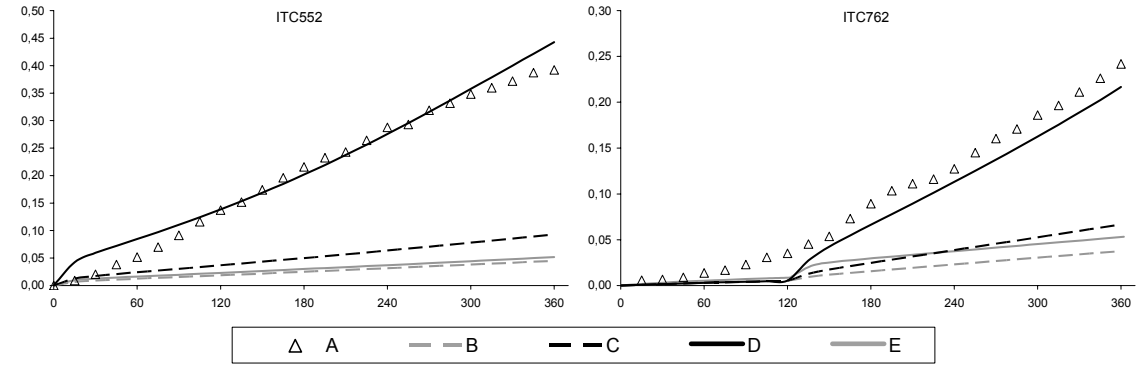

Figure 20: Plots of experimental and calculated D(O_3-NO) (ppm) vs. time (min) for the n-octane – NO_x –air experiments: A – experimental data; B - MCM v3.1a; C - MCM v3.1a with the nitrate and hydroxynitrate yield of 22.6% and 7.0% based in Arey *et al.* (2001); D - MCM v3.1a with the nitrate and hydroxynitrate yield of 7.9% and 2.5% (see discussion in text); E - SAPRC99. ITC552-VOC/NO_x=476; ITC762-VOC/NO_x=35.

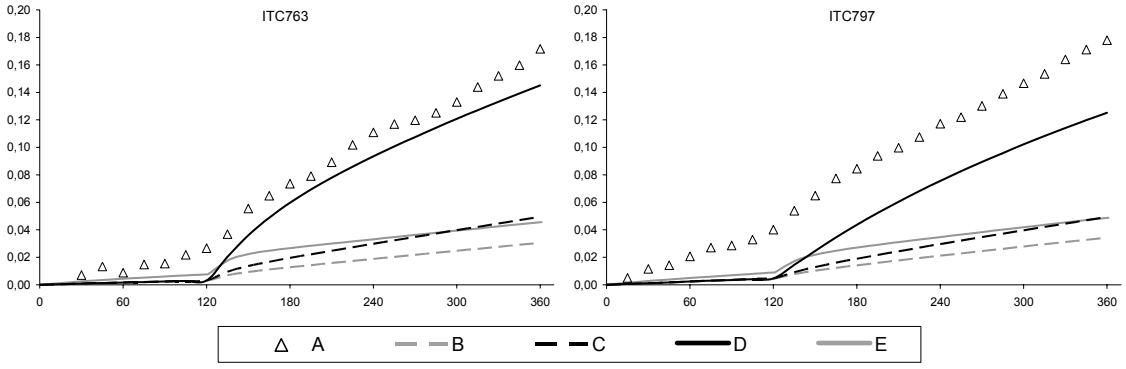

Figure 21: Plots of experimental and calculated D(O_3-NO) (ppm) vs. time (min) for the n-octane – NO_x –air experiments: A – experimental data; B - MCM v3.1a; C - MCM v3.1a with the nitrate and hydroxynitrate yield of 22.6% and 7.0% based in Arey *et al.* (2001); D - MCM v3.1a with the nitrate and hydroxynitrate yield of 0% (see discussion in text); E - SAPRC99. ITC763-VOC/NO_x=3.5; ITC797-VOC/NO_x=1.8.

Another sensitivity test made was related with production of the hydroxycarbonyl product $CH_2CH(OH)CH_2CH_2CH_2CH_2CHO$ from n-heptane degradation. Work from Martin *et al.* (2002) shows evidence for isomerisation and dehydration of such products to form dihydrofuran compounds. Again, the system is very sensitivity to any scheme that changes the radical balance. Besides, as already concluded by Carter and Lurman (1990), it was verified that the runs of n-heptane-NOx-Air and n-octane-NOx-Air in database have large sensitivity to the chamber radical source.

Because of theis extreme sensitivity to radical sources and the fact of the database only having few runs it was decided not to use these runs for mechanism evaluation. A large number of environmental chamber experiments should be carried out, using better chamber characterisation, to allow evaluation of alkane degradation schemes.

5.6 Alkenes Photo-oxidation Mechanism Assessment

Simple alkenes (i.e., excluding dialkenes and terpenes) are typically estimated to account for ca. 7-8 % of anthropogenic non-methane VOC emissions (e.g., Calvert *et al.,* 2000; Goodwin *et al.,* 2001), and being also emitted from biogenic sources (e.g., Klemp *et al.,* 1997). However, their propensity to form O_3 is reported to be disproportionately greater than implied by the fractional emissions contribution, owing to their general high reactivity, as reflected in published scales of photochemical ozone creation potentials (e.g., Derwent *et al.,* 2001; Saunders *et al.,* 2003) and incremental reactivities (e.g. Carter, 1994). Consequently, the oxidation of alkenes is believed to make a major contribution to O_3 formation on local and regional scales, and their degradation is therefore always represented in chemical mechanisms used in urban or regional air-shed models currently applied for research or regulatory purposes.

The representation of alkene degradation has been evaluated in this section, using environmental chamber data on the photo-oxidation of ethene, propene, 1-butene and 1-hexene, which represent the complete database for monoalkenes (excluding α– and β–pinene) for which multiple runs are available.

The set of chamber experimental runs employed in the present evaluation consisted of an extensive database of 31 ethene-NO_X-air and 129 propene-NO_X-air experiments; and a much more limited database of four 1-butene-NO_X-air and four 1-hexene-NO_X-air experiments, carried out in a single chamber (ITC). The range of reagent concentrations relative humidity and NO_2 photolysis constants (k_1) for the considered experiments is presented in Table 4.

5.6.1 Chemistry of alkenes photo-oxidation

The complete degradation chemistry, as represented in MCM v3.1, consists of: 96 reactions of 41 species for ethene; 149 reactions of 61 species for propene; 258 reactions of 97 species for 1-butene and 768 reactions of 256 species for 1-hexene. It can be viewed and downloaded using the subset mechanism assembling facility, available as part of the MCM website. The methodology of mechanism construction has been described in detail by Jenkin *et al.* (1997) and Saunders *et al.* (2003), with chemistry initiated by reaction with OH, O_3 and NO_3 represented for each alkene. Salient features of the OH and O_3-initiated chemistry are summarized below. For the photo-oxidation conditions considered here, the systems are insensitive to the NO_3-initiated chemistry which is therefore not discussed further.

The main features of the OH-initiated degradation chemistry when NO_X is present are summarized in Figure 22.

Table 4: Ranges of reagent concentrations, relative humidity and NO_2 photolysis constants (k_1) for the considered experiments.

Ethene-NOx	Total	CTC	XTC	DTC	ITC	ETC
n.º of available runs	31	-	2	10	3	16
[VOC] (ppm)	0.61-4.04	-	1.91-2.74	1.69-1.89	1.94-3.94	0.61-4.04
[NOx] (ppm)	0.16-0.66	-	0.24-0.52	0.16-0.48	0.45-0.53	0.38-0.66
[VOC]/[NOx]	1.20-11.65	-	5.29-7.95	3.62-11.65	3.75-7.44	1.20-7.86
K_1 (min^{-1})	0.194-0.388		0.246-0.248	0.388[(a)]	0.351	0.351
Relative humidity [(b)]			dry	wet	dry	dry
Propene-NOx						
n.º of available runs	129	36	4	67	18	4
[VOC] (ppm)	0.46-1.63	0.85-1.63	1.1-1.25	0.52-1.30	0.46-1.07	0.90-1.16
[NOx] (ppm)	0.10-0.61	0.42-0.54	0.53-0.56	0.10-0.61	0.45-0.59	0.25-0.60
[VOC]/[NOx]	1.01-5.02	2.04-3.30	2.04-2.32	1.11-5.02	1.01-2.23	1.95-3.64
K_1 (min^{-1})	0.133-0.530	0.133-0.257	0.246-0.251	0.164-0.388	0.351-0.530	0.351-0.388
Relative humidity [(b)]		dry	dry	7 wet; 60 dry	wet	dry
1-Butene-NOx						
n.º of available runs	4	-	-	-	4	-
[VOC] (ppm)	1.06-2.86	-	-	-	1.06-2.86	-
[NOx] (ppm)	0.53-1.09	-	-	-	0.53-1.09	-
[VOC]/[NOx]	1.05-5.31	-	-	-	1.05-5.31	-
k_1 (min^{-1})	0.351				0.351	
Relative humidity [(b)]					wet	
1-Hexene-NOx						
n.º of available runs	4	-	-	-	4	-
[VOC] (ppm)	0.84-1.71	-	-	-	0.84-1.71	-
[NOx] (ppm)	0.51-1.08	-	-	-	0.51-1.08	-
[VOC]/[NOx]	0.87-3.33	-	-	-	0.87-3.33	-
K_1 (min^{-1})	0.351				0.351	
Relative humidity [(b)]					wet	

Notes

(a) One run with $k_6 = 0.194$ min^{-1}.

(b) 'Wet' indicates a relative humidity of ca. 50 %. 'Dry' indicates a relative humidity of < 5 %, typically in the range 2.5 % – 3 %.

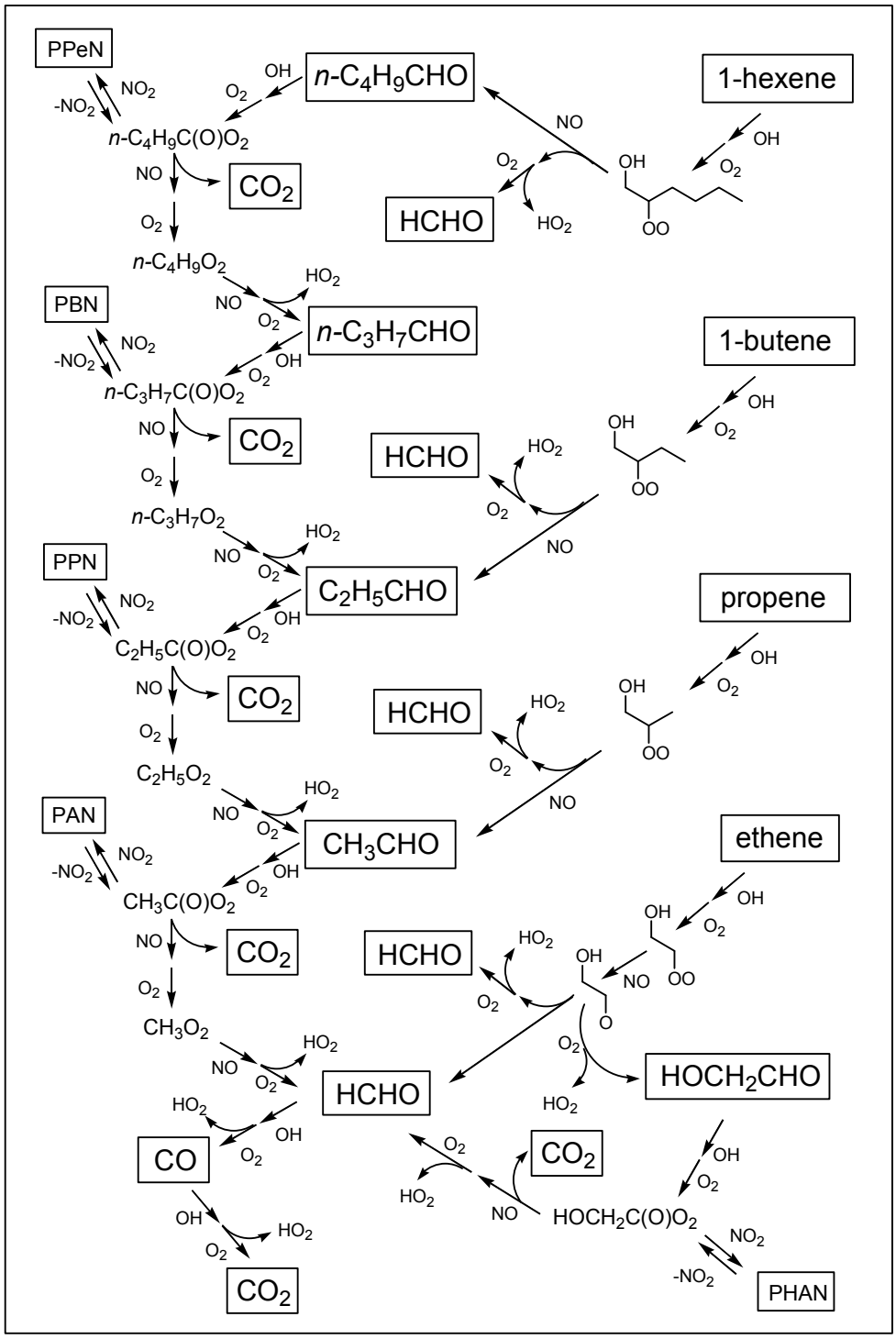

Figure 22: Partial schematic of the MCM representation of the major radical propagation pathways during the OH-initiated degradation of ethene, propene, 1-butene and 1-hexene to CO_2. Reactions of NO with organic peroxy radical intermediates, lead to NO-to-NO_2 conversion and O_3 production (see discussion in text). The reactions of OH with propene, 1-butene, 1-hexene, $HOCH_2CHO$ and *n*-C_4H_9CHO possess additional channels which are fully represented in the mechanism, but not shown in the diagram. (Figure from Pinho *et al.,* 2006)

This figure presents the initial oxidation sequence of the given alkene, $RCH{=}CH_2$ (where R = H, CH_3, C_2H_5 or *n*-C_4H_9), proceeds by addition of OH, leading predominantly to the formation of the aldehydes HCHO and RCHO, with subsequent oxidation leading ultimately to the formation of CO and CO_2. At each oxidation stage, the chemistry is propagated by reactions of peroxy (RO_2) and oxy (RO) radical intermediates. For example, the initial generic oxidation sequence proceeds via the following catalytic cycle:

$$OH + RCH{=}CH_2\ (+O_2) \rightarrow RCH(O_2)CH_2OH \quad \text{(major)} \tag{20}$$

$$\rightarrow RCH(OH)CH_2O_2 \quad \text{(minor)} \tag{21}$$

$$RCH(O_2)CH_2OH + NO \rightarrow RCH(O)CH_2OH + NO_2 \tag{22}$$

$$RCH(O)CH_2OH \rightarrow RCHO + CH_2OH \tag{23}$$

$$CH_2OH + O_2 \rightarrow HCHO + HO_2 \tag{24}$$

$$RCH(OH)CH_2O_2 + NO \rightarrow RCH(OH)CH_2O + NO_2 \tag{25}$$

$$RCH(OH)CH_2O \rightarrow RCHOH + HCHO \tag{26}$$

$$RCHOH + O_2 \rightarrow RCHO + HO_2 \tag{27}$$

$$HO_2 + NO \rightarrow OH + NO_2 \tag{4}$$

The peroxy radicals ($RCH(O_2)CH_2OH$, $RCH(OH)CH_2O_2$ and HO_2) thus provide the coupling with the chemistry of NO_X, which leads to NO-to-NO_2 conversion, and formation of O_3 upon photolysis of NO_2, reactions (1) and (2).

The subsequently-formed oxy radicals determine the identity or identities of the carbonyl products generated from the degradation. In MCM v3.1, thermal decomposition of $RCH(O)CH_2OH$ and $RCH(OH)CH_2O$ via reactions (23) and (26) is assumed to be the exclusive fate for the larger radicals (R = CH_3, C_2H_5 and *n*-C_4H_9). This is consistent with reported experimental studies, although there is evidence that 1,5 H-shift isomerization may be significant in the case of R = *n*-C_4H_9 (Atkinson *et al.,* 1995; Calvert *et al.,* 2000). Decomposition is also the major fate for $HOCH_2CH_2O$, formed from ethene degradation, but competitive reaction with O_2 (to form $HOCH_2CHO$ and HO_2) is also represented (accounting for 22% of its loss at 298 K in 760 Torr air), in accordance with the results of Niki *et al.* (1981) and Barnes *et al.* (1993).

As shown in Figure 22, the further degradation of the larger aldehydes (RCHO), initiated by reaction with OH, leads to further NO-to-NO_2 conversion (and therefore O_3 formation). Consequently, the number of NO-to-NO_2 conversions at each oxidation step, and the lifetimes of the parent alkene and its product aldehydes (which are partially determined by their OH reactivity) have an important influence on the rate of NO oxidation and O_3 formation.

However, other factors may also contribute. Reactions (20)-(27), reaction (4), and the reactions illustrated in Figure 22, are all radical propagation reactions which conserve the radical population in the system. The organic degradation chemistry can also influence oxidation rates, and therefore O_3 formation, through either producing or removing radicals. The photolysis of carbonyl compounds is a potential source of free radicals, which may have an important influence in some systems. Of relevance to the current systems is the photolysis of RCHO (R = CH_3, C_2H_5 and *n*-C_4H_9) and HCHO, for which the following radical-forming photolysis channels are represented in MCM v3.1:

$$RCHO + h\upsilon\ (+2O_2) \rightarrow CO + RO_2 + HO_2 \quad (28)$$

$$HCHO + h\upsilon\ (+2O_2) \rightarrow CO + HO_2 + HO_2 \quad (11)$$

The photolysis parameters assigned to HCHO and CH_3CHO have been tested, and refined for HCHO, during the evaluation of photo-oxidation of butane and intermediate products, MEK, CH_3CHO and HCHO, (see section 5.4.) The sensitivity of the 1-butene and 1-hexene systems to variation of the rates of the photolysis reactions is discussed further below (section 5.6.4). In addition to carbonyl photolysis, photolysis reactions are generally included in MCM v3.1 for products containing nitrate, hydroperoxide and peracid functionalities, as described by Jenkin *et al.* (1997) and Saunders *et al.* (2003).

At the typical concentrations of NO_X in chamber experiments, the reactions of intermediate peroxy radicals with either NO or NO_2 may contribute to radical removal The reactions of the $RCH(O_2)CH_2OH$ and $RCH(OH)CH_2O_2$ with NO possess minor terminating channels generating the corresponding β–hydroxynitrates:

$$RCH(O_2)CH_2OH + NO \rightarrow RCH(ONO_2)CH_2OH \quad (29)$$

$$RCH(OH)CH_2O_2 + NO \rightarrow RCH(OH)CH_2ONO_2 \quad (30)$$

The weighted average branching ratio for the formation of β–hydroxynitrates by these reactions in the MCM v3.1 alkene schemes are 0.5%, 2.1%, 3.9% and 8.9 % for R equal to H, CH_3, C_2H_5 and n-C_4H_9, respectively. As described by Jenkin *et al.* (1997), the branching ratios for β–hydroxynitrate formation from the reactions of β–hydroxy peroxy radicals with NO were assigned values which are 50% of those for the corresponding alkyl peroxy radicals, based on a global comparison for a limited set of data reported for the oxidation of propene, methylpropene and cis-2-butene (Shepson *et al.,* 1985; Muthuramu *et al.,* 1993). More recently, O'Brien *et al.* (1998) have systematically quantified β–hydroxynitrate yields from a series of C_2-C_6 alkenes, with those relevant to the present study being (0.86 ± 0.03) %, (1.5 ± 0.1) %, (2.5 ± 0.2) % and (5.5 ± 1.0) % for ethene,

propene, 1-butene and 1-hexene, respectively. The sensitivity to variations in the β–hydroxynitrate yields, in relation to these newer data, is discussed further below (see sections 5.6.2-5.6.4).

The reactions with NO_2 tend to be most significant for acyl peroxy radicals, leading to the formation of peroxyacyl nitrates. In the case of the present systems, acyl peroxy radicals ($RC(O)O_2$) are formed from the further oxidation of the aldehyde products CH_3CHO, C_2H_5CHO, *n*-C_4H_9CHO and $HOCH_2CHO$ (see Figure 22), and the reversible formation of the corresponding peroxyacyl nitrates from their reactions with NO_2 potentially leads to temporary loss of free radicals:

$$RC(O)O_2 + NO_2 \leftrightarrows RC(O)OONO_2 \qquad (31)$$

As described in detail elsewhere (Jenkin *et al.,* 1997, Jenkin *et al.,* 2003 and Saunders *et al.,* 2003), MCM v3.1 incorporates all the above types of processes explicitly, in addition to competitive reactions which gain in significance at lower concentrations of NO_X.

The kinetics and mechanistic representation of the reactions of O_3 with the series of alkenes is described in detail by Jenkin *et al.* (1997) and Saunders *et al.* (2003). In addition to supplementing the oxidation rate of the alkenes, these reactions have an important secondary influence through being sources of OH and other free radicals. The oxidation is initiated by addition of O_3 to the double bond to form a primary ozonide, which then rapidly decomposes to form two sets of aldehyde plus Criegee biradical products, which possess excess energy (denoted by *):

$$O_3 + RCH{=}CH_2 \rightarrow \alpha(HCHO + [RCHOO]^*) + (1-\alpha)(RCHO + [CH_2OO]^*) \qquad (32)$$

For most 1-alkenes, it has been experimentally shown that α is ≈ 0.5 (Calvert *et al.,* 2000 and references therein), and this assumption is adopted in MCM v3.1. The excited Criegee biradicals, are assigned three possible fates (Jenkin *et al.,* 1997), namely (i) collisional stabilization to produce a stabilized Criegee biradical, (ii) decomposition to generate OH and a co-radical, and (iii) decomposition not generating OH (but usually partially generating other radicals), to account for the balance of the reaction. The reactions are summarized in Table 5 for the present systems. Whereas the branching ratios of 'routes (i) and (ii)' are based on literature data which was available to Jenkin *et al.* (1997), the contributions to 'route (iii)' of reactions forming radicals must be regarded as speculative and are still apparently not well determined (Calvert *et al.,* 2000). Sensitivity of the systems to uncertainties in the yields of OH and other radicals are discussed further below (see sections 5.6.2-5.6.4).

Table 5: Probabilities assigned to the reaction channels of excited Criegee biradicals formed in the alkene systems in MCM v3.1

alkene	stabilization	OH + co-radical formation	other pathways	
			radical[c]	non radical[c]
ethene	0.37[a]	0.13[a]	0.00	0.50
propene, 1-butene and 1-hexene	0.24[b]	0.36[b]	0.10	0.30

Notes

(a) Stabilization and OH yields based on Atkinson (1994); see Jenkin *et al.* (1997) for further details.

(b) Generic values applied to all alkenes of structure $RCH=CH_2$; stabilization yield based on data of Hatekeyama *et al.* (1984) for propene and Paulson and Seinfeld (1992) for 1-octene; OH yield based on the estimation method of Atkinson and Aschmann (1993); see Jenkin *et al.* (1997) for further details.

(c) Balance of reaction not accounted for by stabilization and OH formation divided between radical and non-radical channels for which there was some qualitative evidence; non-radical channel assumed exclusive for $[CH_2OO]^*$ see Jenkin *et al.* (1997) for further details.

The reactions of $O(^3P)$ with alkenes are believed to lead to partial radical formation (e.g. Calvert *et al.,* 2000), and therefore potentially have an influence on the radical balance in the system. Although not normally of great significance in the atmosphere, the reactions of unsaturated organic compounds with $O(^3P)$, formed predominantly by photolysis of NO_2 (reaction (1)), can have a nonnegligible impact under chamber conditions (e.g. Calvert *et al.,* 2000). This is because of the concentrations of NO_x (and therefore NO_2) used in chamber studies tend to be greater than those typically observed in the atmosphere. As shown in Table 4, the NO_x concentrations in the experiments considered here lie in range of 0.1 to 1 ppm, whereas those in urban atmospheres are typically < 0.1 ppm (e.g., Jenkin, 2004, and references therein). In addition to partially intercepting the formation of O_3 by reaction (2), the reactions of $O(^3P)$ with alkenes are believed to lead to partial radical formation (e.g. Calvert *et al.,* 2000), and therefore potentially have an influence on the radical balance in the system.

As part of the present study, reactions of $O(^3P)$ with all the alkenes, and associated chemistry, were incorporated into the mechanism, as summarised in Table 6. The rate coefficients are reasonably well determined, and were based on the recommendations of Calvert *et al.* (2000). The mechanisms and products of the reactions have been reviewed and discussed in detail by Cvetanovic (1987) and Calvert *et al.* (2000). It is well established that the reaction proceeds mainly by addition to the double bond, but there are important uncertainties about the products resulting from this addition.

The resulting biradical adduct can decompose, isomerise, or be collisionally stabilized to form an oxirane. There is some reported information on product channels, with the general indication that radical channels dominate for smaller alkenes, with the formation of molecular channels becoming progressively more important for larger alkenes. However, in the chamber-based evaluation study of SAPRC 99 (using the same data as applied here) it was necessary to reduce radical yields significantly to optimise the alkene degradation mechanisms (Carter, 2000). Consequently, the uncertainty of the impact of the $O(^3P)$ reaction on a given alkene can exceed the sensitivity of the mechanism to other factors which are important under atmospheric conditions, and therefore can potentially introduce bias into the optimisation. As discussed further below the results of simulations for the chamber conditions in the present evaluation are very sensitive to the relative branching ratios assigned to molecular and free radical forming pathways.

Note that the designation MCM v3.1a includes the recent parameter updates based on the evaluation of butane degradation, see section 5.4.1.

Table 6: Product channels and branching ratios assigned to the reactions of $O(^3P)$ with alkenes.

Reaction channel [a]		**ethene (R = H)**		**propene (R = CH_3)**		**1-butene (R = C_2H_5)**		**1-hexene (R = *n*-C_4H_9)**
$O(^3P)$ + $RCH=CH_2$		(b)	(c)	(b)	(c,d)	(b)	(c,e)	(c,f)
→ $RCH^{\cdot}\text{-}O\text{-}CH_2$	(i)	-	**0.40**	0.30	**0.50**	0.44	**0.53**	**1.00**
→ RCH_2CHO	(ii)	-	**0.40**	0.30	**0.50**	0.39	**0.47**	**-**
→ $RCH=C=O + H_2$	(iii)	0.05	**-**	**-**	**-**	**-**	**-**	**-**
→ $RCH_2 + HCO$	(iv)	0.60	**0.12**	0.20	**0.00**	**-**	**-**	**-**
→ $R + CH_2CHO$	(v)	0.35	**0.08**	0.20	**0.00**	0.17	**-**	**-**

Notes

(a) Reaction divided between molecular channels, (i)-(iii), and radical channels, (iv) and (v). Applied total rate coefficients (cm^3 $molecule^{-1}$ s^{-1}), as recommended by Calvert *et al.* (2000): 1.07×10^{-11} exp(-800/T) for ethene; 1.02×10^{-11} exp(-280/T) for propene; 1.34×10^{-11} exp(-315/T) for 1-butene; 1.51×10^{-11} exp(330/T) for 1-hexene. Oxirane products of channel (i) removed by reaction with OH to form products already in mechanism, with rate coefficients (cm^3 $molecule^{-1}$ s^{-1}): 7.3×10^{-14} for R = H; 7.4×10^{-13} for R = CH_3; 2.0×10^{-12} for R = C_2H_5; 4.6×10^{-12} for R = n-C_4H_9.

(b) Branching ratios proposed by Calvert *et al.* (2000).

(c) Final branching ratios used in the present study.

(d) Sensitivity study showed that a combined branching ratio of (iv) and (v) ≤ 0.1 was required for acceptable fit. Zero radical yield was adopted for illustrations (Figure 28– Figure 32).

(e) Radical formation assumed zero. Relative branching ratios for (i) and (ii) based on Calvert *et al.* (2000).

(f) Oxirane formation assumed exclusive based on documented trend of increasing yield for larger alkenes (Calvert *et al.,* 2000).

5.6.2 Ethene-NO_X experiments

The influence of incorporating the $O(^3P)$ initiated chemistry into the MCM v3.1a ethene mechanism was initially investigated, using the reaction pathways and subsequent chemistry summarised in Table 6. Based on the mechanistic information proposed by Calvert *et al.* (2000), the reaction of $O(^3P)$ with ethene was initially assumed to lead to almost exclusive (95%) radical formation. As shown in Figure 23 to Figure 24, inclusion of this chemistry was found to increase the simulated $D(O_3\text{-NO})$ and HCHO formation rates substantially for almost all conditions considered, leading to a significant over-prediction in most experiments, particularly those at lower VOC/NO_X. This behaviour is indicative of systematic errors in the input of radicals to the system (i.e. overestimated sources, underestimated sinks, or both), and possible sensitivity to the radical source and sink reactions described above in section 5.6.1 was therefore tested, within the context of literature uncertainties.

The yield of OH (and a co-radical) from the reaction of O_3 with ethene has an assigned value of 13% in MCM v3.1 (see Table 5). This is consistent with, but at the low end of, the range of 12-18% currently recommended by the IUPAC panel (Atkinson *et al.,* 2005). The reaction is therefore comparatively inefficient at generating radicals, and it is not possible to implement changes to reduce the associated radical input which can be supported by the literature. Nevertheless, a sensitivity study showed that reducing the radical yield to zero leads to an improvement in the simulations, but even this (unsupported) adjustment is insufficient to account fully for the observed over-simulation of $D(O_3\text{-NO})$.

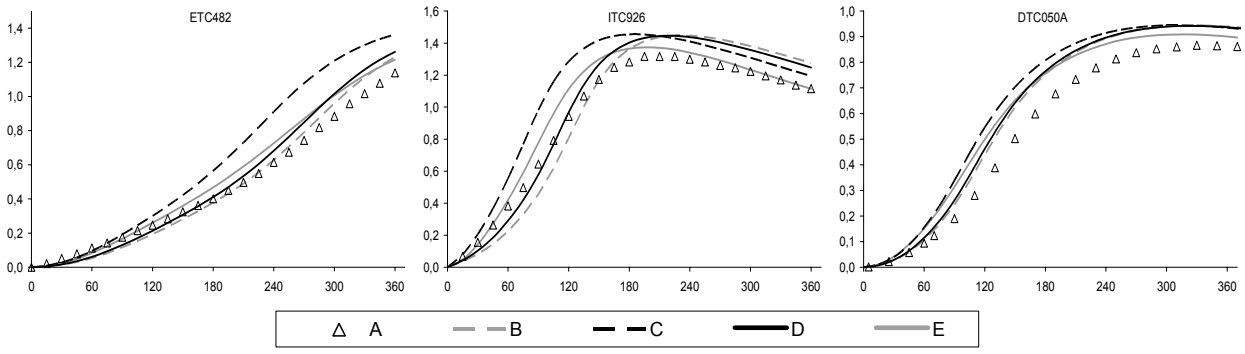

Figure 23: Example plots of experimental and calculated $D(O_3\text{-NO})$ (ppm) vs. time (min) for the ethene – NO_x –air experiments: A – experimental data; B - MCM v3.1a; C - MCM v3.1a with $O(^3P)$ reaction based on Calvert *et al.,* 2000 (see Table 3); D - MCM v3.1a with $O(^3P)$ reaction with optimum radical yield; E - SAPRC99. ETC482-VOC/NO_x=3.8; ITC926-VOC/NO_x=7,4; DTC050A-VOC/NO_x=11.7.

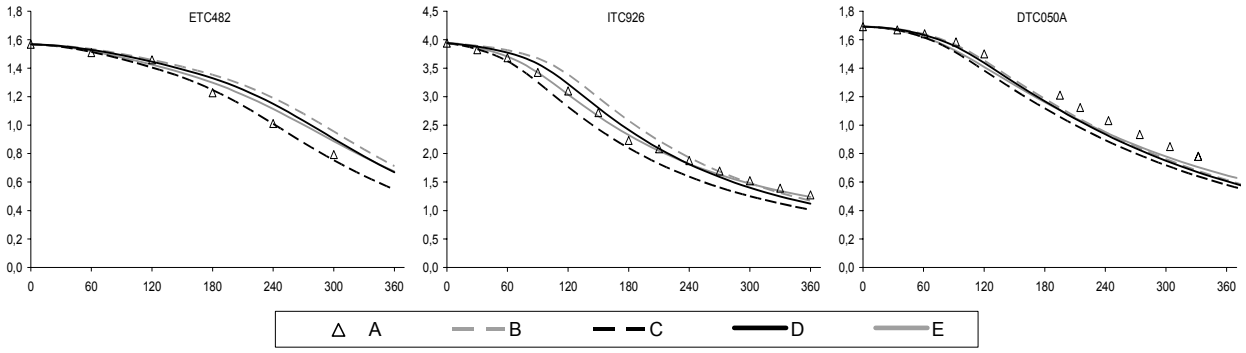

Figure 24: Example plots of experimental and calculated ethene (ppm) vs. time (min) for the ethene – NO_x – air experiments: Legend as in Figure 23.

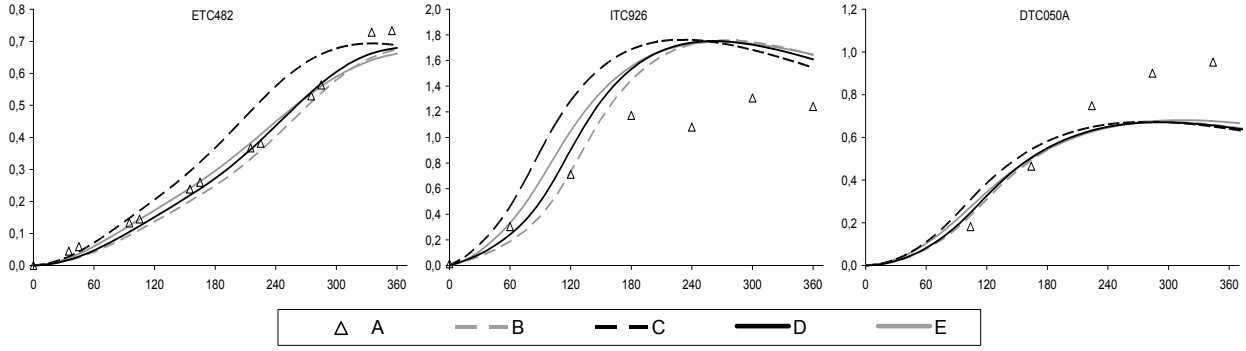

Figure 25: Example plots of experimental and calculated HCHO (ppm) vs. time (min) for the ethene – NO_x – air experiments: Legend as in Figure 23.

The influence of the formation of the β–hydroxynitrate ($HOCH_2CH_2ONO_2$) from reaction type (30) was also investigated. However, because this reaction accounts for a very small fraction of the overall reaction, variation of the nitrate-forming branching ratio from the estimated value of 0.5 % in MCM v3.1 to the value of 0.86 %, reported by O'Brien *et al.* (1998), results in a negligible change in the simulated $D(O_3\text{-NO})$ and HCHO profiles. It is therefore not possible to implement changes to increase radical removal *via* this reaction which can be supported by the literature.

The system is also insensitive to possible changes in the rates of radical formation from the photolysis of carbonyl products. The major product is HCHO, formed with a molar yield of ca. 155 % from the NO_X-catalysed chemistry. As indicated above, MCM v3.1a includes photolysis parameters updated during the evaluation of photo-oxidation of butane and intermediate products and fully tested using the results of HCHO-NO_X photo-oxidation experiments, see section 5.4. The photolysis parameters of the minor product $HOCH_2CHO$ (22%) are subject to some uncertainties, but the system was found to be insensitive to variations in this parameter because secondary radical generation is dominated by HCHO photolysis.

The results were found to be very sensitive to variation of the branching ratios for radical and molecular pathways for the O(^{3}P)-ethene reaction listed in Table 6, with the molecular channels (i) and (ii) adopted for ethene being inferred by analogy with those of larger alkenes (e.g. Calvert *et al.,* 2000). Sensitivity tests demonstrated that it was necessary to increase the molecular channel branching ratios to account for at least 50% of the reaction, in order to get a good representation of the results of the large majority of the experiments, with the optimum being 80% (as shown in Table 6) (see Figure 26 and Figure 27). This conclusion is broadly consistent with the analysis of Carter (2000), who determined an optimised radical yield of 50% during evaluation of the SAPRC-99 mechanism using the same dataset.

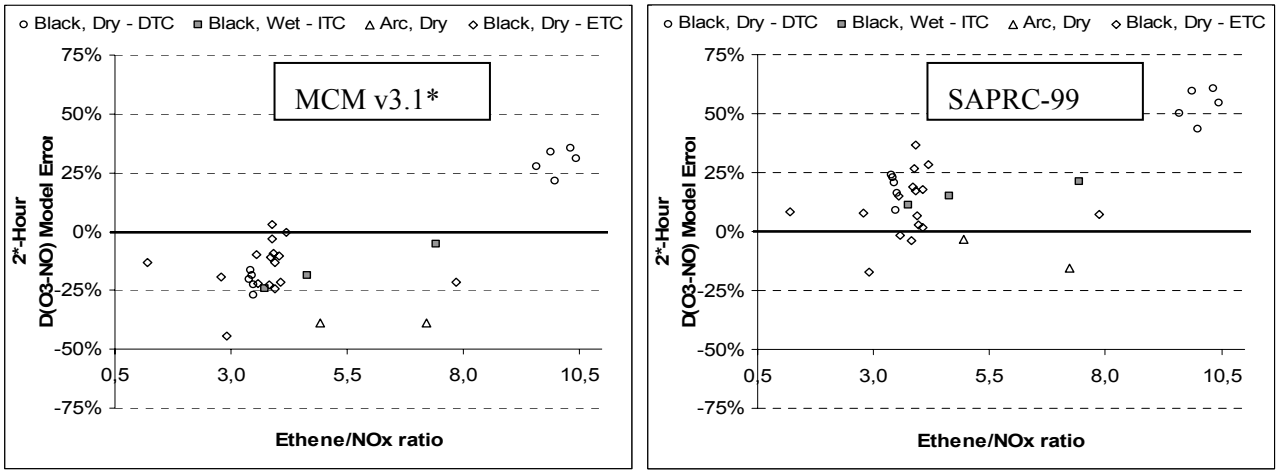

Figure 26: 2 hour* D(O_3-NO) model error *vs*. ethene/NOx ratio. D(O_3-NO) model error = 100 x (calculated value - experimental value)/experimental value. '2-hour*' corresponds to 2 hour equivalent, i.e., the time that corresponds to 2 hours if the NO_2 photolysis coefficient, k_6, was 0.3 min^{-1}. Differences in light intensity were thus accounted for by normalizing the time to the ratio of a standard light intensity (k_6 = 0.3 min^{-1}) to the light intensity of the experiment. 'MCM v3.1*' indicates MCM v3.1a optimised as described in the text. 'Black' indicates illumination with blacklights; 'Arc' indicates experiments in chambers with xenon arc illumination (i.e., CTC and XTC); 'Dry' and 'wet' indicate the relative humidity (see Table 4).

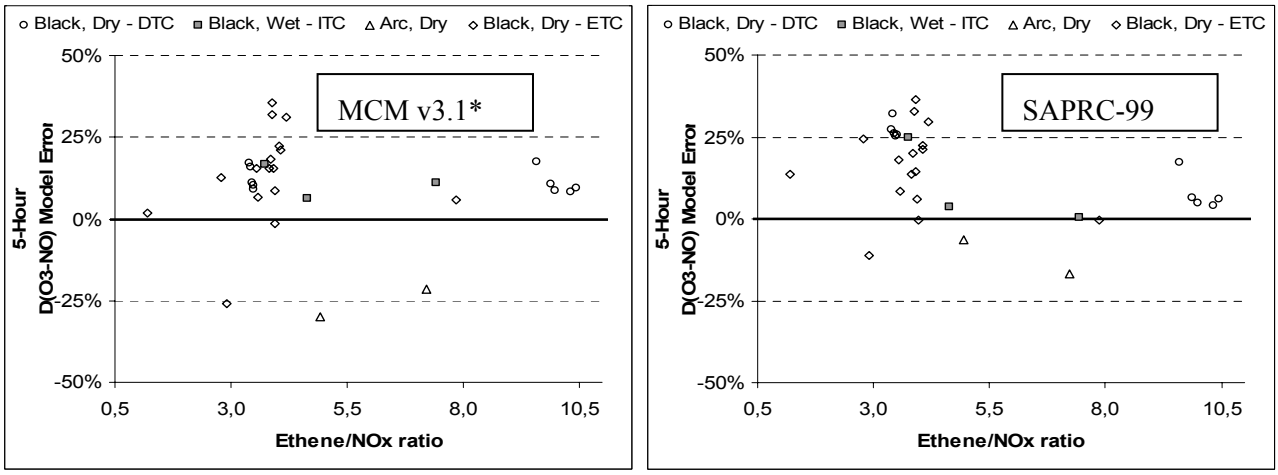

Figure 27: 5 hour* D(O_3-NO) model error *vs*. ethene/NOx ratio. See Figure 26 caption for explanation of legends and definitions.

Zador *et al.* (2005) have recently carried out an evaluation of the MCM v3 ethene mechanism (the same degradation mechanism of MCM v3.1), using chamber data from the European Photoreactor (EUPHORE). For the higher NO_X conditions more typical of the data being considered in the present study, the system was found to be particularly sensitive to uncertainties in the rate coefficient for the reaction of OH with NO_2, which is the major radical sink in the system:

$$OH + NO_2 (+M) \rightarrow HNO_3 (+M) \qquad (33)$$

As referred in section 5.4 the MCM v3.1a uses the JPL (2003) recommendation (k_{33} = 1.05 x 10^{-11} cm^3 molecule s^{-1} at 298 K and 760 Torr; Sander *et al.,* 2003). Additional sensitivity studies on the ethene-NO_X experiments indicate that the results are sensitive to variations in the value of k_{33}, even if compensating changes are made to the chamber radical source to fit the butane-NO_X experiments. Thus, changes in k_{33} of about ± 15 % (i.e., approximately in line with the spread in recent evaluations) lead to corresponding systematic differences in the simulations of the ethene-NO_X experiments, resulting in changes of about ($^{-15}_{+18}$) % in D(O_3-NO), based on the average over the complete series of 31 experiments.

Changes in k_{33} of ± 15 % also lead to systematic differences in the simulations of D(O3-NO) in the other systems, as follows; propene-NO_X, ($^{-5.7}_{+7.4}$) %; 1- butene-NO_x, ($^{-3.4}_{+5.0}$) %; 1-hexene-NO_x, ($^{-5.0}_{+7.5}$) %. This potential source of bias further emphasises the requirement for reducing the uncertainty range in the kinetics of reaction (33).

5.6.3 Propene-NO_X experiments

The O(^{3}P) initiated chemistry was incorporated into the MCM v3.1a propene mechanism, using the reaction pathways and subsequent chemistry summarised in Table 6. Based on the mechanistic information proposed by Calvert *et al.* (2000), the reaction of O(^{3}P) with propene was initially assumed to lead to significant (40 %) radical formation, resulting in a general over-prediction of D(O_3-NO), CH_3CHO and HCHO formation rates in almost all experiments (Figure 28– Figure 32). It is noted that Hynes *et al.* (2005) have also recently reported over-efficient simulation of propene photo-oxidation and ozone formation in three experiments, using MCM v3.1 with the O(^{3}P) reaction implemented on the basis of the same recommendations. Possible sensitivity to the radical source and sink reactions described above in section 5.6.1 was therefore once again considered.

The yield of OH (and a co-radical) from the reaction of O_3 with propene is assigned a value of 36 % in MCM v3.1 (see Table 5). This is based on a generic MCM protocol rule for terminal alkenes (Jenkin *et al.,* 1997), and is reasonably consistent with values reported in the literature for propene, i.e., 33 % (Atkinson and Aschmann, 1993), 35 % (Paulson *et al.,* 1999a), 34 % (Neeb and Moortgat, 1999) and 32 % (Rickard *et al.,* 1999). A slight reduction in line with these data leads to

a small decrease in simulated D(O_3-NO). A sensitivity study showed that an (unsupported) substantial reduction in the radical yield to ≤ 15 % would be required to bring the simulated D(O_3-NO) into reasonable agreement with that observed. The influence of the formation of the β–hydroxynitrates ($CH_3CH(ONO_2)CH_2OH$ and $CH_3CH(OH)CH_2ONO_2$) from reactions type (29) and (30) was also investigated. Once again, however, these channels account for only small fractions of the overall reactions, such that variation of the weighted average nitrate-forming branching ratio from the value of 2.1 % used in MCM v3.1 to the value of 1.5 %, reported by O'Brien *et al.* (1998), results in no discernable changes in the simulated profiles for D(O_3-NO), CH_3CHO and HCHO. Consequently, it is not possible to implement changes supported by the literature, either in the OH yield from the ozonolysis reaction, or in the yield of the β–hydroxynitrates, to improve the agreement between the simulated and observed profiles. Furthermore, the representation of the degradation of both the carbonyl products (HCHO and CH_3CHO) has been validated previously, such that secondary radical production from the photolysis of these species is well represented.

As for the ethene system, the results were found to be very sensitive to variation of the branching ratios for radical and molecular pathways for the O(^{3}P) reaction, with a significant reduction in the importance of the free radical channels (vi) and (v) being required to fit the data. This is consistent with the analysis of Carter (2000), who found it necessary to apply a radical yield of zero (in conjunction with 32 % OH yield from the ozonolysis reaction) during evaluation of the SAPRC-99 propene mechanism using the same dataset. Accordingly, sensitivity studies demonstrated that it was necessary to reduce the importance of the free radical channels of the O(^{3}P) reaction to a combined branching ratio of ≤ 10 % (see Table 6) to provide an acceptable description of the majority of the propene experiments, with the results being insensitive to changes over the range 0-10 %. This result is in fair agreement with the lowest radical yield (18 %) reported in the literature (Anastasi and Sanderson, 1994a,b). The associated illustrations in Figure 28– Figure 32 were performed with a radical yield of zero. As for the ethene system, a systematic error in the rate coefficient applied to the reaction of O(^{3}P) with propene could also explain the apparent need to reduce the radical yield, but would require the rate coefficient to be reduced from the applied recommended value (4.0×10^{-12} cm^3 molecule^{-1} s^{-1} at 298 K: see Table 6) by a factor of ≥ 4. However, such a large reduction is unsupported by the literature, the reported rate coefficients for the O(^{3}P) + propene reaction lying in the range ($4.0 – 5.8$) x 10^{-12} cm^3 molecule^{-1} s^{-1} at 298 K (e.g. Calvert *et al.,* 2000). SAPRC-99 mechanism gives slower O_3 formation than the simulations with the various MCM options since a lower radical formation in the O_3 reaction is used.

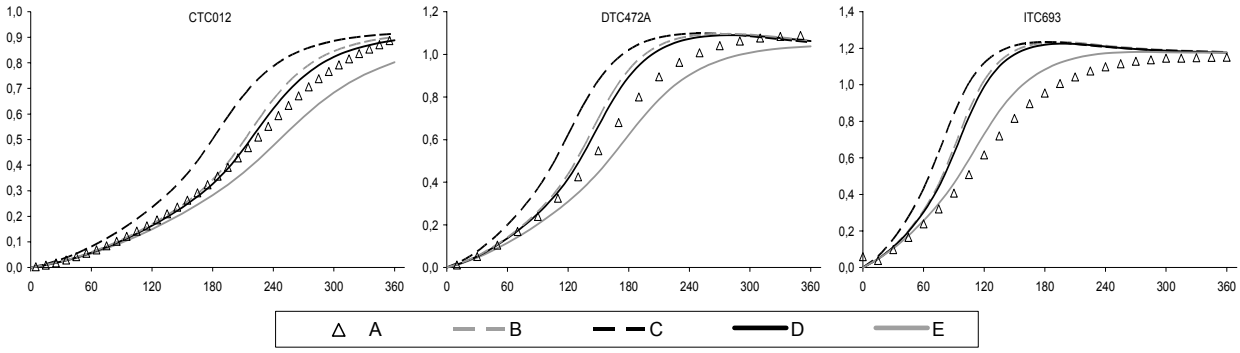

Figure 28: Example plots of experimental and calculated D(O_3-NO) (ppm) vs. time (min) for the propene – NO_x –air experiments: A – experimental data; B - MCM v3.1a; C - MCM v3.1a with O(^{3}P) reaction based on Calvert *et al.,* 2000 (see Table 3); D - MCM v3.1a with O(^{3}P) reaction with zero radical yield; E - SAPRC99. CTC012-VOC/NO_x=2.0; DTC472A=2.2; ITC693- VOC/NO_x=2.2.

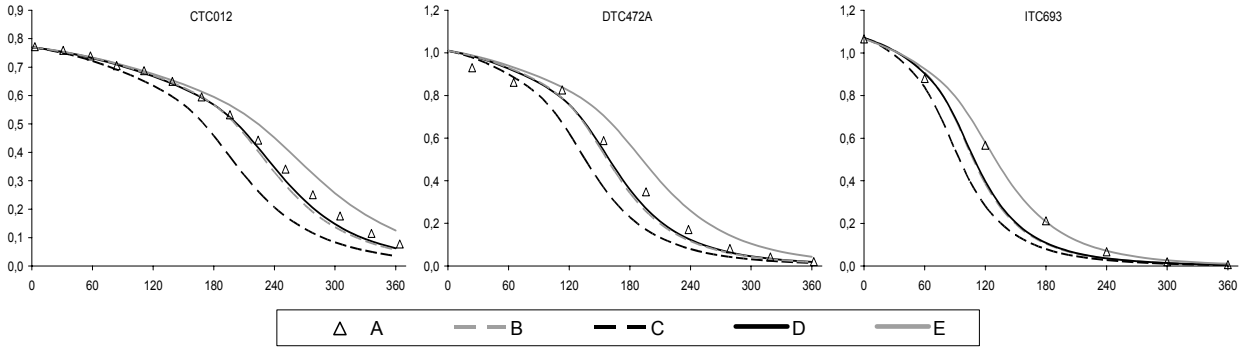

Figure 29: Example plots of experimental and calculated propene (ppm) vs. time (min) for the propene – NO_x –air experiments: Legend as in Figure 28.

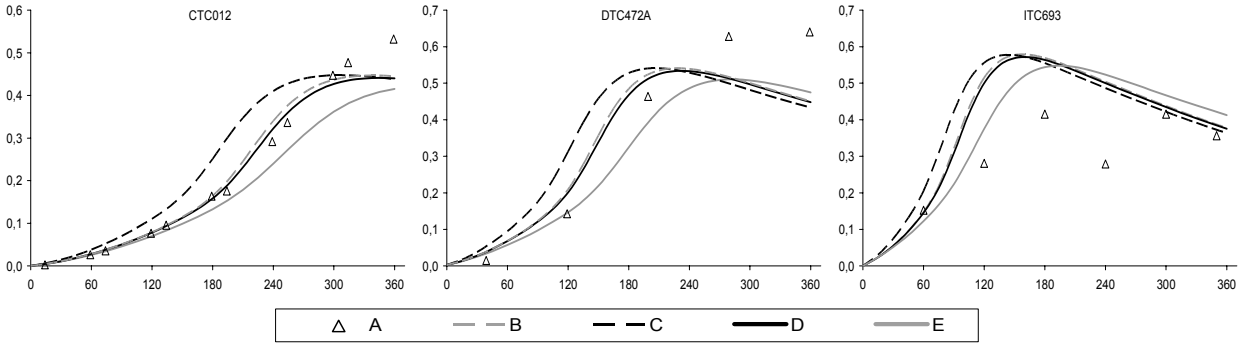

Figure 30: Example plots of experimental and calculated HCHO (ppm) vs. time (min) for the propene – NO_x –air experiments: Legend as in Figure 28.

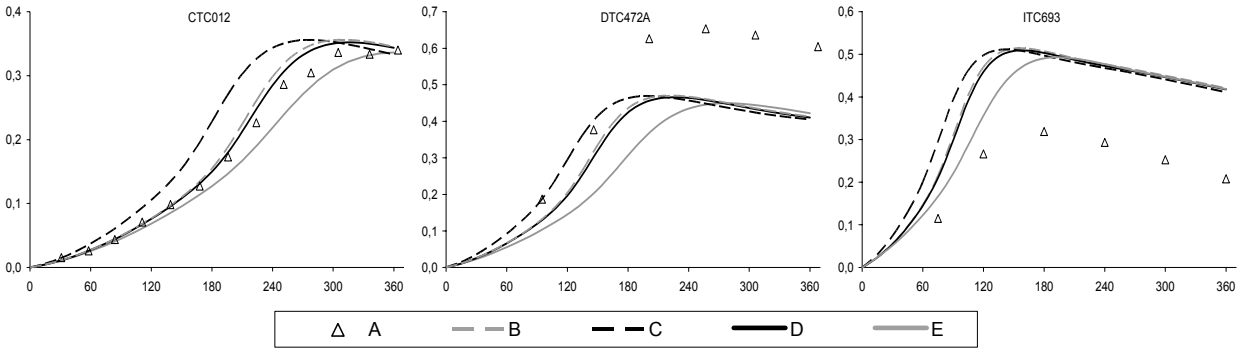

Figure 31: Example plots of experimental and calculated CH_3CHO (ppm) vs. time (min) for the propene – NO_x –air experiments: Legend as in Figure 28.

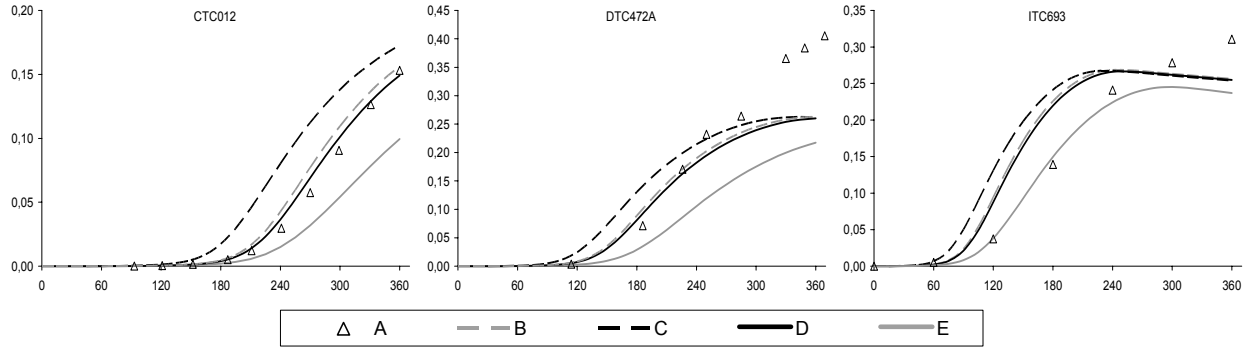

Figure 32: Example plots of experimental and calculated PAN (ppm) vs. time (min) for the propene – NO_x – air experiments: Legend as in Figure 28.

As shown in Table 4, the SAPRC dataset for the propene-NO_X system is very large, consisting of 129 experiments, carried out in 5 different chambers. However, it is apparent (Figure 33 and Figure 34) that the MCM results for D(O_3-NO) in the DTC and ITC chamber experiments (illuminated by blacklights) show a large dispersion, and a tendency towards over-prediction in the case of the ITC dataset. Consequently, the above conclusions with regard to the optimum parameters are mainly governed by the experiments performed in the CTC chamber (illuminated by xenon arc). This is of some concern, because the experiments on the 1-butene and 1-hexene systems, discussed below, were carried out exclusively in the ITC chamber.

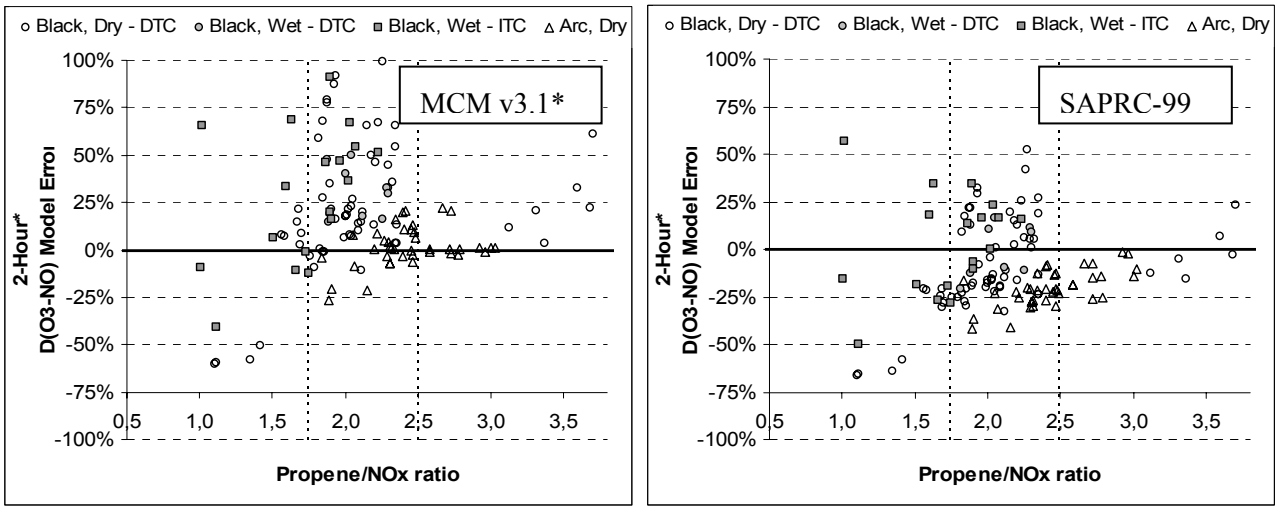

Figure 33: 2 hour* D(O_3-NO) model error *vs*. propene/NOx ratio. D(O_3-NO) model error = 100 x (calculated value - experimental value)/experimental value. '2-hour*' corresponds to 2 hour equivalent, i.e., the time that corresponds to 2 hours if the NO_2 photolysis coefficient, k_6, was 0.3 min^{-1}. Differences in light intensity were thus accounted for by normalizing the time to the ratio of a standard light intensity (k_6 = 0.3 min^{-1}) to the light intensity of the experiment. 'MCM v3.1*' indicates MCM v3.1a optimised as described in the text. 'Black' indicates illumination with blacklights; 'Arc' indicates experiments in chambers with xenon arc illumination (i.e., CTC and XTC); 'Dry' and 'wet' indicate the relative humidity (see Table 4).

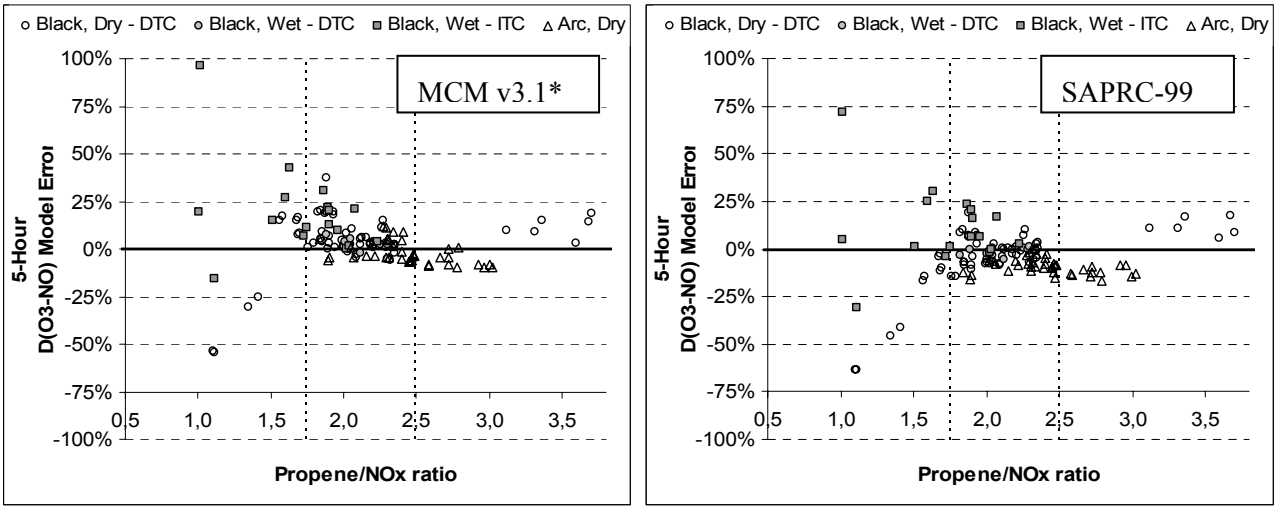

Figure 34: 5 hour* D(O_3-NO) model error *vs*. propene/NOx ratio. See Figure 33 caption for explanation of legends and definitions.

5.6.4 1-Butene-NO_X and 1-hexene-NO_X experiments

$O(^3P)$-initiated chemistry for 1-butene and 1-hexene was incorporated into the MCM v3.1a mechanisms, using the reaction pathways and subsequent chemistry summarised in Table 6. Based on the mechanistic information proposed by Calvert *et al.* (2000), the reaction of $O(^3P)$ with 1-butene has a minor (17%) radical forming channel. However, in view of the results discussed above

for the smaller alkene systems, the reactions involving both 1-butene and 1-hexene were assumed to proceed entirely by the molecular channels (i) and (ii), as shown in Table 6. With this assumption, the incorporation of these reactions resulted in small reductions in the simulated D(O_3-NO) formation rate for both systems. Despite this, the observed formation rates of D(O_3-NO), HCHO and RCHO were consistently and substantially over-predicted in all experiments (Figure 35 – Figure 42). In view of the results described above for the propene-NO_X system in the same chamber, this result is not surprising. Nevertheless, the sensitivity of the simulation to radical source and sink reactions was once again investigated.

The results for both chemical systems were found to be comparatively insensitive to assumptions regarding the yields of the β–hydroxynitrate products. In the case of 1-butene, reduction of the weighted average nitrate-forming branching ratio from the value of 3.9 % used in MCM v3.1 to the value of 2.5 %, reported by O'Brien *et al.* (1998), has only a very minor influence. For the 1-hexene system, use of the yield of 5.5 % reported by O'Brien *et al.* (1998) instead of the higher value of 8.9 % adopted in MCM v3.1, results in a small increase in the simulated D(O_3-NO) formation rate. The sensitivity of the simulations to variation of the photolysis rates applied to the major carbonyl products, C_2H_5CHO and *n*-C_4H_9CHO was also tested. The systems were found to be insensitive for the high [VOC]/[NO_X] experiments, for which even complete omission of the photolysis reactions has only a minor effect. At lower [VOC]/[NO_X], the sensitivity is greater. However, variations which can be supported by the more recent literature (consistent with a ca. 30% decrease in radical formation from *n*-C_4H_9CHO photolysis compared with those applied in MCM (IUPAC, 2002)), do not have a major effect on the simulated D(O_3-NO).

It was found that the simulated profiles can be forced into reasonable agreement with observations, if substantial reductions are made to the assumed radical formation from the ozonolysis reactions (Figure 35 – Figure 42). If it is first assumed that the formation of OH (and a co-radical) is the only radical forming channel in each case (i.e. the yields of other radical pathways in Table 5 are set to zero), reduction of the OH (and co-radical) yields to values of 12 % and 7 % are required for the 1-butene and 1-hexene systems, respectively. Given that these values are substantially lower than even the lowest reported OH yields of 29 % and 18 % for these alkenes (Paulson *et al.,* 1999b), the main conclusion is that it is impossible to reconcile the MCM v3.1 over-simulation of D(O_3-NO) for the 1-butene and 1-hexene systems with the ITC chamber data, even if all parameters influencing radical production are reduced to the smallest values and all parameters influencing radical removal are increased to the highest values, which can currently be justified on the basis of the literature. Carter (2000) reached a similar conclusion during evaluation of the SAPRC-99 mechanism, requiring ozonolysis OH yields of 11.6 % and 8.5 % for the 1-butene and 1-hexene

systems respectively (in conjunction with zero radical production from the $O(^3P)$ reactions) to fit the ITC data.

The corresponding simulations of the aldehyde products in each system are shown in Figure 37, Figure 38, Figure 41 and Figure 42. Even with the above measures applied to force agreement for $D(O_3\text{-NO})$, the simulated concentrations of the aldehyde products in both the 1-butene and 1-hexene systems are greater than observed. In the case of the 1-butene-NO_X experiments, it is difficult to put forward an explanation for this disagreement, given that HCHO and C_2H_5CHO are mainly generated from the predominant OH-initiated, NO_X-catalysed oxidation sequence, reactions (20)-(27) and reaction (4). The near-quantitative (96.1 %) yield of the aldehydes from this chemistry in MCM v3.1 is in good accord with the literature (Atkinson *et al.,* 1995), consistent with exclusive decomposition of the oxy radicals $C_2H_5CH(O)CH_2OH$ and $C_2H_5CH(OH)CH_2O$ *via* reactions type (23) and (26). For the 1-hexene-NO_X experiments, however, it is likely that the assumption of exclusive decomposition for the oxy radicals *n*-$C_4H_9CH(O)CH_2OH$ and *n*-$C_4H_9CH(OH)CH_2O$ in MCM v3.1 leads to over-simulation of the aldehyde products, HCHO and *n*-C_4H_9CHO, owing to the existence of competitive 1,5 H-shift isomerization reactions (see section 5.6.1). A representation of these isomerization reactions, and subsequent chemistry, was therefore implemented, for which the major NO-propagated reaction sequences generate C_6 dihydroxy carbonyl products, for example:

$$n\text{-}C_4H_9CH(O)CH_2OH \rightarrow CH_3CHCH_2CH_2CHOHCH_2OH \quad (34)$$

$$CH_3CHCH_2CH_2CHOHCH_2OH + O_2 \rightarrow CH_3CH(O_2)CH_2CH_2CHOHCH_2OH \quad (35)$$

$$CH_3CH(O_2)CH_2CH_2CHOHCH_2OH + NO \rightarrow CH_3CH(O)CH_2CH_2CHOHCH_2OH + NO_2 \quad (36)$$

$$CH_3CH(O)CH_2CH_2CHOHCH_2OH \rightarrow CH_3CH(OH)CH_2CH_2C(OH)CH_2OH \quad (37)$$

$$CH_3CH(OH)CH_2CH_2C(OH)CH_2OH + O_2 \rightarrow CH_3CH(OH)CH_2CH_2C(=O)CH_2OH + HO_2 \quad (38)$$

Additional simulations including the 1,5 H-shift isomerization reactions and associated chemistry demonstrated (Figure 41 and Figure 42) that a reasonable representation of HCHO and *n*-C_4H_9CHO formation could be achieved with a weighted average of ca. 75 % decomposition of *n*-$C_4H_9CH(O)CH_2OH$ and *n*-$C_4H_9CH(OH)CH_2O$ to occur (i.e., ca. 25 % isomerization), which is at least qualitatively consistent with the conclusions of Atkinson *et al.* (1995), who report ca. 40 % isomerization. Although it is recognised that the present estimate is subject to significant uncertainty (owing to the complications in fitting the data discussed above), the weight of evidence suggests that the generic MCM rule regarding the exclusive decomposition of larger β–hydroxyalkoxy radicals requires revision.

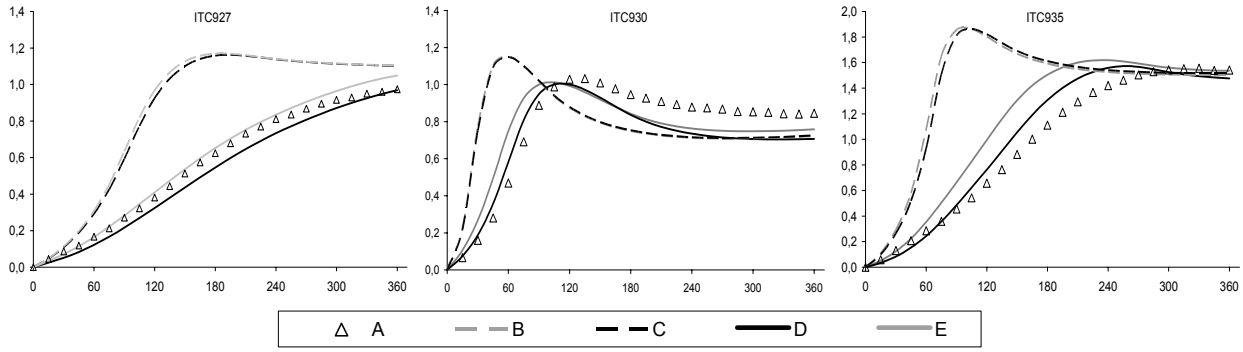

Figure 35: Example plots of experimental and calculated D(O_3-NO) (ppm) vs. time (min) for the 1-butene – NO_x –air experiments: A – experimental data; B - MCM v3.1a; C - MCM v3.1a with O(^{3}P) reaction with 0% radical yield (see Table 6); D - MCM v3.1a with O(^{3}P) with 0% radical yield + reduction of the OH (and co-radical) yields from ozonolysis to 12 %; E - SAPRC99. ITC927- VOC/NO_x=2.0; ITC930- VOC/NO_x=5.3; ITC935- VOC/NO_x=2.6.

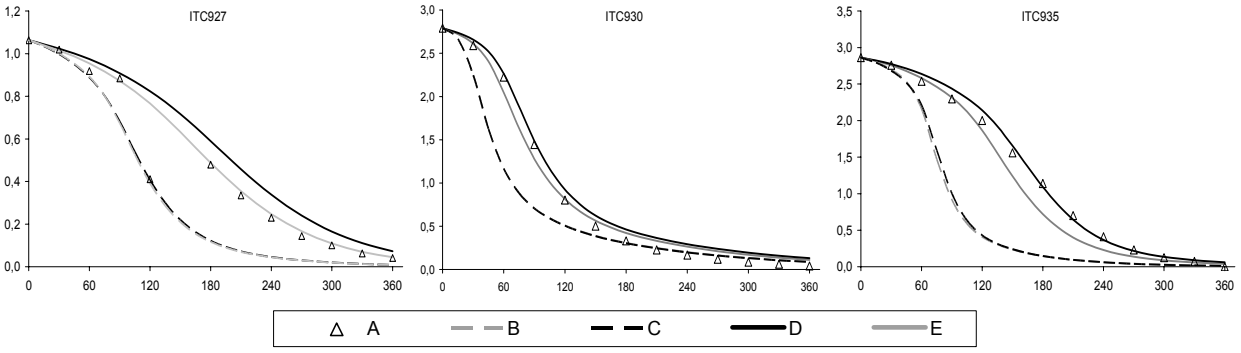

Figure 36: Example plots of experimental and calculated 1-butene (ppm) vs. time (min) for the 1-butene – NO_x –air experiments: Legend as in Figure 35.

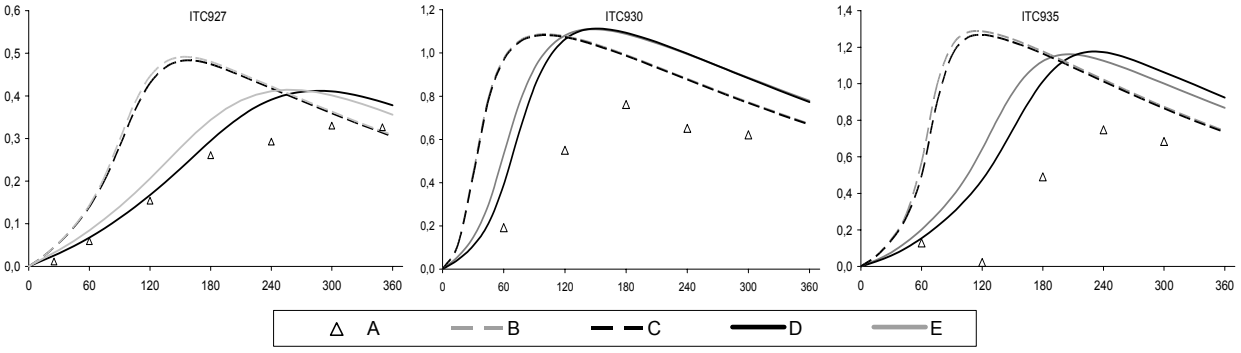

Figure 37: Example plots of experimental and calculated HCHO (ppm) vs. time (min) for the 1-butene – NO_x –air experiments: Legend as in Figure 35.

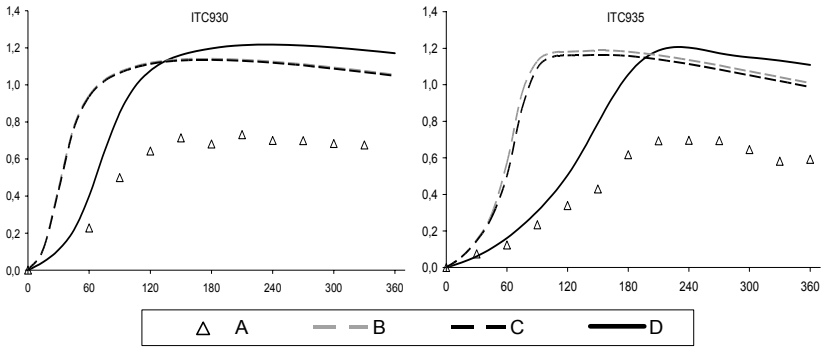

Figure 38: Example plots of experimental and calculated C_2H_5CHO (ppm) vs. time (min) for the 1-butene – NO_x –air experiments: Legend as in Figure 35.

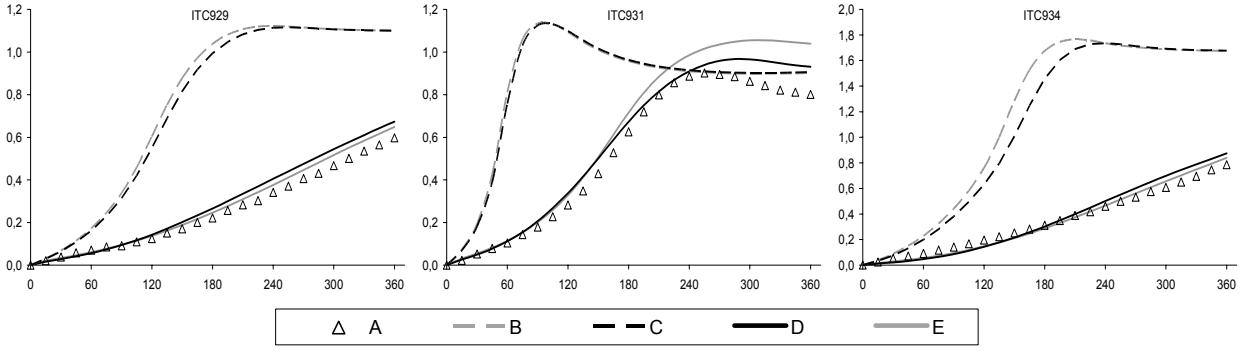

Figure 39: Example plots of experimental and calculated D(O3-NO) (ppm) vs. time (min) for the 1-hexene – NO_x –air experiments: A – experimental data; B - MCM v3.1a; C - MCM v3.1a with O(^{3}P) reaction with 0% radical yield (see Table 6); D - MCM v3.1a with O(^{3}P) reaction with 0% radical yield, reduction of the OH (and co-radical) yields from ozonolysis to 7 %, and with 25 % oxy radical isomerization included; E - SAPRC99.

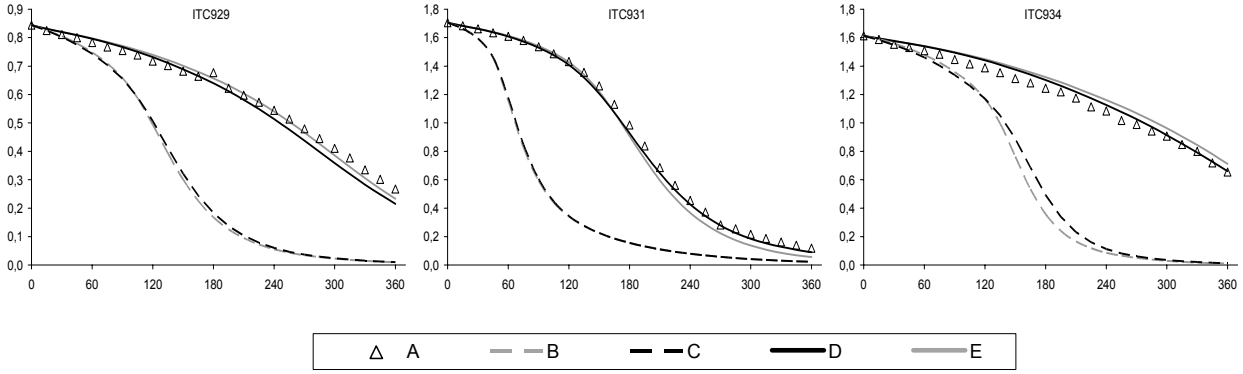

Figure 40: Example plots of experimental and calculated 1-hexene (ppm) vs. time (min) for the 1-hexene – NO_x –air experiments. Legend as in Figure 39.

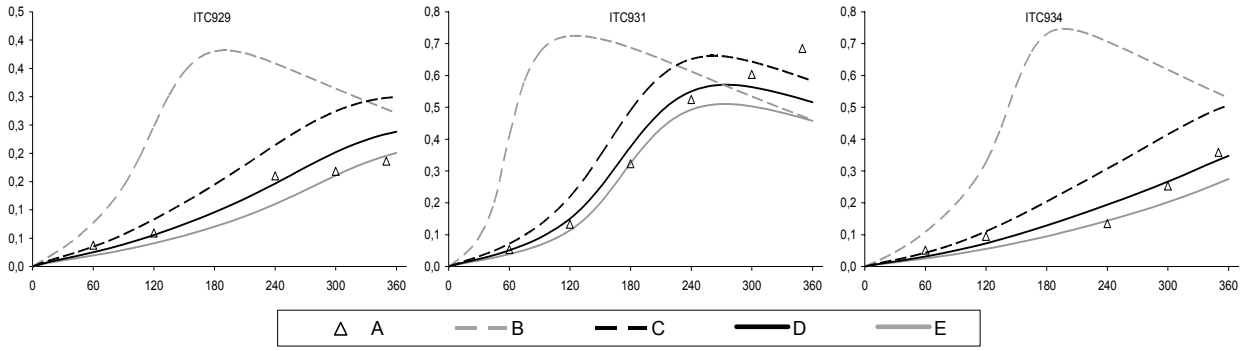

Figure 41: Example plots of experimental and calculated HCHO (ppm) vs. time (min) for the 1-hexene – NO_x –air experiments: A – experimental data; B - MCM v3.1a with insertion of $O(^3P)$ reaction with 0% radical yield (see Table 6); C - MCM v3.1a with insertion of $O(^3P)$ reaction considering 0% radical yield and reduction of the OH (and co-radical) yields from ozonolysis to 7 %; D - MCM v3.1a with insertion of $O(^3P)$ reaction with 0% radical yield, reduction of the OH (and co-radical) yields from ozonolysis to 7 %, inclusion of 25 % oxy radical isomerization; E - SAPRC99.

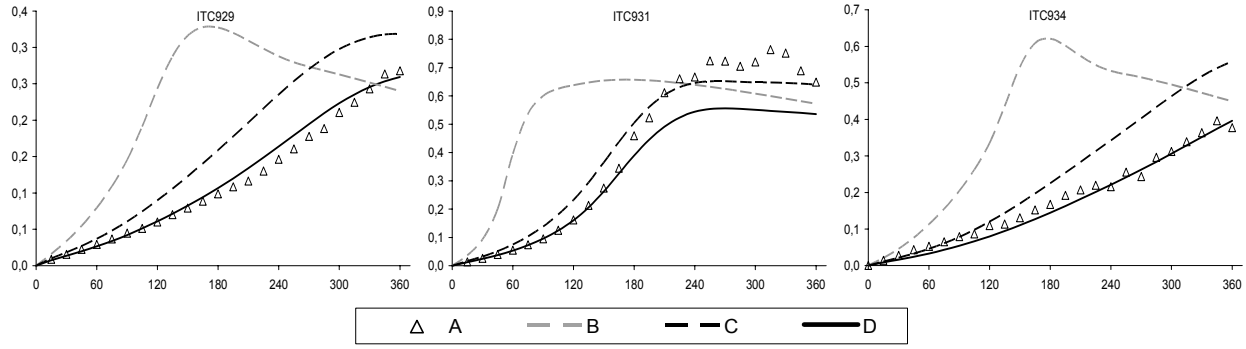

Figure 42: Example plots of experimental and calculated *n*-C_4H_9CHO (ppm) vs. time (min) for the 1-hexene – NO_x –air experiments: A – experimental data; B - MCM v3.1a with insertion of $O(^3P)$ reaction with 0% radical yield (see Table 6); C - MCM v3.1a with insertion of $O(^3P)$ reaction considering 0% radical yield and reduction of the OH (and co-radical) yields from ozonolysis to 7 %; D - MCM v3.1a with insertion of $O(^3P)$ reaction with 0% radical yield, reduction of the OH (and co-radical) yields from ozonolysis to 7 %, inclusion of 25 % oxy radical isomerization.

5.7 Isoprene Photo-oxidation Mechanism Assessment

Isoprene is a, C_5 olefinic volatile organic compound (VOC) ubiquitous in the lower troposphere. Although some anthropogenic sources related to industrial and transport activities are known (Burgess and Penkett, 1993; Derwent *et al.,* 1995; McLaren *et al.,* 1996; Reimann *et al.,* 2000; Clapp and Jenkin, 2001; Borbon *et al.,* 2001; Duane *et al.,* 2002), most isoprene is of natural origin, being emitted largely by vegetation, namely broad leaf trees (e.g. Kesselmeier and Staudt, 1999). Emission rates are species and seasonally dependent, and increase strongly with solar radiation intensity and temperature (e.g. Guenther *et al.,* 1995). As result of the large emission rates and a high chemical reactivity, isoprene plays an important role in atmospheric chemistry, principally in non-urban areas. In addition to the direct impact in processes involving regional photochemical pollution, isoprene is believed to be the most abundant non-methane VOC emitted globally (e.g. Guenther *et al.,* 1995), such that its emission and chemical transformation also plays a significant role in atmospheric processes at a global level.

It is well established that isoprene reacts with the OH, O_3, $O(^3P)$, NO_3 and NO_2 (e.g. Calvert *et al.,* 2000). Because most isoprene is emitted during daylight hours, reaction with OH tends to be the major tropospheric degradation process contributing to isoprene loss, with smaller contributions from reaction with O_3, and possibly with $O(^3P)$ under some conditions (Paulson *et al.,* 1992). However, it is also probable that NO_3 plays a non-negligible role in isoprene oxidation, through reaction with residual isoprene at the end of the day and in the early part of the night (Stroud *et al.,* 2002).

Particular progress has been made in defining the kinetics and mechanisms of the early stages of the gas-phase degradation chemistry of isoprene initiated by reaction with OH, O_3 and NO_3 (e.g. Calvert *et al.,* 2000 and references therein). The major oxidation route, initiated by reaction with OH, has been shown to yield MVK, MACR, HCHO, hydroxyalkyl nitrates and hydroxycarbonyl species as the main oxidation products, when NO_X is present (e.g., Atkinson *et al.,* 1989; Kwok and Atkinson, 1995; Paulson *et al.,* 1992; Grosjean *et al.,* 1993a; Miyoshi *et al.,* 1994; Kwok *et al.,* 1995; Ruppert and Becker, 2000; Sprengnether *et al.,* 2002). The subsequent oxidation chemistry of the carbonyl products has also received some attention (e.g., Raber and Moortgat, 1996; Gierczak *et al.,* 1997), and has been shown to lead to the formation of products such as PAN, peroxymethacrolyl nitrate (MPAN) and highly oxygenated products, such as glyoxal and methylglyoxal. Some of these oxidation products have been detected in the field (Bertman and Roberts, 1991; Lee *et al.,* 1998; Williams *et al.,* 1997), with reasonably well-defined concentration ratios being observed under conditions when isoprene dominates local VOC emissions.

It is fundamental for a complete understanding of atmospheric processes that the atmospheric oxidation of isoprene is well understood and correctly represented in computer airshed models used to simulate urban and regional air quality. Therefore various representations of isoprene photo-oxidation chemistry are included in almost all urban or regional airshed models currently in use for research or regulatory purposes (Carter and Atkinson, 1996).

The photo-oxidation mechanism of isoprene, and photo-oxidation of its degradation products, MACR and MVK, used in MCM v3.1 has been evaluated and refined. Several chamber experimental runs were employed in the present evaluation; 9 isoprene-NO_X-air, 8 MACR-NO_X-air and 5 MVK-NO_X-air. The ranges of reagent concentrations for the considered experiments are presented in Table 7.

Table 7: Ranges of reagent concentrations for the considered experiments.

	Isoprene-NOx	MACR-NOx	MVK-NOx
[VOC] (ppm)	0.27–1.00	1.53–4.41	0.87–2.00
[NOx] (ppm)	0.15–0.60	0.24–0.57	0.51–0.60
[VOC]/[NOx]	0.62-2.08	3.57–9.19	1.73–3.72

5.7.1 Chemistry of isoprene photo-oxidation

The complete degradation chemistry of isoprene, as represented in MCM v3.1, consists of 605 reactions of 201 species. It can be viewed and downloaded using the subset mechanism assembling facility, available as part of the MCM website. The methodology of mechanism construction has been described in detail by Jenkin *et al.* (1997) and Saunders *et al.* (2003). The main features of the OH-initiated degradation chemistry when NO_X is present are summarized in Figure 43. This figure specifically illustrates the major oxidation routes which form the well-established C_4 unsaturated carbonyl products, MVK and MACR, in conjunction with HCHO, as these have most relevance to the evaluation activities described below. These carbonyls account for ca. 60% of the first generation products, with significant additional contributions made by the C_5 unsaturated aldehydes, $HOCH_2C(CH_3)=CHCHO$ and $HOCH_2CH=C(CH_3)CHO$ (not shown in the figure). As represented in MCM v3.1 (and partly shown in Figure 43), the further degradation of the C_4 and C_5 compounds leads ultimately to the generation of CO and CO_2 via intermediate carbonyl products such as methyl glyoxal ($CH_3C(O)CHO$), glycolaldehyde ($HOCH_2CHO$), glyoxal (CH(O)CHO) and HCHO.

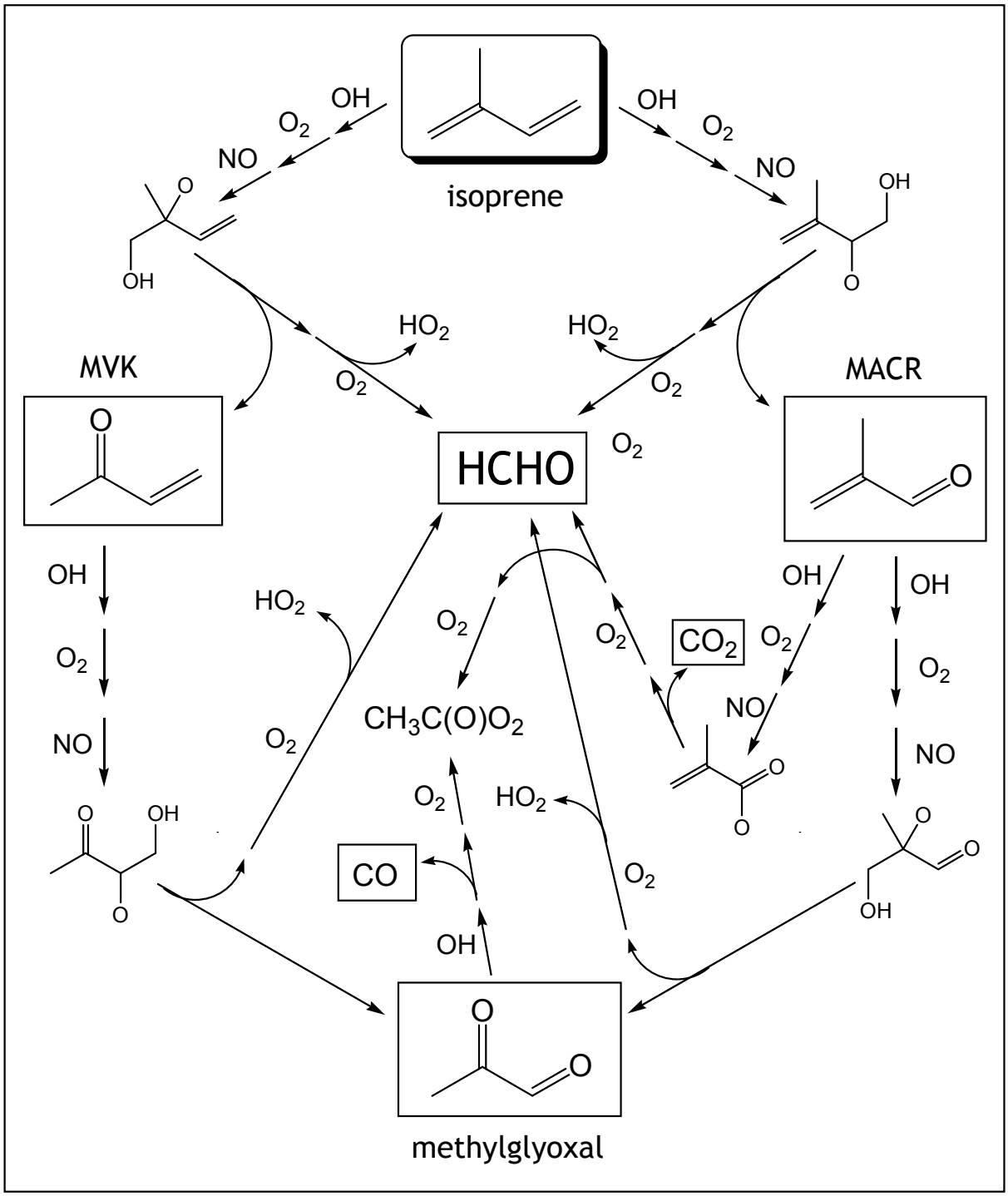

Figure 43: Partial schematic of the MCM representation of the radical propagation pathways of the OH-initiated degradation of isoprene, showing the major routes which proceed through formation of the intermediate products MVK and MACR. The further reactions of HCHO, CO and $CH_3C(O)O_2$ are shown in Figure 3. Reaction steps involving NO are reactions with organic peroxy radical intermediates, which lead to NO-to-NO_2 conversion and O_3 production (see discussion in text). The reactions of OH with isoprene, MVK and MACR possess additional channels which are fully represented in the mechanism, but not shown in the diagram. (Figure from Pinho *et al.,* 2005).

Many of the general VOC oxidation features, described above, also apply to the oxidation of isoprene. Thus, the OH-initiated chemistry at each stage is propagated by reactions of peroxy and oxy radical intermediates, with the number of NO-to-NO_2 conversions at each oxidation step, and the lifetimes of isoprene and the product carbonyl compounds, having an important influence on the rate of NO oxidation and O_3 formation.

The photolysis of the intermediate carbonyl products may have a secondary influence on the system, through photolysis to form free radicals. For example, in the cases of MVK and MACR, the following radical-forming channels are included:

$$MVK + h\upsilon\ (+3O_2) \rightarrow CH_3C(O)O_2 + HCHO + CO + HO_2 \quad (39)$$

$$MACR + h\upsilon\ (+2O_2) \rightarrow CH_2{=}C(CH_3)C(O)O_2 + HO_2 \quad (40)$$

$$MACR + h\upsilon\ (+3O_2) \rightarrow CH_3C(O)O_2 + HCHO + CO + HO_2 \quad (41)$$

Within the complete isoprene scheme, photolysis reactions are also included for other carbonyl products, and generally for products containing nitrate, hydroperoxide and peracid functionalities (Jenkin *et al.,* 1997 and Saunders *et al.,* 2003).

The removal of radicals through reactions of peroxy radical intermediates with NO and NO_2 is important. As discussed further below, the weighted average branching ratio for formation of hydroxyalkenyl nitrates from the reactions of the initially-formed isomeric C_5 hydroxyperoxy radicals with NO (reaction 43), is assigned a value of 10% in MCM v3.1,

$$HOC_5H_8O_2 + NO \rightarrow HOC_5H_8O + NO_2 \quad (42)$$

$$\rightarrow HOC_5H_8ONO_2 \quad (43)$$

and these (and similar) reactions thus have an influence on the radical balance in the system. The formation of PAN, and other peroxyacyl nitrates (generic formula $RC(O)OONO_2$), also occurs during isoprene degradation, leading to temporary radical loss:

$$RC(O)O_2 + NO_2 \leftrightarrows RC(O)OONO_2 \quad (31)$$

This occurs because $CH_3C(O)O_2$ radicals are generated from the degradation of MVK, MACR and methylglyoxal, and a number of other more complex acyl peroxy radicals (e.g. methacrolyl peroxy radicals from MACR degradation) are also represented in the MCM v3.1 scheme.

Because isoprene is an unsaturated hydrocarbon, there are features of the chemistry which have an important impact on its degradation under environmental chamber and atmospheric conditions. Of particular significance are the reactions of O_3 with isoprene itself, and with unsaturated products such as MVK and MACR, the MCM v3.1 formulation of which is described in detail by Jenkin *et*

al. (1997) and Saunders *et al.* (2003). In addition to supplementing the oxidation rate of these species, as already said above (section 5.6.1), these reactions have an important secondary influence through being sources of OH and other free radicals. In MCM v3.1, the yield of OH (and an organic radical formed simultaneously with OH) has assigned values of 27%, 36% and 82% for the reactions of O_3 with isoprene, MVK and MACR, respectively. Whereas the yield for isoprene is based on experimental determinations, the yields for MVK and MACR are based on those for the closest hydrocarbon analogues (Jenkin *et al.,* 1997).

The reactions of $O(^3P)$ with isoprene, MVK and MACR, and associated chemistry, were incorporated into the mechanism, as part of the development of MCM v3.1. This chemistry is summarised in Table 8, and discussed further below.

Table 8: Product channels and branching ratios assigned to the reactions of $O(^3P)$ with isoprene, MVK and MACR.

Reaction	Branching ratio [a]	Comment
isoprene		
$O(^3P) + CH_2=C(CH_3)CH=CH_2 \rightarrow CH_2^{-O-}C(CH_3)CH=CH_2$	0.78	(b)
$O(^3P) + CH_2=C(CH_3)CH=CH_2 (+3O_2) \rightarrow CH_3C(O)CH_2O_2 + HCHO + CO + HO_2$	0.22	(b)
methylvinyl ketone (MVK)		
$O(^3P) + CH_3C(O)CH=CH_2 \rightarrow CH_3C(O)CH^{-O-}CH_2$	0.44	(c)
$O(^3P) + CH_3C(O)CH=CH_2 \rightarrow CH_3C(O)CH_2CHO$	0.39	(c)
$O(^3P) + CH_3C(O)CH=CH_2 (+2O_2) \rightarrow HC(O)CH_2O_2 + HC(O)CH_2O_2$	0.17	(c)
methacrolein (MACR)		
$O(^3P) + CH_2=C(CH_3)CHO \rightarrow CH_2^{-O-}C(CH_3)CHO$	0.44	(d)
$O(^3P) + CH_2=C(CH_3)CHO \rightarrow HC(O)CH(CH_3)CHO$	0.39	(d)
$O(^3P) + CH_2=C(CH_3)CHO (+2O_2) \rightarrow CH_3C(O)CH_2O_2 + CO + HO_2$	0.17	(d)

Notes:

(a) displayed values are those applied with optimized mechanism.

(b) $k = 3.5 \times 10^{-11}$ cm^3 molecule^{-1} s^{-1}, based on Calvert *et al.* (2000). Dominant formation of oxiranes based on the results of Paulson *et al.* (1992). Displayed oxirane is representative of the two possible isomers. Products of radical channel defined by analogy with those suggested for reactions involving simple alkenes (Calvert *et al.,* 2000). Branching ratio optimised as described in the text. Oxirane removed by reaction with OH (estimated $k = 3.5 \times 10^{-11}$ cm^3 molecule^{-1} s^{-1}) to form products already present in mechanism.

(c) Applied $k = 2.11 \times 10^{-12}$ cm^3 molecule^{-1} s^{-1}, based on correlation of OH and $O(^3P)$ reactivities, as reported by Carter (2000). Branching ratios and products based on those for hydrocarbon analogue, 1-butene (Calvert *et al.,* 2000). Oxirane removed by reaction with OH (estimated $k = 2.0 \times 10^{-12}$ cm^3 molecule^{-1} s^{-1}) to form products already present in mechanism.

(d) Applied $k = 6.19 \times 10^{-12}$ cm^3 molecule^{-1} s^{-1}, based on correlation of OH and $O(^3P)$ reactivities, as reported by Carter (2000). Branching ratios and products inferred from those reported for closest hydrocarbon analogue for which data are available, 1-butene (Calvert *et al.,* 2000). Oxirane removed by reaction with OH (estimated $k = 5.3 \times 10^{-13}$ cm^3 molecule^{-1} s^{-1}) to form products already present in mechanism.

Initial simulations were carried out to test the performance of the MCM v3.1 isoprene mechanism against the chamber isoprene-NO_X photo-oxidation data (see Figure 44 to Figure 47). As shown in Figure 44, the MCM v3.1 isoprene mechanism was found to provide a reasonable description of the overall oxidation of NO within the course of the experiments, but tended to underestimate $D(O_3$-NO) in the early stages. In conjunction with this, the simulated decay of isoprene, and formation of the products MVK, MACR, was delayed relative to the observations, see Figure 45 to Figure 47.

As with the butane system, a procedure was adopted in which the available NO_X photo-oxidation runs for the major carbonyl products were used to test and refine the corresponding subsets of the mechanism, prior to a re-evaluation of the full isoprene scheme. This step-by-step approach is advantageous, because it allows compensating errors in the sub-mechanisms to be eliminated. The consideration of HCHO photo-oxidation (as described in section 5.4.1.1) is clearly also of

relevance to the isoprene system, and evaluation of the MACR and MVK chemistry is now described.

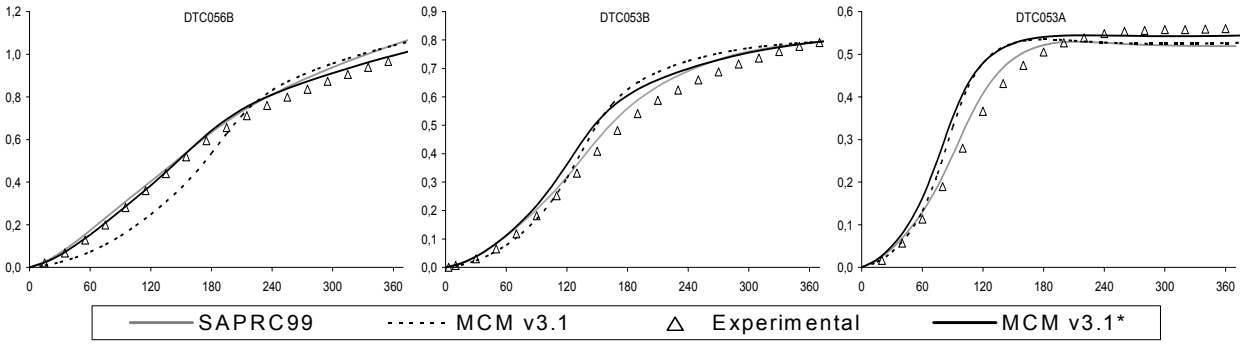

Figure 44: Plots of experimental and calculated D(O_3-NO) (ppm) vs. time (min) for the isoprene – NO_x -air experiments. MCM v3.1* correspond to the MCM after the refine of the butane scheme (MCM v3.1a) plus the refine of isoprene scheme.

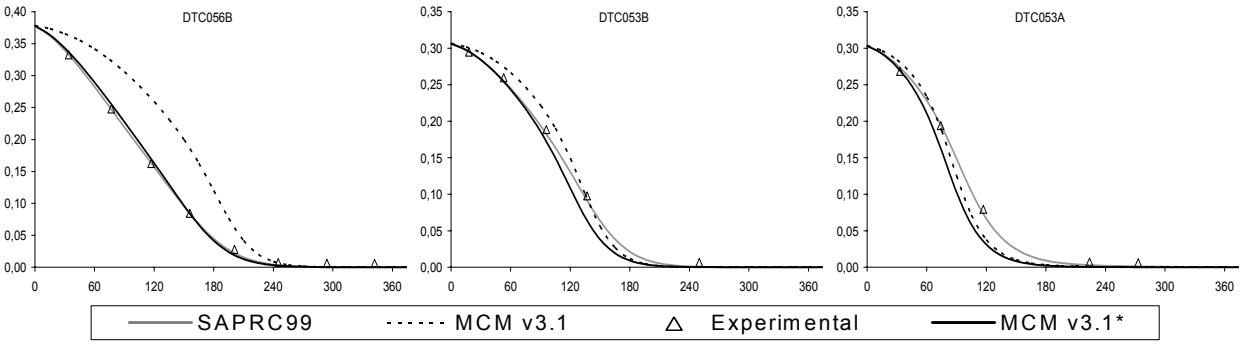

Figure 45: Plots of experimental and calculated isoprene (ppm) vs. time (min) for the isoprene – NO_x -air experiments. Legend as in Figure 44.

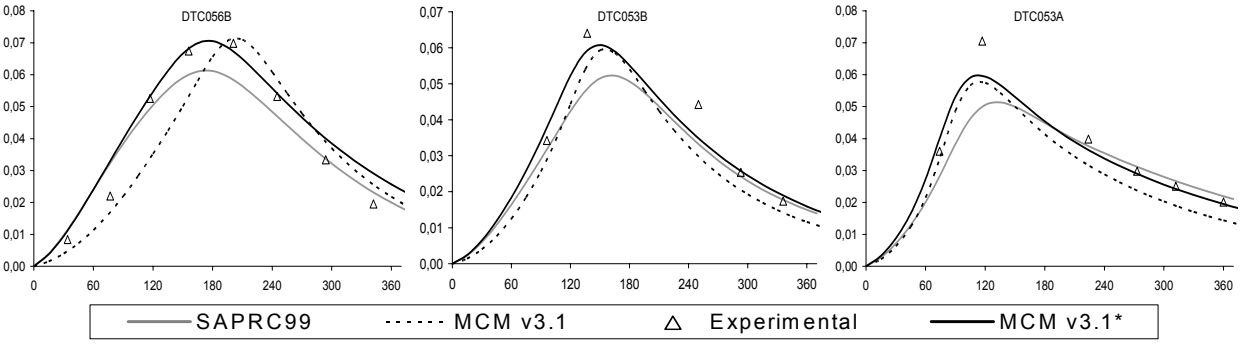

Figure 46: Plots of experimental and calculated MVK (ppm) vs. time (min) for the isoprene – NO_x - air experiments. Legend as in Figure 44.

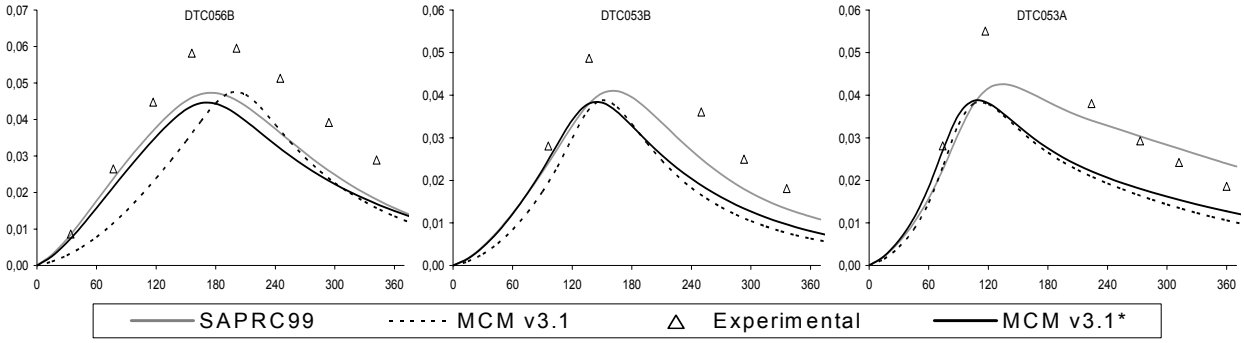

Figure 47: Plots of experimental and calculated MACR (ppm) vs. time (min) for the isoprene – NOx -air experiments. Legend as in Figure 44.

5.7.2 MACR-NO_X experiments

As shown in Figure 48, MCM v3.1 was found to over-predict significantly the observed D(O_3-NO) in the initial stages of the experiments, but with the final values being slightly lower than those observed. This behaviour was indicative of systematic errors in the input of radicals to the system, and a number of modifications were therefore considered to insert in MCM v3.1. Within the existing mechanistic framework, the representation of the radical yields from MACR photolysis and from its reaction with O_3 was revised. In addition to this, the reaction of O(^{3}P) with MACR, which may partially produce radicals, was incorporated into the mechanism.

As indicated above (section 5.7.1), the OH yield from the ozonolysis of MACR, as represented in MCM v3.1, is 82%. Based on the results of Aschmann *et al.* (1996), this value was reduced significantly to 20% during the isoprene system refine. This had a small, but significant effect on the calculated radical input to the system, typically leading to a slightly reduced rate of increase in D(O_3-NO) in the middle stages of the experiments and a small delay in achieving the maximum value.

There have been no studies of the kinetics, or products of the reaction, of O(^{3}P) reaction with MACR. However this reaction could play a role in MACR degradation under environmental chamber conditions. For the present study, therefore, the reactions presented in Table 8 were incorporated into the refined MCM v3.1 mechanism. Carter (2000) has demonstrated that available rate coefficients for reactions of alkenes with O(^{3}P) and OH show a good degree of correlation, providing the basis of an estimation method for O(^{3}P) rate coefficients. As part of that study, a rate coefficient of 6.19 x 10^{-12} cm^{-3} $molecule^{-1}$ s^{-1} was estimated for the reaction of O(^{3}P) with MACR, and this value is also adopted in the present work. By analogy with reported data for simple alkenes (Calvert *et al.,* 2000), three assumed product channels, resulting from initial addition of O(^{3}P) to the double bond, were included. As shown in Table 8, two of these channels have molecular

products, forming either the corresponding oxirane, or the isomeric carbonyl, 2-methyl-malonaldehyde. The third channel, accounting for 17% of the reaction, was assumed to proceed *via* adduct fragmentation, leading to the ultimate generation of the free radicals, $CH_3C(O)CH_2O_2$ and HO_2 (see Table 8). Although it was necessary to include the reaction of MACR with $O(^3P)$ for completeness, the effect of its inclusion was found to be very minor.

Raber and Moortgat (1996) demonstrated that the photolysis quantum yield for MACR is substantially below unity. They reported an upper limit quantum yield of 0.03, which was adopted for use in MCM v3.1 (Jenkin *et al.,* 1997; Saunders *et al.,* 2003). More recently, Gierczak *et al.* (1997) and the EU RADICAL consortium (RADICAL, 2002), have reported reduced upper limit quantum yields of <0.01 and <0.004, respectively. In conjunction with the above changes for the O_3 and $O(^3P)$ reactions, the quantum yield was therefore varied in MCM v3.1 to optimize the description of the MACR-NO_X chamber data. The results were found to be very sensitive to this parameter, and a best fit value of 0.0036 was obtained, which is fully consistent with the more recent studies above. This value is also consistent with the value of 0.0041 derived by Carter (2000), during optimization of the SAPRC-99 mechanism.

The overall influence of the above changes is shown in Figure 48 to Figure 50, with the change in the applied quantum yield for MACR photolysis being mainly responsible for the difference between the performance of the MCM v3.1 and MCM v3.1* schemes (MCM v3.1* correspond to MCM after the refine of the butane scheme (MCM v3.1a) plus the refine of isoprene scheme). MCM v3.1* thus provides a much improved description of the initial D(O_3-NO) values, although a tendency towards slight under-prediction at longer experimental durations remains.

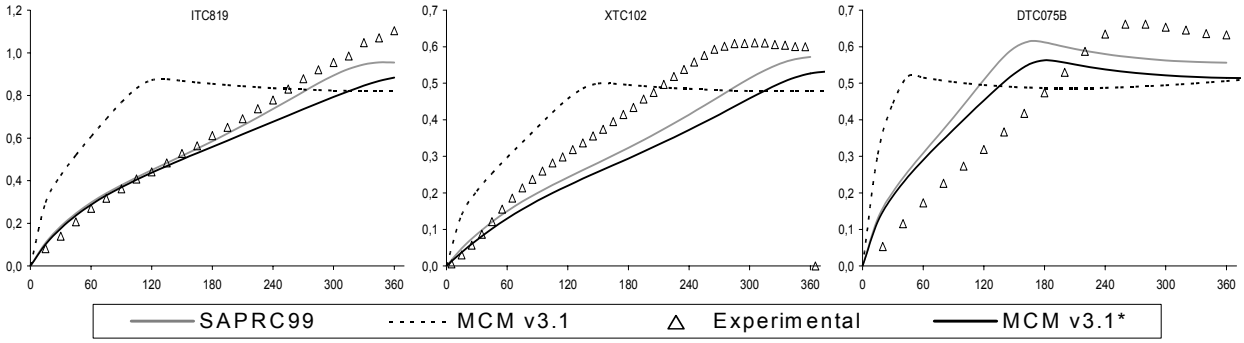

Figure 48: Plots of experimental and calculated D(O_3-NO) (ppm) vs. time (min) for the MACR – NO_x –air experiments. MCM v3.1* correspond to MCM after the refine of the butane scheme (MCM v3.1a) plus the refine of isoprene scheme.

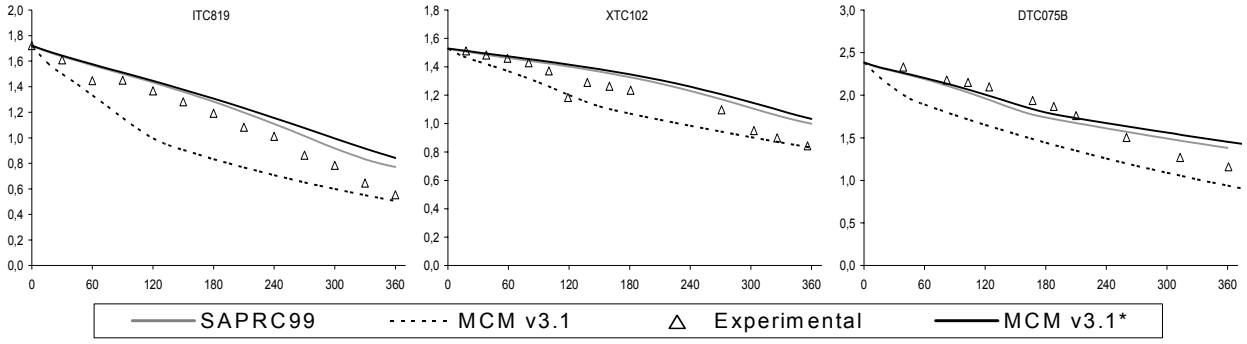

Figure 49: Plots of experimental and calculated MACR (ppm) vs. time (min) for the MACR – NO_x –air experiments. Legend as in Figure 48.

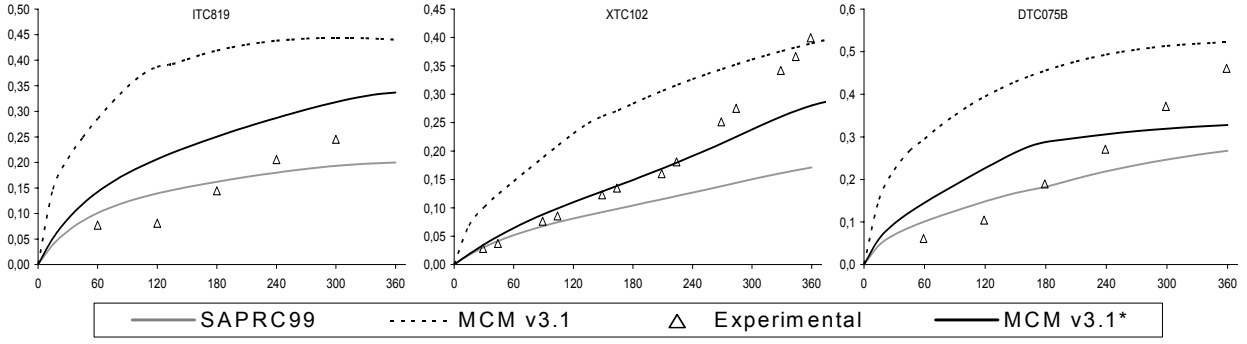

Figure 50: Plots of experimental and calculated HCHO (ppm) vs. time (min) for the MACR – NO_x –air experiments. Legend as in Figure 48.

5.7.3 MVK-NO_X experiments

Similarly to the MACR-NO_X system, MCM v3.1 was found to over-predict significantly the observed D(O_3-NO) in the initial stages of the MVK-NO_X experiments, but with the final values being slightly lower than those observed (see Figure 51). Once again, therefore, modifications were made to the representation of the radical yields from MVK photolysis and reaction with O_3; the reaction of $O(^3P)$ with MVK was also incorporated into the MCM mechanism.

As indicated above (section 5.7.1), the OH yield from the ozonolysis of MVK, as represented in MCM v3.1, is 36%. Based on the results of Aschmann *et al.* (1996) and Paulson *et al.* (1998), this value was reduced to 16% during the isoprene system refine. This had a notable effect on the calculated radical input to the system, which resulted in a reduced rate of increase in D(O_3-NO) middle stages of the experiments and a small, but significant delay in achieving the maximum value.

In the absence of studies of the reaction of $O(^3P)$ with MVK, the kinetics and mechanism inserted in the refined version of the mechanism were once again defined by analogy, as shown in Table 8. The assigned rate coefficient, 2.11 x 10^{-12} cm^{-3} $molecule^{-1}$ s^{-1}, was based on the estimate of Carter (2000) using the correlation with OH reactivity described above. Three product channels were included for the reaction, which were defined by analogy with reported data for the closest hydrocarbon analogue, 1-butene (Calvert *et al.,* 2000). In this case, the two molecular channels are assumed to form either the corresponding oxirane, or the isomeric carbonyl, 3-oxo-butyraldehyde. The third channel, accounting for 17% of the reaction, was assumed to lead to the ultimate generation of $HC(O)CH_2O_2$, as shown in Table 8. Once again, however, inclusion of the reaction of MVK with $O(^3P)$ was found to have only a very minor influence on the simulations.

In MCM v3.1, a quantum yield of 0.05 is assigned to the photolysis of MVK, based on the upper limit value of Raber and Moortgat (1996). More recently, Gierczak *et al.* (1997) measured quantum yields, as a function of pressure and wavelength, which confirmed that MVK is photolysed inefficiently at atmospheric pressure, the values being lower on average than the upper limit of Raber and Moortgat (1996). Subsequently, the EU RADICAL consortium (RADICAL, 2002) has reported an overall upper limit quantum yield of <0.004 for photolysis in natural sunlight. In conjunction with the above changes for the O_3 and $O(^3P)$ reactions, the quantum yield expression recommended by Gierczak *et al.* (1997) was implemented in the refined version of MCM.

The combined effect of the above modifications is shown in Figure 51 to Figure 54. The change in the applied quantum yield for MVK photolysis is the most important factor responsible for the difference between the performance of the MCM v3.1 and MCM v3.1* schemes (MCM v3.1* corresponds to MCM after the refine of the butane scheme (MCM v3.1a) plus the refine of isoprene scheme), with the reduction in the radical yield from the O_3 reaction having a smaller, but still significant, effect.

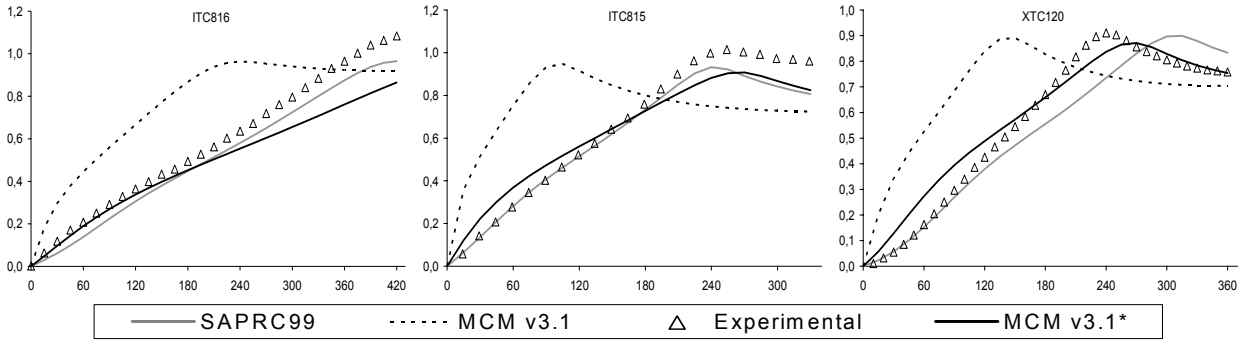

Figure 51: Plots of experimental and calculated $D(O_3\text{-}NO)$ (ppm) vs. time (min) for the MVK – NO_x –air experiments. MCM v3.1* correspond to MCM after the refine of the butane scheme (MCM v3.1a) plus the refine of isoprene scheme.

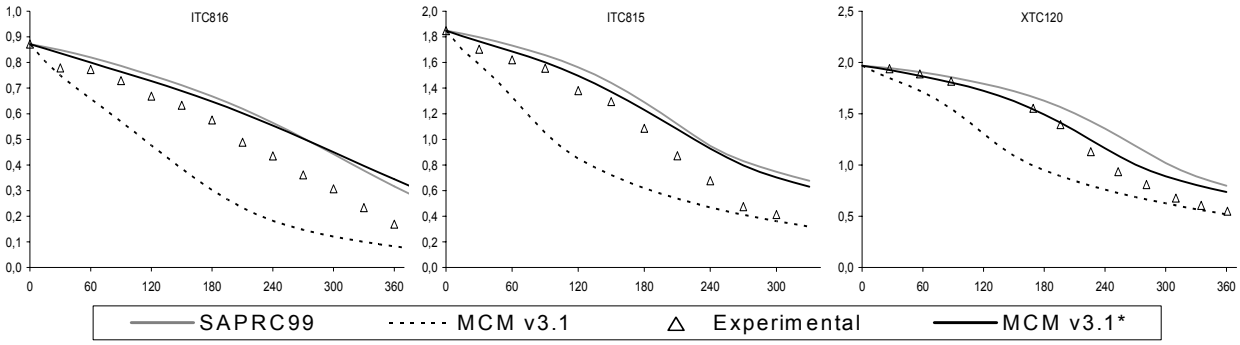

Figure 52: Plots of experimental and calculated MVK (ppm) vs. time (min) for the MVK – NO_x –air experiments. Legend as in Figure 51.

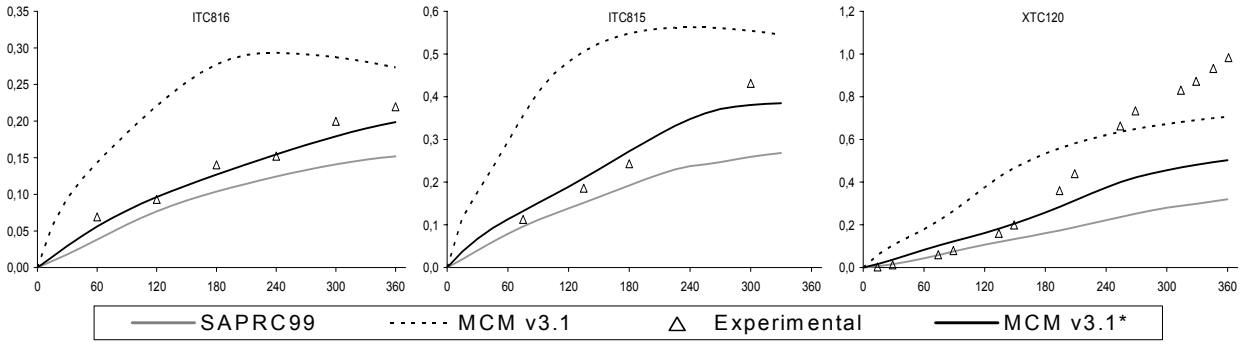

Figure 53: Plots of experimental and calculated HCHO (ppm) vs. time (min) for the MVK – NO_x –air experiments. Legend as in Figure 51.

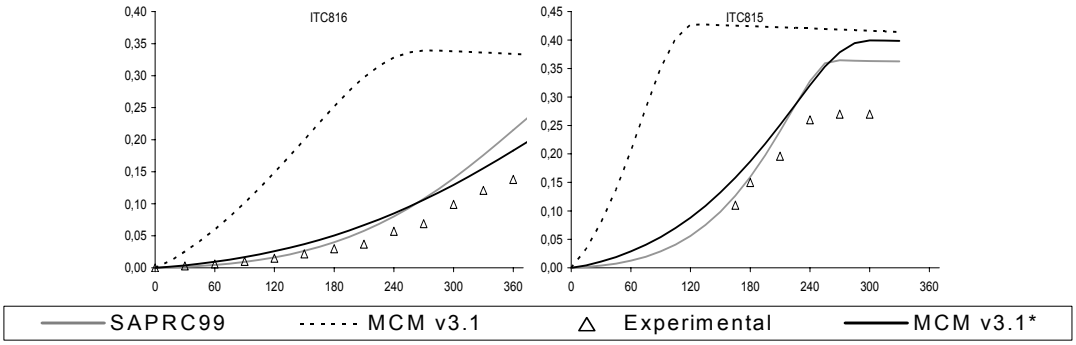

Figure 54: Plots of experimental and calculated PAN (ppm) vs. time (min) for the MVK – NO_x –air experiments. Legend as in Figure 51.

5.7.4 Isoprene-NO_X experiments

Prior to re-evaluation of the full isoprene mechanism (with the above changes for MACR and MVK included), the reaction of $O(^3P)$ with isoprene was also incorporated, using the reaction steps shown in Table 8. This reaction has been studied by Paulson *et al.* (1992), who concluded that the

reaction leads predominantly to the formation of oxiranes (85±9)%, following addition of $O(^3P)$. This is also consistent with the reported dominant formation of oxiranes and other molecular products (ca. 75-90%) from the reactions of $O(^3P)$ with $>C_3$ alkenes in general (Calvert *et al.,* 2000) and 1,3-butadiene, suggesting that radical forming channels are likely to be restricted to ca. 10-25% of the isoprene + $O(^3P)$ reaction (Carter *et al.,* 1996 and references therein). The precise radical yield value was therefore optimized on the basis of the chamber experiments, leading to a best fit value of 22% which is consistent with the above range. The remaining 78% of the reaction was assumed to lead to oxirane formation, which is compatible with the results of Paulson *et al.* (1992). Figure 44 to Figure 47 demonstrate that the resultant optimized MCM v3.1 mechanism provides an improved representation of $D(O_3\text{-NO})$, isoprene decay, and formation of HCHO, MVK and MACR, when compared with the chamber experimental data series. Although the modifications to the treatment of HCHO, MACR and MVK described above have a slight effect on the performance of the parent isoprene mechanism, the differences betweens the simulations using the MCM v3.1 and MCM v3.1* schemes are mainly due to inclusion of the $O(^3P)$ reaction in MCM v3.1*. This indicates that the two mechanisms would perform similarly in atmospheric models, under conditions when the $O(^3P)$ reaction is unimportant.

It was also clear that the value assigned to the branching ratio for radical production from the $O(^3P)$ reaction can be influenced by assumptions concerning the formation of hydroxyalkenyl nitrates from reaction (43), since this also has an impact on the radical balance in the system. The value of 10% adopted in MCM v3.1, for the branching ratio $k_{43}/(k_{42}+ k_{43})$, is based on the results of a number of studies (see Jenkin *et al.,* 1998 and references therein). However, reported values cover the range from as low as 4.4% (Chen *et al.,* 1998), to as high as 14% (Paulson *et al.,* 1992), indicating that some uncertainty exists in this parameter value. Consequently, it is possible that compensating changes can be made to the radical yield from the $O(^3P)$ reaction, and the extent of radical loss by reaction (43), leading to similar simulated results. The optimization procedure was therefore repeated with $k_{43}/(k_{42}+ k_{43})$ varied over the reported range. As expected, the use of lower values of $k_{43}/(k_{42}+ k_{43})$ resulted in smaller optimized radical yields from the $O(^3P)$ reaction, and *vice-versa*. However, the results with other optimized combinations were never as good as those simulated with the base case values, and particularly poor fits were obtained if the radical yield from the $O(^3P)$ reaction was assumed to be zero. The best description of the system was therefore obtained with $k_{43}/(k_{42}+ k_{43}) = 0.1$, and with the radical channel of the $O(^3P)$ reaction accounting for 22% of the total. These conclusions are similar to those of Carter (Carter, 2002), who determined simultaneously optimized values of $k_{43}/(k_{42}+ k_{43}) = 0.088$, and 25% for the $O(^3P)$ radical-forming channel, during the evaluation of SAPRC-99 mechanism.

5.8 α-Pinene and β-pinene Photo-oxidation Mechanism Assessment

Like isoprene, the monoterpenes α-pinene and β-pinene are volatile organic compound ubiquitous in the lower troposphere. α-Pinene and β-pinene are of natural origin, being emitted largely by vegetation, namely coniferous plants as well as on members of the families *Lami-aceae, Apiaceae, Rutaceae, Myrtaceae and Asteraceae, QuercusIlex and Quercus robur* (e.g. Kesselmeier and Staudt, 1999 and references therein).

Emission rates of monoterpenes are species and seasonally dependent, and increase exponentially with temperature (e.g. Guenther *et al.,* 1995). As result of the large emission rates (estimates for the global carbon input by monoterpenes range 127 Tg C yr^{-1} (Guenther *et al.,* 1995)), and a high chemical reactivity, monoterpenes play an important role in atmospheric chemistry, principally in non-urban areas, but also in atmospheric processes at a global level.

Much emphasis has been placed on α- and β-pinene, since measurements of monoterpene speciation suggest that these make a particularly significant contribution to global monoterpenes emissions (e.g., Guenther *et al.,* 1994 and references therein), and also because they are representative of classes of monoterpene having either a cyclic double bond (in the case of α-pinene) or an exocyclic double bond (in the case of β-pinene) (Jenkin *et al.,* 2000a).

It is well established that α-pinene and β-pinene react with OH, O_3, $O(^3P)$ and NO_3 (e.g. Calvert *et al.,* 2000). During daylight the reaction with OH and with O_3 tends to be the major tropospheric degradation processes contributing to α-pinene and β-pinene loss. NO_3 plays a non-negligible role in oxidation during the night (e.g. Wängberg *et al.,* 1997; Hallquist *et al.,* 1999).

Particular progress has been made in defining the kinetics and mechanisms of the early stages of the gas-phase degradation chemistry of α-pinene and β-pinene initiated by reaction with OH, O_3 and NO_3 (e.g., Calvert *et al.,* 2000 and references therein; Atkinson and Arey, 2003 and references therein).

The major oxidation route, initiated by reaction of α-pinene with OH, has been shown to yield pinonaldehyde, organic nitrates, formaldehyde and acetone as the main oxidation products, when NO_X is present (e.g., Arey *et al.,* 1990; Hatakeyama *et al.,* 1991; Hakola *et al.,* 1994; Noziere *et al.,* 1999; Ruppert *et al.,* 1999; Orlando *et al.,* 2000; Wisthaler *et al.,* 2001; Aschmann *et al.* 2002). The reaction of α-pinene with O_3, besides giving origin to the same oxidation products obtained from reaction with OH, produces OH (e.g., Atkinson *et al.,* 1992b; Chew and Atkinson, 1996; Paulson *et al.,* 1998; Rickard *et al.,* 1999; Siese *et al.,* 2001.)

The OH-initiated degradation chemistry, of β-pinene has been shown to yield nopinone, formaldehyde and acetone as the main oxidation products, when NO_X is present (e.g., Arey *et al.,* 1990; Hatakeyama *et al.,* 1991; Hakola *et al.,* 1994; Aschmann *et al.,* 1998; Orlando *et al.,* 2000; Wisthaler *et al.,* 2001). Also OH is obtained by reaction of β-pinene with O_3 (Atkinson *et al.,* 1992a), as well as nopinone and formaldehyde (e.g., Hatakeyama *et al.,*1989; Grosjean *et al.,* 1993b; Ruppert *et al.,* 1999; Yu *et al.,* 1999; Winterhalter *et al.,* 2000).

Like for isoprene, is important for a complete understanding of atmospheric processes that the atmospheric oxidation of α-pinene and β-pinene is well understood and correctly represented in computer airshed models used to simulate urban and regional air quality. Therefore various representations of α-pinene and β-pinene photo-oxidation chemistry are included in urban or regional airshed models currently in use for research or regulatory purposes (e.g. Carter, 2000; Saunders *et al.,* 2003).

The set of chamber experimental runs employed in the present evaluation consisted of a database of 6 α–pinene-NO_X-air, 6 β–pinene-NO_X-air and 5 acetone-NO_X-air experiments. The range of reagent concentrations for the considered experiments is presented in Table 9.

Table 9: Ranges of reagent concentrations, relative humidities and NO_2 photolysis constants (k_6) for the considered experiments.

	α-pinene-NOx	β-pinene-NOx	acetone-NOx
n.º of available runs	6	6	5
[VOC] (ppm)	0.263-0.445	0.265-0.968	8.461-15.000
[NOx] (ppm)	0.132-0.534	0.137-0.293	0.137-0.286
[VOC]/[NOx]	0.523-2.128	0.946-3.301	37.338-102.810

5.8.1 Chemistry of α-pinene and β-pinene photo-oxidation

The complete degradation chemistry, as represented in MCM v3.1, consists of: 925 reactions of 321 species for α–pinene; and 1149 reactions of 400 species for β–pinene. The methodology of mechanism construction of α- and β-pinene has been described in detail by Saunders *et al.* (2003), with chemistry initiated by reaction with OH, O_3 and NO_3 represented in each case. Salient features of the OH and O_3-initiated chemistry are now summarized. For the photo-oxidation conditions considered here, the systems are insensitive to the NO_3-initiated chemistry which is therefore not discussed further.

The main features of the OH-initiated degradation chemistry to first generation products when NO_X is present are summarized in Figure 55. Oxidation of both α– and β–pinene in MCM v3.1 proceeds

by sequential addition of OH and O_2 leading, in each case, to the initial formation of three isomeric hydroxyl-substituted peroxy radicals (RO_2). Addition of OH at the more substituted sites, followed by O_2 addition, leads to the formation of the secondary and primary radicals, APINBO2 and BPINBO2. Addition of OH at the less-substituted sites generates hydroxy-substituted tertiary organic radicals, which are assumed to isomerise partially, prior to O_2 addition, following the mechanism suggested by Noziere *et al.* (1999) and Vereecken and Peeters (2000) for α-pinene. The importance of the isomerisation mechanism is set such that the primary yield of the isomerised radicals (APINCO2 and BPINCO2) is 7.5 %, this constraint being guided by the yields of acetone reported in the literature (see below). In each case, therefore, the hydroxy-substituted tertiary organic radicals mainly react with O_2 (i.e., in preference to isomerisation) to generate the major radicals APINAO2 and BPINAO2 (see Figure 55).

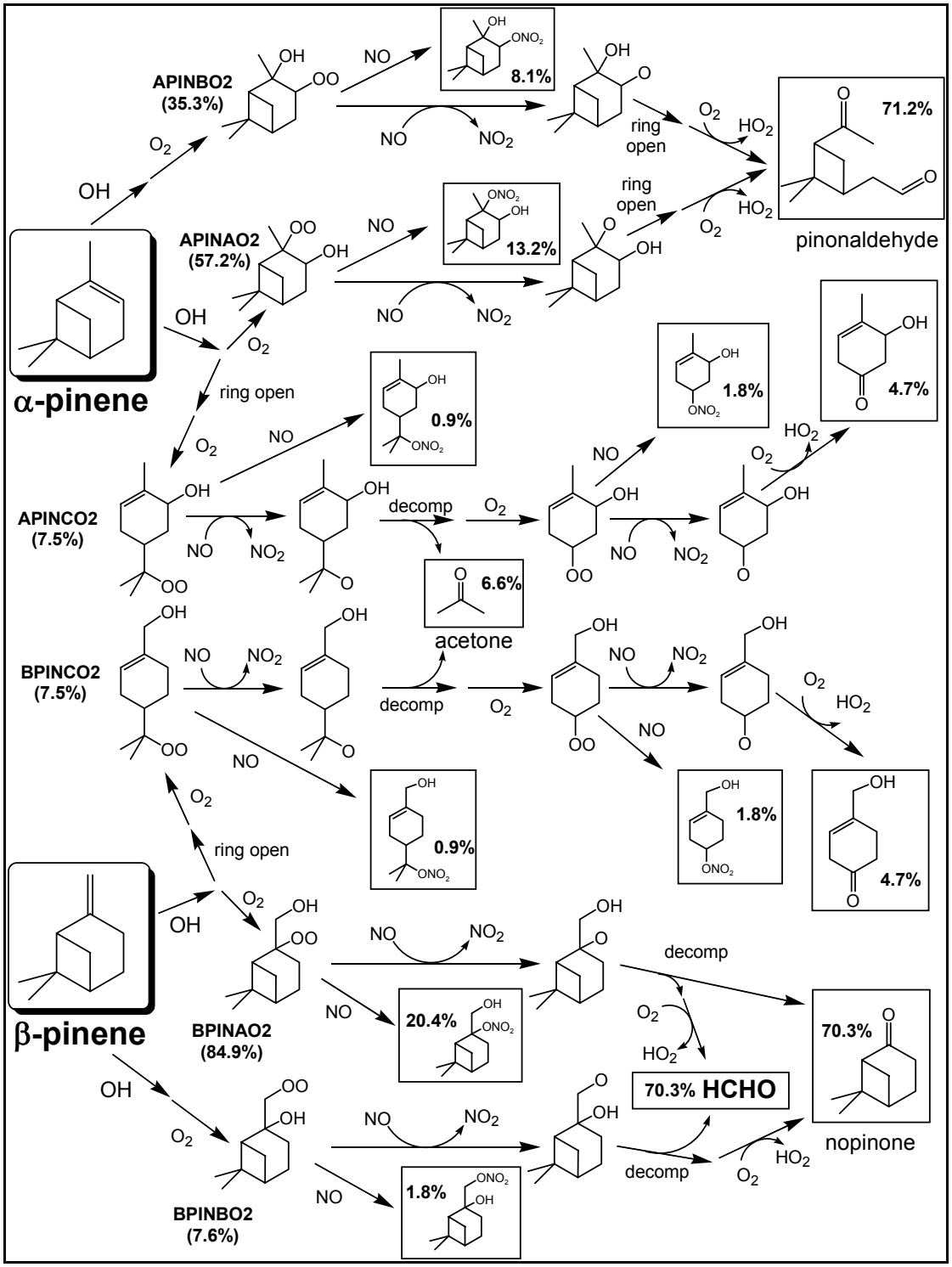

Figure 55: Partial schematic of the MCM representation of the radical propagation pathways of the OH-initiated degradation of α- and β-pinene, showing the major routes which proceed through formation of the intermediate products pinonaldehyde and nopinone.

As described by Saunders *et al.* (2003), the initial OH addition ratios applied in MCM v3.1 were estimated using the SAR method of Peeters *et al.* (1994). More recently Peeters *et al.* (2001) and Capouet *et al.* (2004) have calculated and applied substantially modified ratios for the initial RO_2 radical distribution. This is considered further below in the sensitivity studies (section 5.8.3).

The general VOC oxidation features, described in sections above, also apply to the oxidation of α- and β-pinene. Thus, the subsequent chemistry in the presence of NO_X leads predominantly to the formation of carbonyl products, with their subsequent oxidation leading ultimately to the formation of CO and CO_2. At each oxidation stage, the chemistry is propagated by reactions of peroxy (RO_2) and oxy (RO) radical intermediates. For example, the initial oxidation sequence involving BPINAO2 proceeds via the following catalytic cycle:

$$OH + \beta\text{–pinene } (+O_2) \rightarrow BPINAO2 \quad (44)$$

$$BPINAO2 + NO \rightarrow BPINAO + NO_2 \quad (45)$$

$$BPINAO \rightarrow nopinone + CH_2OH \quad (46)$$

$$CH_2OH + O_2 \rightarrow HCHO + HO_2 \quad (24)$$

$$HO_2 + NO \rightarrow OH + NO_2 \quad (4)$$

The peroxy radicals (RO_2 and HO_2) thus provide the coupling with the chemistry of NO_X, which leads to NO-to-NO_2 conversion, and formation of O_3 upon photolysis of NO_2, reactions (1) and (2).

The subsequently-formed oxy radicals determine the identity or identities of the carbonyl products generated from the degradation. In MCM v3.1, the radicals APINAO, APINBO, BPINAO and BPINBO are assumed to undergo exclusive C-C bond scission, leading to the formation of the major carbonyl products, pinonaldehyde (in the case of α–pinene) and nopinone and HCHO (in the case of β–pinene), resulting in molar yields of ca. 70 % in each case from the NO_X-propagated chemistry. These are generally at the high end of the yield ranges reported in the literature (Arey *et al.,* 1990; Hatakeyama *et al.,* 1991; Hakola *et al.,* 1994; Noziere *et al.,* 1999; Wisthaler *et al.,* 2001; Aschmann *et al.* 2002): (28–87) % for pinonaldehyde; (25–79) % for nopinone; (45–54) % for HCHO. A number of studies have considered potentially competing 1,5-H atom shift isomerisation reactions for the above oxy radicals, particularly in relation to the observed formation of HCHO as a first generation product of α–pinene oxidation (Noziere *et al.,* 1999; Orlando *et al.,* 2000; Peeters *et al.,* 2001).

The radicals APINCO and BPINCO are also assumed to undergo exclusive C-C bond scission in MCM v3.1, leading in each case to the formation of acetone and an unsaturated hydroxy-substituted C_7 cyclic radical. The resultant yield of acetone from the NO_X-propagated chemistry in

both terpene systems (6.6 %) is consistent with the ranges reported in the literature (Aschmann *et al.,* 1998; Noziere *et al.,* 1999; Orlando *et al.,* 2000; Wisthaler *et al.,* 2001): (5−15) % for α−pinene; (2−13) % for β−pinene. As shown in Figure 55, the cyclic radicals, formed in conjunction with acetone, are assumed to be oxidised mainly to form cycloketone products, via conventional reactions of the corresponding RO_2 and RO intermediates with NO and O_2, respectively.

The further degradation of the first (and subsequent) generation carbonyl products by reaction with OH, leads to further NO-to-NO_2 conversion (and therefore O_3 formation). Consequently, the number of NO-to-NO_2 conversions at each oxidation step, and the lifetimes of the parent terpene and its product carbonyls (which are partially determined by their OH reactivity) have an influence on the rate of NO oxidation and O_3 formation. Whereas the chemistry of the simple carbonyl products (i.e., HCHO and acetone) is well established (and represented in MCM v3.1), there is comparatively little experimental information on the oxidation mechanisms of the more complex species, in particular the major products pinonaldehyde and nopinone. Their degradation is therefore based on the generic rules described in the MCM protocols (Jenkin *et al.,* 1997; Saunders *et al.,* 2003). In the case of pinonaldehyde, the NO_X-propagated degradation chemistry (*via* two H atom abstraction channels), follows two sequences, each leading to the ultimate formation of HCHO, acetone and a C_5 tricarbonyl. Because these sequences include a number of isomerisation and decomposition/ring-opening steps, and thus each involves five intermediate RO_2 radicals (and NO-to-NO_2 conversions), the oxidation of pinonaldehyde into these second generation products is comparatively efficient at generating ozone. A more detailed theoretical appraisal of the OH initiated degradation of pinonaldehyde has been performed by Fantechi *et al.* (2002), and subsequently applied by Capouet *et al.* (2004). The impacts of the recommendations of this appraisal on the present chamber simulations are considered in the sensitivity studies described below (section 5.8.3).

The NO_X propagated degradation chemistry of nopinone in MCM v3.1 proceeds via four H atom abstraction channels. Similarly to pinonaldehyde, a substantial proportion (ca. 80 %) of this chemistry follows reaction sequences with a number of isomerisation and decomposition/ring-opening steps, leading to the formation of acetone and C_6 tricarbonyl co-products. However, a notable proportion (ca. 20 %) proceeds via a short reaction sequence, in which the relevant RO radical reacts with O_2 to generate a diketone product (6,6-dimethyl-bicyclo[3.1.1]heptane-2,4-dione) which retains the bicyclic carbon skeleton. This latter sequence is thus comparatively inefficient a generating ozone, both intrinsically, and also because the bicyclic diketone product is estimated to be of lower reactivity than nopinone by a factor of ca. 3.

The chemistry represented in the previous set of reactions (44, 45, 46, 24, 4) consists entirely of propagation reactions which conserve the radical population in the system. The organic degradation chemistry can also influence oxidation rates, and therefore O_3 formation, through either producing or removing radicals, and such processes have generally been shown to have a major influence on mechanism performance. The photolysis of carbonyl compounds is a potential source of free radicals, which may have an important influence. Of relevance to the current systems is the photolysis of the simple carbonyls, HCHO and acetone, and of some of the more complex carbonyls, such as pinonaldehyde and related species.

The sensitivity of the α–pinene simulations to the implementation of molecular product channels for pinonaldehyde and related species photolysis is discussed further below (section 5.8.3).

At the typical concentrations of NO_X in chamber experiments, the reactions of intermediate peroxy radicals with either NO or NO_2 may contribute to radical removal. The reactions of RO_2 with NO generally possess terminating channels, forming the corresponding organic nitrate product, the branching ratios of which are sensitive to the size and structure of the RO_2 radical:

$$RO_2\cdot + NO + M \rightarrow RONO_2 + M \qquad (19)$$

As indicated by the total nitrate product yields shown in Figure 55, the weighted average branching ratios, for first generation nitrate product formation in MCM v3.1 are assigned values of 24 % and 25 % for the oxidation of α– and β–pinene, respectively, based on the data reported by Ruppert *et al.* (1999) for a series of monoterpenes. The sensitivity to variations in the α–pinene nitrate yields, within the context of literature uncertainties, is discussed further below (section 5.8.3).

The reactions with NO_2 tend to be most significant for acyl peroxy radicals, leading to the formation of peroxyacyl nitrates. The MCM v3.1 degradation schemes for α– and β–pinene include the respective formation of ca. 20 and ca. 30 acyl peroxy radicals (of generic formula $RC(O)O_2$). These include the acetyl peroxy radical, $CH_3C(O)O_2$, but are mainly constituted by complex multifunctional species. The reversible reactions of the $RC(O)O_2$ radicals with NO_2, to form the corresponding peroxyacyl nitrates, potentially leads to temporary loss of free radicals:

$$RC(O)O_2 + NO_2 \leftrightarrows RC(O)OONO_2 \qquad (31)$$

As described in detail elsewhere (Jenkin *et al.,* 1997, Jenkin *et al.,* 2003 and Saunders *et al.,* 2003), MCM v3.1 incorporates all the above types of process explicitly, in addition to competitive reactions which gain in significance at lower concentrations of NO_X.

The kinetics and mechanistic representation of the reactions of O_3 with α– and β–pinene is described in detail by Jenkin *et al.* (2000) and Saunders *et al.* (2003). In addition to supplementing

the oxidation rate of the terpenes, these reactions have an important secondary influence through being sources of OH and other free radicals. The mechanism proceeds in each case *via* addition of O_3 to the double bond, leading initially to formation of energy rich ozonides. In the case of α–pinene (which contains an endocyclic double bond), the ozonide decomposes rapidly by two ring opening channels to form isomeric C_{10} carbonyl-substituted Criegee biradicals, which also possess excess energy. In the case of β–pinene (which contains an exocyclic double bond), the ozonide decomposes by two possible channels, forming either HCHO and an energy rich C_9 Criegee biradical, or nopinone and the energy rich Criegee biradical, $[CH_2OO]^*$. The energy rich Criegee biradicals are assumed to be either collisionally stabilized, or to decompose to yield OH and an additional organic radical. As described by Saunders *et al.* (2003), the representations in MCM v3.1, based in part on the structure-reactivity method proposed by Rickard *et al.* (1999), lead to overall fractional yields of OH (and the co-radicals) of 80 % and 35 % respectively, which are consistent with the ranges reported in experimental studies: (68 – 91) % for α–pinene (Atkinson *et al.,* 1992; Chew and Atkinson, 1996; Paulson *et al.,* 1998; Rickard *et al.,* 1999; Siese *et al.,* 2001; Aschmann *et al.*, 2002; Berndt *et al.*, 2003); (24 –35) % for β–pinene (Atkinson *et al.,* 1992; Rickard *et al.,* 1999).

As part of the present study, reactions of $O(^3P)$ with α– and β–pinene, and associated chemistry, were incorporated into the mechanism, as summarised in Table 10, and discussed further below.

Table 10: Product channels and branching ratios assigned to the reactions of $O(^3P)$ with α- and β-pinene in MCM v3.1a.

Reaction	Branching ratio	Comment
α-pinene		
$O(^3P)$ + 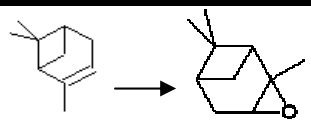	0.77	(a)
$O(^3P)$ + 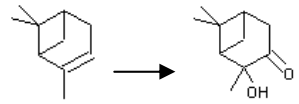	0.23	(a)
β-pinene		
$O(^3P)$ + 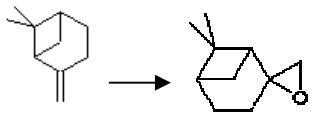	0.77	(b)
$O(^3P)$ + 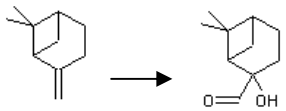	0.23	(b)

(a) k = 3.2 x 10^{-11} cm^3 $molecule^{-1}$ s^{-1}, based on the recommendation of Calvert *et al.* (2000). Branching ratios are based on the results of Alvarado *et al.* (1998), who observed the formation of α–pinene oxide and two carbonyl products isomeric with α-pinene oxide. The carbonyl products are represented by the displayed species, which is already formed from α–pinene degradation in MCM v3.1, appearing as APINBCO. α–pinene oxide removed by reaction with OH (estimated k = 1.2 x 10^{-11} cm^3 $molecule^{-1}$ s^{-1}) to form products already present in mechanism.

(b) k = 2.7 x 10^{-11} cm^3 $molecule^{-1}$ s^{-1}, based on the recommendation of Calvert *et al.* (2000). Branching ratios are inferred from the results of Alvarado *et al.* (1998) for α-pinene (see note (a)). The displayed carbonyl product is isomeric with β–pinene oxide, and is already formed from β–pinene degradation in MCM v3.1, appearing as C918CHO. β–pinene oxide removed by reaction with OH (estimated k = 1.2 x 10^{-11} cm^3 $molecule^{-1}$ s^{-1}) to form products already present in mechanism.

5.8.2 Acetone/NO_X experiments

The simulated D(O_3-NO) and HCHO formation rates, and acetone loss rates were found to be well described for the series of acetone-NO_X photo-oxidation experiments, using MCM v3.1 (see Figure 56 to Figure 58).

For consistency, the photolysis parameters for acetone were revised in line with the latest recommendation of the IUPAC panel (Atkinson *et al.,* 2005). As described by Jenkin *et al.* (1997), those in MCM v3.1 were previously based on the absorption cross-sections of Martinez *et al.* (1992) and the quantum yields of Meyrahn *et al.* (1986). The revised absorption cross sections are based on the measurements of Gierczak *et al.* (1998), which agree well with those reported by Martinez *et al.* (1992) at room temperature. The revised quantum yields are based on the appraisal of Warneck (2001), and are greater than those reported by Meyrahn *et al.* (1986) by ca. 40 % on

average over the wavelength range 280-320 nm at room temperature and 1 bar. Consequently, the revision leads to increased radical formation, and slightly increased D(O_3-NO) and HCHO formation rates, and acetone loss rates, although these are still in acceptable agreement with the experimental results. It is also apparent from the figures that the loss rate of acetone is very slow (typically ca. 4 % in 6 hours), by virtue of its low OH reactivity and photolysis rate, with notable formation of D(O_3-NO) and HCHO resulting from the very high mixing ratios of acetone employed. In the terpene systems, therefore, the further oxidation of product acetone is negligible on the timescale of chamber experiments and cannot contribute significantly to ozone formation.

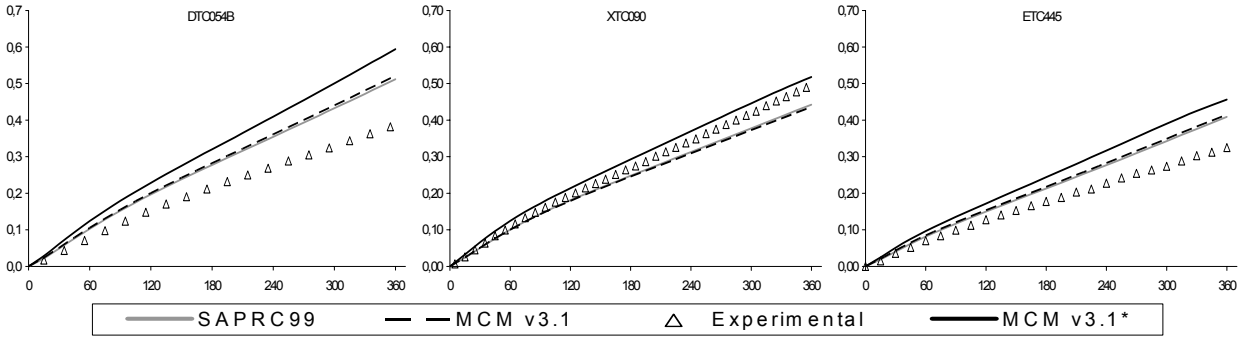

Figure 56: Example plots of experimental and calculated D(O_3-NO) (ppm) vs. time (min) for the acetone – NO_x –air experiments. MCM v3.1* relate to MCM v3.1a with the upgrade in photolysis coefficient. DTC054B-VOC/NO_x=38.3; XTC090-VOC/NO_x=49.6; ETC445-VOC/NO_x=61.9.

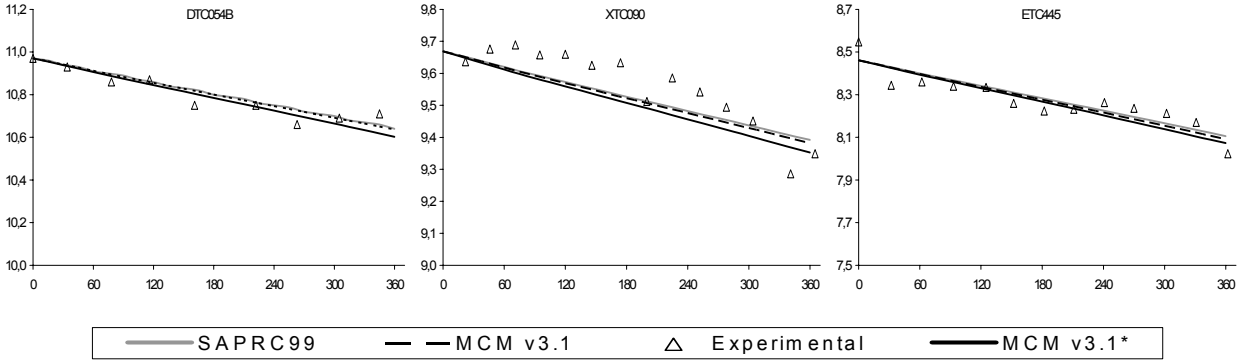

Figure 57: Example plots of experimental and calculated acetone (ppm) vs. time (min) for the acetone – NO_x –air experiments. MCM v3.1* relate to MCM v3.1a with the upgrade in photolysis coefficient. DTC054B-VOC/NO_x=38.3; XTC090-VOC/NO_x=49.6; ETC445-VOC/NO_x=61.9.

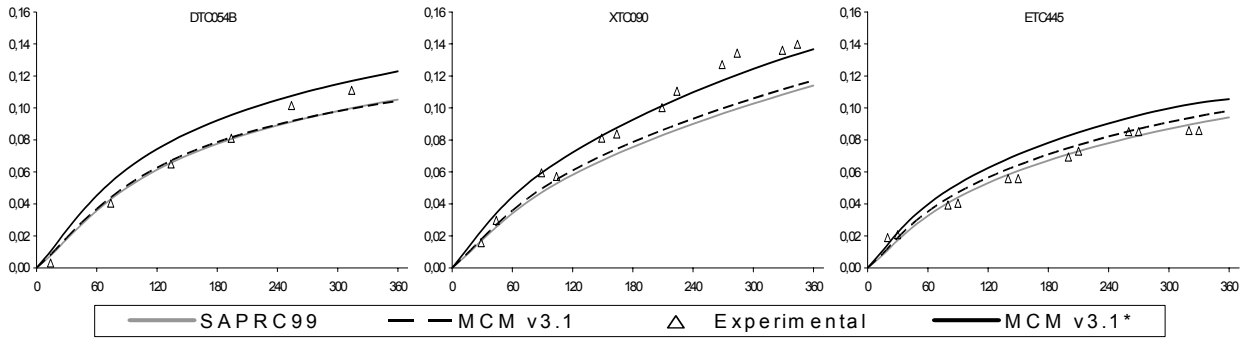

Figure 58: Example plots of experimental and calculated HCHO (ppm) vs. time (min) for the acetone – NO_x –air experiments. MCM v3.1* relate to MCM v3.1a with the upgrade in photolysis coefficient. DTC054B-VOC/NO_x=38.3; XTC090-VOC/NO_x=49.6; ETC445-VOC/NO_x=61.9.

5.8.3 α-pinene-NO_X experiments

The MCM v3.1 α-pinene mechanism was found to overestimate D(O_3-NO) specially for low VOC/NO_x ratios. In conjunction with this, the simulated decay of α-pinene was in advance and formation of the product HCHO was underpredicted relative to the observations.

The influence of incorporating the O(^{3}P) initiated chemistry into the MCM v3.1 α–pinene mechanism was investigated, using the reaction pathways and subsequent chemistry summarised in Table 10. Alvarado *et al.* (1998) concluded that O(^{3}P) reaction with α-pinene leads predominantly to the formation of α-pinene oxide (0.77±0.06) and two isomeric ketones ($C_{10}H_{16}O$) with a yield of (0.18±0.03 and 0.06±0.02), following addition of O(^{3}P). The assigned rate coefficient, 3.2 x 10^{-11} cm^{-3}.$molecule^{-1}$.s^{-1}, was recommended by Calvert *et al.* (2000). Although it was necessary to include the reaction with O(^{3}P) for completeness, the effect of this inclusion was found to be small, (see Figure 59). The chemistry mechanism was developed by Dr. Michael Jenkin.

As refered in section 5.4 designation MCM v3.1a includes the parameter updates, based on evaluation of butane degradation, updating of the photolysis parameters for HCHO, MEK and change in the assigned rate coefficient for the reaction of OH with NO_2 from a value (at 298 K and 760 Torr) of 1.19 x 10^{-12} cm^{-3}.$molecule^{-1}$.s^{-1} (based on value recommended by IUPAC), to a value of 1.05 x 10^{-11} cm^{-3}.$molecule^{-1}$.s^{-1} (based on Jet Propulsion Laboratory (JPL), Sander *et al.,* 2003). MCM v3.1a updates have negligible or zero impacts on the α-pinene – NO_x –air experiments evaluation.

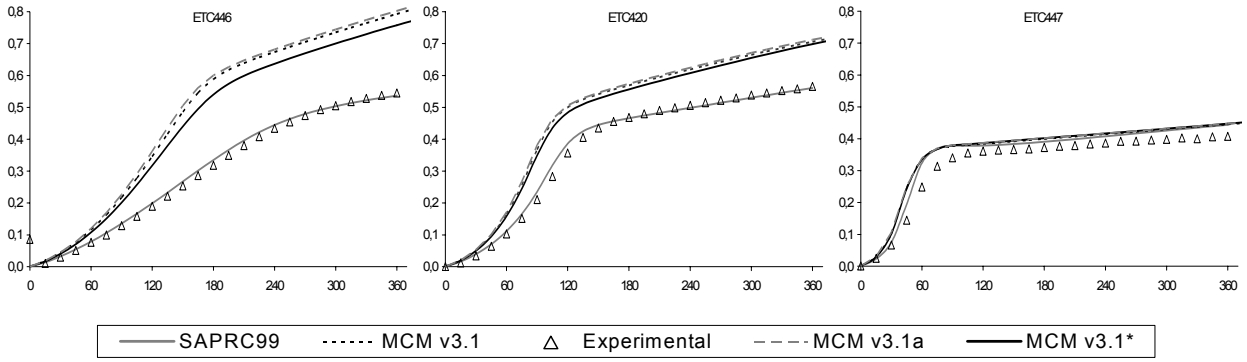

Figure 59: Example plots of experimental and calculated $D(O_3\text{-}NO)$ (ppm) vs. time (min) for the α-pinene – NO_x –air experiments. MCM v3.1* relate to MCM v3.1a with insertion of $O(^3P)$ reaction with α-pinene. ETC446-VOC/NO_x=0.52; ETC420-VOC/NO_x=0.91; ETC447-VOC/NO_x=2.13.

The intermediate carbonyl products may have a secondary influence on the system, through photolysis to form free radicals. For example, in the cases of pinonaldehyde and norpinonaldehyde, the following radical-forming channels are included in MCM v3.1:

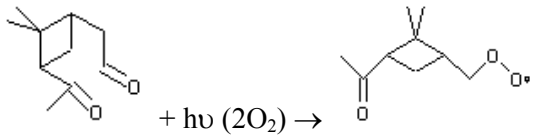

(47)

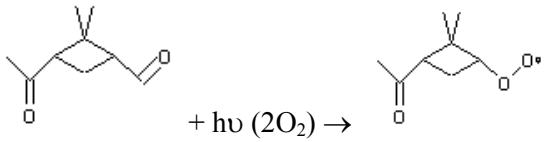

(48)

A means of reducing radical yield in the system is to increase molecular products from pinonaldehyde and norpinonaldehyde photolysis. The EU RADICAL consortium (RADICAL, 2002) investigated photolysis of a series on n-aldehydes C4-C6 and showed that although the photolysis rate was quite constant, the yield of radicals dropped from *ca.* 80% for butanal to less than 20% for pentanal and hexanal. Also Capouet *et al.* (2004) and references there in indicate that the molecular channels of aldehydes photolysis increase slowly with chain length. So, based on the appraisal of Capouet *et al.* (2004) and also consistent with the trend of decreasing photolysis radical yields with carbon chain length for aldehydes, photolysis parameters and photolysis product channels for pinonaldehyde, norpinonaldehyde and hydroxypinonaldehydes were revised. In each case, the photolysis was changed in a way to give 74% of molecular products and 24% of radicals, reactions (47) and (48) The effect of this change was found to be small, of the same order of

inclusion of reaction with $O(^3P)$. The simultaneous inclusion of the two changes add a small but significant change in $D(O_3\text{-NO})$ parameter for low VOC/NOx ratios, see Figure 60.

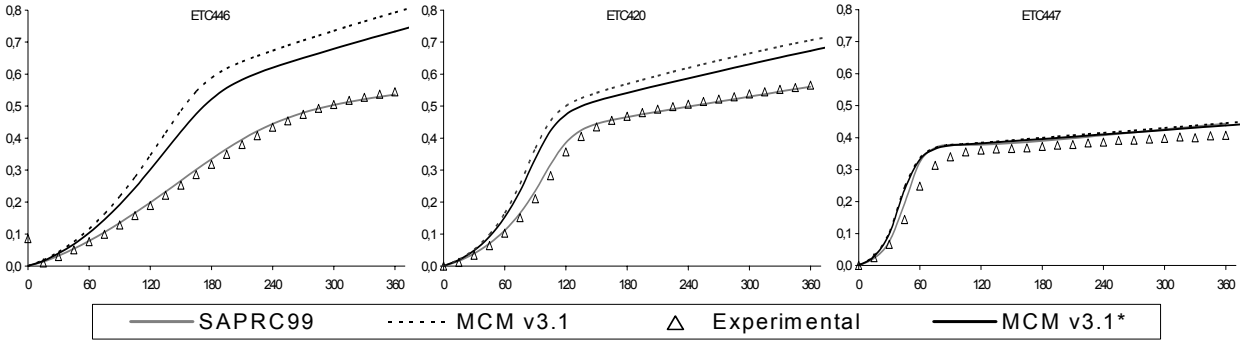

Figure 60: Example plots of experimental and calculated $D(O_3\text{-NO})$ (ppm) vs. time (min) for the α-pinene – NO_x –air experiments. MCM v3.1* relate to MCM v3.1a with insertion of $O(^3P)$ reaction with insertion of $O(^3P)$ reaction with α-pinene and change in photolysis product channels for pinonaldehyde, norpinonaldehyde and hydroxypinonaldehydes (see text).

The OH initiated degradation chemistry for pinonaldehyde was revised taken account of the detailed theoretical appraisal of Fantechi *et al.* (2002), including 3 initiation channels and the increased formation of intermediate carbonyls such as norpinonaldehyde. Some compatible revisions have also been applied to the chemistry of the related aldehydes. The revisions on chemistry mechanism were developed by Dr. Michael Jenkin. These changes add a significant effect in $D(O_3\text{-NO})$ parameter, moving the model in the right trend to fit the experimental data, (see Figure 61), but also decrease the HCHO formation, moving the model in the wrong trend to fit the experimental data.

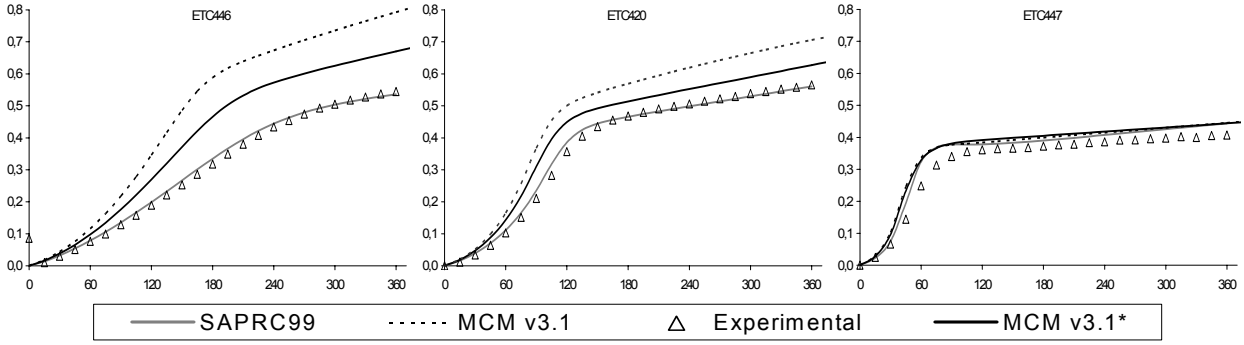

Figure 61: Example plots of experimental and calculated $D(O_3\text{-NO})$ (ppm) vs. time (min) for the α-pinene – NO_x –air experiments. MCM v3.1* relate to MCM v3.1a with insertion of $O(^3P)$ reaction with α-pinene, with change in photolysis product channels for pinonaldehyde, norpinonaldehyde and hydroxypinonaldehydes and with change in OH initiated degradation chemistry for pinonaldehyde (see text).

In MCM v3.1, a nitrate yield of 24% (when NO_x is present) was assigned based on data from Ruppert *et al.* (1999). Since the mechanism can only be reconciled with the data by reducing the radical yield in the system this is well achieved by increasing the nitrate yield radical sink (RO2+NO = RONO2). The nitrate yields from the initially formed RO2 radicals were increased to 27%, a value at the extremity of the yield uncertainty range of Noziere *et al.* (1999). The organic nitrate yield is indicated by Noziere *et al.* (1999) as 18± 9 %. This change improves the early stages of the simulation, (see Figure 62).

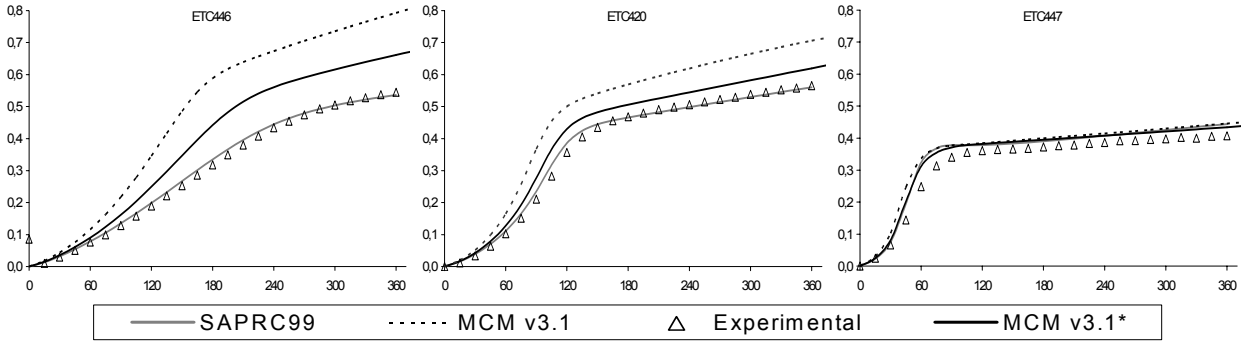

Figure 62: Example plots of experimental and calculated D(O_3-NO) (ppm) vs. time (min) for the α-pinene – NO_x –air experiments. MCM v3.1* relate to MCM v3.1a with insertion of O(^{3}P) reaction with α-pinene, with change in photolysis product channels for pinonaldehyde, norpinonaldehyde and hydroxypinonaldehydes, with change in OH initiated degradation chemistry for pinonaldehyde and change in nitrate yields from the initially formed RO2 radicals (see text).

Since α-pinene is an unsaturated hydrocarbon, there are additional features of the chemistry which have an important impact on its degradation under environmental chamber and atmospheric conditions. Of particular significance is the reaction with O_3, which is described in detail by Jenkin *et al.* (2000) and Saunders *et al.* (2003). In addition to supplementing the oxidation rate, this reaction has an important secondary influence through being source of OH. Experimental studies of OH yields lie in the range 68%-91% (e.g., Atkinson *et al.,* 1992b, Chew and Atkinson, 1996, Paulson *et al.,* 1998, Rickard *et al.,* 1999, Siese *et al.,* 2001; Aschmann *et al.*, 2002; Berndt *et al.*, 2003).

The OH yield with the MCMv3.1 representation is 80%, (see section 5.8.1.), in the middle of reported range. Decreasing the OH yield to 70%, a significant effect, improving the data fitting for the D(O_3-NO) parameter and for decay of α-pinene was verified, (see Figure 63 and Figure 64). However the underprediction of HCHO is enlarged, (see Figure 65).

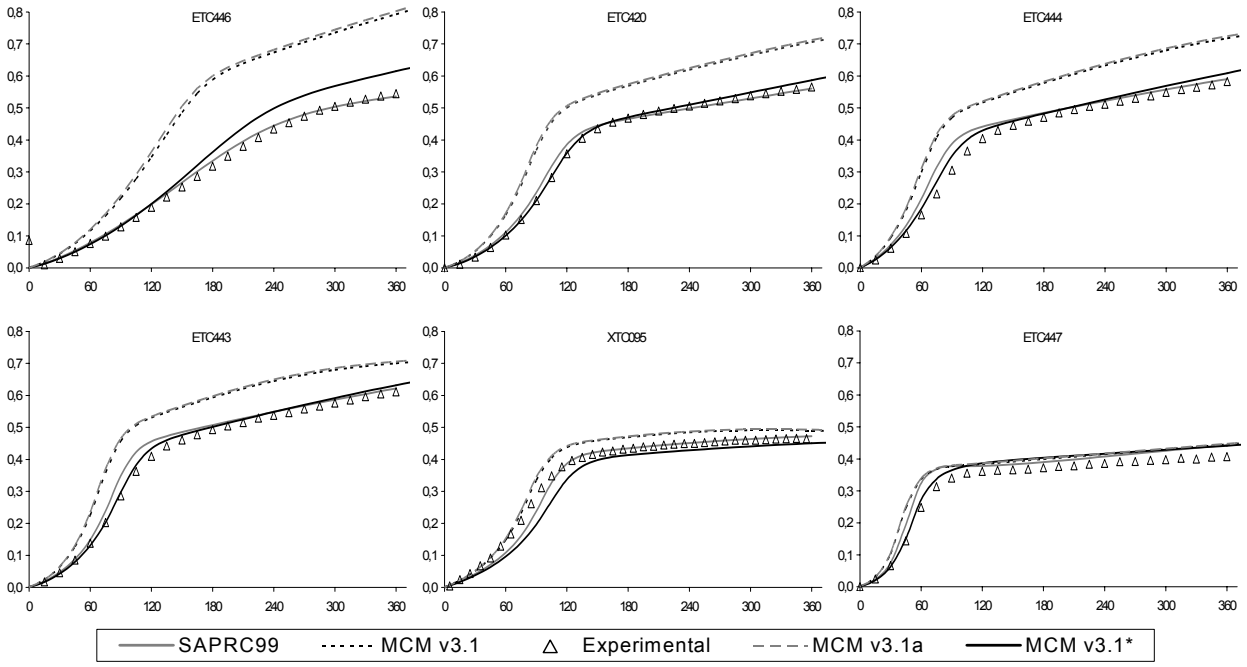

Figure 63: Example plots of experimental and calculated D(O_3-NO) (ppm) vs. time (min) for the α-pinene – NO_x –air experiments. MCM v3.1* relate to MCM v3.1a with insertion of $O(^3P)$ reaction with α-pinene, with change in photolysis product channels for pinonaldehyde, norpinonaldehyde and hydroxypinonaldehydes, with change in OH initiated degradation chemistry for pinonaldehyde, change in nitrate yields from the initially formed RO2 radicals and OH yield from O_3+α-pinene was decreased from 80% to 70% (see text). ETC446-VOC/NO_x=0.52; ETC420-VOC/NO_x=0.91; ETC444-VOC/NO_x=0.94; ETC443-VOC/NO_x=1.09; XTC095-VOC/NO_x=1.84 ; ETC447-VOC/NO_x=2.13.

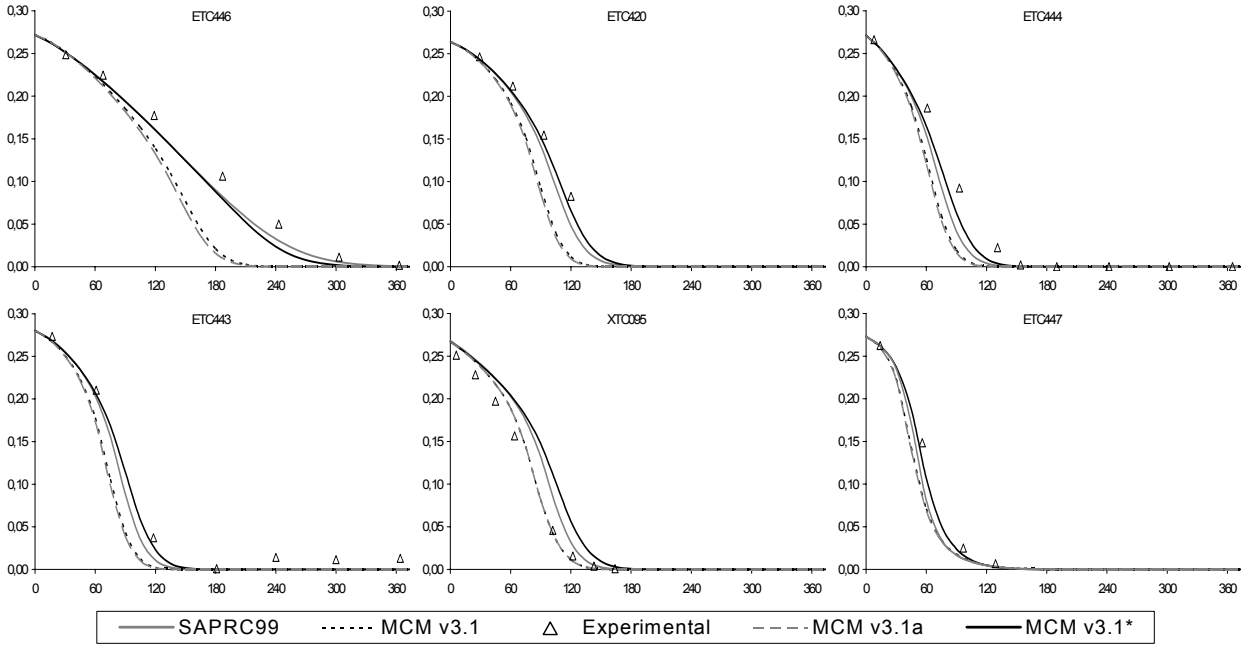

Figure 64: Example plots of experimental and calculated α-pinene (ppm) vs. time (min) for the α-pinene – NOx –air experiments. Same legend as Figure 63.

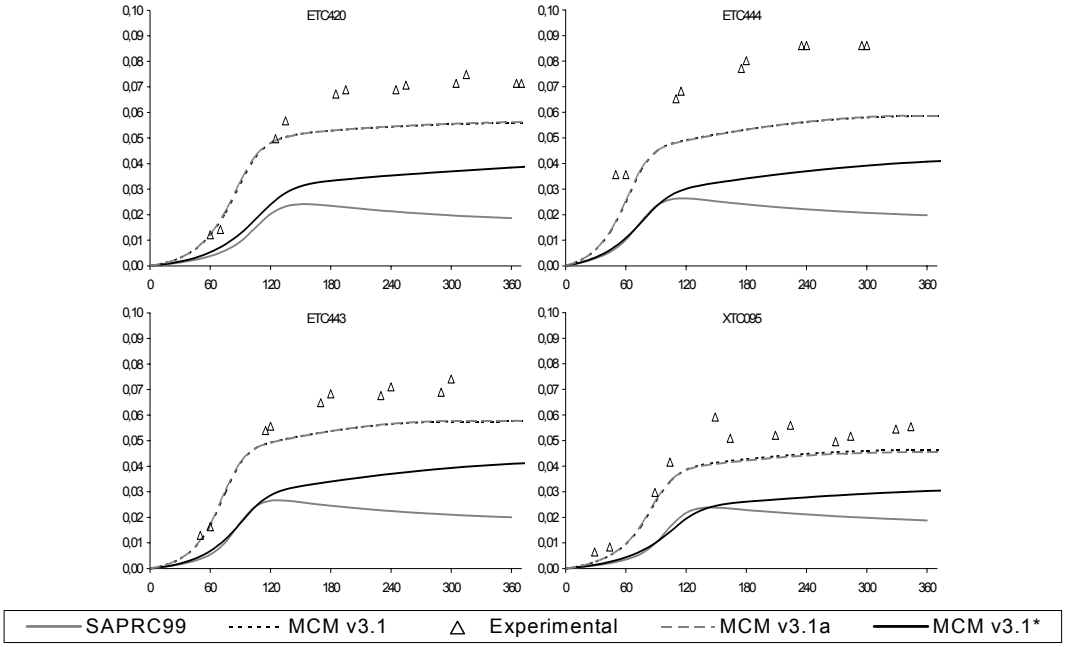

Figure 65: Example plots of experimental and calculated HCHO (ppm) vs. time (min) for the α-pinene – NOx –air experiments. Same legend as Figure 63.

Recent studies (Noziere *et al.,* 1999, Orlando *et al.,* 2000) indicate that HCHO is probably formed as a first generation product, with a yield near 20%. However, such a route is not currently represented in the MCM scheme, partly because the details are not clear and the routes tentatively proposed in the literature do not yet been backed up with theoretical calculations. However, the inclusion of primary HCHO formation route from β-hydroxyalkoxy isomerisation was tested. The chemistry mechanism was developed by Dr. Michael Jenkin based on processes discussed by Capouet *et al.* (2004) and references therein. The HCHO formation couldn't be conciliated without compromising the D(O_3-NO) formation and α-pinene decay.

5.8.4 β-pinene-NO_X experiments

The D(O_3-NO) formation rate and β–pinene loss rate, simulated using MCM v3.1, were broadly comparable with the experimental observations, but with a tendency to overestimation at low VOC/NO_X.

The influence of incorporating the O(^{3}P) initiated chemistry into the MCM v3.1 β–pinene mechanism was investigated, using the reaction pathways and subsequent chemistry summarised in Table 10. The chemistry mechanism was developed by Dr. Michael Jenkin based in the studies of Alvarado *et al.* (1998) on the reaction of O(^{3}P) with α-pinene. The assigned rate coefficient, 2.7 x 10^{-11} cm^{-3}.$molecule^{-1}$.s^{-1}, was recommended by Calvert *et al.* (2000). As for α-pinene, although it

was necessary to include the reaction with $O(^3P)$ for completeness, the effect of its inclusion was found to be small, see Figure 66.

The MCM v3.1a resulted from the updates made on evaluation of butane degradation; update the photolysis parameters for HCHO, MEK and update in the assigned rate coefficient for the reaction of OH with NO_2, have an increasing effect in ozone production from the β-pinene degradation. This effect, not observed in α-pinene MCM degradation mechanism, is mainly caused by the high yield of HCHO.

Furthermore HCHO yields in the literature cover the range 45%-55% (Hatakeyama *et al.,* 1991, Orlando *et al.,* 2000), with the MCM yield (*ca.* 70% when NO_x is present) being higher than the range in the literature.

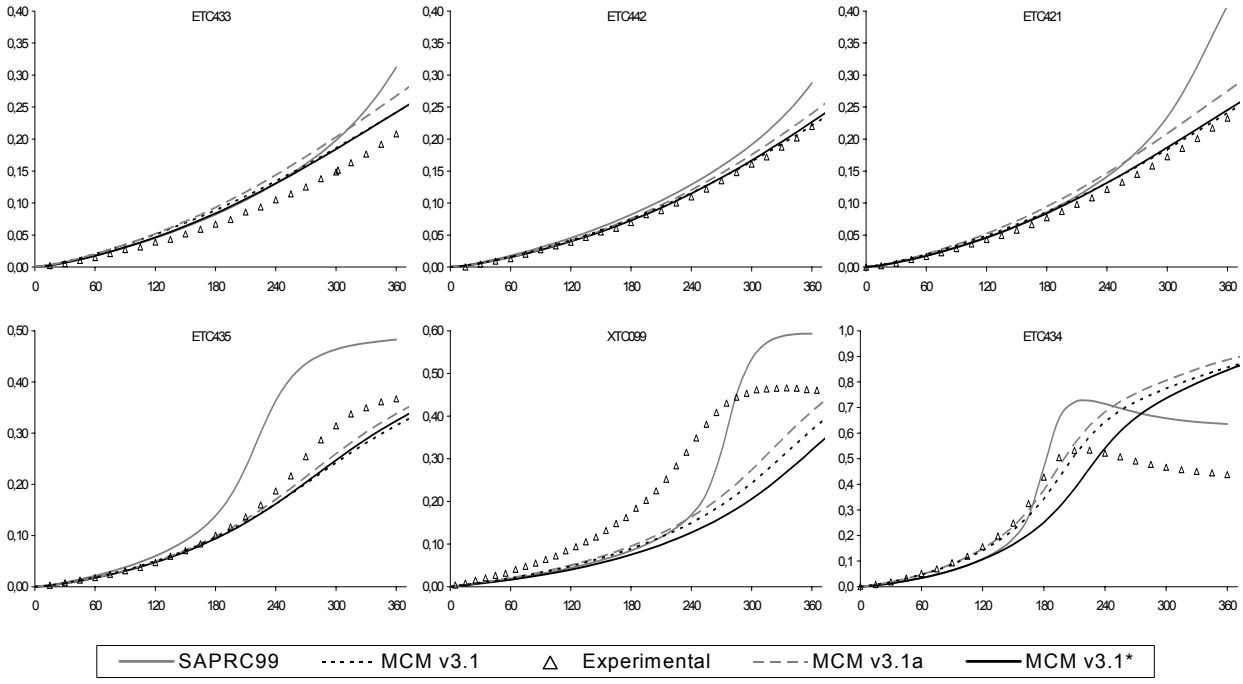

Figure 66: Example plots of experimental and calculated $D(O_3\text{-NO})$ (ppm) vs. time (min) for the β-pinene – NO_x –air experiments. MCM v3.1* relate to the MCM v3.1a with insertion of $O(^3P)$ reaction with β-pinene.

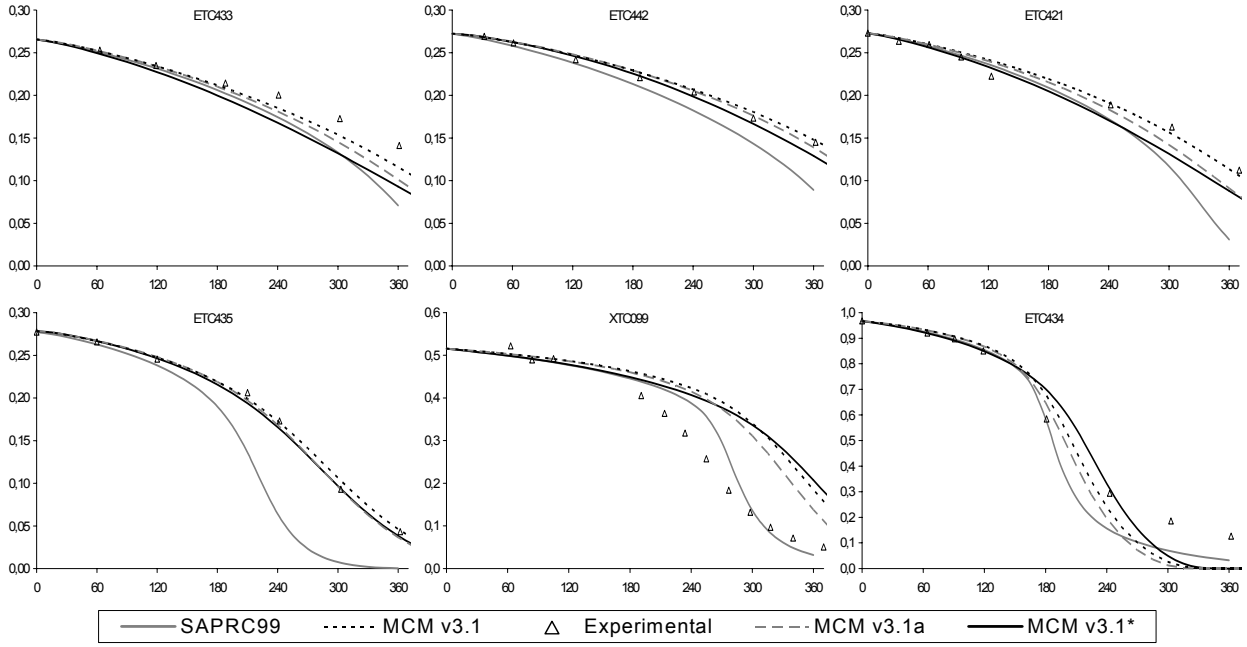

Figure 67: Example plots of experimental and calculated β-pinene (ppm) vs. time (min) for the β-pinene – NO_x –air experiments. MCM v3.1* relate to the MCM v3.1a with insertion of $O(^3P)$ reaction with β-pinene.

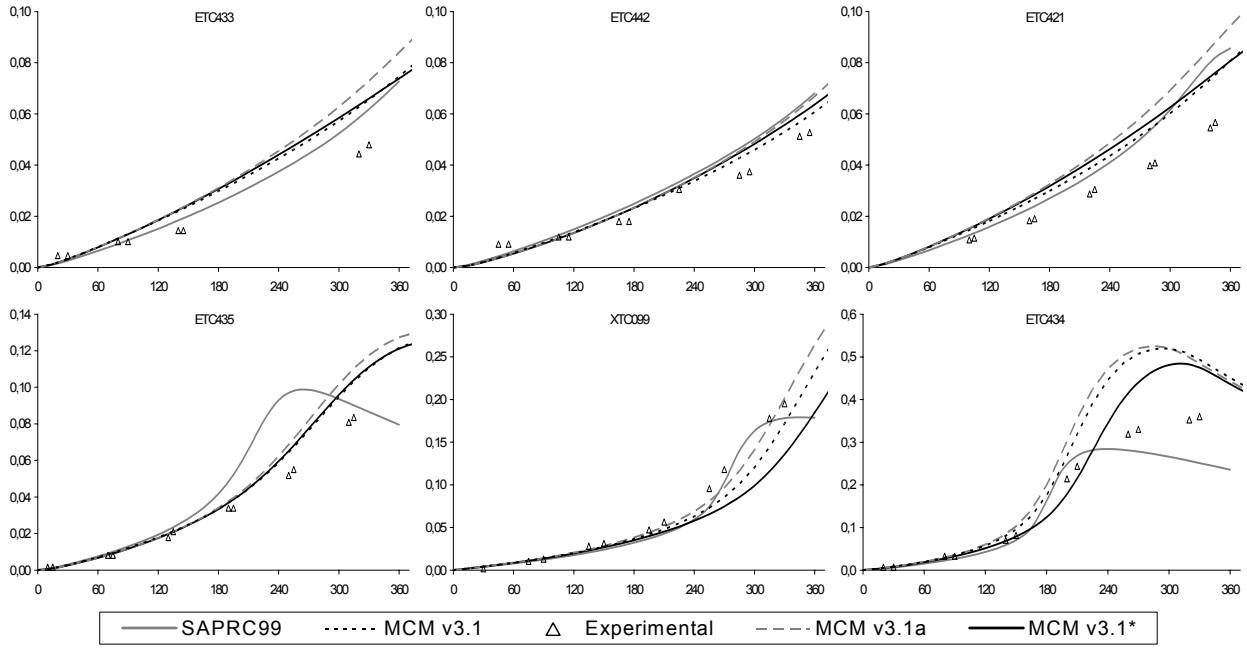

Figure 68: Example plots of experimental and calculated HCHO (ppm) vs. time (min) for the β-pinene – NO_x –air experiments. MCM v3.1* relate to the MCM v3.1a with insertion of $O(^3P)$ reaction with β-pinene.

The nopinone yields in the literature cover a wide range 25%-79% (Arey *et al.,* 1990, Hatakeyama *et al.,* 1991, Hakola *et al.,* 1994, Wisthaler *et al.,* 2001). The nopinone yield in MCM (*ca.* 70%) is within the reported range. A significant change to the initiation branching ratios was tested; (see reactions (49), (50) and (51)). A change in initial branching ratios from 84.9%: 7.6%: 7.5% for

BPINAO2: BPINBO2: BPINCO2 to 43.5%: 13.0%: 43.5% for BPINAO2: BPINBO2: BPINCO2 was applied. Simultaneously a representation of a ring-closure reaction for BPINCO2 was also tested. The chemistry mechanism was developed by Dr. Michael Jenkin based on processes discussed by Capouet *et al.* (2004) and references therein. The result of these changes didn't improve the fitting of the modelled with the experimental data.

β-pinene + OH → 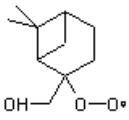 (BPINAO2) (49)

β-pinene + OH → 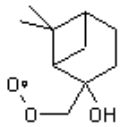 (BPINBO2) (50)

β-pinene + OH → 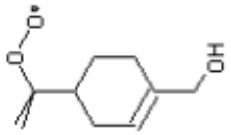 (BPINCO2) (51)

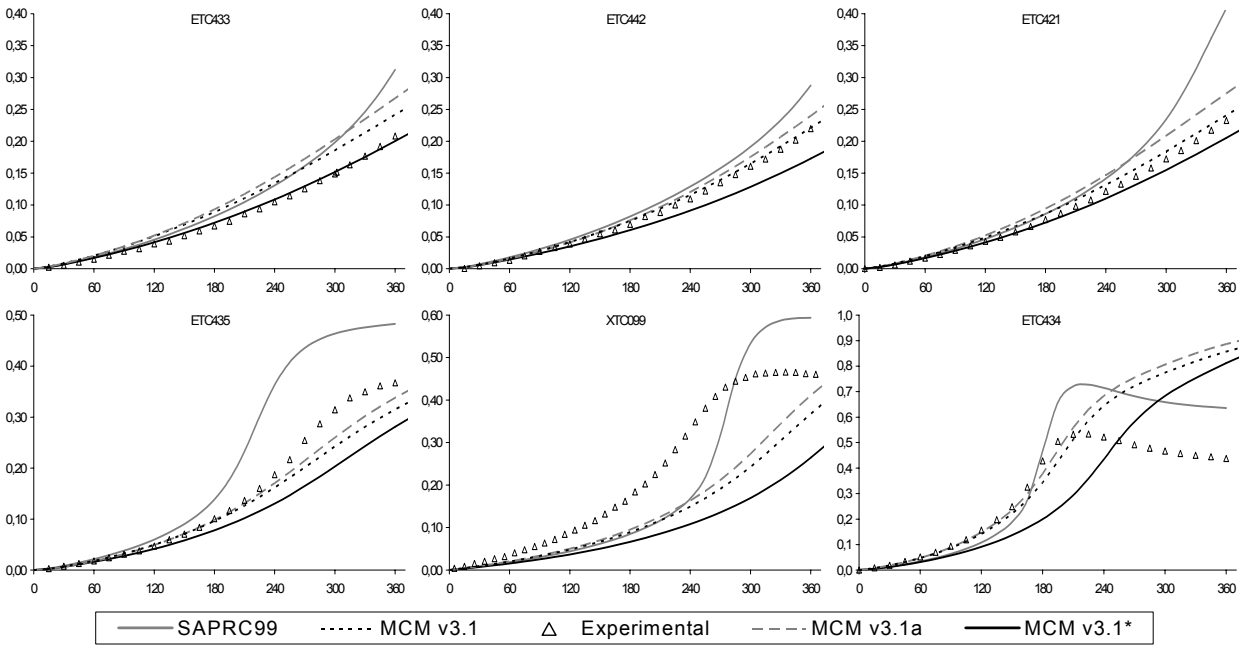

Figure 69: Example plots of experimental and calculated D(O_3-NO) (ppm) vs. time (min) for the β-pinene – NO_x –air experiments. MCM v3.1* relate to the MCM v3.1a with insertion of O(^{3}P) reaction with β-pinene, change to the initiation branching ratios and a representation of a ring-closure reaction for BPINCO2.

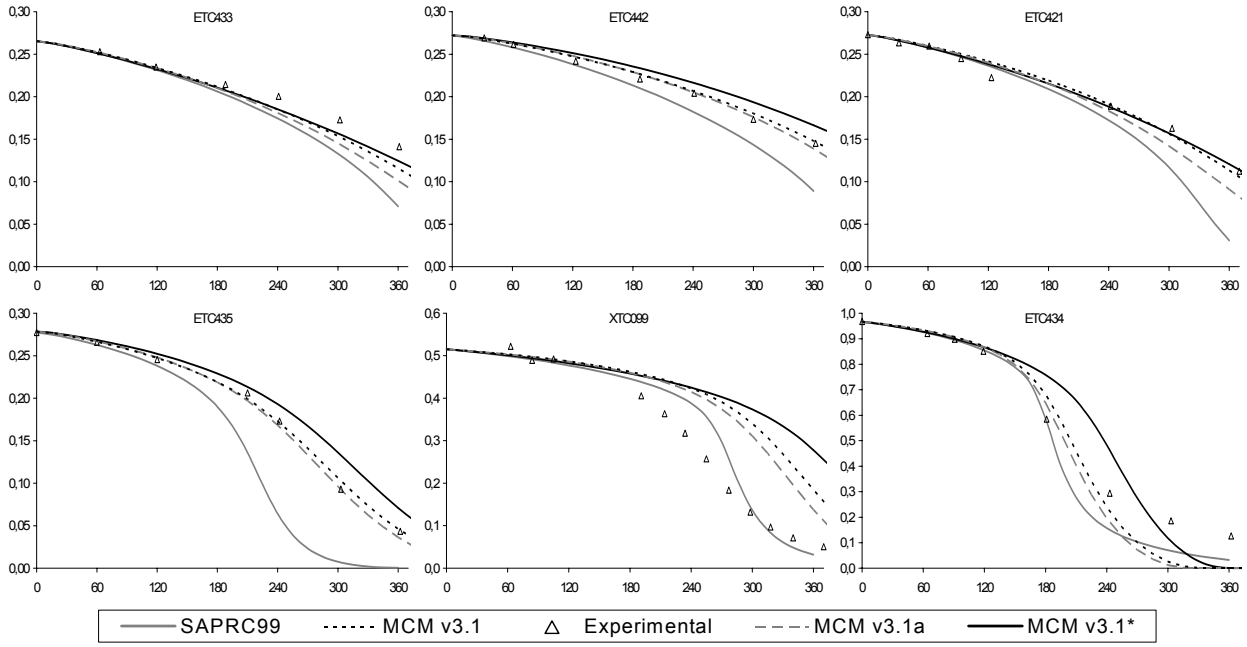

Figure 70: Example plots of experimental and calculated β-pinene (ppm) vs. time (min) for the β-pinene – NO_x –air experiments. MCM v3.1* relate to the MCM v3.1a with insertion of $O(^3P)$ reaction with β-pinene, change to the initiation branching ratios and a representation of a ring-closure reaction for BPINCO2.

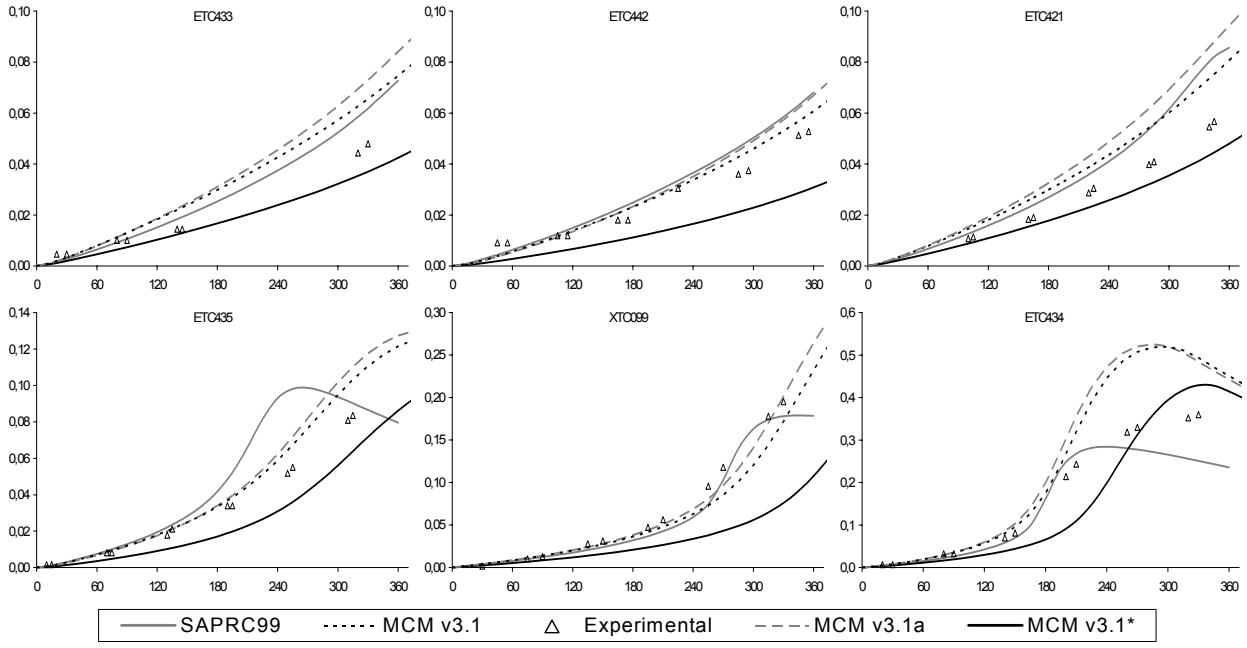

Figure 71: Example plots of experimental and calculated HCHO (ppm) vs. time (min) for the β-pinene – NO_x –air experiments. MCM v3.1* relate to the MCM v3.1a with insertion of $O(^3P)$ reaction with β-pinene, change to the initiation branching ratios and a representation of a ring-closure reaction for BPINCO2.

5.9 Summary and Conclusions

Butane, ethene, propene, 1-butene, 1-hexene, isoprene, α-pinene and β-pinene, formaldehyde, acetaldehyde, methacrolein, acetone, methylethyl ketone and methylvinyl ketone degradation mechanism included in version 3.1 of the Master Chemical Mechanism were evaluated using Statewide Air Pollution Research Center at the University of California environmental chamber datasets.

Photo-oxidation of butane and its degradation products, MEK, CH_3CHO and HCHO were evaluated in conjunction with an initial evaluation of the chamber-dependent auxiliary mechanisms. The MCM v3.1 mechanism for butane was found to provide an acceptable reaction framework for describing the NO_X-photo-oxidation experiments, although a number of parameter modifications and refinements were identified and introduced, resulting in an improved performance. These generally relate to the magnitude of sources of free radicals from carbonyl photolysis processes. Specifically, recommendations are made to update the photolysis parameters for HCHO, MEK, either in line with data reported since the MCM mechanism development protocol (Jenkin *et al.,* 1997), or on the basis of optimization in the current study. The performance of MCM v3.1 and the adaptation, MCM v3.1a, was simultaneously compared with that of the SAPRC-99 mechanism. The performance of MCM v3.1a was found to be very similar to that of SAPRC-99.

The simulations for the ethene and propene systems were found to be sensitive to the branching ratios assigned to molecular and free radical forming pathways. In broad agreement with the conclusions of Carter (2000), acceptable fitting of these systems is best achieved by the assumption that the $O(^3P)$ reactions mainly generate molecular products, although it is recognised that this result is inconsistent with the literature consensus (e.g. Calvert *et al.,* 2000; Baulch *et al.,* 2005) which indicates significant radical formation from the reactions of $O(^3P)$ with ethene and propene at room temperature and atmospheric pressure. With this constraint, the MCM v3.1 mechanisms for ethene and propene generally perform well, providing a reasonable description of the data obtained in the majority of SAPRC chambers.

The evaluation of the 1-butene and 1-hexene degradation mechanisms, using a limited dataset from one chamber, was found to be inconclusive. The results of the sensitivity studies demonstrate that it is impossible to reconcile the simulated and observed formation of ozone in these systems for ranges of parameter values which can currently be justified on the basis of the literature.

Photo-oxidation of isoprene was evaluated simultaneously with its degradation products, methacrolein and methylvinyl ketone. The MCM v3.1 mechanism for isoprene was found to provide an acceptable reaction framework for describing the NO_X-photo-oxidation experiments on the above systems, although a number of parameter modifications and refinements were identified which resulted in an improved performance. These all relate to the magnitude of sources of free radicals from organic chemical process, such as carbonyl photolysis rates and the yields of radicals from the reactions of O_3 with unsaturated oxygenates. Specifically, recommendations are made to update the photolysis parameters for MACR and MVK, and the OH yields from the reactions of O_3 with MACR and MVK, either in line with new data reported since the development of MCM mechanism protocol (Jenkin *et al.,* 1997), or on the basis of optimization in the current study. In addition to this, representations of the reactions of $O(^3P)$ with isoprene, MACR and MVK (which were not previously treated in MCM) were included. The influence of the reactions involving MACR and MVK was found to be very minor. In contrast, inclusion of the reaction of $O(^3P)$ with isoprene was the major factor responsible for the differences in the simulations of the parent isoprene system performed with MCM v3.1 and with MCM v3.1 including the refinements. The performance of MCM v3.1 including the refinements was found to be very similar to that of SAPRC-99, suggesting that they would perform comparably in simulations of isoprene oxidation under tropospheric conditions.

The performance of the MCM v3.1 α-pinene mechanism against the chamber α-pinene -NO_X photo-oxidation data were made and the MCM v3.1 α-pinene mechanism was found to overestimate $D(O_3\text{-NO})$ specially for low VOC/NO_x ratios. In conjunction with this, the simulated decay of α-pinene was in advance and formation of the product HCHO is underpredicted relative to the observations. MCM v3.1a updates have negligible or zero impacts on the α-pinene – NO_x –air experiments evaluation. The mechanism can only be reconciled with the data by reducing the radical yield in the system. The reaction of $O(^3P)$ with α-pinene was incorporated, using the reaction steps based in data from literature. Although it was necessary to include the reaction with $O(^3P)$ for completeness, the effect of its inclusion was found to be small. The nitrate yields from the initially formed RO2 radicals were increased from 24% to 27%, a change to the extremity of the yield uncertainty range of Noziere *et al.* (1999). This change improves the early stages of the simulation. Decreasing the OH yield from reaction with O_3 on 80% to 70% implies a significant effect improving the data fitting for the $D(O_3\text{-NO})$ parameter and for decay of α-pinene. However the underprediction of HCHO is enlarged. The inclusion of primary HCHO formation route from β-hydroxyalkoxy isomerisation was tested with a chemistry mechanism based on processes

discussed by Capouet *et al.* (2004) and references therein. However it was not possible to conciliate the HCHO formation without compromise the D(O_3-NO) formation and α-pinene decay.

Also the performance of the MCM v3.1 β-pinene mechanism against the chamber β-pinene -NO_X photo-oxidation data were made. However, in half of the runs the curve shapes of experimental ozone production is very different from the other runs and from the modelled ones. So, it was not possible to conciliate three of the runs without compromise the other three. The updates resulted from the evaluation of butane degradation (MCM v3.1a) causes an increasing effect in ozone production. This effect, not observed in α-pinene MCM degradation mechanism, is mainly due to the high yield of HCHO. The reaction of O(^{3}P) with β-pinene was incorporated for completeness, using the reaction steps based in data from literature, but the effect of its inclusion was found to be small. A significant change in initial branching ratios from 84.9%: 7.6%: 7.5% for BPINAO2: BPINBO2: BPINCO2 to 43.5%: 13.0%: 43.5% was applied. Simultaneously a representation of a ring-closure reaction for BPINCO2 was tested. The chemistry mechanism was developed based on processes discussed by Capouet *et al.* (2004) and references therein. The result of this change didn't improve significantly the fitting of the modelled with the experimental data. More environmental chamber experiments should be carried out, using better chamber characterisation, to allow a full evaluation of β-pinene degradation scheme.

Table 11 gives the summary of the results of the evaluated degradation mechanism.

Table 11: Summary of the results of the degradation mechanism, included in version 3.1 of the Master Chemical Mechanism, evaluated using Statewide Air Pollution Research Center at the University of California environmental chamber datasets.

Degradation mechanism	Comments
Butane	Used for initial assessment of the auxiliary mechanism parameters. Evaluated in conjunction with its degradation products, MEK, CH_3CHO and HCHO and the chamber-dependent auxiliary mechanisms. Update of photolysis parameters for HCHO, MEK and adjustment of Carter chamber radical source values used in the SAPRC evaluation (Carter, 2000) by a factor of 1.35 for the ITC chamber, and by a factor of 1.2 for the DTC, CTC and XTC chambers. **Generally good fits to D(O_3-NO) data in butane–NO_X photo-oxidation experiments. The scatter in the results was indicative of run-to-run variability, with most of the data being fit by the mechanism to within +/- 30%, with no consistent biases.**
Ethene	**Tendency to overestimate D(O_3-NO) data in most of etene–NO_X photo-oxidation experiments.** Good representation of D(O_3-NO) data in large majority of the experiments if considering the molecular pathways for the O(^{3}P)-ethene reaction to account for at least 50% of the reaction, with the optimum being 80%, although it is recognised that this values are inconsistent with the literature consensus.
Propene	**Tendency to overestimate D(O_3-NO) data in most of propene–NO_X photo-oxidation experiments.** Good representation of D(O_3-NO) data in large majority of the experiments if considering the molecular pathways for the O(^{3}P)-propene reaction to account for <10%, although it is recognised that this values are inconsistent with the literature consensus.
1-butene	**Tendency to overestimate D(O_3-NO) data in 1-butene–NO_X photo-oxidation experiments.** Reasonable agreement with observations, if considering the molecular pathways for the O(^{3}P)-1-butene reaction to account for 100 % and if assumed radical formation from the ozonolysis reactions to be 12 %, although it is recognised that this values are inconsistent with the literature consensus.
1-hexene	**Tendency to overestimate D(O_3-NO) data in 1-hexene–NO_X photo-oxidation experiments.** Good agreement with observations, if considering the molecular pathways for the O(^{3}P)-1-hexene reaction to account for 100 %, the radical formation from the ozonolysis reactions to be 7 % and 25 % oxy radical isomerization, although it is recognised that considered radical yields from O(^{3}P) and O_3 reactions with 1-hexene are inconsistent with the literature consensus.
Isoprene	**Generally good fits to D(O_3-NO) data in isoprene–NO_X photo-oxidation experiments. Tendency to underestimate D(O_3-NO) in the early stages.** Evaluated in conjunction with its degradation products, MACR and MVK. Update the photolysis parameters for MACR and MVK, update the OH yields from the reactions of O_3 with MACR and MVK and insertion of the reactions of O(^{3}P) with isoprene, MACR and MVK. MCM v3.1 including the refinements provides an improved representation of D(O_3-NO), isoprene decay, and formation of HCHO, MVK and MACR. The influence of the reactions involving MACR and MVK was found to be very minor. The inclusion of the reaction of O(^{3}P) with isoprene was the major factor responsible for the differences in the simulations of the parent isoprene system performed with MCM v3.1 and with MCM v3.1 including the refinements.

α-pinene	**Tendency to overestimate D(O_3-NO) specially for low VOC/NO_x ratios.** Good agreement with observations, if considering the insertion of O(^{3}P) reaction with α-pinene, change in photolysis product channels for pinonaldehyde, norpinonaldehyde and hydroxypinonaldehydes, change in OH initiated degradation chemistry for pinonaldehyde, increased from 24% to 27% the nitrate yields from the initially formed RO2 radicals and decrease OH yield from O_3+α-pinene from 80% to 70%.
β-pinene	**Generally fits to D(O_3-NO) for low VOC/NO_x ratios and not fit for high VOC/NO_x ratios.** Not possible to implement changes which bring simulation into agreement with observation for the entire VOC/NOx range.
Formaldehyde	**Tendency to under-predict D(O_3-NO) in many (but not all) of the runs.** Good agreement with observations, if applied new absorption cross section and quantum yield data for the photolysis of HCHO. Cross sections being based on the data of Meller and Moortgat, (2000) and the quantum yields based on data from Smith *et al.* (2002).
Acetaldehyde	**Good description of D(O_3-NO) in the complete set of CH_3CHO-NO_X chamber experiments.**
Methacrolein	**Tendency to overestimate significantly the observed D(O_3-NO) in the initial stages of the experiments, but with the final values being slightly lower than those observed.** A much improved description of the initial D(O_3-NO) values, although a tendency towards slight under-prediction at longer experimental durations, is obtained if considering decrease OH yield from ozonolysis of MACR from 82% to 20%, O(^{3}P) reaction with MACR and decrease in quantum yield for MACR to a value of 0.0036 (quantum yield for MACR was obtained by best fit, however is consistent with the literature). The change in the applied quantum yield for MACR photolysis is the most important factor responsible for best performance.
Acetone	**Good description of D(O_3-NO) in the complete set of CH_3COCH_3-NO_X chamber experiments.** The update of photolysis parameters for acetone increased radical formation and slightly increased D(O_3-NO) and HCHO formation rates, and acetone loss rates, although these are still in acceptable agreement with the experimental results. Cross sections being based on the data of Gierczak *et al.* (1998) and the quantum yields based on data from Warneck (2001).
Methylethyl ketone	**The MCM v3.1 mechanism has tendency to over-predict D(O3-NO) in many of the chamber runs, particularly in the early stages of the experiment.** Good agreement with observations if reducing the quantum yield for the photolysis of MEK. Best fit for quantum yield value of 0.17, which is close to the extremity of the uncertainty limit of the determination of Raber and Moortgat (1996). MCM v3.1a systematically overestimates the formation of HCHO in the system. The production of HCHO could be well described if 1,5 H shift isomerisation reaction of α-carbonyl oxy radical accounts for ca. 70%.
Methylvinyl ketone	**Tendency to overestimate significantly the observed D(O_3-NO) in the initial stages of the experiments, but with the final values being slightly lower than those observed.** A much improved description of D(O_3-NO) values is obtained, if considering decrease OH yield from ozonolysis of MVK from 36% to 16%, O(^{3}P) reaction with MVK and decrease in quantum yield for MVK based Gierczak *et al.* (1997). The change in the applied quantum yield for MVK photolysis is the most important factor responsible for best performance.

As a result of chamber evaluation of MCM, it is possible to make a number of suggestions and recommendations for future work, in relation to gaps and uncertainties in the kinetic and mechanistic database, and the availability of chamber data.

Confidence in chamber evaluations requires the uncertainty to be reduced on the kinetics of the reaction of OH with NO_2, which is often the major radical sink in the system.

Chamber evaluation of VOC systems requires confirmatory information on their reactions with $O(^3P)$, particularly on the relative contributions made by molecular and free radical product channels under chamber conditions. This is a major factor influencing the fitting of several systems in the present study, even though these reactions are generally regarded as insignificant under atmospheric conditions and are not usually included in atmospheric mechanisms. Uncertainty in this area therefore seriously compromises the evaluation procedure.

Although the reactions of ozone with alkenes and with unsaturated oxygenates have received considerable attention, further information is required to quantify fully free radical formation from these reactions under atmospheric conditions. Particular uncertainties relate to improving the characterisation of decomposition channels for excited Criegee intermediates which do not form OH, and quantifying the extent to which these channels generate free radical products, and whether this is independent of the parent alkene from which a given Criegee biradical is generated. In addition, to avoid experimental complications, studies of OH formation have generally been derived from ozone-VOC experiments performed in the absence of NO_X. It is therefore not clear if the presence of NO_X influences the mechanisms forming OH and/or other radicals.

The SAPRC database provides a comprehensive experimental dataset for many VOC. However, chamber data for longer chain alkanes and alkenes are comparatively limited. Full evaluation of atmospheric organic chemistry mechanisms, such as the MCM, ideally requires more chamber data on these systems.

6 Atmospheric Simulation and Testing

One of the aims of the current study is the application of MCM, after applied refinements resulting from chamber evaluation, to a concrete environmental situation where photochemical pollution formation is well established and defined in order to further test the Photochemical Trajectory Model and the modifications introduced in MCM.

Photochemical pollution episodes with elevated levels of tropospheric ozone have been registered in different rural zones worldwide, which are far away from urban and industrial areas (e.g. Donev *et al.,* 2002; Dueñas *et al.,* 2004). This is related with diverse phenomena of secondary pollutants formation and transport in the atmosphere. In particular, studies realized in Portugal revealed frequent photochemical pollution episodes, on regional-scale, in rural areas during summer period under sea breeze conditions that need to be understood in their causes and formation processes (Bonsang *et al.,* 2001; Harder *et al.,* 2001). These previous works highlighted an important role of sea breezes in the air circulation during summer on Portuguese coastal regions.

The field study was the application of a Photochemical Trajectory Model (PTM) to a real situation in the Portuguese west coast: the air mass transported by the sea breeze, from the coast line (Aveiro) to a location, approximately 65 kilometres inland, (Covelo). The PTM was applied for the days June 29 and 30 of 2001. A field campaign, developed during summer 2001[2], consisted in simultaneous measurements of meteorological and air quality data at three locations, at Portuguese coast oriented in-line with the penetration of sea breezes. The Field Campaign is described in detail in Evtyugina, 2004 and Evtyugina *et al.,* 2006a. Figure 72 presents the study domain with the identification of measurement sites in CZCM field campaign 2001, Lota, Sangalhos and Covelo. The figure also shows the location of two permanent meteorological stations; Aveiro and Anadia.

The first sampling place, Lota, was located close to salt pan farms at the delta of the river Vouga, northwest of the Aveiro urban zone. This place is located in an open area that, when under the influence of N-NW sea breeze winds, has no significant local anthropogenic pollutants emissions, permitting the measurement of air masses freshly transported from the sea across the salt pan delta estuary areas. The second sampling place was located in the small town of Sangalhos. This is a relatively populated area with several small mills and some agricultural activity (mainly maize and vine farming). The third sampling site was located in the small village of Covelo Baixo considered a rural/forest zone (Evtyugina *et al.,* 2006a).

[2] The experimental campaign was sponsored by Coastal and Maritime Zone Centre (CZCM - Centro das Zonas Costeiras e do Mar).

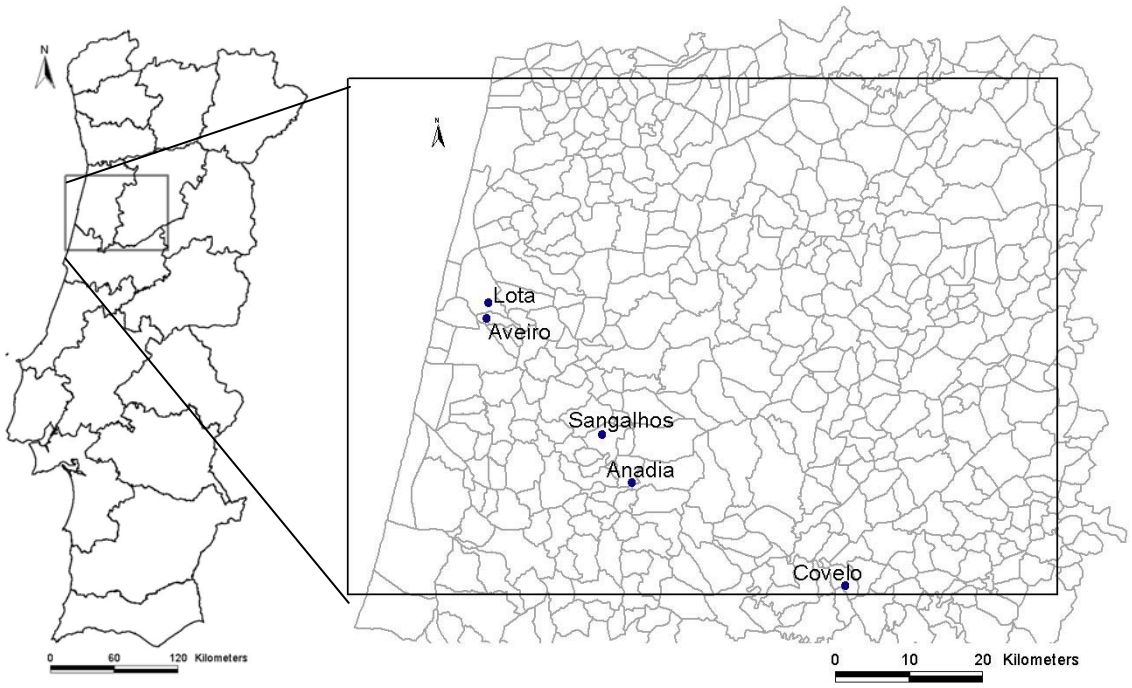

Figure 72: Study domain with identification of measurement sites in CZCM field campaign 2001; Lota, Sangalhos and Covelo and the site location of two permanent meteorological stations; Aveiro and Anadia.

6.1 Photochemical Trajectory Model (PTM)

The Photochemical Trajectory Model (PTM) used in this study was a trajectory, one layer box, model, with a Lagrangian approach, using MCM as the chemical mechanism. The MCM version used in this study was the MCM v3.1 and the MCM v3.1 with changes resultant from previous described chamber studies.

The chemical development of the species *i*, in an air parcel, in terms of its concentration rate of change with time, is described by a series of differential equations, see equation below:

$$\frac{dC_i}{dt} = \frac{E_i}{h_{mix}} + P_i - L_i C_i - \frac{V_d}{h_{mix}} C_i \qquad (52)$$

where C_i is the species concentration in the air parcel, E_i the local emission rate from pollution sources, h_{mix} the time-dependent boundary layer depth, P_i the instantaneous production from photochemistry, L_iC_i the instantaneous loss rate by photochemistry, V_d the species-dependent dry deposition velocity. Dry depositions used in PTM are the ones available in the "One Layer Photochemical Air Pollution Model". This Model was put together by Dick Derwent (from Atmospheric Processes Research Meteorological Office) in 1996 and available for download at the website http://mcm.leeds.ac.uk/MCM.

The PTM simulates the chemical development in a vertically well-mixed boundary layer air parcel being advected along trajectories. This is reasonable, when the starting time of the first daily wind trajectory takes place after the breakdown of night time inversion resulting in a well mixed boundary layer. The PTM considers that the entire column, from the bottom to the top, has the same trajectory. The approximation could be considered reasonable since the selected period for the PTM application were days of well formed sea breeze.

The model was integrated with variable order Gear's method FACSIMILE (Curtis and Sweetenham, 1987) using software FACSIMILE[3].

6.1.1 Chemical Mechanism

The MCM is described in section 2 and a more detailed description could be obtained in Jenkin *et al.* (1997), Saunders *et al.* (2003), Jenkin *et al.* (2003) and Bloss *et al.* (2005b).

6.1.1.1 Photolysis coefficients

MCM considers photolysis reactions for inorganic species: O_3; H_2O_2; NO_2; NO_3; HONO; HNO_3 and for many organic species, from simple carbonyl compounds, such as aldehydes and ketones (both emitted into the troposphere and formed as degradation products), and also for many other complex carbonyl compounds, hydroperoxides and organic nitrates which are generated as degradation products (Jenkin *et al.,* 1997).

Equations for photolysis coefficients calculation, as function of solar zenith angle to model application, are available for download at, the website http://mcm.leeds.ac.uk/MCM. These equations are based in photon flux determined using a Two Stream Isotropic Scattering Model for clear sky conditions at an altitude of 0.5 km (Hough, 1988 *in* Jenkin *et al.,* 1997). However, in this work a new photon flux was used for the photolysis coefficients calculation since some changes were made in absorption cross-section and quantum yield and the Two Stream Isotropic Scattering Model wasn't available.

Absorption cross-section and quantum yield for the photolysis reactions considered in this study are given in Table 12. Photolysis rates as a function of solar zenith angle were determined using Tropospheric Ultraviolet and Visible Radiation Model (NCAR/ACD TUV[4]), for clear sky conditions at an altitude of 0.5 km. The Photolysis reactions and parameters assigned as function of solar zenith angle (χ) are present in Appendix I.

[3] FACSIMILE for Windows, version 3.5.5, ©UES Software 2000.

[4] NCAR/ACD TUV: Tropospheric Ultraviolet & Visible Radiation Model. NCAR Atmospheric Chemistry Division (ACD). (http://gcmd.nasa.gov/records/UCAR_TUV.html)

Table 12: Source references for absorption cross sections and quantum yield for photolysis reactions considered in this study.

J (MCM FACSIMILE code)	**Absorption cross-sections**	**Quantum yields**
O3 = O1D	Molina and Molina, 1986	Sander *et al.,* 2000
O3 = O	Molina and Molina, 1986	Sander *et al.,* 2000
H2O2 = OH + OH	DeMore *et al.,* 1997	DeMore *et al.,* 1997
NO2 = NO + O	DeMore *et al.,* 1997	DeMore *et al.,* 1997
NO3 = NO	Wayne *et al.,* 1991	Johnston *et al.,* 1996
NO3 = NO2 + O	Wayne *et al.,* 1991	Johnston *et al.,* 1996
HONO = OH + NO	Bongartz *et al.,* 1991	Bongartz *et al.,* 1991.
HNO3 = OH + NO2	Burkholder *et al.,* 1993	Johnston *et al.,* 1974
HCHO = CO + HO2 + HO2	DeMore *et al.,* 1994	DeMore *et al.,* 1994
HCHO = H2 + CO	DeMore *et al.,* 1994	DeMore *et al.,* 1994
CH3CHO = CH3O2 + HO2 + CO	Martinez *et al.,* 1992	Atkinson and Lloyd, 1984
C2H5CHO = C2H5O2 + HO2 + CO	Martinez *et al.,* 1992	Heicklen *et al.,* 1986
n-C3H7CHO = NC3H7O2 + CO + HO2	Martinez *et al.,* 1992	Förgeteg *et al.,* 1978
n-C3H7CHO = CH3CHO + C2H4	Martinez *et al.,* 1992	Förgeteg *et al.,* 1978
i-C3H7CHO = i-C3H7O2 + HO2 + CO	Martinez *et al.,* 1992	DeSai *et al.* 1986
CH_2=C(CH_3)CHO = CH3CO3 + HCHO + CO + HO2	Raber and Moortgat 1996	Raber and Moortgat 1996
CH_2=C(CH_3)CHO = CH_2=C(CH_3)COO2 +HO2	Raber and Moortgat 1996	Raber and Moortgat 1996
CH3C(O)CH3 = CH3CO3 + CH3O2	Martinez *et al.,* 1992	Meyrahn *et al.,* 1986
CH3C(O)C2H5 = CH3CO3 + C2H5O2	Martinez *et al.,* 1992	Raber and Moortgat 1996
CH3C(O)CH=CH2 = C3H6 + CO	Raber and Moortgat 1996	Raber and Moortgat 1996
CH3C(O)CH=CH2 = CH3CO3 + HCHO + CO + HO2	Raber and Moortgat 1996	Raber and Moortgat 1996
$(CHO)_2$ = CO + CO + H2	Plum *et al.,* 1983	Plum *et al.,* 1983 and Langford and Moore, 1984
$(CHO)_2$ = HCHO + CO	Plum *et al.,* 1983	Plum *et al.,* 1983 and Langford and Moore, 1984
$(CHO)_2$ = CO + CO + HO2 + HO2	Plum *et al.,* 1983	Plum *et al.,* 1983 and Langford and Moore, 1984
CH3C(O)CHO = CH3CO3 + CO + HO2	Meller *et al.,* 1991	Raber and Moortgat 1996
CH3C(O)C(O)CH3 = CH3CO + CH3CO	Plum *et al.,* 1983	Plum *et al.,* 1983
CH3OOH = CH3O + OH	Vaghjiani and Ravishankara, 1990	Vaghjiani and Ravishankara, 1990
CH3NO3 = CH3O + NO2	Roberts and Fajer, 1989	Talukdar *et al.,* 1997
C2H5NO3 = C2H5O + NO2	Roberts and Fajer, 1989	Zhu and Ding, 1997
n-C3H7NO3 = NC3H7O + NO2	Roberts and Fajer, 1989	Luke *et al.,* 1989
IC3H7NO3 = IC3H7O + NO2	Roberts and Fajer, 1989	Luke *et al.,* 1989
t-C4H9NO3 = TC4H9O + NO2	Roberts and Fajer, 1989	Luke *et al.,* 1989
CH3C(O)CH2ONO2 = CH3C(O)CH2O + NO2	Roberts and Fajer, 1989	Jenkin *et al.,* 1997
CH3C(O)CH2ONO2 = CH3CO + HCHO + NO2	Roberts and Fajer, 1989	Jenkin *et al.,* 1997

Figure 73 shows the ratio between the photolysis coefficients calculated using Tropospheric Ultraviolet and Visible Radiation Model for clear sky conditions at an altitude of 0.5 km with the absorption cross sections and quantum yield presented in Table 12 and the photolysis coefficients calculated by application of equations available for download at, the website http://mcm.leeds.ac.uk/MCM. Most of the values are in acceptable agreement; a systematic

difference might be expected because solar intensities, obtained by the two different models, are different.

The value of J33 is opposite to the general trend, in the figure; therefore the photolysis model used to calculate the J values based on a Two Stream Isotropic Scattering Model was analysed. The code which was first developed by Adrian Hough in 1988, contains the Plum *et al.* (1983) cross sections for glyoxal. However, the present analysis allowed to identify an error in one cross sections value which has been propagated in a number of photolysis model codes since 1988. Some differences are, also, related with the fact that in this work the absorption cross sections and quantum yield values were obtained by interpolation for 1nm intervals, a more rigorous approach than in models based in the Hough 1988 model.

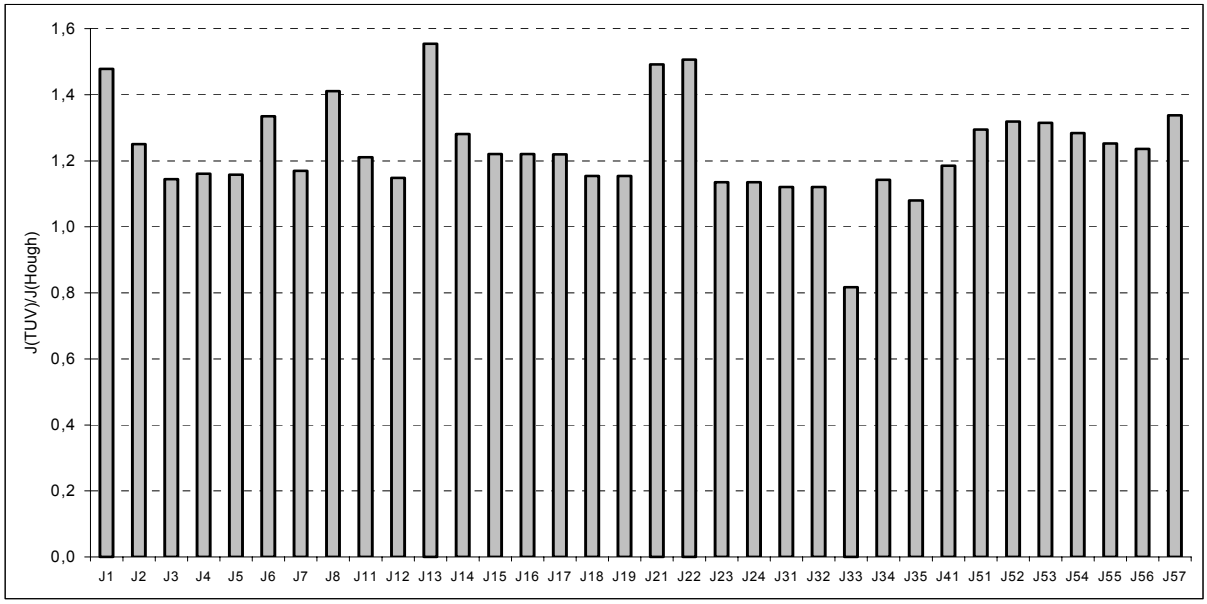

Figure 73: Ratio of photolysis coefficients calculated using photon flux determined by Tropospheric Ultraviolet and Visible Radiation Model (J-TUV) and photolysis coefficients calculated using photon flux determined a Two Stream Isotropic Scattering Model for clear sky conditions at an altitude of 0.5 km (as available for download by internet, Hough, 1988 *in* Jenkin *et al.,* 1997) (J-Hough).

As result of chamber evaluation of MCM v3.1, quantum yield for photolysis reactions of formaldehyde, MEK, MACR and MVK and absorption cross sections of formaldehyde were updated. The new values and respective photolysis reactions are presented in Table 13 and Appendix I.

Table 13: Source references for absorption cross sections and quantum yield for photolysis reactions considered after the refinements obtained in chamber evaluation

J (MCM FACSIMILE code)	**Absorption cross-sections**	**Quantum yields**	**Coments**
HCHO = CO + HO2 + HO2	Meller and Moortgat, 2000.	Smith *et al.,* 2002	σ and ϕ recommended by IUPAC (Data Sheet P1 updated in 16th May 2002)
HCHO = H2 + CO	Meller and Moortgat, 2000.	Smith *et al.,* 2002	σ and ϕ recommended by IUPAC (Data Sheet P1 updated in 16th May 2002)
CH3C(O)CH3 = CH3CO3 + CH3O2	Gierczak *et al.,* 1998	Warneck, 2001	σ and ϕ recommended by IUPAC (Data Sheet P7 updated in 21st January 2003)
CH_2=C(CH_3)CHO = CH3CO3 + HCHO + CO + HO2	Raber and Moortgat 1996	Pinho *et al.,*2005	σ (IUPAC recommends Gierczak *et al.,* 1997) ϕ obtained by optimization and in accordance with Gierczak *et al.,* 1997 and RADICAL, 2002.
CH_2=C(CH_3)CHO = CH_2=C(CH_3)COO2 +HO2	Raber and Moortgat 1996	Pinho *et al.,*2005	σ (IUPAC recommends Gierczak *et al.,* 1997) ϕ obtained by optimization and in accordance with Gierczak *et al.,* 1997 and RADICAL, 2002.
CH3C(O)C2H5 = CH3CO3 + C2H5O2	Martinez *et al.,* 1992	Pinho *et al.,*2005	σ recommended by IUPAC (Data Sheet P8 updated in 16th May 2002); ϕ obtained by optimization
CH3C(O)CH=CH2 = C3H6 + CO	Gierczak *et al.,* 1997	Gierczak *et al.,* 1997	σ and ϕ recommended by IUPAC (Data Sheet P11 updated in 16th May 2002); ϕ/2
CH3C(O)CH=CH2 = CH3CO3 + HCHO + CO + HO2	Gierczak *et al.,* 1997	Gierczak *et al.,* 1997	σ and ϕ recommended by IUPAC (Data Sheet P10 updated in 9th August 2002); ϕ/2

6.1.2 Transport Model

The PTM uses a trajectory one layer box model. The PTM was applied to a real situation in the Portuguese west coast: the air mass transported by the sea breeze, during the period of June 29 to June 30 (2001), from the coast line (Aveiro) to a location, approximately 65 kilometres inland (Covelo).

Air masses trajectories were calculated based in a back-trajectory principle. The trajectories were calculated, for 30 minutes intervals, relatively to the arrival of the air mass at Covelo and imply a period of transport between Lota and Covelo of 3:30 – 5:00 hours, under sea breeze (see Table 14). The trajectories were calculated using wind measurements taken at 10 meters height obtained in Aveiro and Sangalhos sites; see Figure 74 and Figure 75. The wind data used were from the Aveiro meteorological station instead Lota and the data from Covelo were not used since in the acquisition of wind data from Lota and Covelo, during the CZCM field campaign 2001, had problems (see explanation in following pages).

Table 14: Considered initial, end and run time for each modelled trajectory for June 29 and June 30, 2001.

June 29	Initial (h:min)	End (h:min)	Run time (h:min)	June 30	Initial (h:min)	End (h:min)	Run time (h:min)
T1	12:30	16:30	4:00	T1	11:25	16:00	4:35
T2	13:15	17:00	3:45	T2	12:10	16:30	4:20
T3	13:55	17:30	3:35	T3	12:25	17:00	4:35
T4	14:25	18:00	3:35	T4	12:40	17:30	4:50
T5	14:55	18:30	3:35	T5	12:45	18:00	5:15
T6	15:30	19:00	3:30	T6	13:10	18:30	5:20
T7	15:55	19:30	3:35	T7	14:10	19:00	4:50
T8	16:20	20:00	3:40	T8	14:35	19:30	4:55
T9	16:45	20:30	3:45	T9	14:55	20:00	5:05

The time domain of these field application is in same order of those used in chamber runs, evaluated in the first part of this study. Most of the MCM field applications were in Photochemical Trajectories Models with the air parcel being advected along multi-day trajectories over Europe (Derwent *et al.,* 1991; Derwent *et al.,* 1998; Derwent *et al.,* 2001; Derwent *et al.,* 2005; Utembe *et al.,* 2005).

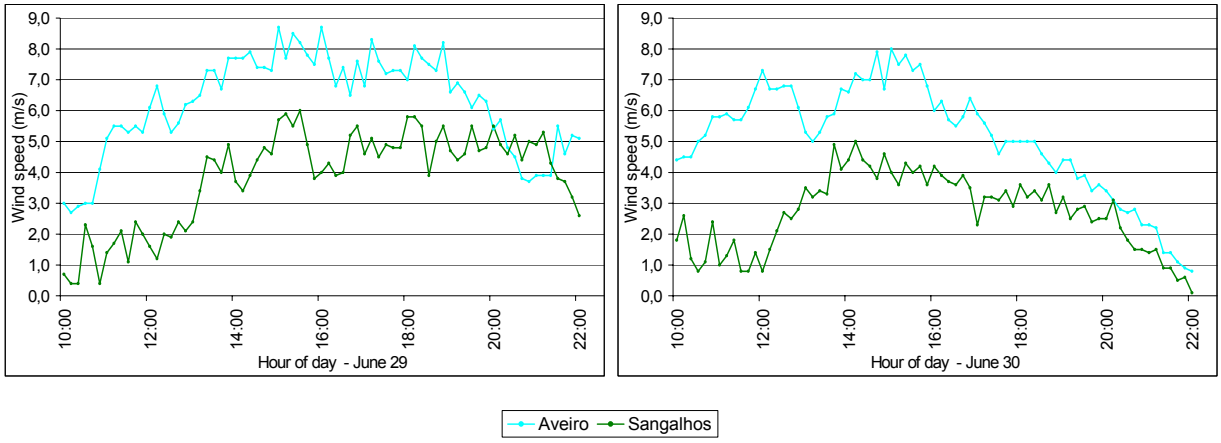

Figure 74: Wind speed measured in Aveiro and Sangalhos during June 29 and 30 (2001).

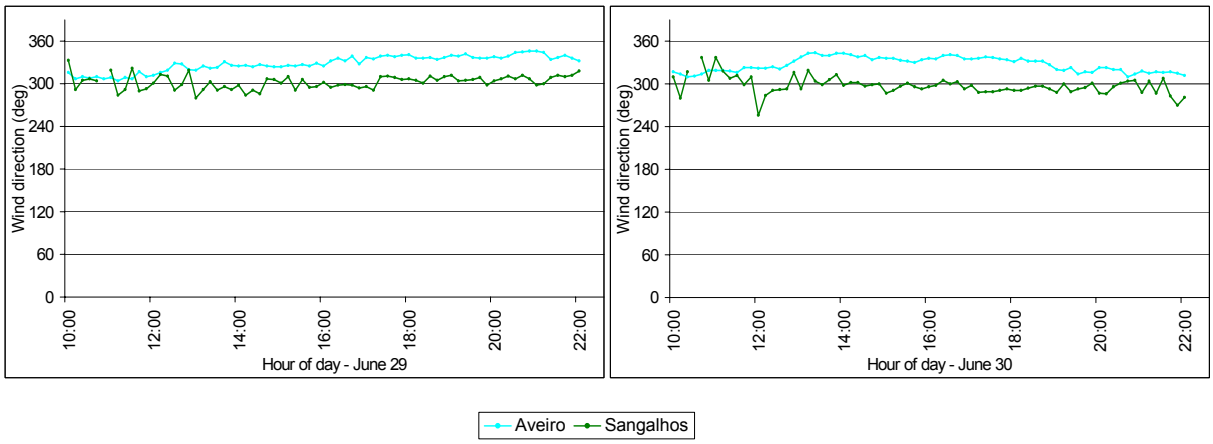

Figure 75: Wind direction measured in Aveiro and Sangalhos during June 29 and 30 (2001).

The present study considered 9 different trajectories calculated to 30 minutes intervals arriving air mass at Covelo. The trajectories obtained for day June 29 and June 30 are presented in Figure 76 and Figure 77 respectively.

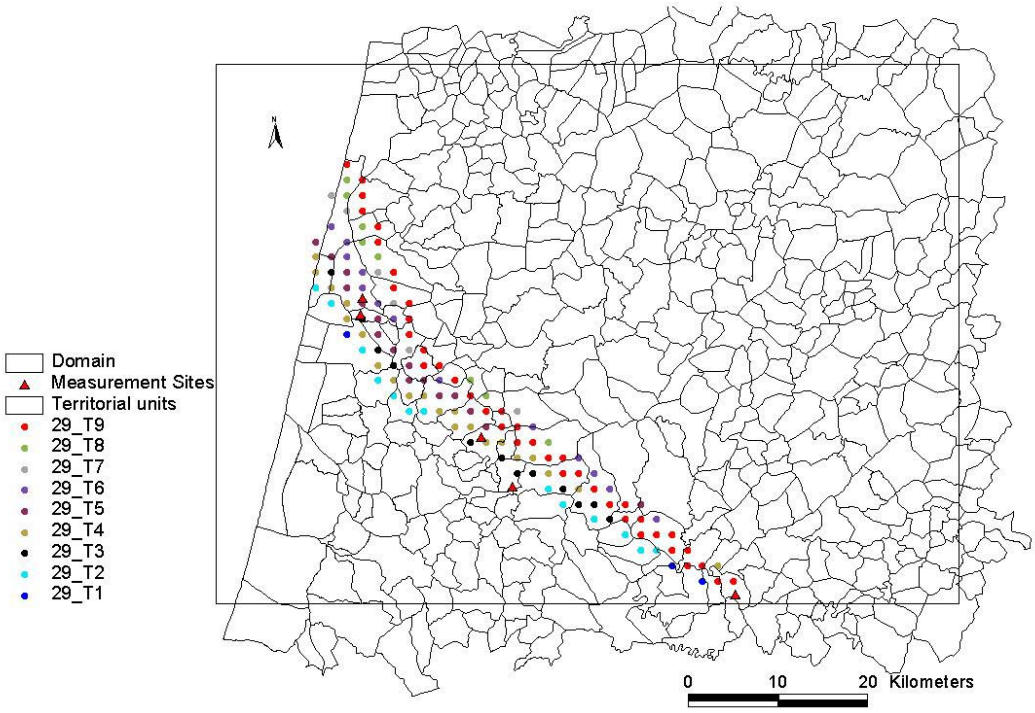

Figure 76: Trajectories of air masses for June 29 of 2001 for 30 minutes intervals of Covelo arriving air mass.

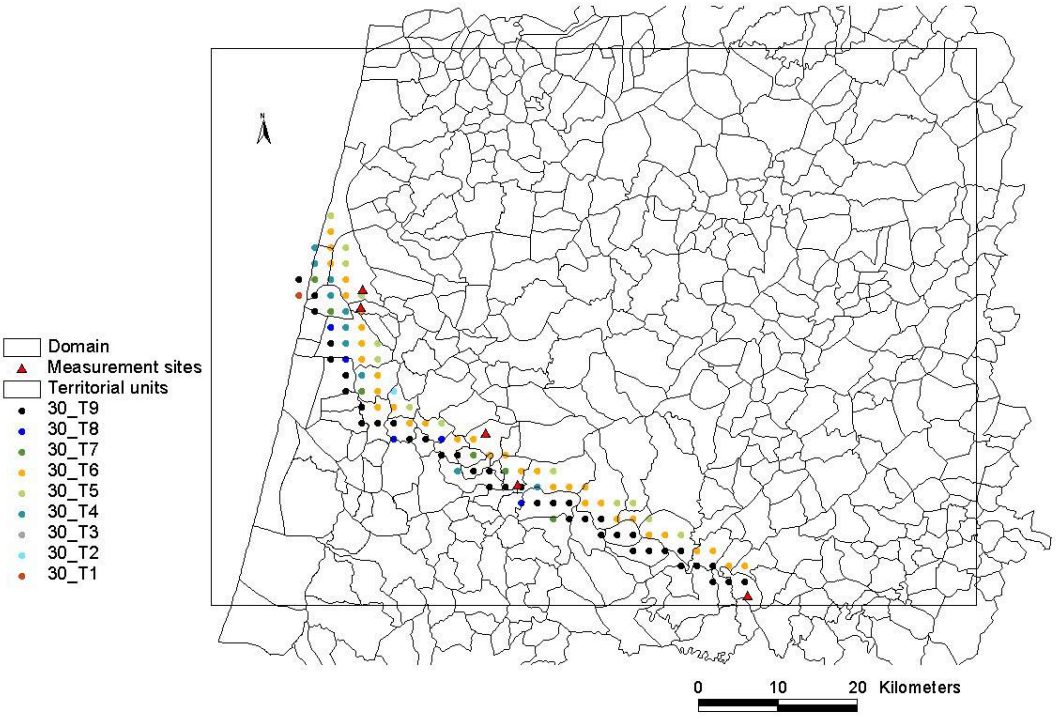

Figure 77: Trajectories of air masses for June 30 of 2001 for 30 minutes intervals of Covelo arriving air mass.

To establish the box height used in the PTM, the vertical temperature profile obtained by balloon measurements made during the CZCM field campaign 2001 in Sangalhos was used. Figure 78 shows the temperature *vs.* height for June 29 and 30. The box height, function of day time, used in the PTM, for June 29 and 30, is presented in Figure 79.

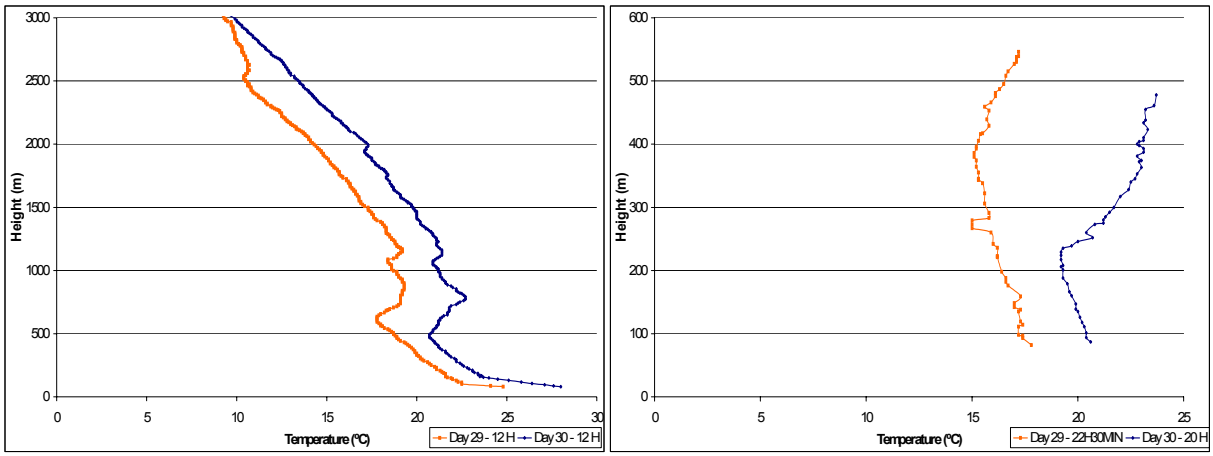

Figure 78: Temperature vs. height. Measurements obtained by balloon made during the CZCM field campaign 2001 in Sangalhos, for June 29 and 30.

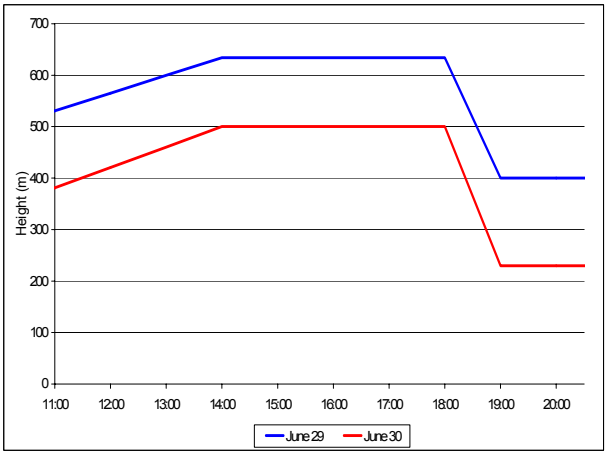

Figure 79: Box height, function of day time, used in the Photochemical Trajectorie Model for June 29 and 30.

6.1.3 Air Quality and Meteorological Data

The initial concentrations of O_3, NO_x and VOC used in PTM were obtained from the CZCM field campaign 2001, see Figure 80 e Figure 81.

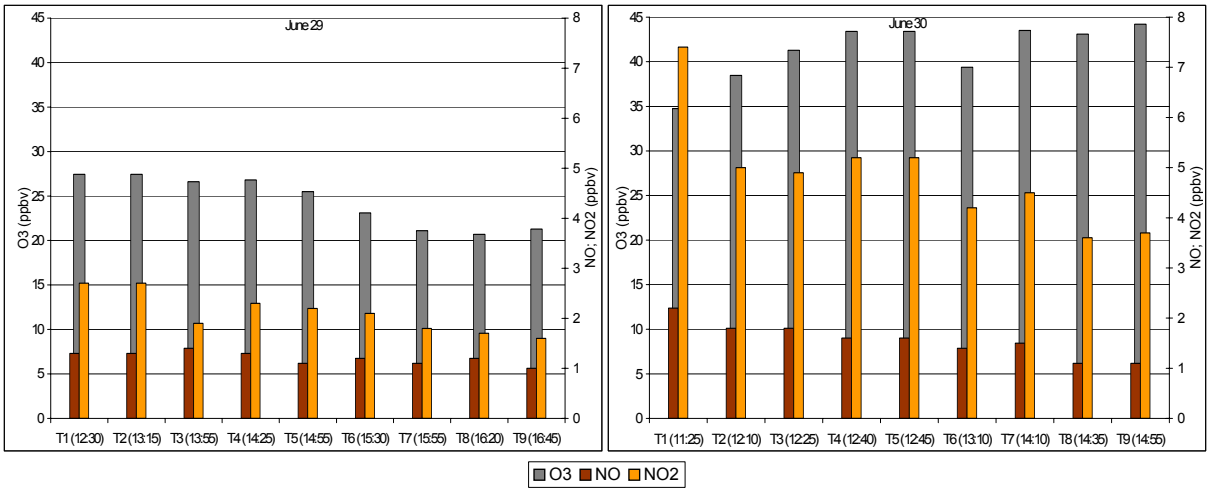

Figure 80: Initial concentrations of O_3 and NO_x used in PTM, data from CZCM field campaign 2001, resulting from measurements at Lota.

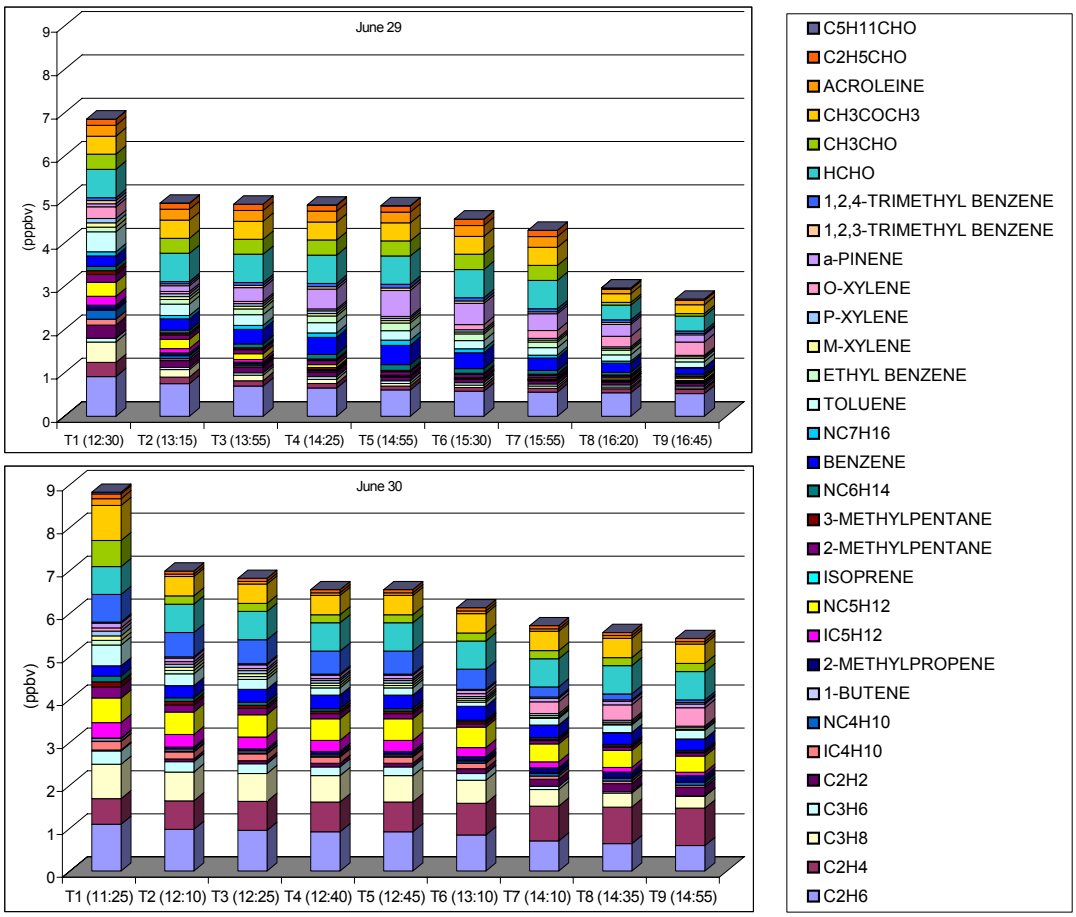

Figure 81: Initial concentrations of VOC used in PTM, data from CZCM field campaign 2001, resulting from measurements at Lota.

The meteorological data used for PTM were obtained from the CZCM field campaign 2001 and from permanent meteorological stations at Aveiro, Anadia, Coimbra and Oporto. Selection of the data was made considering its availability and quality. The wind speed and direction is present in the section 6.1.2. The Photosynthetic Active Radiation (PAR) used was calculated based in measurements of Global Radiation (W/m^2) from the Oporto meteorological station. The PAR (W/m^2) was considered 0.45 of the Global Radiation and the photon flux of PAR ($\mu mol.m^{-2}.s^{-1}$) was calculated considering that the energy of a photon of 550 nm as representative of the average energy of the PAR photons (Nunes 1996 and references therein), see Figure 82. The Global Radiation was only used for PAR calculation but was not used for the photolysis coefficients since no spectral measurements were made during field campaign. Besides the days chosen had perfect clear skies, without clouds that could interfere with estimations taken pour sun inclination.

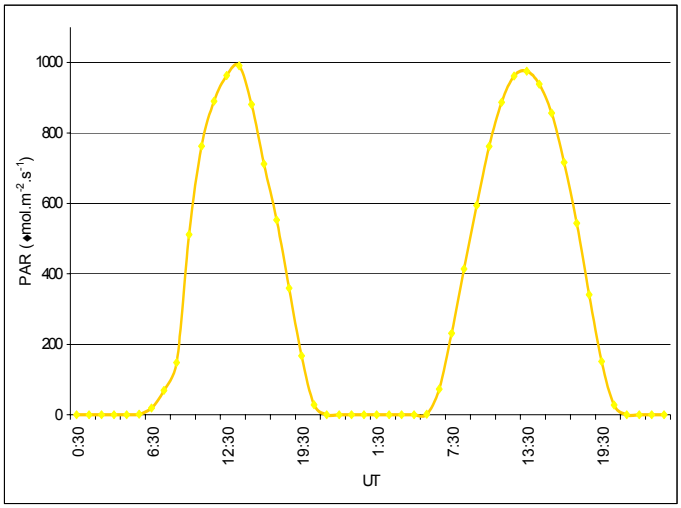

Figure 82: Photosynthetic Active Radiation calculated from Oporto Global Radiation measurements during June 29 and 30 of 2001.

The temperature and relative humidity used in PTM for each grid cell was calculated by interpolation of temperature measurements at Aveiro and Anadia meteorological stations and measurements in Covelo during CZCM field campaign 2001 (see Figure 83 and Figure 84).

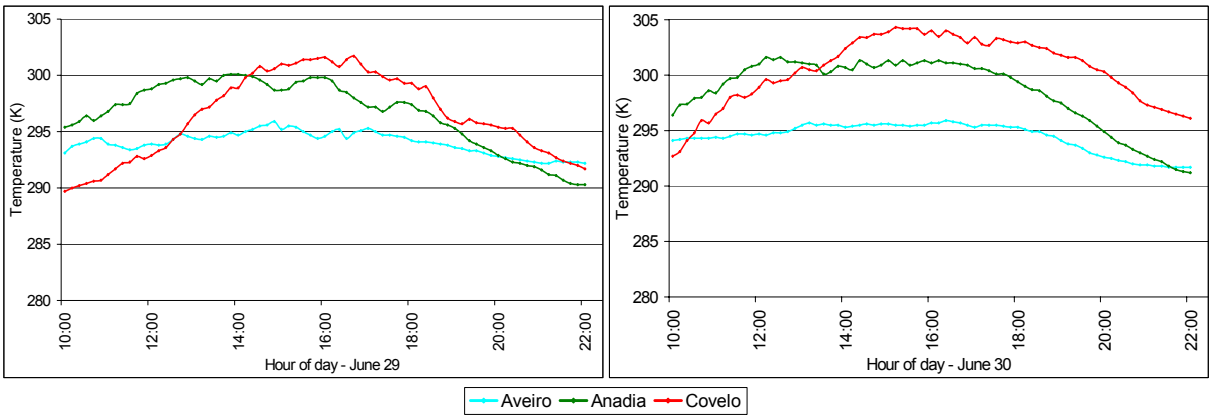

Figure 83: Temperature measured in Aveiro, Anadia and Covelo during June 29 and 30 (2001).

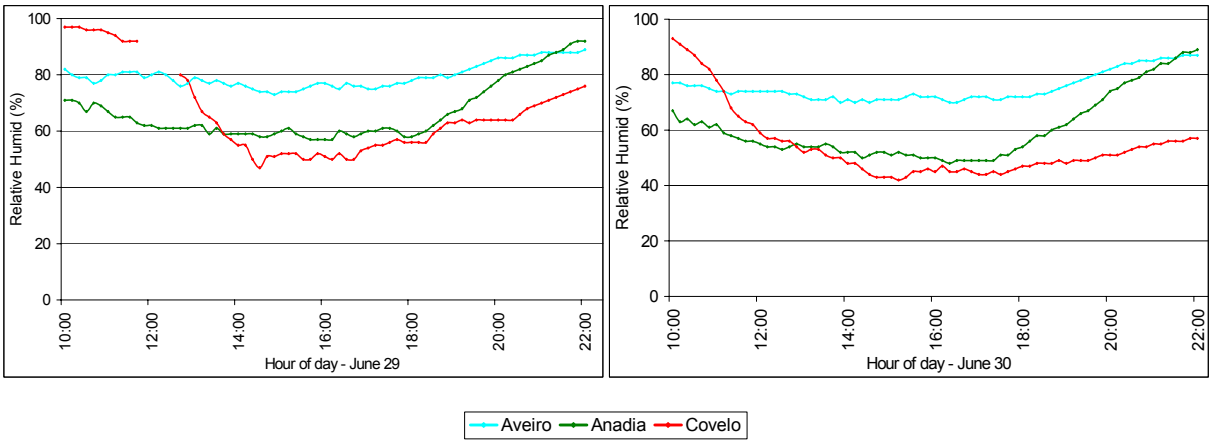

Figure 84: Relative humid in Aveiro, Anadia and Covelo during June 29 and 30 (2001).

6.1.4 Emissions Database

6.1.4.1 Biogenic Emissions Inventory

Although on a worldwide basis VOCs from biogenic sources dominate over those from anthropogenic sources by a factor greater than 10, in urban areas anthropogenic VOCs often dominate (e.g. Atkinson and Arey, 2003). The European Continent is unique, since most of the emissions of VOC come from anthropogenic sources rather than natural sources (e.g. Simpson *et al.,* 1999). However, the VOC emissions in Mediterranean areas are dominated by emissions from forests during summer time (e.g. Pio *et al.,* 1993; Simpson *et al.,* 1999). Considering the study domain, the inventory of biogenic emissions assumes a key role.

The overview and discussion of emission, physiology and ecology of biogenic volatile organic compounds are well documented (e.g. Tingey *et al.,* 1980; Tingey *et al.,* 1981; Guenther *et al.*

1993; Harley *et al.*; 1999; Kesselmeier and Staudtt, 1999) and taking in account the goal of this work, this section only describes the used methodology.

There are two main approaches to assign emission factors to an area. One is to quantify the species composition within that area, assign an emission rate to each species and aggregate the resulting emissions from each species. The other is to assign an emission rate directly to the ecosystem type in the study area (Guenther *et al.,* 1995).

The construction of global VOC emission inventories depends on the use of algorithms describing VOC emission rates under different environmental conditions. If these algorithms and their underlying assumptions are incorrect, estimations of VOC fluxes, ozone concentrations and other model outputs will also be incorrect (e.g. Guenther *et al.* 1993; Guenther*,* 1997; Simon *et al.,* 2005).

In the present study, only the inventory for isoprene and monoterpenes emissions was performed, because these conpounds groups are the more relevant and MCM v3.1 does not have the mechanism reactions for other biogenic compounds. In the study domain the monoterpene emissions are mainly associated with the Pine (*Pinus Pinaster*) forests, therefore the monoterpene emissions were splited; 60% α-pinene and 40% β-pinene (Pio *et al.,* 1993).

There are two general models that can be used to simulate VOC emissions variations due to changes in light and leaf temperature (Guenther *et al.,* 1993). The emission of isoprene and monoterpenes show clear temperature dependence. Additionally, isoprene emissions have been shown to be function of light, as a result of the direct link between isoprene emission and synthesis from photosynthetic products. As no large isoprene pool exists, synthesis and hence emission will cease within minutes, in absence of photosynthetic active radiation (PAR). Monoterpenes emissions are generally regarded as light independent, because after synthesis they are stored in organs, such as resin ducts or glands, exhibiting quite large storage pools compared to emission rates (e.g. Tingey *et al.,* 1980; Tingey *et al.,* 1981; Guenther *et al.* 1993; Harley *et al.*; 1999; Kesselmeier and Staudtt, 1999).

For the mathematical description of isoprene and monoterpene emissions, semi empirically designed algorithms are used.

Guenther *et al.* (1993) recommended the following algorithm to estimate the emission flux of isoprene,

$$I = I_S C_T C_L \tag{53}$$

where I [μg.g^{-1}(dry mass).h^{-1}] is isoprene emission rate at a temperature T(K) and PAR flux L(μmol.m^{-2}.s^{-1}), I_S [μg.g^{-1}(dry mass).h^{-1}] is isoprene emission rate at a standard temperature, T_S = 303 K and a standard PAR flux (1000 μmol.m^{-2}.s^{-1}). C_L and C_L factors are defined as,

$$C_L = \frac{\alpha C_{L1} PAR}{\sqrt{1+\alpha^2 PAR^2}} \tag{54}$$

$$C_T = \frac{\exp\left[\frac{C_{T1}(T-T_S)}{RT_S T}\right]}{C_{T3} + \exp\left[\frac{C_{T2}(T-T_M)}{RT_S T}\right]} \tag{55}$$

where α (0.0027), C_{L1} (1.066), R is a constant (8.314 J.K^{-1}.mol^{-1}), C_{T1} (95000 J.mol^{-1}), C_{T2} (230000 J.mol^{-1}), T_M (314 K), T_S (303 K) are empirical coefficients obtained by measurements emission rates of eucalyptus, sweet gum, aspen and velvet bean (Guenther *et al.,* 1993). The value of coefficient C_{T3} should be 0.961 (Guenther, 1997). As seen in Figure 85 the temperature and radiation factors have a large influence in the isoprene emissions.

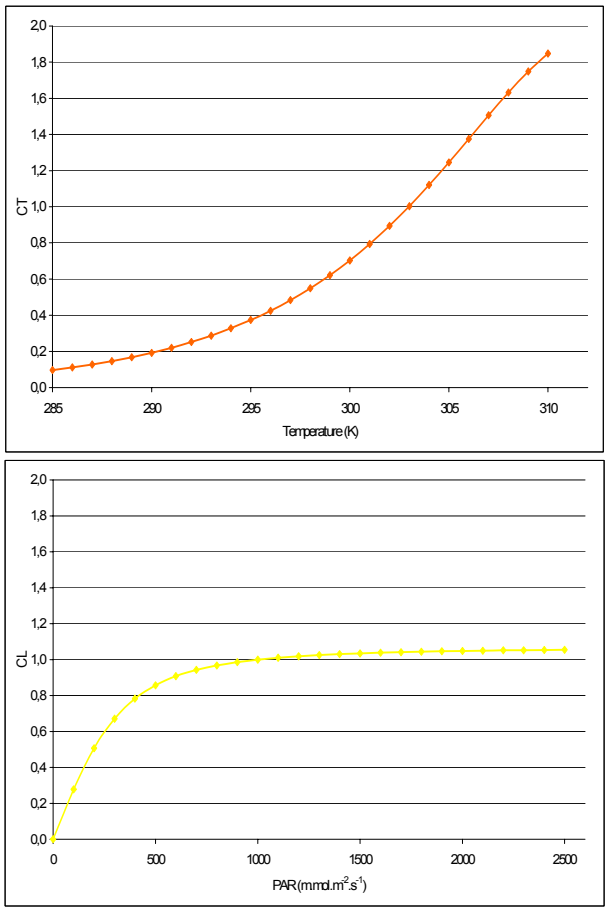

Figure 85: Temperature (CT) and radiation (CL) factors, from the Guenther *et al.* (1993) recommended algorithm to estimate the emission flux of isoprene, function of temperature and radiation respectively.

Emissions of monoterpenes are controlled by volatilization of stored VOC for a large variety of plants and the emission response to temperature shows an exponential increase with temperature (e.g. Tingey *et al.,* 1980; Guenther *et al.,* 1993). Biogenic emissions models typically use the following equation to simulate the temperature dependence of monoterpene emission rates (Guenther *et al.,* 1993 and references there in),

$$M = M_S \exp(\beta(T - T_S)) \quad (56)$$

where M [μg.g^{-1}(dry mass).h^{-1}] is the monoterpene emission rate at temperature T(K), M_S [μg.g^{-1}(dry mass).h^{-1}] is the monoterpene emission rate at a standard temperature, T_S = 303 K and β (K^{-1}) is an empirical coefficient. The coefficient β establishes the temperature dependence. β estimates vary from 0.057 to 0.144 K^{-1} (Guenther *et al.,* 1993 and references there in). Guenther *et al.* (1993) recommended the use of β equal to 0.09 K^{-1}. Using a β value of 0.09 K^{-1}, the temperature effect in flux emissions of monoterpenes is very similar to the effect of the factor CT in flux emissions of isoprene, see Figure 86.

The natural VOC emissions, F [μg.h^{-1}.m^{-2}] can be estimated as:

$$F = ED \quad (57)$$

where E is emission rate of natural VOC per mass of leaf dry mass [μg.g^{-1}(dry mass).h^{-1}] and the D [g (dry mass).m^{-2}] is foliar density of biogenic species.

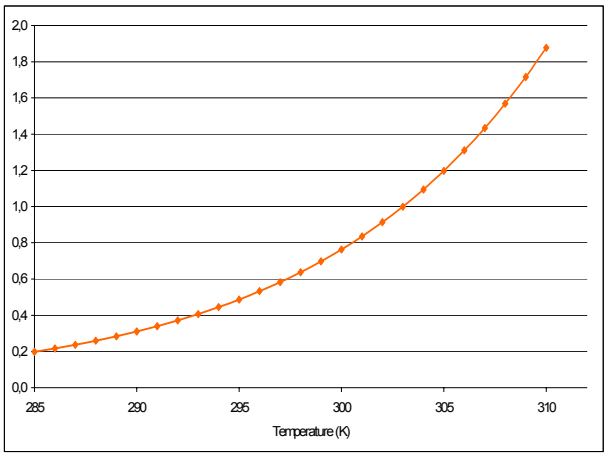

Figure 86: Temperature factor accounting the exponential increase of flux emissions of monoterpenes with temperature, considering the value 0.09 K^{-1} to β parameter as recommended by Guenther *et al.* (1993).

The inventory of the biogenic emissions to the studied domain was performed using the land use data from the CNIG - Centro Nacional de Informação Geográfica (National Centre of Geographic Information).

For the domain, 41 land use maps 10x16 km (scale 1:25000) were used. In these maps land use is divided in six different classes (Forest; Agricultural; Social; Aquatic surfaces; Uncultivated; Unproductive) resulting in more than 800 different codes used by CNIG. Land use classification attributed by CNIG is divided into individual polygons each having different species, percentage of occupied area and dominant specie.

Spatial information for polygons was converted to a spatial grid with cell dimensions of 100x100 metres using a Geographical Information Software (Arcview). This methodology results in very small losses of information.

To each CNIG code an emission flux of isoprene and monoterpenes ($\mu g.m^{-2}.h^{-1}$) for standard conditions (T_S = 303 K e PAR = 1000 $\mu mol.m^{-2}.s^{-1}$) was obtained, using emission factors. Emission factors are usually expressed by specie. The emission factors used in this study were obtained in the literature (see Appendix II).

However, Pio *et al.* (1993) concluded, from the emission measurements and the spatial distribution of vegetation, that only a few species including the maritime pine, the eucalyptus, the cork oak, the holm oak and some shrubs such as the spurge laurel and the rock-rose (which are important emitters of monoterpenes and very frequent in uncultivated areas) need to be considered to produce a correct emission inventory in Portugal.

Fluxes of emission for cells of 2x2 kilometres were obtained associating individual 100x100 metres cells. The cell dimension of 2x2 kilometres were selected in a way to decrease the error associated with trajectories imprecision. Each of these cells represents an average air mass in terms of surface emissions.

For the study domain the isoprene emissions, associated mainly with *Eucalyptus globulus*, prevail in a centre-south band. This area, between Anadia and Tábua, has a dense Eucalyptus forest (*Eucalyptus globulus*) and consequently important emissions of isoprene. Monoterpene emissions are located in the south-west and north-east of the domain. These emissions are mainly associated with the Pine (*Pinus Pinaster*) forests.

Figure 87 and Figure 88 show isoprene and monoterpenes emission rate at standard conditions.

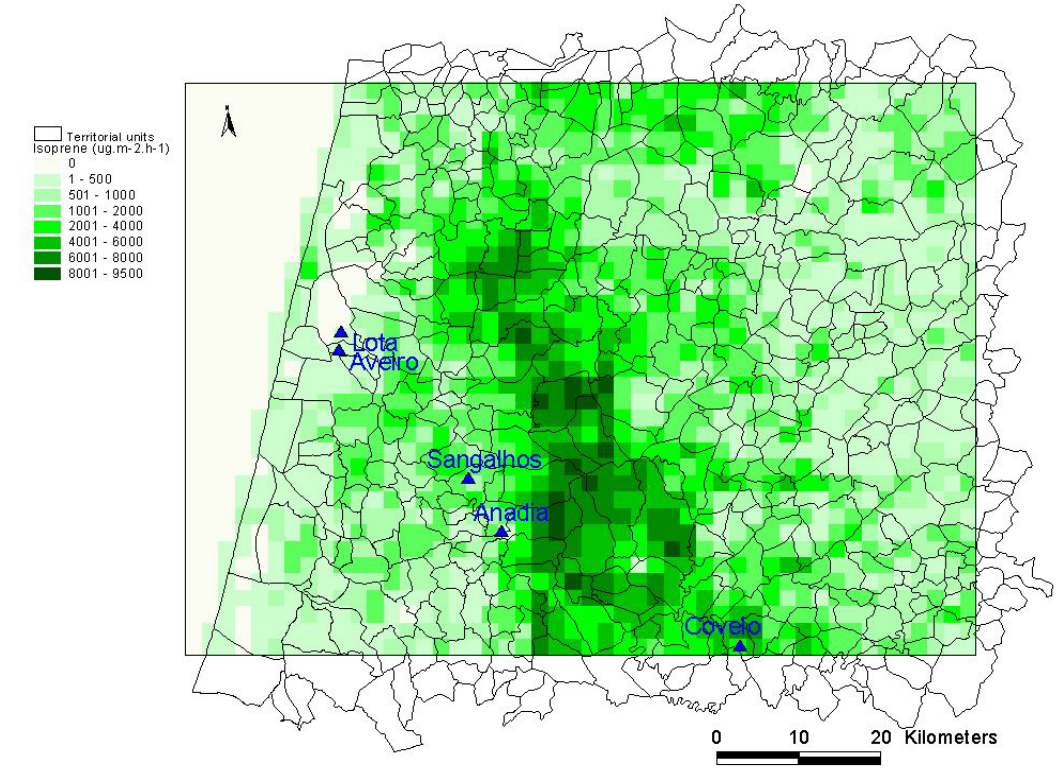

Figure 87: Mass emissions of isoprene ($\mu g.m^{-2}.h^{-1}$) for the study domain converted to a 2x2 km grid, for standard conditions Ts = 303 K and PAR = 1000 ($\mu mol.m^{-2}.s^{-1}$).

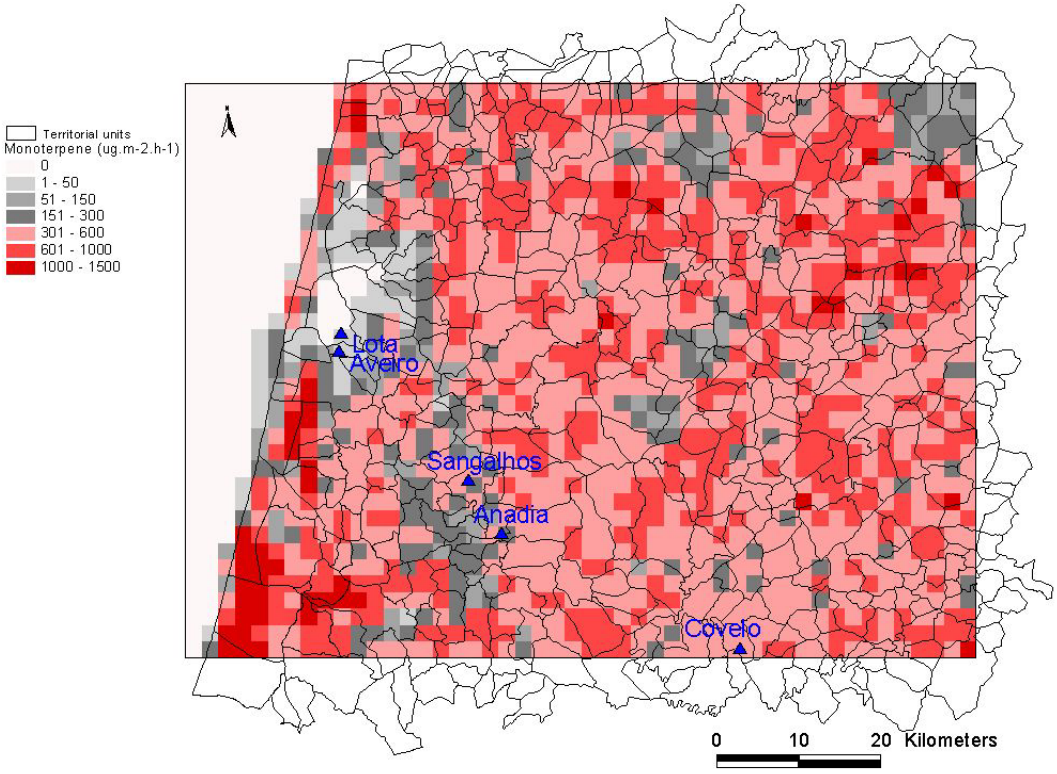

Figure 88: Mass emissions of monoterpenes ($\mu g.m^{-2}.h^{-1}$) for the study domain converted to a 2x2 km grid, for standard conditions Ts = 303 K and PAR = 1000 ($\mu mol.m^{-2}.s^{-1}$).

6.1.4.2 Motor Vehicle Emission Inventory

In order to apply correctly the Photochemical Trajectory Model (PTM) it is essential to have a Motor Vehicle Emission Inventory (MVEI) with high spatial and temporal resolution. As described above, the PTM, in this study, is applied on a 2x2 km grid domain and during the diurnal period. Each cell needs an average emission factor (mass of pollutant.area^{-1}.time^{-1}) depending on time of the day; so the only way to obtain this information would be to know exactly the traffic in each road as function of time and the individual vehicle emissions. Since the motor vehicle emissions depends, namely, on fuel, velocity, load, class, age and driving cycle, it is almost impossible to obtain this information with accuracy for a large area like the study domain.

There are, essentially, two methods to establish, temporally and spatially, quantification of emissions originated from traffic data: top-down and bottom-up approaches (e.g. Borrego *et al.,* 2000). In the present study both approaches were applied.

In a top-down study using fuel-based approach, on-road measurements of motor vehicle emissions, expressed as mass of pollutant emitted per unit of fuel consumed, are combined with fuel sales data to estimate total pollutant (e.g. Borrego *et al.,* 2000; Singer and Harley, 2000; Pokharel *et al.,*2002; Yli-Tuomi *et al.,* 2005). In the present study, data from fuel sales discriminated for large territorial units, were disaggregated to small territorial unit, based in population density. The fuel-based emission factors (g.(kg fuel)$^{-1}$) were obtained considering the vehicle distribution by classes circulating in Portugal in the end of year 2000 and the emission factors calculated using the methodology proposed by European Environment Agency to be used by EEA member countries for the compilation of CORINAIR emission inventories and described by Ntziachristos and Samaras (2000).

The fuel-based emission factors (g.(kg fuel)$^{-1}$) take under consideration the speed dependency emissions from vehicles of different age (consequently submitted to different EC Directives). The fuel-based emission factors (g.(kg fuel)$^{-1}$) were obtained by considering the hot emissions function of speed (g.km^{-1}.vehicle^{-1}) and the fuel consumption function of speed ((g fuel). km^{-1}.vehicle^{-1}).

The information about vehicle distribution by classes circulating in Portugal in the year 2000 was obtained from the Portuguese Car Sales Association (ACAP - Associação do Comércio Automóvel de Portugal), see Appendix III. Emission factors were calculated considering an average speed, considering the vehicle distribution circulating in Portugal at the end of year 2000 and the percentages of fuel sales in the study domain (see Appendix III).

The mass emission flux was converted to a 2x2 km grid using Geographical Information Software (Arcview). Figure 89 shows mass emissions of NO_x (μg.m^{-2}.h^{-1}) for the study domain converted to a 2x2 km grid.

The mass emission flux obtained by top-down methodology is not correlated with the roads distribution, instead relates with the spatial distribution of the sales. Other disadvantage of this methodology is the fact that it considers a spatial identity between fuel sales and the fuel consumption, which is a rough approximation, especially when the study domain is crossed by several main roads and a highway. The total emissions for the study domain, obtained by application of top-down methodology, are: 12102 $kg.day^{-1}$ of NO_x and 3841 $kg.day^{-1}$ of VOC.

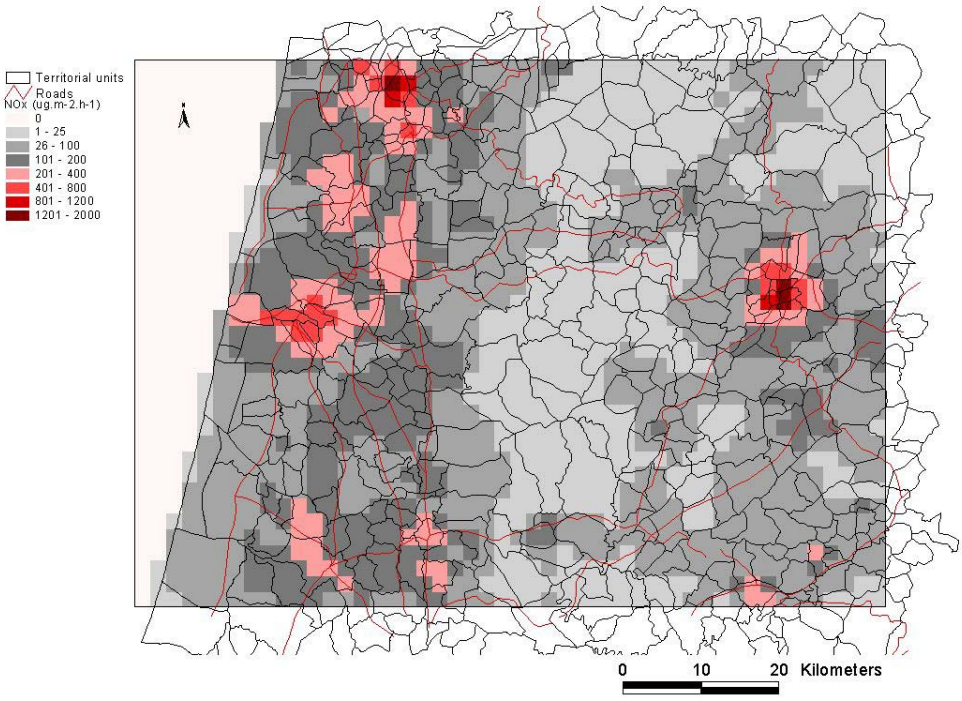

Figure 89: Mass emissions of NO_x ($\mu g.m^{-2}.h^{-1}$), from Motor Vehicle Emission Inventory applying the top-down methodology, for the study domain converted to a 2x2 km grid.

In the bottom-up approach, main roads were processed as line sources and hot on-road emissions were calculated based on daily mean traffic and emission factors. The emission factors were based in speed dependency emissions from vehicles of different age (consequently submitted to different EC Directives). The average emission factors, obtained considering the distribution by vehicle type circulating in Portugal by the end of year 2000, are presented in Appendix III.

Data related to the Daily Mean Traffic (DMT) for 68 counting points inside the study domain were obtained from the National Road Agency. The road segments length was calculated within a Geographical Information System. Line sources have been subdivided, taking into account the existent crossroads. The described methodology was applied for the estimation of NO_x and VOC

emissions associated with main roads; in the study domain no urban roads were considered. The main disadvantage of this methodology is the fact that it doesn't considers the urban and local roads.

The emission factors obtained by the applied methodologies have several factors contributing to uncertainty, namely the use of average speeds in hot emissions calculation. The emissions are higher for cold start than for drive conditions corresponding hot emissions (hot engine and warmed-up catalyst), but the major fuel consumption are in drive conditions corresponding to hot emissions. However, cold start emissions seem to be important contributors for urban driving (Ntziachristos and Samaras 2000).

Another factor contributing to uncertainty was the way evaporative VOC emissions were considered. Evaporative VOC emissions only are fully described for gasoline passenger cars (Ntziachristos and Samaras 2000). In the current study evaporative VOC emissions were not calculated by the methodology proposed by Ntziachristos and Samaras (2000) but indexed to calculated VOC hot emissions. The index factor was obtained from the Portuguese National Inventory submitted to UNECE/EMEP. The reported National NMVOC emission ratio between the NFR sector, *1 A 3 b v - R.T., Gasoline evaporation* relative to *1 A 3 b Road Transportation* was 28% in 2001.

The total emissions for the study domain, obtained by application of bottom-up methodology, are 13898 $kg.day^{-1}$ of NO_x and 3956 $kg.day^{-1}$ of VOC.

Roads considered in Motor Vehicle Emission Inventory are represented in Figure 90 and the mass emissions of NO_x ($\mu g.m^{-2}.h^{-1}$), obtained by application of bottom-up methodology, are represented in Figure 91.

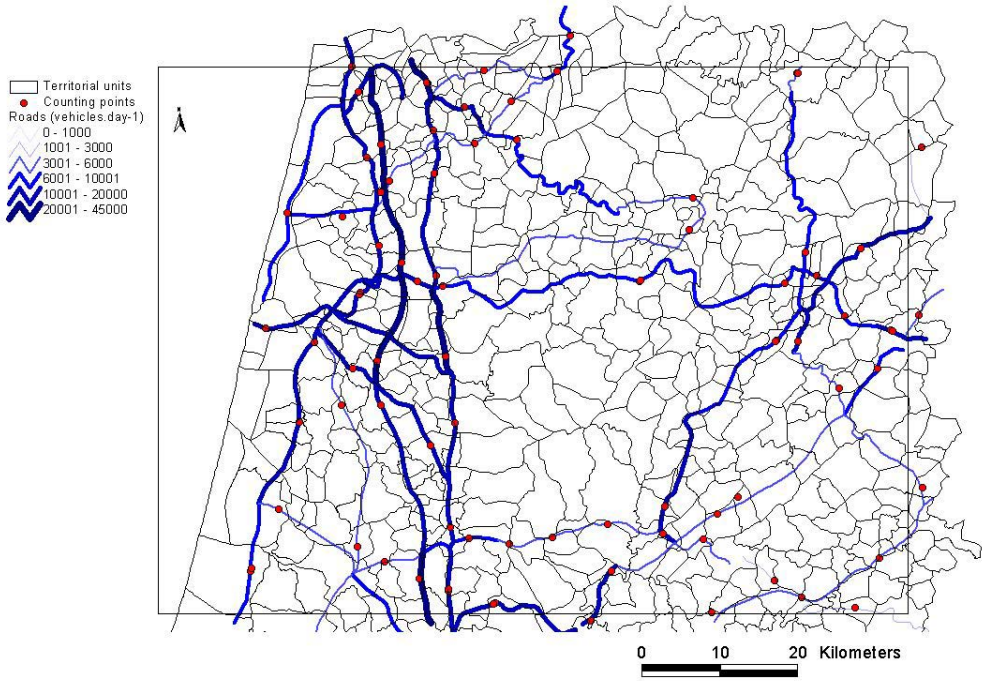

Figure 90: Roads considered in Motor Vehicle Emission Inventory applying the bottom-up methodology and traffic counting points.

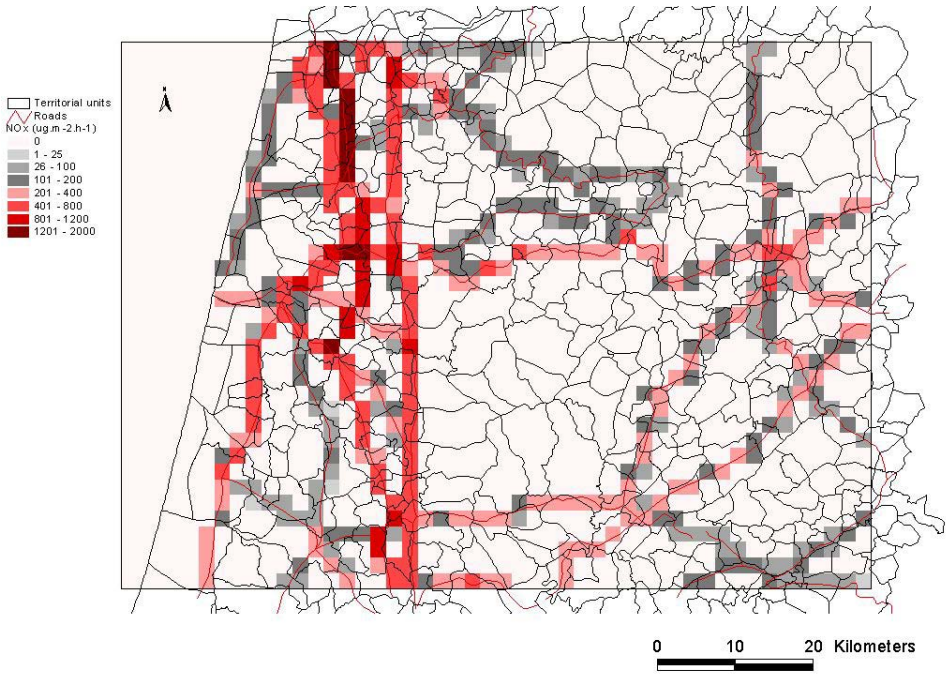

Figure 91: Mass emissions of NO_x ($\mu g.m^{-2}.h^{-1}$), from Motor Vehicle Emission Inventory applying the bottom-up methodology, for the study domain converted to a 2x2 km grid.

The top-down methodology has some advantages and some disadvantages relatively to a bottom-up methodology. The great advantage is the comparatively easier application and the great disadvantage is, obviously, no correlation between the emissions and road traffic as in the bottom-up methodology.

The comparison of emission data obtained by these two approaches demonstrates a good agreement for total values, but a significant difference for spatial distribution of the data. To ensure completeness of the data, to improve their spatial resolution and also to analyse the impact of the traffic emissions, a combination of the two approaches was applied to generate the emission data used by PTM.

The emission data considers total emissions from bottom-up calculation adding to these emissions 30% of top-down emission. This assumption was based in the relation between kilometres per year that Portuguese vehicles run in long distance and urban/suburban travels (DGGE, 1999)

The total emissions for the study domain, obtained by application of final methodology, are; 17529 $kg.day^{-1}$ and 4350 $kg.day^{-1}$ of NO_x and VOC respectively. The spatial distribution for NO_x ($\mu g.m^{-2}.h^{-1}$) is presented in Figure 92.

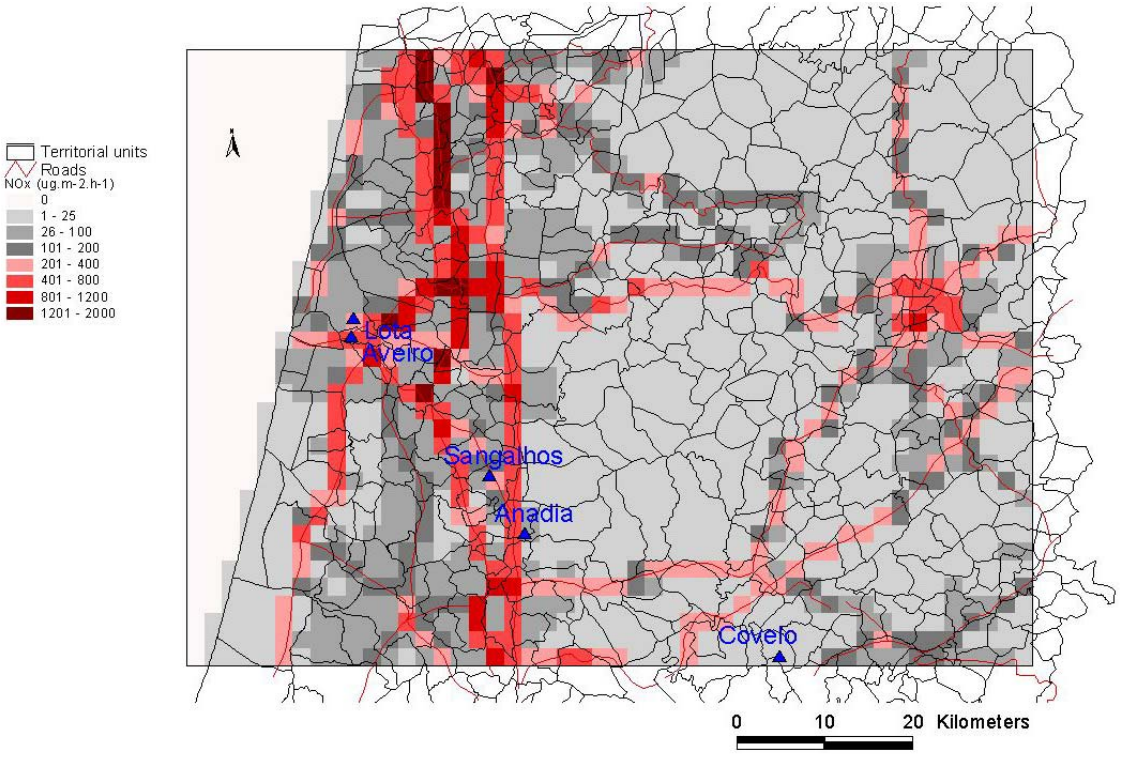

Figure 92: Mass emissions of NO_x ($\mu g.m^{-2}.h^{-1}$), from Motor Vehicle Emission Inventory, for the study domain converted to a 2x2 km grid.

The speciation of emitted NMVOC's was made based in literature (Ntziachristos and Samaras 2000), considering the distribution by vehicle type and fuel sales. NMVOC speciation considering motor vehicles emissions are presented in Appendix III.

The traffic emissions depend on hourly variation patterns. However, patterns are not constant from day to day or from season to season (e.g. Transportation Research Board, 2000; Jenkin *et al.,* 2000c). Hourly variation patterns, used in current PTM application, see Appendix, were based in typical patterns described in Jenkin *et al.* (2000c).

6.1.4.3 Anthropogenic Emission Inventory – SNAP sectors 2, 3, 4, 5, 6 and 8

The UNECE/EMEP emission database (http://webdab.emep.int/) gives access to national total and sector emissions for each year, pollutants/activity classes and total/sector categories.

Portuguese National Anthropogenic Emission Inventory (NAEI) was obtained in UNECE/EMEP emission database. The data obtained from Expert Estimated Emissions (Vestreng *et al.,* 2005), are based on officially reported emissions as far as possible. However, some of the officially reported data have been corrected and gaps have been filled. The road transport emissions (S(7)) were not considered, in this section, since they were object of an especial treatment, see Motor Vehicle Emission Inventory. The (S10) - Agriculture and forestry, land use and wood stock change and (S11) - Other sources and sinks had zero emissions (Vestreng *et al.,* 2005). The (S9) - Waste treatment and disposal were not considered because of difficulties on disaggregatting the emissions, this sector correspond only to ≈1% of NMVOC emissions.

The Anthropogenic Emission Inventory (AEI), presented in this section, accounts for the following SNAP (Selected Nomenclature for Air Pollution) sectors defined in UNECE/EMEP emission database: (S2) - Non-industrial combustion plants (stationary sources); (S3) - Combustion in manufacturing industry (stationary sources); (S4) - Production processes (stationary sources); (S5) - Extraction and distribution of fossil fuels and geothermal energy; (S6) - Solvent use and other product use and (S8) - Other mobile sources and machinery, see Portuguese emissions of NMVOC and NO_x in 2001 in Appendix IV.

Like in MVEI, the emissions were disaggregated to smaller territorial units.

For the sectors; (S2) - Non-industrial combustion plants (stationary sources), (S3) - Combustion in manufacturing industry (stationary sources), (S4) - Production processes (stationary sources) and

(S8) - Other mobile sources and machinery, the emissions were disaggregated based on data from fuel (butane; propane; gasoline, diesel and fuel oil) sales obtained for the territorial unit.

For the sector (S5) - Extraction and distribution of fossil fuels and geothermal energy, the emissions were disaggregated based in data from gasoline sales obtained for territorial unit. For the sector (S6) - Solvent use and other product use, the emissions were disaggregated based on population density for the territorial unit. For all sectors, the emissions were disaggregated, from the large territorial unit to smaller territorial units, based on population density.

For the study domain the point sources were considered independently. Point sources emission estimates were provided by the CORINAIR inventory (EEA-ETC/AE-CORINAIR, 1996) and are present in Appendix IV.

The mass emission flux was converted to a 2x2 km grid using a Geographical Information Software (Arcview). Figure 89 shows mass emissions of NO_x ($\mu g.m^{-2}.h^{-1}$) for the study domain, converted to a 2x2 km grid.

The total emissions from, SNAP sectors (2, 3, 4, 5, 6 and 8) and point sources, for the study domain are 12243 $kg.day^{-1}$ of NO_x and 30121 $kg.day^{-1}$ of NMVOC.

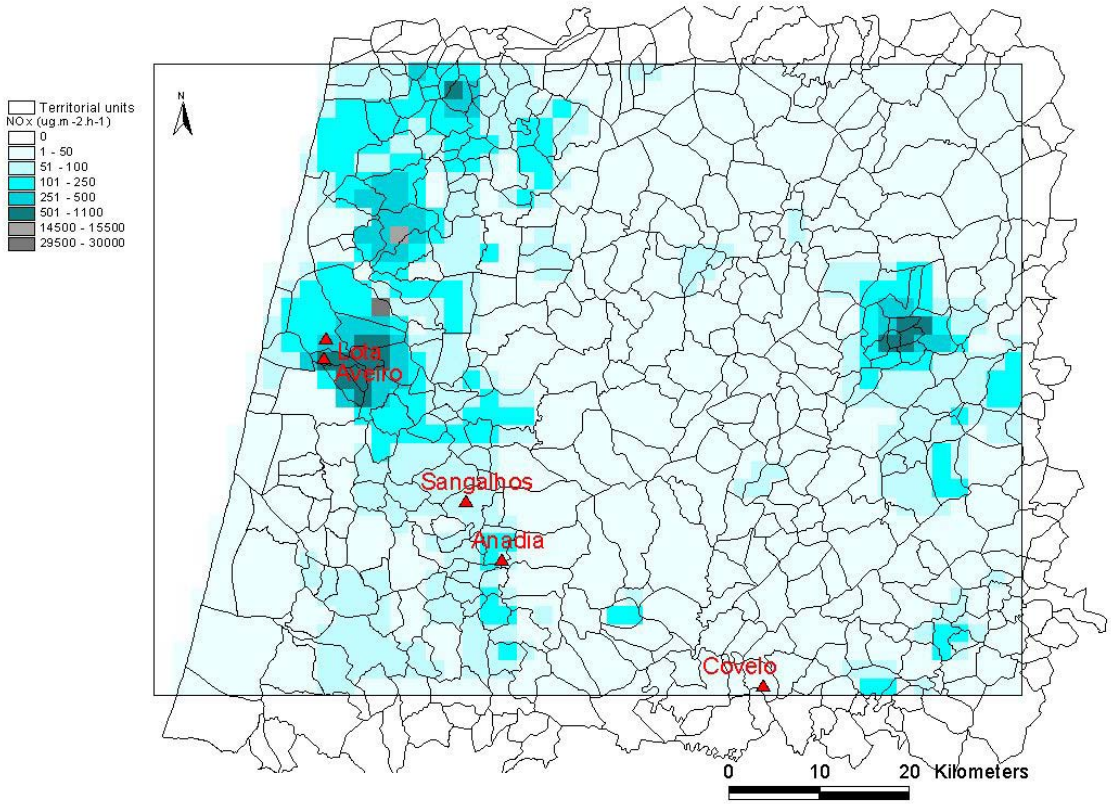

Figure 93: Mass emissions of NO_x ($\mu g.m^{-2}.h^{-1}$), from SNAP sectors (2, 3, 4, 5, 6 and 8), for the study domain converted to a 2x2 km grid.

To apply the PTM it is essential to have the speciation of emitted NMVOC's. The speciation of the emitted NMVOC for the SNAP sectors (2, 3, 4, 5, 6 and 8) was based on data from the UK NAEI (Jenkin *et al.,* 2000b) are presented in Appendix IV.

The temporal variations applied to the emissions of NMVOC and NO_x were based on those estimated for the UK by Jenkin *et al.* (2000c), and are also presented in Appendix IV.

6.2 Evaluation of the Photochemical Trajectory Model Application

In the following analysis, different designations are attributed to the chemical mechanism applied in PTM: MCM v3.1 is related to the MCM as available for download in internet; MCM v3.1a is the adapted version of MCM v3.1, resulting from identified modifications during the optimization of butane and intermediate products of it oxidation; MCM v3.1b is the adapted version of MCM v3.1, resulting from identified modifications during chamber evaluation of photo-oxidation of butane, isoprene, ethene, propene and α-pinene.

The ozone concentrations obtained by application of PTM, using the chemical mechanism MCM v3.1b and the above described database (initial concentrations, meteorological data, and emissions inventories), are in a good approximation to the measured values in Sangalhos and Covelo, see Figure 94.

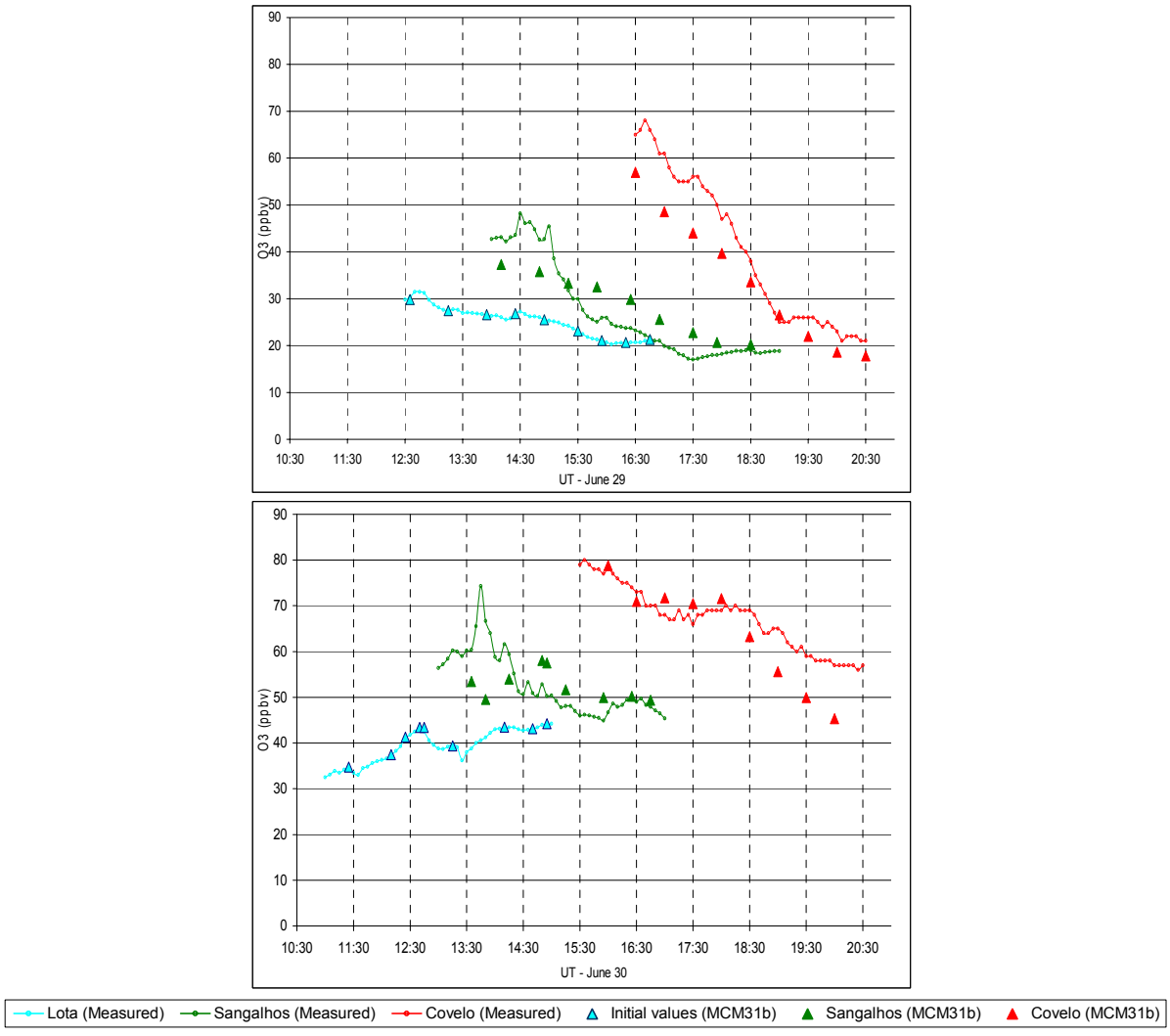

Figure 94: Ozone concentrations obtained by application of PTM, using chemical mechanism MCM v3.1b, and measured values obtained in Sangalhos and Covelo for June 29 and 30 (2001). The points represent the simulated concentrations with 30 minutes arriving intervals at Covelo.

As pointed out in section 6.1.1.1, during this work some changes were inserted in photolysis coefficients calculation, namely a change in the photon flux: use of photon flux determined by Tropospheric Ultraviolet and Visible Radiation Model (NCAR/ACD TUV[5]), for clear sky conditions at an altitude of 0.5 km, instead of photon flux determined using a Two Stream Isotropic Scattering Model for clear sky conditions at an altitude of 0.5 km (Hough, 1988 *in* Jenkin *et al.,* 1997). Also some quantum and absorption cross section, for some species were update, relatively to the data usually used in MCM applications and applied to obtain the expressions available for download in MCM internet site. Figure 95 and Figure 96 show a significant effect in calculated ozone concentration for the different air masses moving from Coast to Covelo site using the two photolysis coefficient calculation models. Obviously, the effect is larger for the air masses arriving earlier in the day and exposed to larger radiation. The use of photon flux determined by Tropospheric Ultraviolet and Visible Radiation Model (NCAR/ACD TUV) instead of photon flux determined using a Two Stream Isotropic Scattering Model (Hough, 1988) implies an average increase of ozone concentrations of ca. 11% with a maximum increase of ca. 21% for the first air mass arriving Covelo at June 30 (2001).

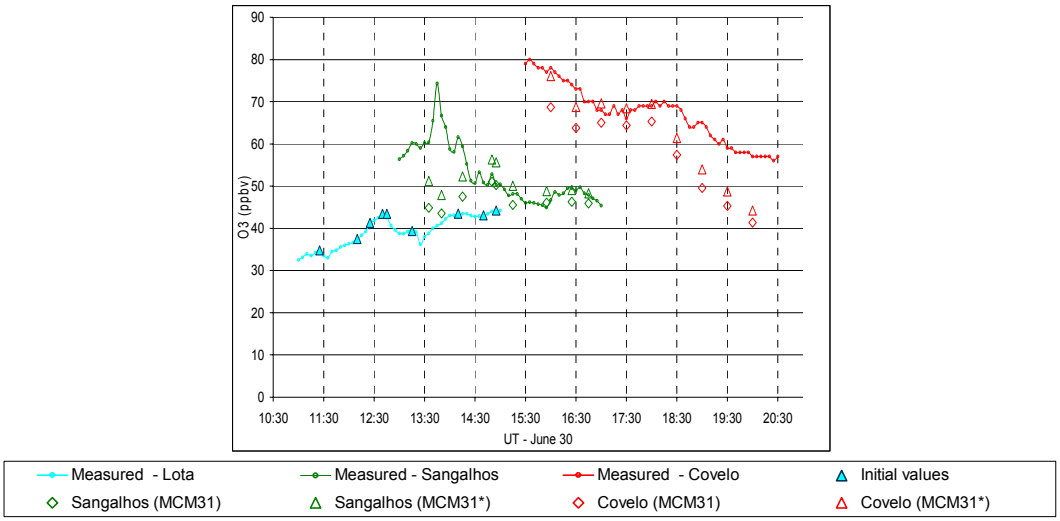

Figure 95: Comparison of observed and simulated ozone concentrations for June 30 (2001). The points represent the simulated concentrations with 30 minutes arriving intervals at Covelo. The legend MCM31 relate to the MCM v3.1 as available for download in internet and the legend MCM31* relate to the same version with change in photolysis coefficient calculation model.

[5] NCAR/ACD TUV: Tropospheric Ultraviolet & Visible Radiation Model. NCAR Atmospheric Chemistry Division (ACD). (http://gcmd.nasa.gov/records/UCAR_TUV.html)

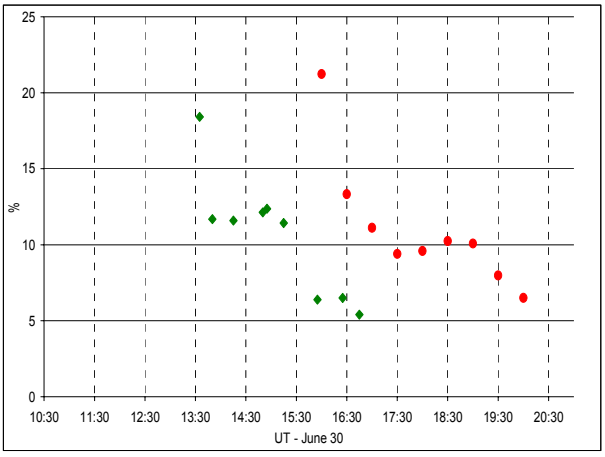

$$\% = \left| \left(\frac{Local(CalculatedMCM31^{*}) - Initial(Observed)}{Initial(Observed)} \right) * 100 \right| - \left| \left(\frac{Local(CalculatedMCM31) - Initial(Observed)}{Initial(Observed)} \right) * 100 \right|$$

Figure 96: Difference of percentage of difference between values obtained by application of MCM31* and MCM31, for Sangalhos (green symbol) and Covelo (red symbol) and the initial ozone concentrations observed in Lota for June 30 (2001). The points represent the simulated concentrations with 30 minutes arriving intervals at Covelo. The legend MCM31 relate to the MCM v3.1 as available for download in internet and the legend MCM31* relate to the same version with change in photolysis coefficient calculation model.

The change in the assigned rate coefficient for the reaction of OH with NO_2 from $1.19x10^{-12}$ $cm^3.molecule^{-1}.s^{-1}$ (at 298K and760 Torr) (based on IUPAC, 2002) to a value of $1.05x10^{-12}$ $cm^3.molecule^{-1}.s^{-1}$ (based on JPL, 2003) was also tested in the current field application. As shown in previous sections this change had significant effects in MCM chamber evaluation. However, as Figure 97 and Figure 98 show, this change has a small although observable effect in ozone concentration calculated for the different air masses moving from the Coast to Covelo site.

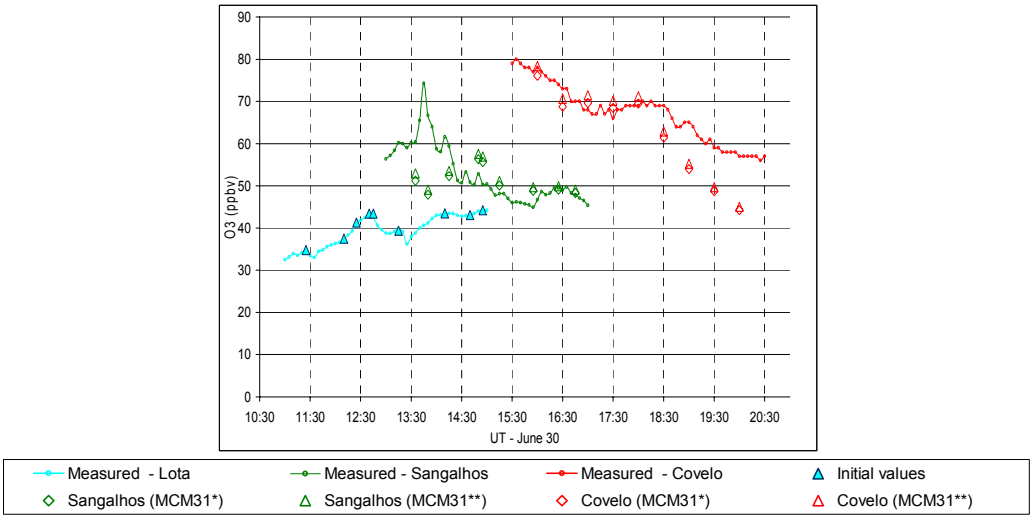

Figure 97: Comparison of observed and simulated ozone concentrations for June 30 (2001). The points are the simulated concentrations with 30 minutes arriving intervals at Covelo. The legend MCM31* relates to the MCM v3.1 as available for download in internet with the change in photolysis coefficient calculation model, the legend MCM31** relates to MCM31* with the change in rate coefficient for the reaction of OH with NO_2 from the value based on IUPAC, 2002 to a value based on JPL, 2003 (see text).

The decrease in the assigned rate coefficient for the reaction of OH with NO_2 implies an average increase of ca. 3% with a maximum increase of ca. 7% for the first air mass arriving Covelo at June 30 (2001).

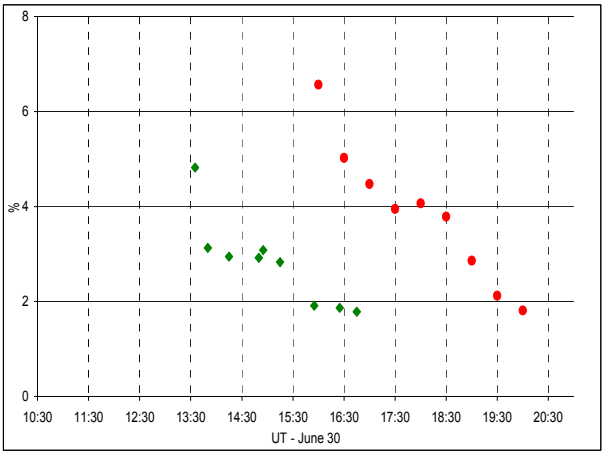

$$\% = \left| \left(\frac{Local(CalculatedMCM31**) - Initial(Observed)}{Initial(Observed)} \right) * 100 \right| - \left| \left(\frac{Local(CalculatedMCM31*) - Initial(Observed)}{Initial(Observed)} \right) * 100 \right|$$

Figure 98: Difference of percentage of difference between values obtained by application of MCM31* and MCM31, for Sangalhos (green symbol) and Covelo (red symbol) and the initial ozone concentrations observed in Lota for June 30 (2001). The points are the simulated concentrations with 30 minutes arriving intervals at Covelo. The legend MCM31* relates to the MCM v3.1 as available for download in internet with the change in photolysis coefficient calculation model, the legend MCM31** relates to MCM31* with the change in rate coefficient for the reaction of OH with NO_2 from the value based on IUPAC, 2002 to a value based on JPL, 2003 (see text).

The changes proposed in previous sections as result of chamber evaluation of: photo-oxidation of butane, and its degradation products, methylethyl ketone (MEK), acetaldehyde (CH_3CHO) and formaldehyde (HCHO); photo-oxidation of isoprene and its degradation products, methacrolein (MACR) and methylvinyl ketone (MVK), photo-oxidation of ethene and propene and photo-oxidation of α-pinene were tested against the field data. The proposed refinements have very small effects on the ozone concentrations, presenting only a small change when applied to these field conditions (see Figure 99 and Figure 100).

As expected, the insertion of reaction of $O(^3P)$ with the indicated VOC has a null effect in field conditions. Also the update in OH yield from the ozonolysis of MACR and MVK has a null effect in ozone concentration when applied to these field conditions; this result agrees with the chamber evaluation indications.

The effect of all changes considered together implies an average increase of ca. 1% for June 30 (2001) and a increase for the firsts runs and a decrease for the last runs of June 29 (2001).

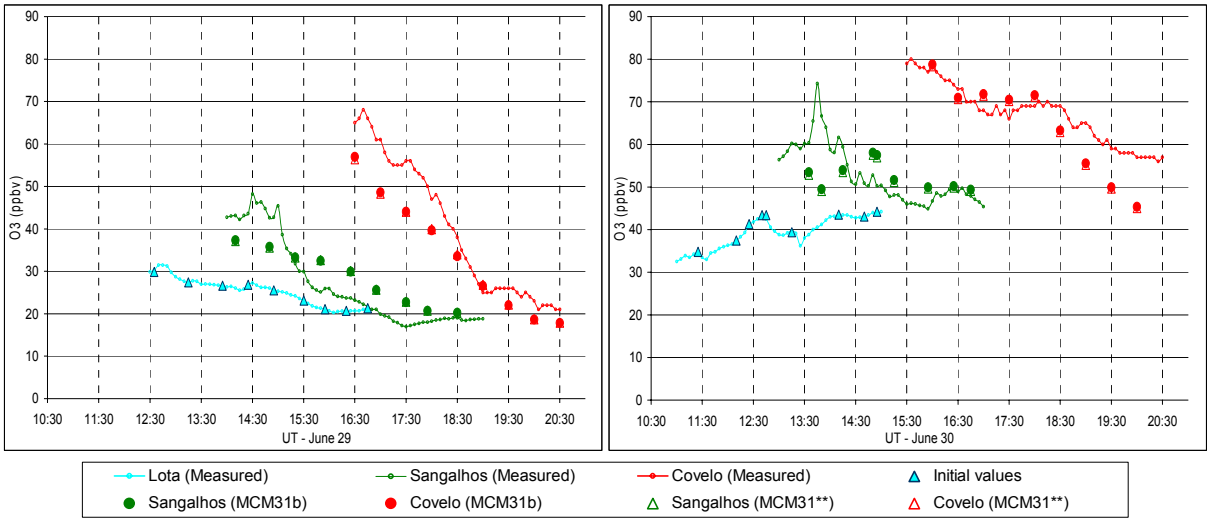

Figure 99: Comparison of observed and simulated ozone concentrations for June 30 (2001). The points are the simulated concentrations with 30 minutes intervals arriving at Covelo. The legend MCM31** relates to the MCM v3.1 as available for download in internet with the change in photolysis coefficient calculation model and with the change in rate coefficient for the reaction of OH with NO_2 from the value based on IUPAC, 2002 to a value based on JPL, 2003, the legend MCM31b relates to MCM31** with the refinements resulting from chamber evaluation of photo-oxidation of butane, isoprene, ethane, propene and α-pinene (see text).

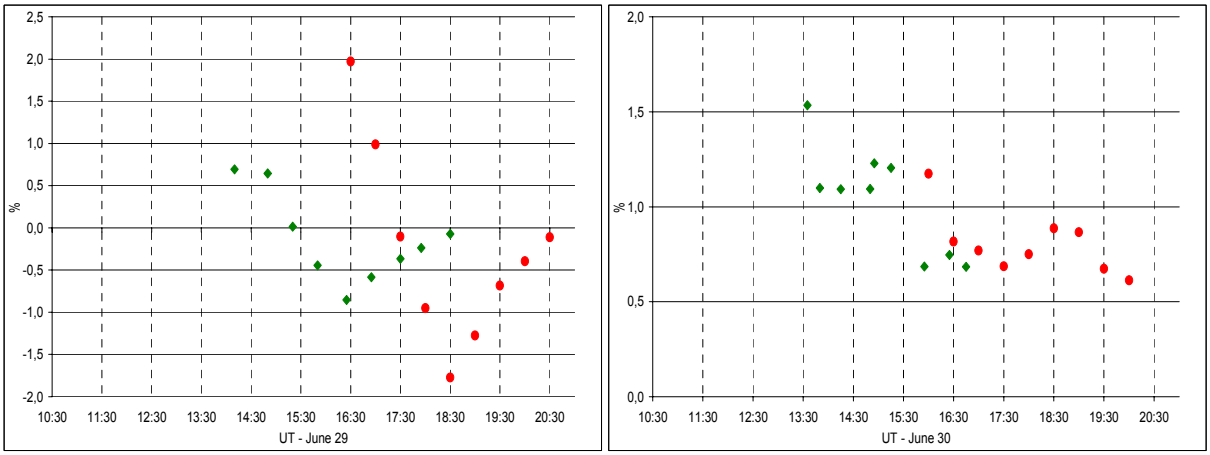

$$\% = \left| \left(\frac{Local(CalculatedMCM31b) - Initial(Observed)}{Initial(Observed)} \right) * 100 \right| - \left| \left(\frac{Local(CalculatedMCM31**) - Initial(Observed)}{Initial(Observed)} \right) * 100 \right|$$

Figure 100: Difference of percentage of difference between values obtained by application of MCM31* and MCM31, for Sangalhos (green symbol) and Covelo (red symbol) and the initial ozone concentrations observed in Lota for June 30 (2001). The points are the simulated concentrations with 30 minutes arriving intervals at Covelo. The legend MCM31** relates to the MCM v3.1 as available for download in internet with the change in photolysis coefficient calculation model and with the change in rate coefficient for the reaction of OH with NO_2 from the value based on IUPAC, 2002 to a value based on JPL, 2003, the legend MCM31b relates to MCM31** with the refinements resulting from chamber evaluation of photo-oxidation of butane, isoprene, ethane, propene and α-pinene (see text).

Simulated and measured concentrations of nitrogen oxides showed discrepancy (see Figure 101 and Figure 102). Unfortunately no NO_x measurements exists for Sangalhos site, and for June 29 no available data exists for Covelo due to problems with the measurement equipment.

This divergence of results could be related with the predominant NO_x emission near the ground level wich implies a predictably vertical gradient and the PTM assumption that pollutants are completely mixed in the box representing the average concentration inside of the boundary layer and not the surface concentration. The concentration of NO and NO_2 observed near the ground level presented a variation with peaks of short term that could indicate closest emission sources, being thus the pollutant predictably badly distributed in the vertical direction (Evtyugina *et al.,* 2006b). On the other hand, measured vertical profiles of O_3 revealed a good vertical mixture during the day in the sea breeze boundary layer (Evtyugina *et al.,* 2006a).

It is important to point that NO_2 measurements were made with a chemiluminescent detector with thermal converter. So, NO_2 include many other oxidised N compounds, especially PAN and higher PANs (which decompose in the converter) and also organic nitrates in general, HONO and a fraction of HNO_3. The contribution of these species, to NO_2 concentration, is very important and drastically reduces the difference between measured and modelled values, see Figure 104.

The inventory of emissions of mobile sources underlying the modelling does not contemplate the urban and suburban road emissions. Therefore, the emissions of NO_x estimated are not significant for the Covelo area. Nevertheless, this location can suffer influence from the local emissions proceeding from nearby villages and vehicles on local and regional roads.

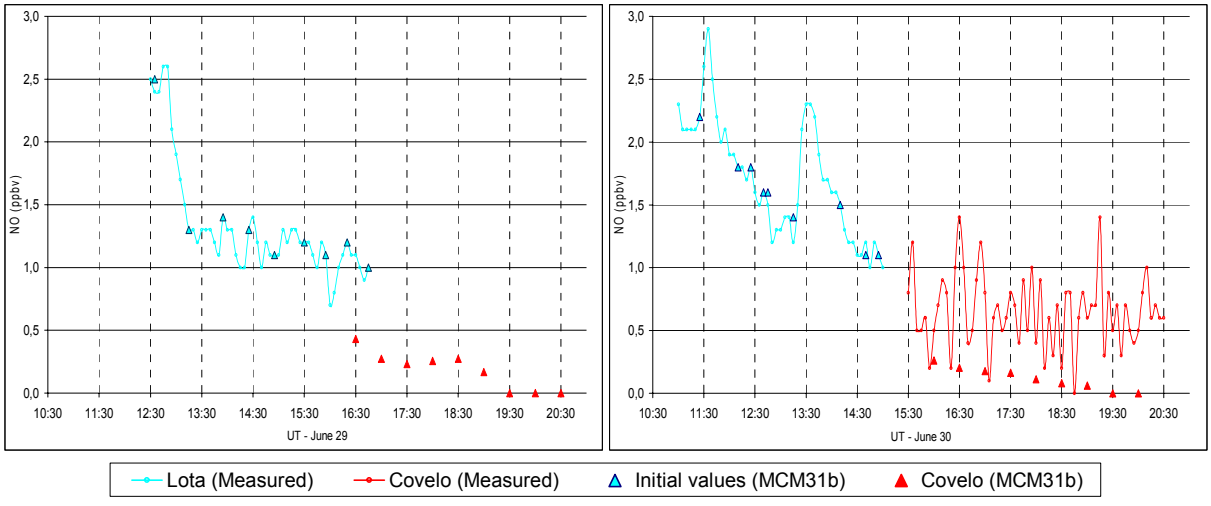

Figure 101: NO concentrations obtained by application of PTM, using chemical mechanism MCM v3.1b, and measured values obtained in Covelo for June 29 and 30 (2001). The points represent the simulated concentrations with 30 minutes arriving intervals at Covelo.

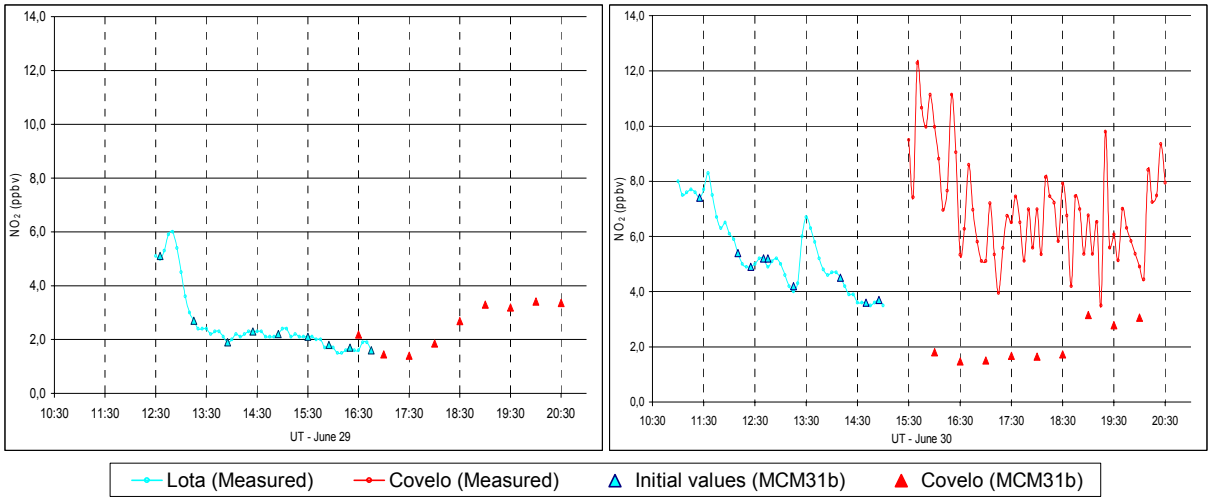

Figure 102: NO_2 concentrations obtained by application of PTM, using chemical mechanism MCM v3.1b, and measured values obtained in Covelo for June 29 and 30 (2001). The points represent the simulated concentrations with 30 minutes arriving intervals at Covelo.

The analysis of O_3, NO, NO_2, HNO_3 and peroxiacilnitrates (PANT) concentration, obtained by PTM application, along the respective trajectories (see Figure 103 and Figure 104) allow a better understanding of the species trend during the transport:

- The air masses leaving the Coast before ≈3 p.m. and arriving to Covelo before ≈ 6 p.m. show an increasing in O_3 concentration during the transport. The O_3 increasing ratio during the first trajectories is much higher. After ≈ 6 p.m. a decrease in O_3 concentration is obtained by modelling;

- The NO decrease during the transport for all studied trajectories;

- For June 29 the air masses leaving the Coast after ≈3 p.m. shows a increasing in NO_2 concentration during the transport. This increase in NO_2 is also observed in June 30, however only after ≈4 p.m and the ratio of increase is smaller;

- HNO_3 concentrations showed increased values along trajectories, with constant final for June 29, and a diminishing during the last half of the trajectories for June 30;

- The peroxiacilnitrates (PANT) concentration increase during the transport for all studied trajectories.

This O_3 trend could be explained by the natural decreasing of NO_2 photolysis coefficient with decrease in radiation by the end of the day. At 6 pm the radiation is about 50% of the day maximum. The decreasing of NO concentration along the trajectories is explicated by NO reaction with RO2 and with O_3, originating NO_2. This also explains the increase in NO_2 observed in the latter hours of afternoon, since the remotion processes are not efficient. At this day period NO_2 has a small photolysis coefficient and the availability of OH radical is smaller, (see Figure 105).

HNO_3 trend along trajectories, with a diminishing during the final part, should be related with decrease OH in the end of trajectory (no HNO_3 is formed by the reaction of NO_2 + OH) and with deposition during the transport of air masses. The HNO_3 deposition is more effective in June 30 since the air masses transport takes, in average, on extra hour travelling from Coast to Covelo, comparing to June 29 (see Table 14).

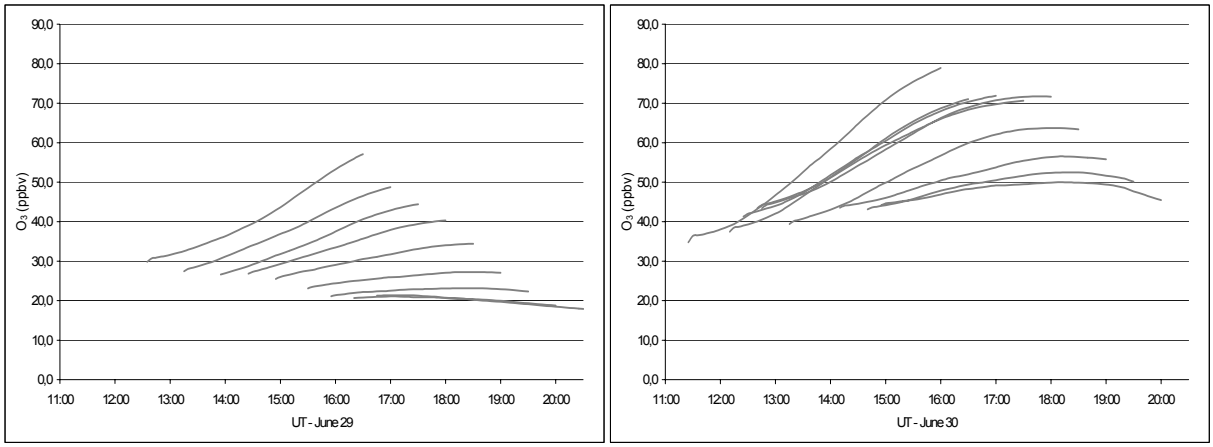

Figure 103: Evolution of O_3 concentration along the respective trajectories for June 29 and 30 (2001), obtained by application of PTM, using chemical mechanism MCM v3.1b.

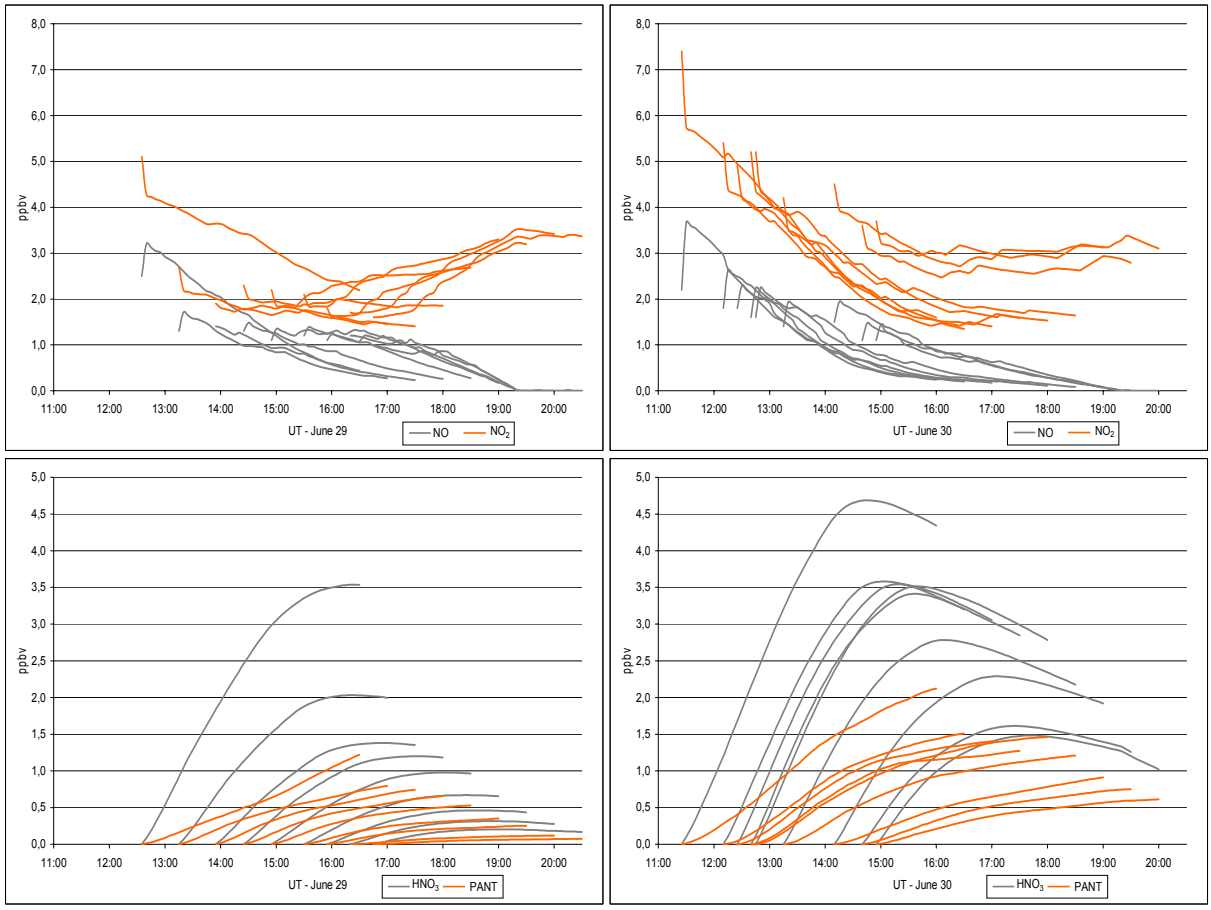

Figure 104: Evolution of NO, NO_2, HNO_3 and peroxiacilnitrates (PANT) concentration along the respective trajectories for June 29 and 30 (2001), obtained by application of PTM, using chemical mechanism MCM v3.1b.

Figure 105 shows the evolution of OH, HO_2 and RO2 concentration along the respective trajectories, obtained by application of PTM. As expected, by the end of the day the OH radical concentration decreases since the photolysis of O_3 decreases implying less $O(^1D)$ formation and consequently OH production (see Figure 1). The evolution of radical RO2 concentration results essentially from the following competition: RO2 is produced by oxidation of VOC with OH and consumed by reaction with NO and in a smaller scale by reaction with HO_2 and itself. The increase in the beginning of trajectories is resultant from a prevalence of VOC oxidation with OH comparatively with removal reactions. When OH radicals are insufficient to react with VOC and NO_2, the RO2 concentration stops increasing and stabilizes, following by a decrease if the dominance of removal reactions is observed. The fast increase in RO2 concentration, by the end of the latter trajectories, could be understood as a result of NO extinguish.

The evolution of radical HO_2 results also from the oxidation of VOC by OH and from reaction with NO, regenerating OH and producing NO_2 and in a smaller scale from selfreaction and reaction with RO2.

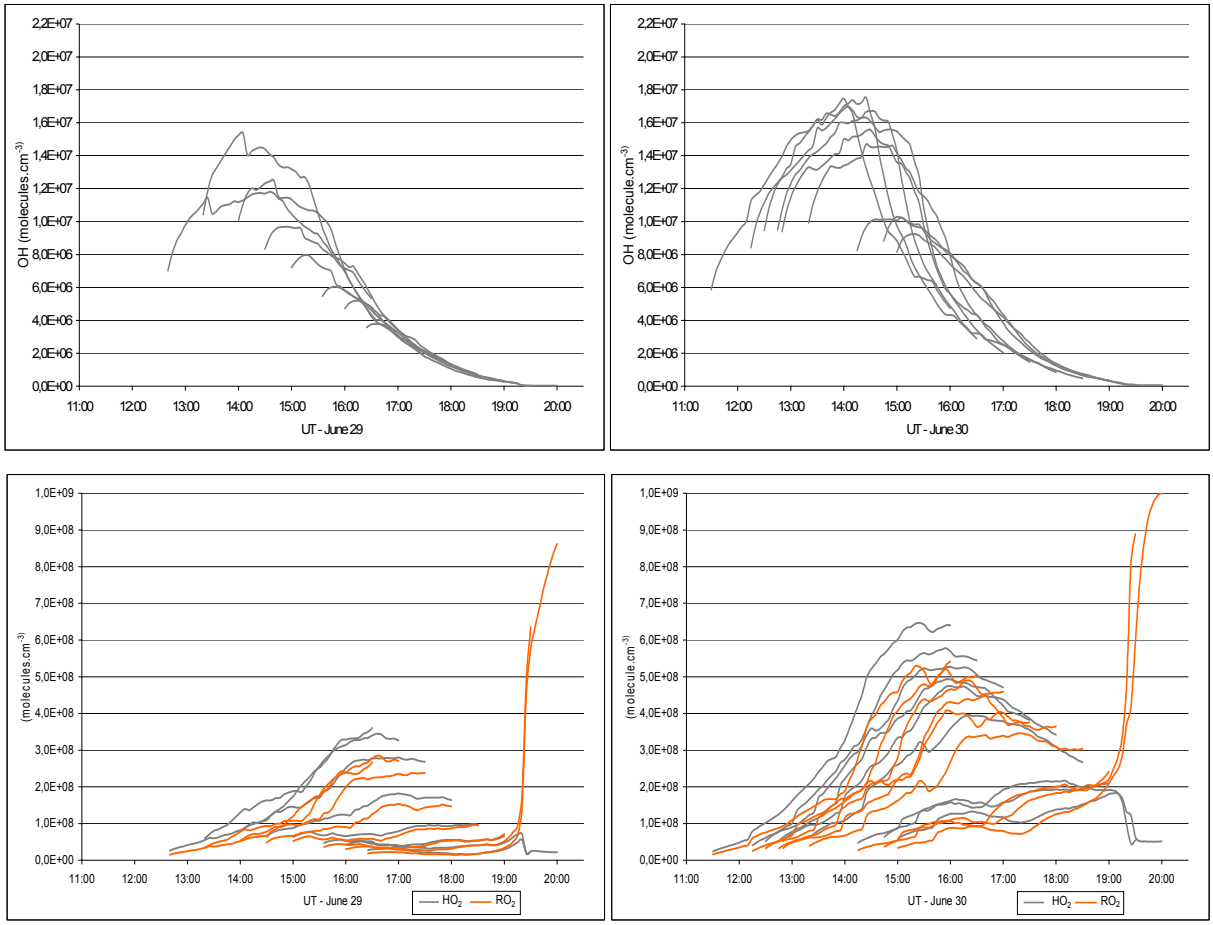

Figure 105: Evolution of OH and RO2 concentration along the respective trajectories for June 29 and 30 (2001), obtained by application of PTM, using chemical mechanism MCM v3.1b.

The MCMv3.1 considers the oxidation mechanisms of 135 volatile organic compounds. So, theoretically, it is possible to compare the results of the obtained modelled values, of all 135 organic compounds and the resultant oxidation products, with the real values obtained from field measurements.

However, usually only a partial set of VOCs are measured during a field experiment. During the CZCM field campaign 2001, 31 compounds were measured (see details in Evtyugina, 2004 and Evtyugina *et al.,* 2006a). The measured aldehydes and ketones (formaldehyde, acetaldehyde, acetone, acroleine, propanal, hexanal) were obtained on 4 hour averages, starting at 8 a.m. until 8 p.m. The VOCs (ethane, ethene, propane, propene, acetylene, isobutane, n-butane, 1-butene, isobutene, isopentane, n-pentane) were measured in 2h intervals, starting at 9h and ending at 19h. The other measured VOCs (isoprene, 2-metilpentane, 3-metilpentane, n-hexane, benzene, n-heptane, toluene, ethylbenzene, m-xylene, p-xylene, o-xylene, α-pinene, 1.3.5-trimethyl benzene, 1.2.4- trimethyl benzene) were measured in 30 min averages, at 1h 30 min intervals, starting at 8h 45 min and ending at 19h 15 min. From this set of measured VOCs the following species are here evaluated: HCHO, CH_3CHO, CH_3COCH_3, isoprene and α-pinene.

The concentration of the HCHO obtained by modelling is compared with measured values in Figure 106. Figure 106 shows a reasonable agreement between HCHO measured values and those obtained by model application, taking into account the measurement uncertainties and the limitations of a box model. The reasonable agreement obtained for HCHO is a good indication of the capacities of this kind of model for predicting photochemical atmospheric processes. The HCHO is directly emitted and also formed in large quantities by VOCs oxidation, in this case, especially, by isoprene oxidation. As expected, the evolution obtained by application of PTM, shows an increase in HCHO concentrations along transport, (see Figure 107). The rate of HCHO formation increases when the air mass arrives to the Eucalyptus forest and the isoprene concentrations rise as result of biogenic emissions. Secondary HCHO represents, almost, the total HCHO concentration observed.

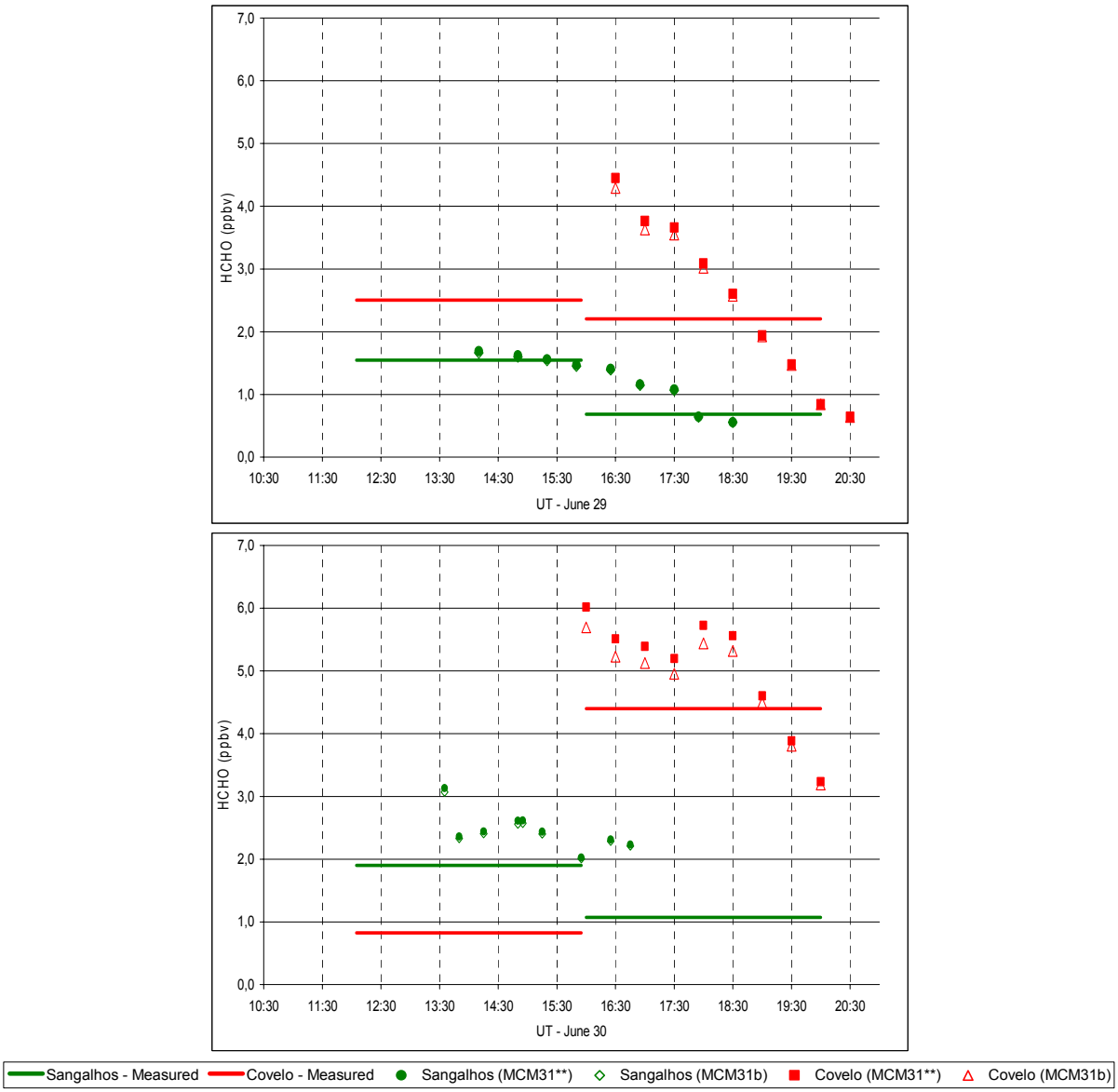

Figure 106: Comparison of observed and simulated HCHO concentrations for June 29 and 30 (2001). The points are the simulated concentrations at 30 minutes intervals arriving at Covelo. The legend MCM31** relates to the MCM v3.1 as available for download in internet with the change in photolysis coefficient calculation model and with the change in rate coefficient for the reaction of OH with NO_2 from the value based on IUPAC, 2002 to a value based on JPL, 2003, the legend MCM3.1b relates to MCM31** with the refinements that results from chamber evaluation of photo-oxidation of butane, isoprene, ethane, propene and α-pinene (see text).

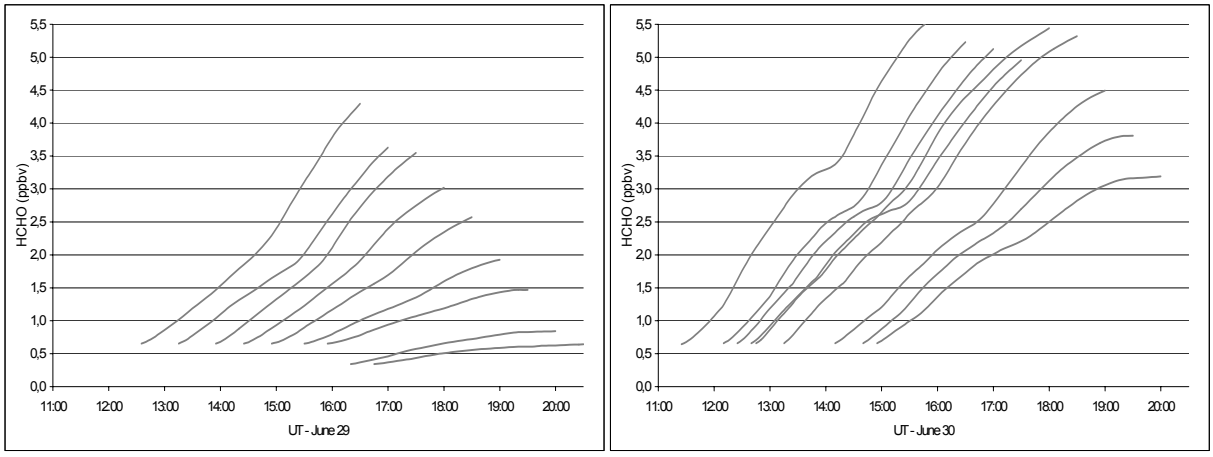

Figure 107: Evolution of HCHO concentration along the respective trajectories for June 29 and 30 (2001), obtained by application of PTM, using chemical mechanism MCM v3.1b.

Figure 108 also shows some agreement between CH_3CHO measured values and values obtained by model application, but only for June 29. For June 30 the measured values are approximately double of the modelled ones. This different trend verified for the two days is difficult to explain with the available data. However, it is important to remember that transports and industrial emissions increase with temperature and this fact is not taken under consideration on the database inserted in the PTM.

The CH_3CHO is emitted in a much smaller scale than HCHO and the production by VOC oxidation is also smaller in a domain where isoprene emissions have a so strong role. The observed concentrations of CH_3CHO are small, implying a larger uncertainty in the measurements.

The evolution of CH_3CHO concentration along the trajectories, obtained by application of PTM, for June 29 shows a small decrease in the beginning of the first trajectories, probably as result of by CH_3CHO photolysis and reaction with OH. Later on the radiation decreases and CH_3CHO concentration stabilizes (see Figure 109). In June 30, CH_3CHO concentration shows a small increase in the beginning of the first trajectories, resulting from the dominance of CH_3CHO production (oxidation CH_3CHO precursors) relatively to removal processes. The initial concentration of VOC for the two analysed days is different (see Figure 81); in June 30 the concentration of CH_3CHO precursors (e.g. propene, 1-butene) was considered higher than in June 29.

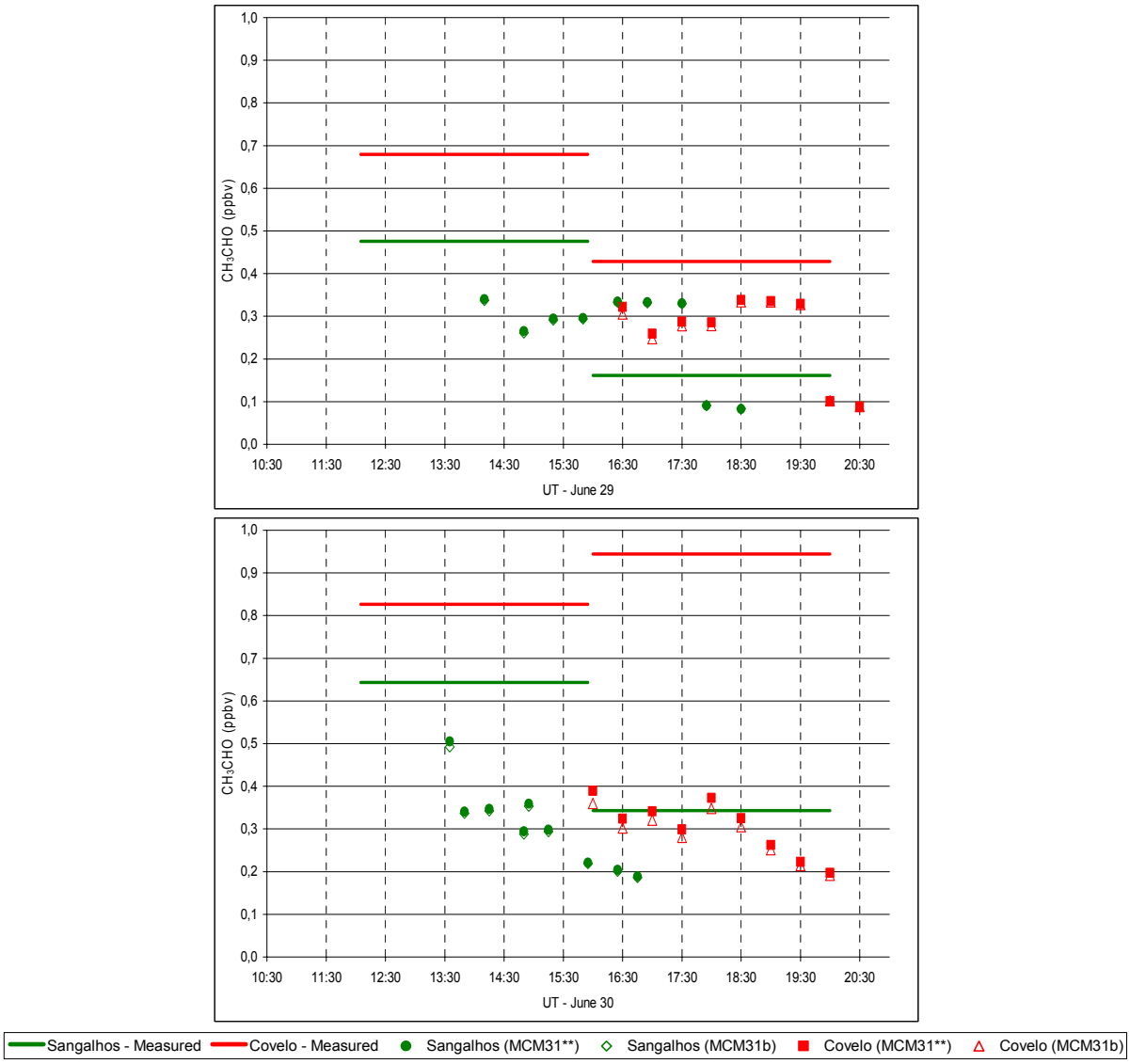

Figure 108: Comparison of observed and simulated CH_3CHO concentrations for June 29 and 30 (2001). The same legend as in Figure 106.

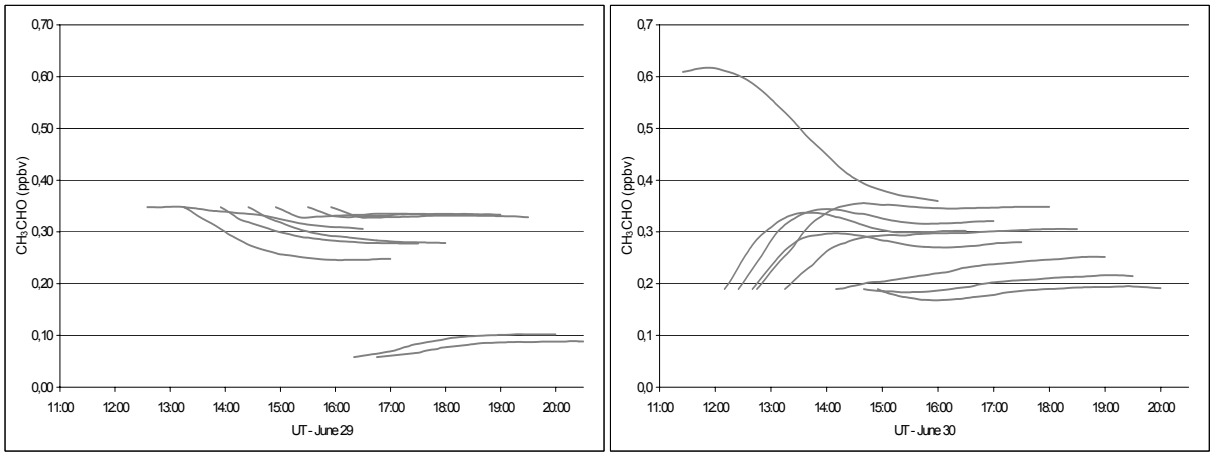

Figure 109: Evolution of CH_3CHO concentration along the respective trajectories for June 29 and 30 (2001), obtained by application of PTM, using chemical mechanism MCM v3.1b.

Figure 110 presents modelled and measured concentrations for acetone. Likewise for CH_3CHO, CH_3COCH_3 measured and modelled results are in a better agreement for June 29 than for June 30.

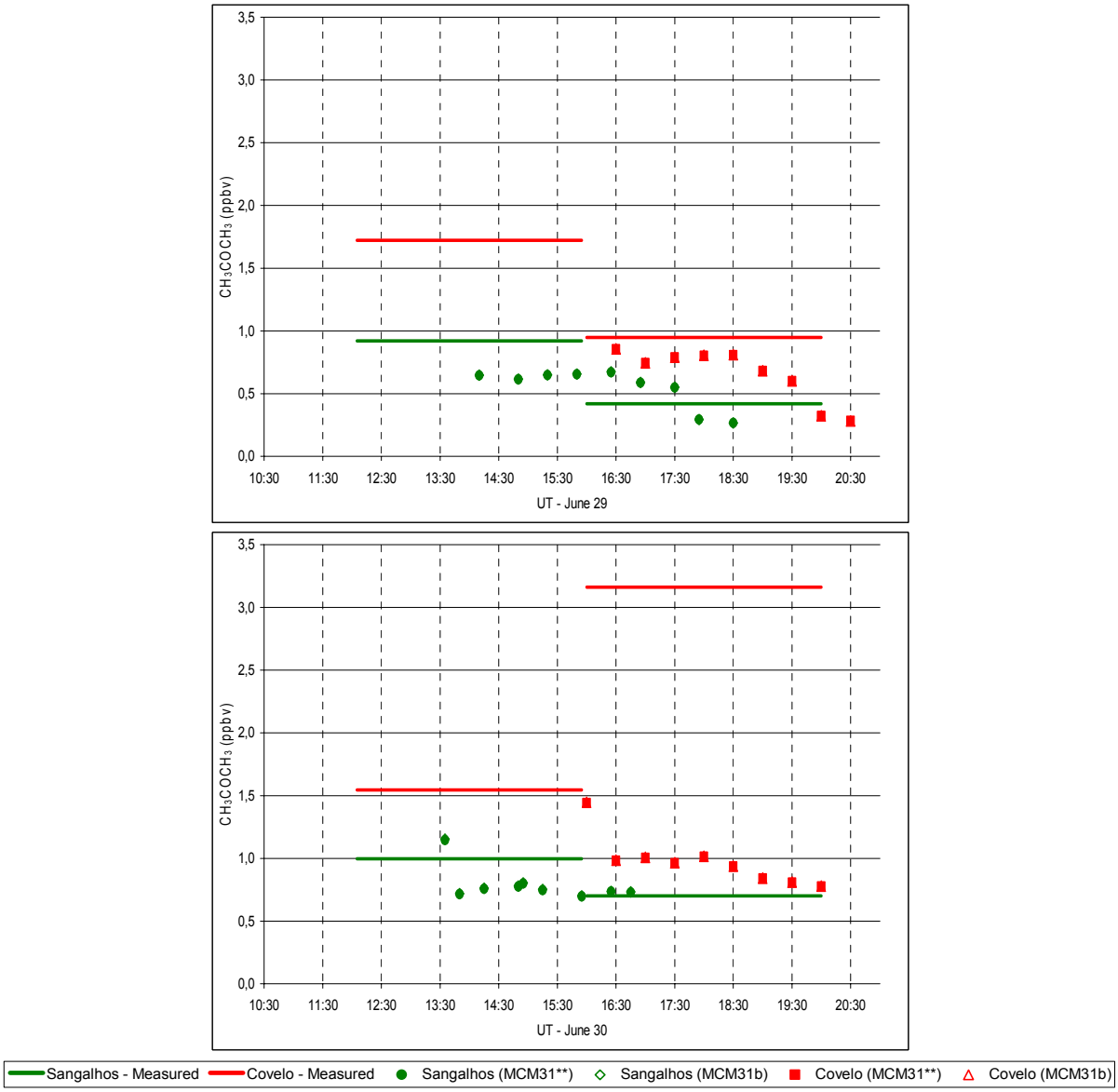

Figure 110: Comparison of observed and simulated $CH_3C(O)CH_3$ concentrations for June 29 and 30 (2001). The same legend as in Figure 106.

Figure 111 presents the evolution of CH_3COCH_3 concentration along the trajectories, obtained by application of PTM. As expected, the evolution obtained by application of PTM, shows an increase in CH_3COCH_3 concentrations during transport inland as result of the oxidation of precursors (e.g. propane, isobutane, isopentane) and the large lifetime of CH_3COCH_3 (photolysis and reaction with OH, result in a global mean lifetime of the order of a month (Gierczak *et al.,* 1998)).

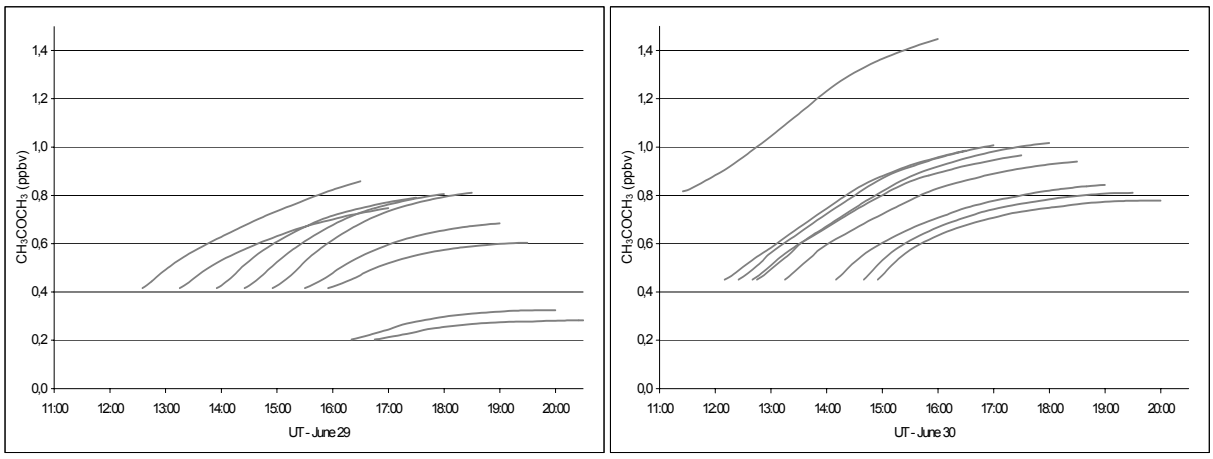

Figure 111: Evolution of CH_3COCH_3 concentration along the respective trajectories for June 29 and 30 (2001), obtained by application of PTM, using chemical mechanism MCM v3.1b.

Figure 112 shows the concentration of isoprene obtained by modelling and by measurement, in Sangalhos and Covelo sites.

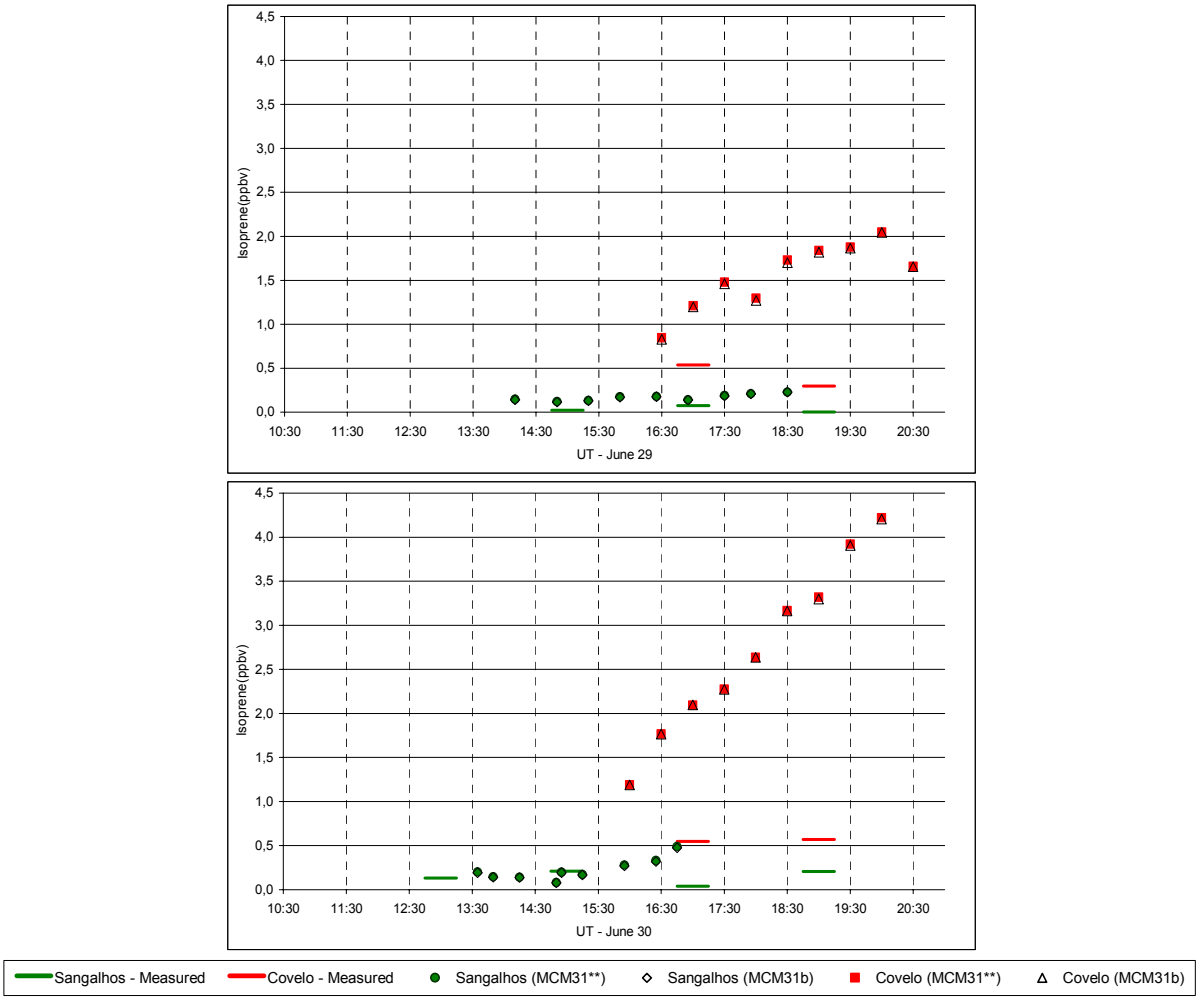

Figure 112: Comparison of observed and simulated isoprene concentrations for June 29 and 30 (2001). The same legend as in Figure 106.

The measured values of isoprene observed in Sangalhos are of the same order than the modelled results. But in Covelo the model strongly overpredicts the values of isoprene concentration. This difference is much more evident in June 30. Figure 112 also shows that the necessary refinements inserted in MCM v3.1 as result of chamber evaluation, including the update in OH yield from the ozonolysis of MACR and MVK, have a null effect in isoprene concentration calculations when applied to these field conditions. These results agree with the conclusions of chamber evaluation.

The difference observed in model outputs in the two days results from the higher temperatures, applied to the model during June 30, and consequently higher emissions (see Figure 113) and from the small box height considered during June 30 (Figure 79).

However, these different conditions should also be reflected in measured values.

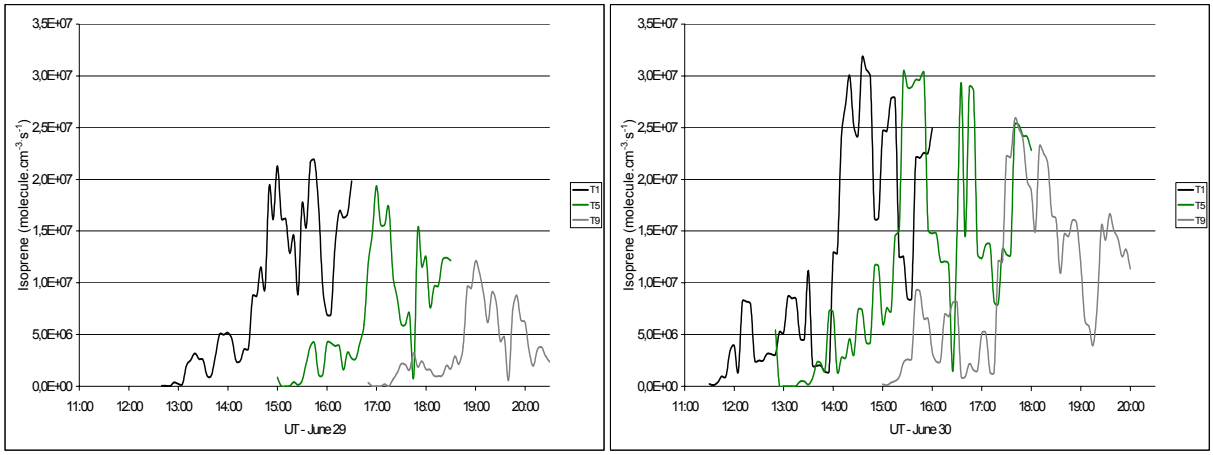

Figure 113: Emission flux of isoprene along three trajectories (first, fifth and nineth) for June 29 and 30 (2001), obtained by application of PTM.

As can be seen in section 6.1.4.1 the biogenic emission database considers a huge emission flux of isoprene between Sangalhos and Covelo, resulting from the Eucalyptus forest (Figure 87). It is possible that this emission flux is overestimated; Simpson *et al.* (1999) indicated discrepancies of up to a factor of 5 in isoprene emissions determinations. Also box height, considered in PTM, has uncertainties, namely because only measurements at one site were available. An underestimation of the boundary layer depth has a large effect in isoprene concentration obtained by modelling, since the PTM assumes a homogeneous concentration inside the box.

The possible overestimation of biogenic emissions do not implies, necessarily, a large model overprediction in ozone production since in most of the trajectory the system is NO_x limited and in the end of trajectory no OH is available to react with isoprene. In these conditions Isoprene reacts mainly with O_3.

Notice that a sensitivity test to biogenic emissions applied by Pinho (2000) (to the same domain and similar meteorological conditions) for one trajectory (air mass arrived inland at 16 hours and 30 minutes) showed that a reduction of biogenic emission by a factor of five would result in a change in ozone production ca. 10%.

The effect of overprediction of biogenic emissions in ozone formation is smaller in air masses arriving at inland locations latter in the afternoon, since no OH is available to react with isoprene in the end of the day. Figure 114 shows that for June 29, for the last air mass arriving to Covelo, the observed isoprene concentration represents almost the total isoprene emitted during the air mass transport.

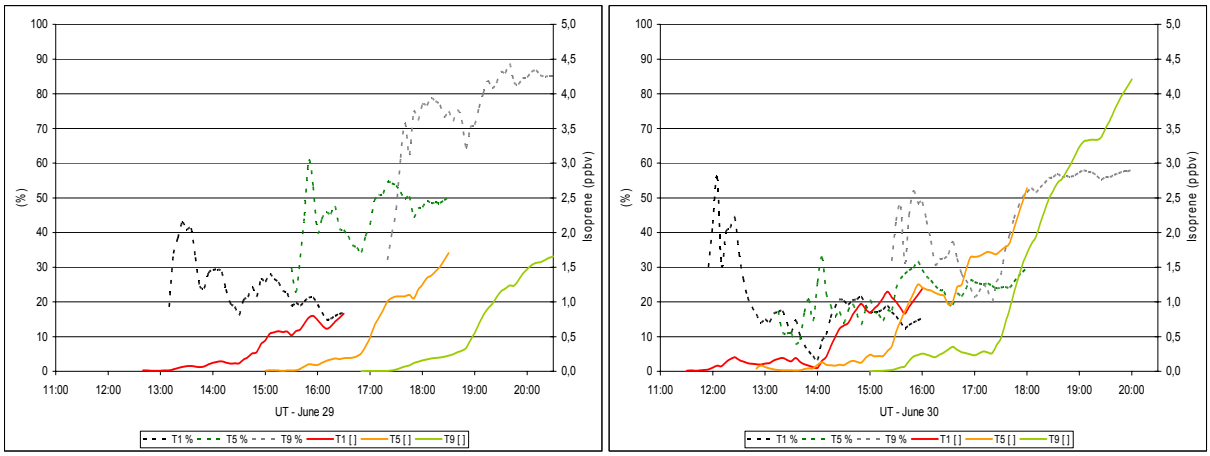

Figure 114: Isoprene concentration along three trajectories (first, fifth and nineth) and percentage of isoprene observed concentration relatively to the total isoprene concentration resulting from air emission, without consumption, until that moment. Data for June 29 and 30 (2001), obtained by application of PTM, using chemical mechanism MCM v3.1b.

Figure 115 presents the concentration of α-pinene obtained by modelling and by measurement, in Sangalhos and Covelo sites.

The measured values of α-pinene observed in Sangalhos are much higher than model outputs. But in Covelo the measured values are lower than model results. This indicates a possible underestimation of α-pinene emissions before the air mass arrival at Sangalhos and an overestimation of α-pinene emissions between Sangalhos and Covelo.

The evolution of α-pinene modelled concentration along the trajectories, obtained by application of PTM, shows a decrease in the beginning of the trajectories, resulting from the oxidation of α-pinene by OH, followed by an increase in concentrations resulting from estimated biogenic emissions (see Figure 117). Since the initial concentration of α-pinene considered for June 29 was high, approximately near 3 p.m., the increase in concentrations as result of biogenic emissions was not so effective.

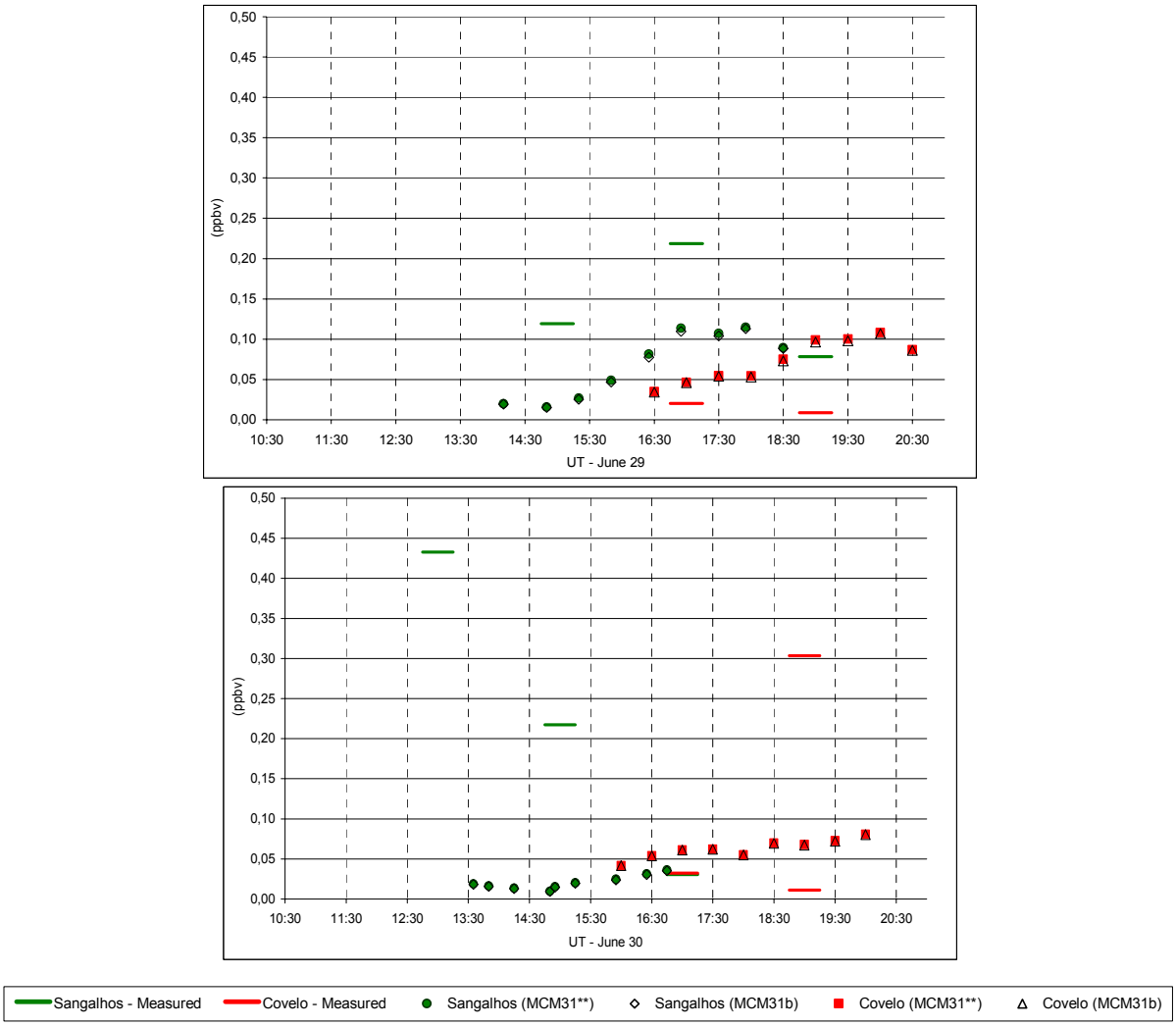

Figure 115: Comparison of observed and simulated α-pinene concentrations for June 29 and 30 (2001). The same legend as in Figure 106.

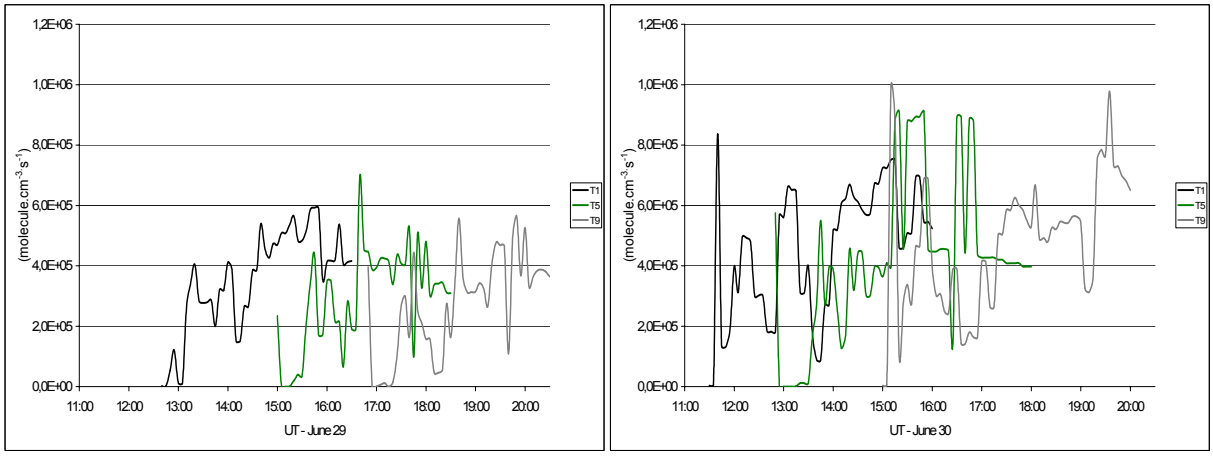

Figure 116: Emission flux of α-pinene along three trajectories (first, fifth and nineth) for June 29 and 30 (2001), obtained by application of PTM.

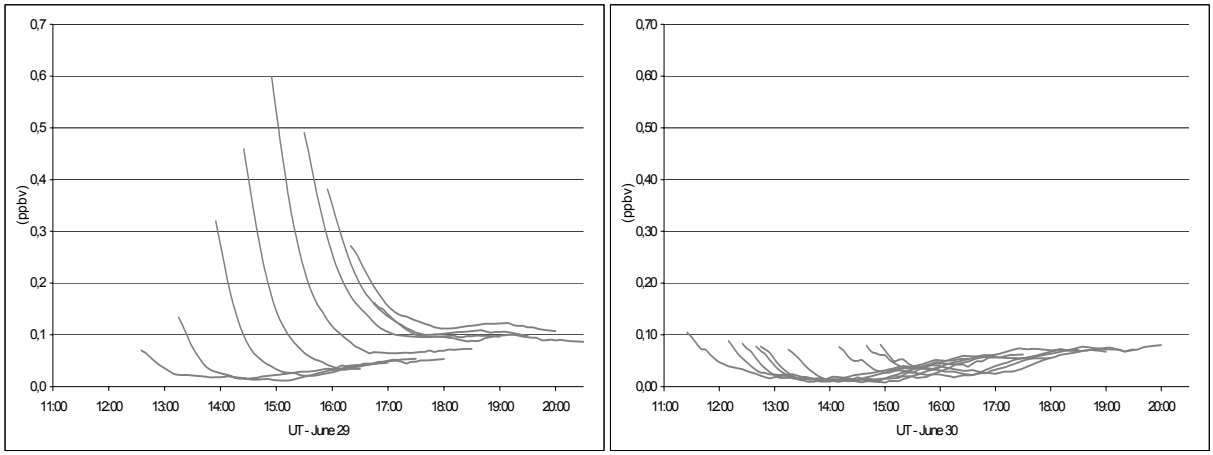

Figure 117: Evolution of α-pinene concentration along the respective trajectories for June 29 and 30 (2001), obtained by application of PTM, using chemical mechanism MCM v3.1b.

6.3 Sensitivity Tests

In this study a sensitivity test, relatively to the effect in ozone concentration *via* change in ambient temperature were made: a change in temperature of 5 degrees has a large effect in calculated ozone concentrations, see Figure 118, Figure 119 and Figure 120.

In order to better understand the reaction mechanism effect on ozone concentration *via* temperature change one test was made changing only the temperature in the calculation algorithm of biogenic emissions and another changing the temperature data used to calculate the rate coefficients of all rates depending on temperature, without changing the rate of emissions.

A change by 5 degrees in temperature used in the algorithm of biogenic emission rates, has, as expected, a significant effect in biogenic emissions (see discussion in section 6.1.4.1, Figure 85 and Figure 86) and consequently in ozone concentration, see Figure 119, (the temperature variation between June 29 and 30 (2001) was approximately 5 degrees). Clearly this effect is more effective in Covelo than in Sangalhos, since there is a large forest between these two places.

The change in temperature data used to calculate the rate coefficients of all kinetic transformations depending on temperature has a significant effect, on both studied places, Sangalhos and Covelo.

Clearly, the effect of changing temperature in calculating the algorithm of biogenic emissions and the effect of changing the temperature data used to calculate the rate coefficients is almost cumulative, for the tested conditions and has a quite similar quantitative effect on ozone production for the studied field conditions.

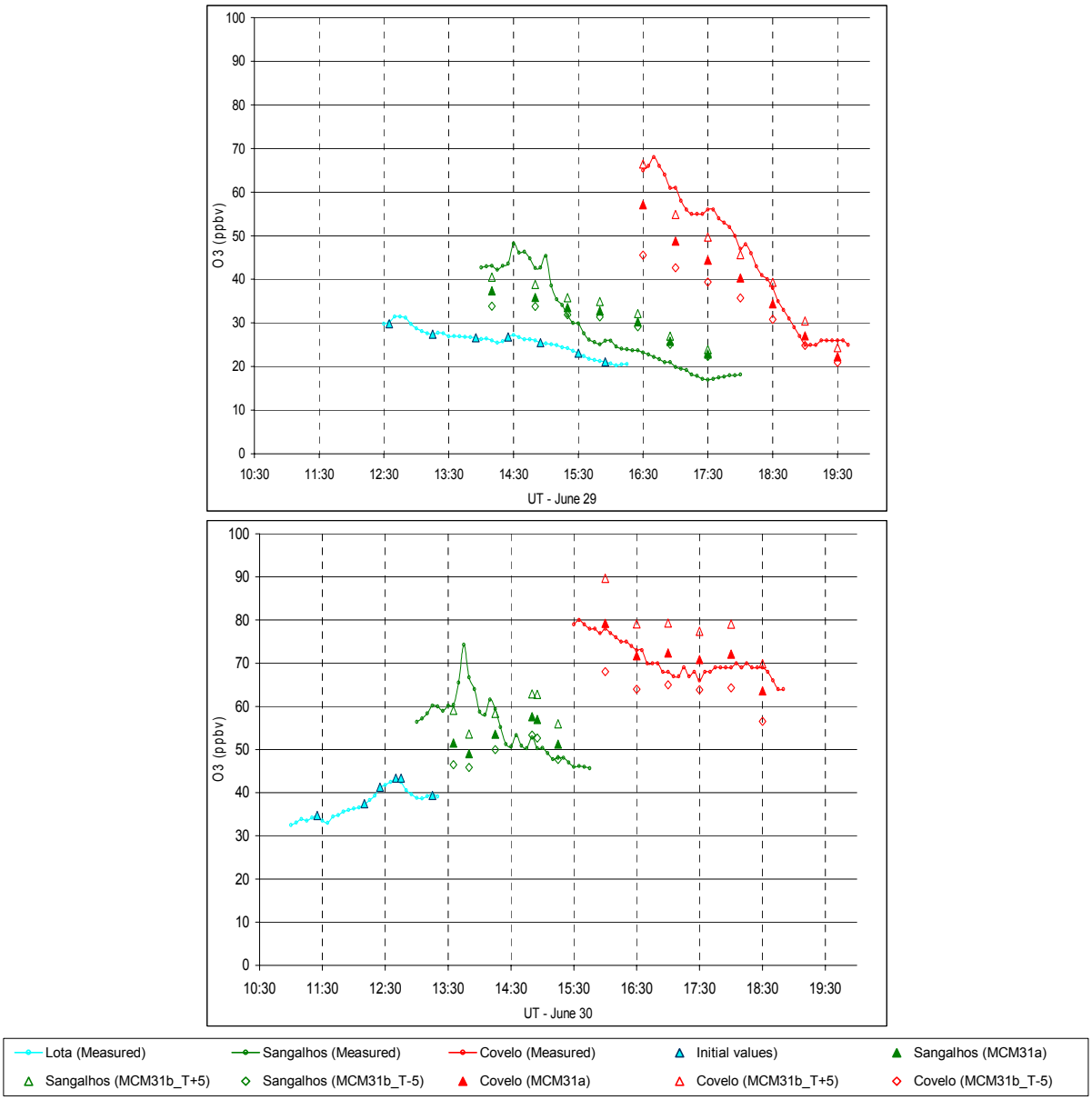

Figure 118: Ozone concentrations obtained by application of PTM, changing the temperature by 5 degrees, using as chemical mechanism MCM v3.1b, and measured values obtained in Sangalhos and Covelo for June 29 and 30 of 2001. The points represent the simulated concentrations at 30 minutes intervals arriving at Covelo.

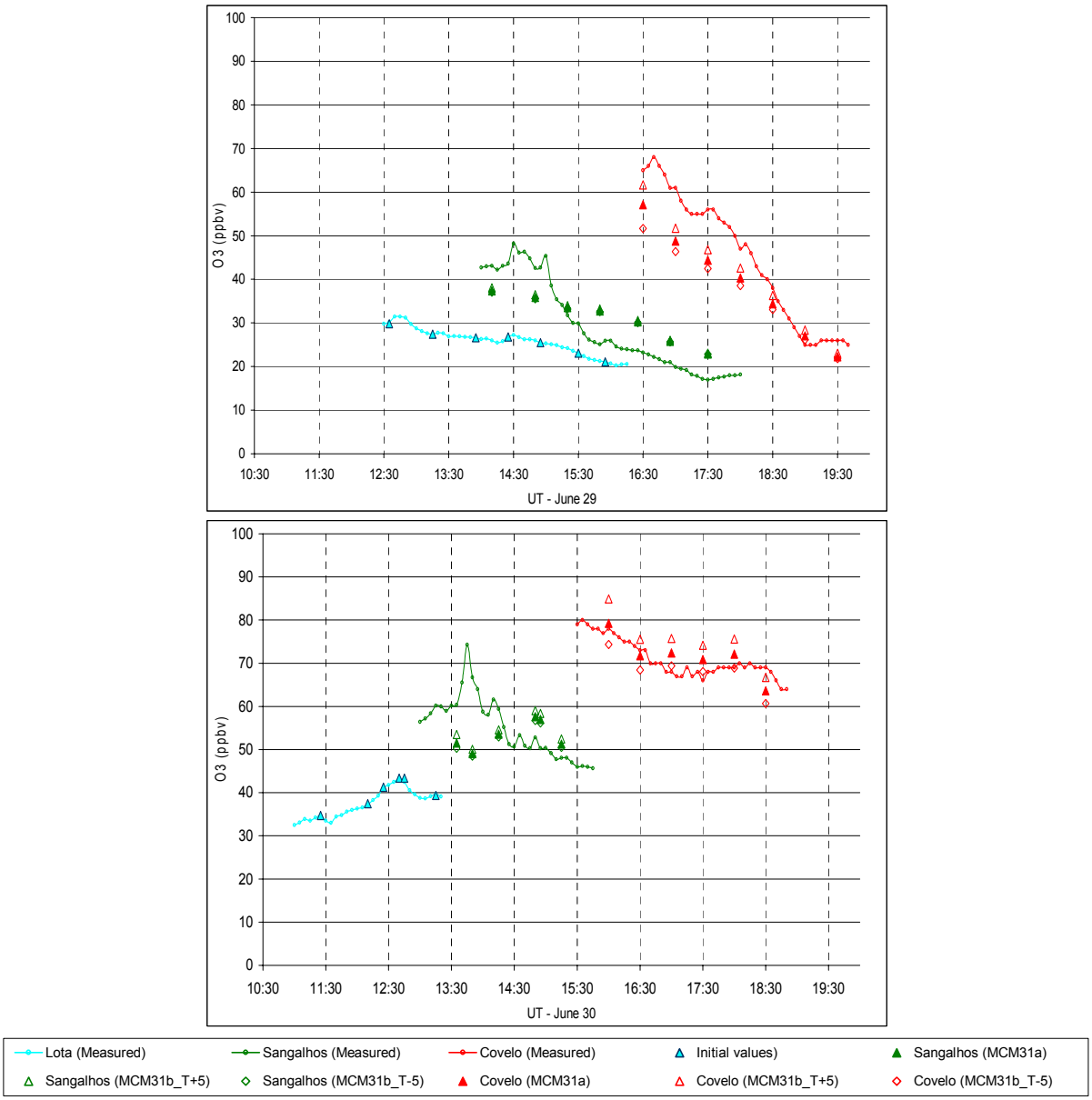

Figure 119: Ozone concentrations obtained by application of PTM, changing the temperature used in algorithm of biogenic emissions calculation, by 5 degrees, using as chemical mechanism MCM v3.1b, and measured values obtained in Sangalhos and Covelo for June 29 and 30 of 2001. The points represent the simulated concentrations at 30 minutes intervals arriving at Covelo.

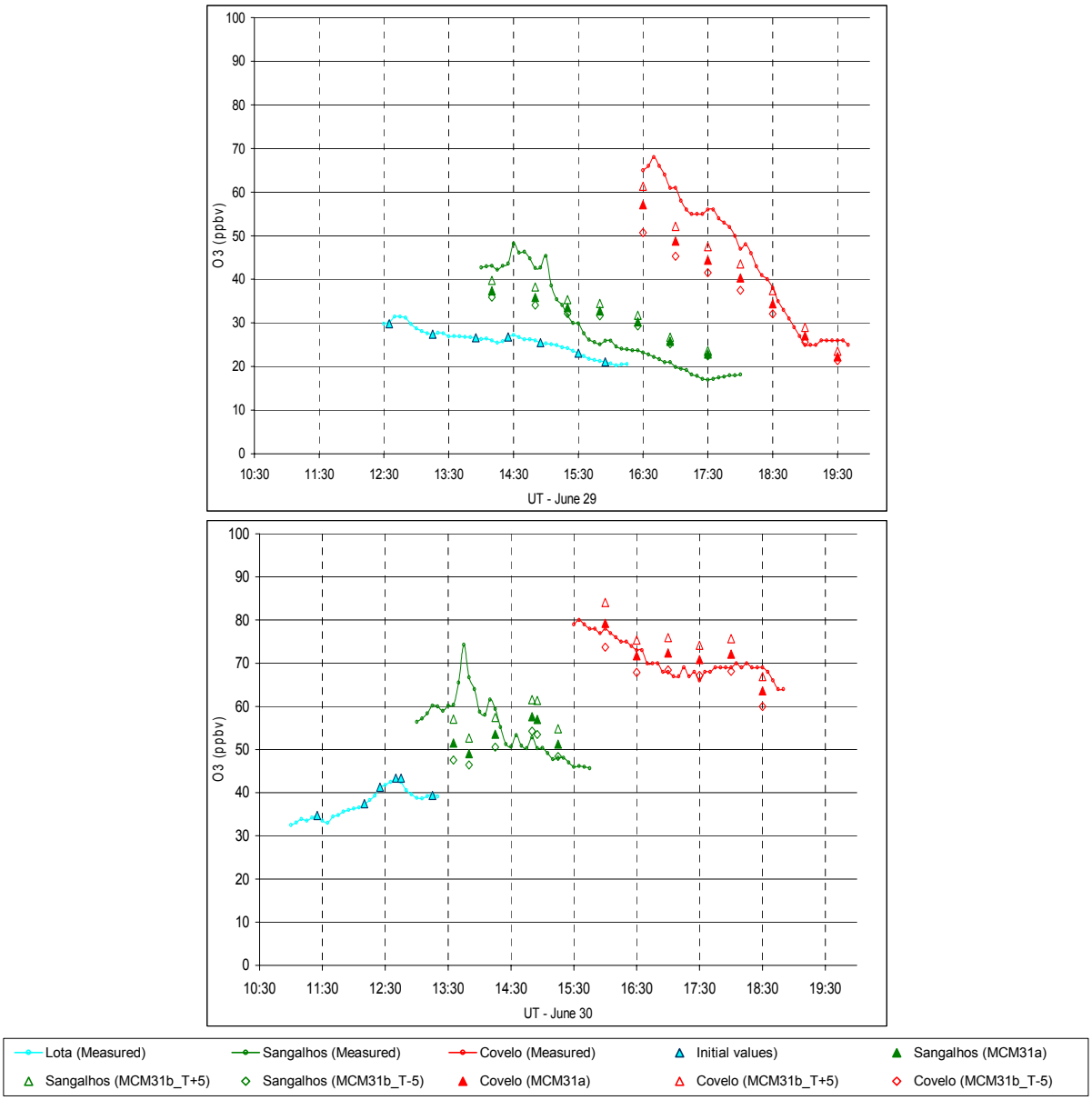

Figure 120: Ozone concentrations obtained by application of PTM, changing the temperature data used to calculate the rate coefficients of all rates depending on temperature, by 5 degrees, using as chemical mechanism MCM v3.1b, and measured values obtained in Sangalhos and Covelo for June 29 and 30 (2001). The points represent the simulated concentrations at 30 minutes intervals arriving at Covelo.

6.4 Summary and Conclusions

The MCM v3.1 was incorporated into a one layer Photochemical Trajectory box Model (PTM) using a Lagrangian approach. The PTM was used to evaluate and intercompare the original and adapted versions of MCM v3.1, (resulting from refinements provided by the chamber evaluation described in sections 5.4-5.7), at normal environmental conditions, in the polluted boundary layer atmosphere. The PTM was applied to a real situation in the Portuguese west coast, during an ozone summer episode, by following the air mass transported by sea breeze, from the coast line (Aveiro) to a location, approximately 65 kilometres inland (Covelo). The PTM was applied during the period of June 29 and 30, 2001, using meteorological and air quality data, obtained from a field campaign. The ozone concentrations obtained by application of PTM, using as chemical mechanism the MCM v3.1 and the described initial concentrations, meteorological data, and emissions inventories, are a good approximation to the measured values in Sangalhos and Covelo.

The use of new photolysis expressions in PTM, relatively to expressions available for download in the MCM internet site, shows a significant effect in ozone concentration calculated for the different air masses moving from Coast to Covelo site.

The change in the assigned rate coefficient for the reaction of OH with NO_2 was tested in the field application. Because concentrations of NO_x in the studied atmosphere are much smaller than those observed in the experiments considered in chamber database, this change, wich has a significant impact in MCM chamber evaluation, has only a small effect in ozone concentration calculated in the current field study. The refinements in MCM v3.1 resulting from chamber evaluation of photo-oxidation of butane, and its degradation products, methylethyl ketone (MEK), acetaldehyde (CH_3CHO) and formaldehyde (HCHO), photo-oxidation of isoprene and its degradation products, methacrolein (MACR) and methylvinyl ketone (MVK) and photo-oxidation of ethane, propene and α-pinene, cause only a very small change in ozone concentrations when applied to these coastal field conditions. The insertion of reaction of $O(^3P)$ with the indicated VOCs, as expected, has a null effect in field conditions.

Sensitivity tests, performed to account for the effect in ozone production by changing temperature, were made. These sensitivity tests show that a change in temperature by 5 degrees has a large effect in calculated ozone concentrations. The change in temperature used in algorithm of biogenic emissions calculation, by 5 degrees, has as expected a significant effect in biogenic emissions and consequently

in ozone concentration. Clearly the effect is more effective in Covelo than in Sangalhos since there is a large forest between these two places. The change in temperature data used to calculate the rate coefficients of all transformation processes depending on temperature has also a significant effect on ozone, at both studied locations, Sangalhos and Covelo. The effect of changing temperature in calculation algorithm of biogenic emissions and the effect of changing the temperature data used to calculate the rate coefficients is almost cumulative, for the tested conditions.

The field evaluation of MCM v3.1 inserted in a photochemical trajectory model confirms that exist too many uncertainties in the model to make a quantitative analysis for several of the species represented in MCM. The evaluation of a chemical mechanism using only field experiments is, at this moment, not possible since the uncertainties plus insufficiency of the database and the unpredictable errors in the transport module could not be taken apart from the chemical mechanism. So it is not possible to index the errors to the chemical mechanism and to avoid the compensation of the error by the different modules of the Model.

Nevertheless, the photochemical trajectory model gave sufficient accurate information about ozone concentrations. Besides, a model that describes detailed emitted VOC speciation and has a chamber-evaluated detailed mechanism is more able to assess the roles played by individual VOC in atmospheric chemistry generally, and in ozone formation in particular. A chamber-evaluated detailed mechanism permits the examining of detailed organic composition inside of air mass, e.g. to simulate the generation of speciated organic intermediates (e.g. multifunctional carbonyls, hydroperoxides and nitrates).

The knowledge of the air composition in a specific moment and in a specific place in atmosphere is not achievable, since atmosphere is a very complex system with several interfaces and with a turbulent flux that could not be physically represented. However, the development of mathematical models describing the chemistry, meteorology, and deposition (Airshed models) allow the development and assessment of effective control strategies.

References

Alvarado A, Tuazon E. C., Aschmann S. M., Atkinson R. and Arey J., 1998. Product of the gas phase reactions of O(^{3}P) atoms and O_3 with α-pinene and 1,2-dimethyl-1-cyclo-hexene. Journal of Geophysical Research, 103, 25541-25551.

Anastasi C. and Sanderson M., 1994a. Reaction of Atomic Oxygen with Some Simple Alkenes - Part 1 .-Low-pressure Studies on Reactions involving Ethene, Propene and (*E*)-But-2-ene. Journal of the Chemical Society Faraday Transactions, 90, 3617-3624.

Anastasi C. and Sanderson M., 1994b. Reaction of Atomic Oxygen with Some Simple Alkenes - Part 2 .-Reaction Pahways involving Ethene, Propene and (*E*)-But-2-ene at Atmospheric Pressure. Journal of the Chemical Society Faraday Transactions, 90, 3625-3631.

Aschmann S. M., Arey J. and Atkinson R., 1996. OH radical formation from gas-phase reactions of O_3 with methacrolein and methyl vinyl ketone. Atmospheric Environment, 30, 2939-2943.

Aschmann S. M., Reissell A., Atkinson R. and Arey J., 1998. Products of the gas phase reactions of the OH radical with α- and β-pinene in the presence of NO. Journal of Geophysical Research – Atmospheres, 103 (D19), 25553-25561.

Aschmann S. M., Arey J. and Atkinson R., 2002. OH radical formation from the gas-phase reactions of O_3 with a series of terpenes. Atmospheric Environment, 36, 4347-4355.

Arey J., Atkinson R. and Aschmann S. M., 1990. Product study of the gas-phase reactions of monoterpenes with the OH radical in the presence of NO_x. Journal of Geophysical Research, 95, 18539-18546.

Arey J., Aschmann S. M., Kwok E. S. C. and Atkinson R., 2001. Alkyl Nitrate, Hydroxylalkyl Nitrate, and Hydroxycarbonyl Formation from the NOx-Air Photooxidations of C5-C8 n-Alkanes. Journal of Physical Chemistry A, 105, 1020-1027.

Atkinson R. and Lloyd A. C., 1984. Evaluation of Kinetic and Mechanistic Data For Modeling of Photochemical Smog. Journal of Physical and Chemical Reference Data, 13, 315-444 .

Atkinson R., 1989. Kinetics and mechanisms of gas-phase reactions of the hydroxyl radical with organic compounds. Journal of Physical and Chemical Reference Data, Monograph 1, 1-246.

Atkinson R., Aschmann S. M., Arey J. and Shorees, B., 1992a. Formation of OH radicals in the gas-phase reactions of O_3 with a series of terpenes. Journal of Geophysical Research, 97, 6065-6073.

Atkinson R., Baulch D. L., Cox R. A., Hampson R. F., Kerr J. A. and Troe J., 1992b. Evaluated kinetic and photochemical data for atmospheric chemistry, Supplement IV : IUPAC subcommittee on gas kinetic data evaluation for atmospheric chemistry. Journal of Physical and Chemical Reference Data, 21, 1125-1568.

Atkinson R. and Aschmann S. M., 1993. OH radical production from the gas phase reactions of O_3 with a series of alkenes under atmospheric conditions. Environmental Science and Technology, 27, 1357-1363.

Atkinson R., 1994. Gas-phase tropospheric chemistry of organic compounds. Journal of Physical and Chemical Reference Data, Monograph 2.

Atkinson R., Tuazon E. C. and Aschmann S. M., 1995. Products of the gas-phase reactions of a series of 1-alkenes and 1-methylcyclohexene with the OH Radical in the presence of NO. Environmental Science and Technology, 29, 1674-1680.

Atkinson R., 1997a. Atmospheric reactions of alkoxy and β-hydroxyalkoxy radicals. International Journal of Chemical Kinetics, 29, 99-111.

Atkinson R., 1997b. Gas-Phase Tropospheric Chemistry of Volatile Organic Compounds: 1. Alkanes and Alkenes. Journal of Physical Chemical Reference Data, *26*, 215-290.

Atkinson R., 2000. Atmospheric chemistry of VOCs and NOx. Atmospheric Environment, 34, 2063-2101.

Atkinson R. and Arey J., 2003. Gas-phase tropospheric chemistry of biogenic volatile organic compounds: a review. Atmospheric Environment, 37, Supplement No. 2 S197–S219.

Atkinson R., Baulch D. L., Cox R. A., Crowley J. N., Hampson R. F., Hynes R. G., Jenkin M. E., Rossi M. J. and Troe J., 2005. Evaluated kinetic and photochemical data for atmospheric chemistry. Volume II: reactions of organic species. Atmospheric Chemistry and Physics Discussions, 5, 6295-7168.

Barnes I., Becker K. H., Ruppert L, 1993. FTIR Product study of the self-reaction of beta-hydroxyethyl peroxi-radicals. Chemical Physics Letters, 203, 295-301.

Berndt T., Böge O., Stratmann F., 2003. Gas-Phase Ozonolysis of α-Pinene: Gaseous Products and Particle Formation. Atmospheric Environment, 37, 3933-3945.

Bertin N., Staudtt M., Hansen U., Seufert G., Ciccioli P., Foster P., Fugit J-L. and Torres L., 1997: The BEMA-project: Diurnal and seasonal course of monoterpene emissions from *Quercus ilex* under natural conditions – application of light and temperature algorithms, Atmospheric Environment, 31, 135–144.

Bertman S. B. and Roberts J. M., 1991. A PAN Analog from Isoprene Photooxidation. Geophysical Research Letter, 18, 1461 - 1464, 10.1029/91GL01852.

Bloss C., Wagner V., Bonzanini A., Jenkin M. E., Wirtz K., Martin-Reviejo M. and Pilling M. J., 2005a. Evaluation of detailed aromatic mechanisms (MCMv3 and MCMv3.1) against environmental chamber data. Atmospheric Chemistry and Physics, 5, 623-639.

Bloss C., Wagner V., Jenkin M. E., Volkamer R., Bloss W. J., Lee J. D., Heard D. E.,'Wirtz K., Martin-Reviejo M., Rea G., Wenger J. C. and Pilling M. J., 2005b. Development of a detailed chemical mechanism (MCMv3.1) for the atmospheric oxidation of aromatic hydrocarbons. Atmospheric Chemistry and Physics, 5, 641-664.

Bongartz A., Kames J., Welter F. and Schurath U., 1991. Near-UV Absorption Cross Sections and Trans/Cis Equilibrium of Nitrous Acid. Journal of Physical Chemistry, 95, 1076-1082.

Bonn B., von Kuhlmann R. and Lawrence M. G., 2004. High contribution of biogenic hydroperoxides to secondary organic aerosol formation. Geophysical Research Letters, 31, L10108, doi: 10.1029/2003GL019172.

Bonsang, B., Moortgat, G. K. and Pio, C. A., 2001. Overview of the FIELDVOC'94 experiment in a eucalyptus forest of Portugal. Chemosphere, 3, 211-226.

Borbon A., Fontaine H, Veillerot M., Locoge N., Galloo J. C. and Guillermo R., 2001. An investigation into the traffic-related fraction of isoprene at an urban location. Atmospheric Environment, 35, 3749-3760.

Borrego C., Tchepel O., Barros N. and Miranda A. I., 2000. Impact of road traffic emissions on air quality of the Lisbon region. Atmospheric Environment, 34, 468-4690.

Burgess R. A. and Penkett S. A., 1993. Ground-based non-methane hydrocarbon measurements in England. Proceedings of the EUROTRAC'92 Symposium, Garmisch-Partenkirchen, March 1992. Academic Publishing, The Hague, The Netherlands, 165-169.

Burkholder J. B., Talukdar R. K., Ravishankara A. R. and Solomon, S., 1993. Temperature dependence of the HNO_3 UV absorption cross sections, Journal of Geophysical Research, 98, 22937-22948.

Capouet M., Peeters J., Nozière B. and Müller J.F., 2004. Alpha-pinene oxidation by OH: simulations of laboratory experiments. Atmospheric Chemistry and Physics, 4, 2285–2311.

Calvert J. G., Atkinson R., Kerr J. A., Madronich S., Moortgat G. K., Wallington T. J. and Yarwood G., 2000. The mechanisms of atmospheric oxidation of alkenes. Oxford University Press, New York. ISBN 0195131770.

Carter W. P. L. and Atkinson R., 1987. An experimental study of incremental hydrocarbon reactivity. Environmental Science and Technology, 21, 670-679.

Carter, W. P. L., and F. W. Lurmann, 1990. Evaluation of the RADM Gas-Phase Chemical Mechanism. EPA-600/3-90-001. U.S. Environmental Protection Agency.

Carter W. P. L. and Lurmann F. W., 1991. Evaluation of a Detailed Gas-Phase Atmospheric Reaction Mechanism using Environmental Chamber Data. Atmospheric Environment, 25A, 2771-2806.

Carter W. P. L., 1994. Development of Ozone Reactivity Scales for Volatile Organic Compounds. Journal of the Air and Waste Management Association, 44, 881 - 899.

Carter W. P. L., Luo D., Malkina I. L. and Fitz D., 1995a. The University of California, Riverside Environmental Chamber Data Base for Evaluating Oxidant Mechanisms: Indoor Chamber Experiments Through 1993. EPA/600/SR-96/078, U.S. Environmental Protection Agency, Research Triangle Park, NC. Available at http://www.cert.ucr.edu/~carter/absts.htm#databas

Carter W. P. L., Luo D., Malkina I. L. and Pierce J. A., 1995b. Environmental Chamber Studies of Atmospheric Reactivities of Volatile Organic Compounds. Effects of Varying Chamber and Light Source. Final report to National Renewable Energy Laboratory, Contract XZ-2-12075, Coordinating Research Council, Inc., Project M-9, California Air Resources Board, Contract A032-0692, and South Coast Air Quality Management District, Contract C91323. Available at http://www.cert.ucr.edu/~carter/absts.htm#explrept.

Carter, W. P. L. and Atkinson, R., 1996: Development and Evaluation of a Detailed Mechanism for the Atmospheric Reactions of Isoprene and NOx, International Journal of Chemical Kinetics, 28, 497-530.

Carter W. P. L., 2000. Documentation of the SAPRC-99 Chemical Mechanism for VOC reactivity Assessment. Final Report to California Air Resources Board Contract 92-329 and Contract 95-308, Air Pollution Research Center and College of Engineering Center for Environmental Research and Technology University of California Riverside, California. Available at http://www.cert.ucr.edu/~carter/absts.htm#saprc99 and http://www.cert.ucr.edu/~carter/reactdat.htm

Carter W. P. L., Seinfeld J. H., Fitz D. R. and Tonnesen G. S., 2002. Development of a Next-Generation Environmental Chamber Facility for Chemical Mechanism and VOC Reactivity Research. Draft Research Plan and First Progress Report to the United States Environmental Protection Agency Cooperative Agreement CR 827331-01-0 for the period July 1, 1999 through October 16, 2001. Center for Environmental Research and Technology College of Engineering University of California Riverside.

Chen X., Hulbert D. and Shepson P., 1998. Measurement of the organic nitrate yield from OH reaction with isoprene. Journal of Geophysical Research, 103, D9, 25563-25568.

Chew A. A. and Atkinson R., 1996. OH radical formation yields from the gas-phase reactions of O_3 with alkenes and monoterpenes. Journal of Geophysical Research, 101, 28649-28653.

Clapp L. J. and Jenkin M. E., 2001. Analysis of the relationship between ambient levels of O_3, NO_2 and NO as a function of NOx in the UK. Atmospheric Environment, 35, 6391-6405.

Curtis A. R. and Sweetenham W. P., 1987. FACSIMILE release H user's manual. AERE Report R11771 (HMSO). London.

Cvetanovic R. J., 1987. Evaluated Chemical Kinetic Data for the Reactions of Atomic Oxygen $O(^3P)$ with Unsaturated Hydrocarbons. Journal of Physical and Chemical Reference Data, 16, 261-326.

DeMore W. B., Sander S. P., Golden D. M., Hampson R. F., Kurylo M. J., Howard C. J., Ravishankara A. R., Kolb C. E. and Molina M. J., 1994. Chemical Kinetics and Photochemical Data for Use in Stratospheric Modeling, Evaluation Number 11. JPL Publication 97-4, Jet Propulsion Laboratory, California Institute of Technology, Pasadena, CA.

DeMore W. B., Sander S. P., Golden D. M., Hampson R. F., Kurylo M. J., Howard C. J., Ravishankara A. R., Kolb C. E. and Molina M. J., 1997. Chemical Kinetics and Photochemical Data for Use in Stratospheric Modeling, Evaluation Number 12. JPL Publication 97-4, Jet Propulsion Laboratory, California Institute of Technology, Pasadena, CA.

DeSai J., Heicklen J., Bahta A. and Simonaitis R. 1986. The photo-oxidation of i-C3H7CHO vapour. Journal of Photochemistry, 34, 137-164.

DGGE, 1999. A Procura de Energia em Portugal 2000-2020 - Sector dos Transportes. Direcção Geral de Geologia e Energia.

Dodge M. C., 2000. Chemical oxidant mechanisms for air quality modeling: critical review. Atmospheric Environment, 34, 2103-2130.

Derwent R. G. and Jenkin M. E., 1991. Hydrocarbons and the long-range transport of ozone and PAN across Europe. Atmospheric Environment, 25A, 1661-1678.

Derwent R. G., Middleton D. R., Field R. A., Goldstone M. E., Lester J. N. and Perry R., 1995 Analysis and interpretation of air quality data from an urban roadside location in central London over the period from July 1991 to July 1992. Atmospheric Environment, 29, 923-946.

Derwent R. G., Jenkin M. E., Saunders S. M. and Pilling M. J., 1998. Photochemical ozone creation potentials for organic compounds in North-West Europe calculated with a Master Chemical Mechanism. Atmospheric Environment, 32, 2429-2441.

Derwent R. G., Jenkin M. E., Saunders S. M. and Pilling M. J., 2001.Characterization of the reactivities of volatile organic compounds using a master chemical mechanism. Journal of the Air and Waste Management Association, 51, 699-707.

Derwent R. G., Jenkin M. E., Saunders S. M., Pilling M. J. and Passant N. R., 2005. Multi-day ozone formation for alkenes and carbonyls investigated with a master chemical mechanism under European conditions. Atmospheric Environment, 39, 625-625.

Donev E., Zeller K. and Avramov A., 2002. Preliminary background ozone concentrations in the mountain and coastal areas of Bulgaria. Environmental Pollution, 117, 281-286.

Duane M., Poma B., Rembges D., Astorga C. and Larsen B. R., 2002. Isoprene and its degradation products as strong ozone precursors in Insubria, Northern Italy. Atmospheric Environment, 36, 3867-3879.

Dueñas, C., Fernández, C. M., Cañete, S., Carretero, J. and Liger, E., 2004. Analyses of ozone in urban and rural sites in Málaga (Spain). Chemosphere, 56, 631-639.

EEA-ETC/AE-CORINAIR, 1996. Summary Report 1, EEA Topic Report 7. EEA, Copenhagen.

Evtyugina, M. G., 2004. Photochemical Pollution in Portuguese Coast. (in Portuguese) Ph.D. Thesis, University of Aveiro, Portugal.

Evtyugina M. G., Nunes T., Pio C. A. and Costa C. S., 2006a. Photochemical pollution under sea breeze conditions, during summer, at the Portuguese West Coast. Submitted to Atmospheric Environment.

Evtyugina M. G., Pio C. A., Nunes T. and Pinho P. G., 2006b. Photochemical ozone formation investigated with a master chemical mechanism at Portugal West Coast under sea breeze conditions. Submitted to Atmospheric Environment.

Fantechi G., Vereecken L. and Peeters J., 2002. The OH-initiated atmospheric oxidation of pinonaldehyde: Detailed theoretical study and mechanism constructiony. Physical Chemistry Chemical Physics, 4, 5795-5805.

Finlayson-Pitts B. J. and Pitts J. N., 2000. Chemistry of the upper and lower atmosphere: theory, experiments and applications. Academic Press.

Förgeteg S., Dóbé S. and Bérces T., 1978. Effect of pressure on the primary photochemical processes of n-butyraldehyde at 313 nm. Reaction Kinetics and Catalysis Letters, 9, 331-336.

Gery M. W., Whitten G. Z. and Killus J. P., 1988. Development and testing of the CBM-IV for urban and regional modeling. Report to the U.S. Environmental Protection Agency, EPA/600/3-88-012.

Gierczak T., Burkholder J. B., Talukdar R. K., Mellouki A., Barone S. B., Ravishankara, A. R., 1997. Atmospheric Fate of Methyl Vinyl Ketone and Methacrolein. Journal of Photochemistry and Photobiology A: Chemistry, 110, 1-10.

Gierczak, T., Burkholder J. B., Bauerle S. and Ravishankara A. R., 1998. Photochemistry of acetone under tropospheric conditions. Chemical Physics, 231, 229– 244.

Gierczak, T., Burkholder J. B., Bauerle S. and Ravishankara A. R., 1998. Photochemistry of acetone under tropospheric conditions. Chemical Physics, 231, 229– 244.

Goodwin J. W. L., 2001. UK Emissions of Air Pollutants 1970 - 1999. Report AEAT/ENV/R/0798.

Grosjean D., Williams E. L. and Grosjean E., 1993a. Atmospheric chemistry of isoprene and its carbonylproducts. Environmental Science and Technology, 27, 830-840.

Grosjean D., Williams E. L., Grosjean E., Andino J. M. and Seinfeld J. H., 1993b. Atmospheric oxidation of biogenic hydrocarbons: reaction of ozone with β-pinene, δ-limonene and trans caryophyllene. Environmental Science and Technology, 27, 2754-2758.

Guenther A. B., Zimmerman P., Harley P., Monson R. and Fall R., 1993. Isoprene and monoterpene emission rate variability: Model evaluation and sensitivity analysis. Journal Geophysical Research, 98, 12609-12617.

Guenther, A. B., Zimmerman P. and Wildermuth M., 1994. Natural volatile organic compound emission rate estimates for U.S. woodland landscapes. Atmospheric Environment, 28, 1197-1210.

Guenther A. B., Hewitt C. N., Erickson D., Fall R., Geron C., Graedel T., Harley P., Klinger L., Lerdau M., McKay W. A., Pierce T., Scholes B. Steinbrecher R., Tallamraju R., Taylor J. and Zimmerman P., 1995. A global model of natural volatile organic compound emissions. Journal Geophysical Research, 100, 8873-8892.

Guenther A. B., Greenberg J., Harley P., Helmig D., Klinger L., Vierling L., Zimmerman P. and Geron C., 1996. Leaf, branch, stand and landscape scale measurements of volatile organic compound fuxes from US woodlands. Tree Physiology, 16, 17-24.

Guenther A. B., 1997. Seasonal and spatial variations in natural volatile organic compound emissions. Ecological Applications, 7, 34–45.

Hakola H., Arey J., Aschmann S.M. and Atkinson R., 1994. Product formation from the gas-phase reactions of OH radicals and O_3 with a series of monoterpenes. Journal of Atmospheric Chemistry, 18, 75-102.

Hakola H., Rinne J. and Laurila T., 1998. The hydrocarbon emission rates of tea-leafed willow (*Salix phylicifolia*), silver birch (*Betula pendula*) and European aspen (*Populus tremula*). Atmospheric Environment, 32, 1825-1833.

Hallquist M., Wängberg I., Ljungström E., Barnes I. and Becker, K. H., 1999. Aerosol and product yields from NO3 radical- initiated oxidation of selected monoterpenes. Environmental Science and Technology, 33, 553 – 559.

Hansen U., Van Eijk J., Bertin N., Staudtt M., Kotzias D., Seufert G., Fugit J. L., Torres L., Cecinato A., Brancaleoni E., Cicciolo P. and Bomboi, T., 1997: Biogenic emissions and CO2 gas exchange investigated on four Mediterranean shrubs, Atmospheric Environment, 31, 157–167.

Harder H., Pätz, W., Volz-Thomas A., Fischer H. and Zenkes T., 2001, Measurements of nitrogen oxides, ozone, and carbon monoxide during the FIELDVOC'94 campaign in Tábua, Ed. Khalil, M.A.K., Atmospheric Chemistry of Volatile Organic Compounds in a Eucalyptus Forest (FIELDVOC'94). Chemosphere, 3, 227-237.

Harley P. C., Monson R. K. and Lerdau M. T., 1999. Ecological and evolutionary aspects of isoprene emission from plants. Oecologia, 118, 109-123.

Heicklen J., DeSai J., Bahta A., Harper, C. and Simonaitis R., 1986. The temperature and wavelength dependence of the photo-oxidation of propionaldehyde. Journal of Photochemistry, 34, 117-135.

Hatakeyama S., Kobayashi H. and Akimoto H., 1984: Gas-phase oxidation of SO_2 in the ozone-olefin reactions, Journal Physical Chemistry, 88, 4736–4739.

Hatakeyama S., Izumi K., Fukuyama T. and Akimoto H., 1989. Reactions of ozone with α–pinene and β–pinene in air: yields of gaseous and particulate products. Journal of Geophysical Research, 94, 13013-13024.

Hatakeyama S, Izumi K., Fukuyama T. and Akimoto H., 1991: Reactions of OH with α-pinene and β-pinene in air, estimate of global CO production from the atmospheric oxidation of terpenes. Journal of Geophysical Research, 96, 947-958.

Hynes R. G., Angove D. E., Saunders S. M., Haverd V. and Azzi M., 2005. Evaluation of two MCM v3.1 alkene mechanisms using indoor environmental chamber data. Atmospheric Environment, 39, 7251-7262.

IUPAC Subcommittee on Gas Kinetic Data Evaluation, http://www.iupac-kinetic.ch.cam.ac.uk/.

Jeffries H. E., Gery M. W., Carter W. P. L., 1992. Protocols for evaluating oxidant mechanisms for urban and regional models. EPA 600/R-92/112. Atmospheric Research and Exposure Assessment Laboratory, ORD, USEPA, Research Triangle Park, North Carolina.

Jenkin M. E., Saunders S.M and Pilling M. J., 1997. The tropospheric degradation of volatile organic compounds: A protocol for mechanism development. Atmospheric Environment, 31, 81-104.

Jenkin M. E., Boyd A. A. and Lesclaux R., 1998. Peroxy radical kinetics resulting from the OH-initiated oxidation of 1,3-butadiene, 2,3-dimethyl-1,3-butadiene and isoprene. Journal of Atmospheric Chemistry, 29, 267–298.

Jenkin M. E. and Clemitshaw K. C., 2000 Ozone and other secondary photochemical pollutants: chemical processes governing their formation in the planetary boundary layer. Atmospheric Environment, 34, 2499-2527.

Jenkin M. E., Shallcross D. E. and Harvey J. N., 2000a. Development and application of a possible mechanism for the formation of cis-pinic acid from the ozonolysis of α- and β-pinene. Atmospheric Environment, 34, 2837-2850.

Jenkin M. E., Passant N. R. and Rudd H. J., 2000b. Development of Species Profiles for UK Emissions of VOCs. A report produced for the Department of the Environment, Transport & the Regions. AEAT\EPSC-0044, AEA Technology.

Jenkin M. E., Murrells T. P. and Passant N. R., 2000c. The Temporal Dependence of Ozone Precursor Emissions: Estimation and Application. A report produced for the Department of the Environment, Transport & the Regions. AEAT/R/ENV/0355, AEA Technology.

Jenkin M. E., Saunders S. M., Derwent R. G. and Pilling M. J., 2002. Development of a reduced speciated VOC degradation mechanism for use in ozone models. Atmospheric Environment, 36, 4725-4734.

Jenkin M. E., Saunders, S. M., Wagner, V. and Pilling, M. J., 2003. Protocol for the development of the Master Chemical Mechanism, MCM v3, Part B: tropospheric degradation of aromatic volatile organic compounds. Atmospheric Chemistry and Physics, 3, 181-193.

Jenkin M. E., 2004. Analysis of sources and partitioning of oxidant in the UK - Part 1: the NOx -dependence of annual mean concentrations of nitrogen dioxide and ozone. Atmospheric Environment, 38, 5117 –5129.

Johnston H. S., Chang S. and Whitten G., 1974. Photolysis of nitric acid vapour. Journal of Physical Chemistry, 78, 1-7.

Johnston H. S., Davis H. F. and Lee Y. T., 1996. NO_3 Photolysis Product Channels: Quantum Yields from Observed Energy Thresholds. Journal of Physical Chemistry, 100, 4713-4723.

Kesselmeier J. K. and Staudtt M., 1999. Biogenic volatile organic compounds (VOC): An overview on emission, physiology and ecology. Journal of Atmospheric Chemistry, 33, 23–88.

Killus J. P. and Whitten G. Z., 1990. Backgroud reactivity in smog chambers. International Journal of Chemical Kinetics, 22, 547-575.

Klemp D., Kley D., Kramp F., Buers H.J., Pilwat G., Flocke F., Pätz H.W. and Volz- Thomas A., 1997. Long-term measurements of light hydrocarbons (C_2-C_5) at Schauinsland (Black Forest), Journal of Atmospheric chemistry, 28, 135-171.

König G., Brunda M., Puxbaum H., Hewitt C. N., Duckham S. C. and Rudolph J., 1995. Relative contribution of oxygenated hydrocarbons to the total biogenic VOC emissions of selected mid-European agricultural and natural plant species. Atmospheric Environment, 29, 861–874.

Kwok, E. S. C. and Atkinson R., 1995. Estimation of hydroxyl radical rate constants for gas-phase organic compounds using a structure-reactivity relationship: an update. Atmospheric Environment, 29, 1685-1695.

Kwok E. S. C., Atkinson R. and Arey J., 1995. Observation of hydroxycarbonyls from the OH radical-initiated reaction of isoprene, Environmental Science and Technology, 29**,** 2467-2469.

Langford A. O., Petek H. and Moore C. B., 1984. Collision Complex Formation in the Reactions of Formyl Radicals with Nitric Oxide and Oxygen. Journal of Physical Chemistry, 80, 4211-4221.

Lee Y. N., Zhou X., Kleinman L. I., Nunnermacker L. J., Springston S. R., Daum P. H., Newman L., Keigley W. G., Holdren M. W., Spicer C. W., Parrish D. D., Holloway J., Williams J., Roberts J. M., Ryerson T. B., Fehsenfeld F. C., Young V. and Fu B., 1998. Atmospheric chemistry and distribution of formaldehyde and several multi-oxygenated carbonyl compounds during the 1995 Nashville/Middle Tennessee ozone study. Journal of Geophysical Research, 103, 22449-22462.

Luke W. T., Dickerson R. R. and L. J. Nunnermacker, 1989. Direct Measurements of the Photolysis Rate Coefficients and Henry's Law Constants of Several Alkyl Nitrates. Journal of Geophysical Research, 94, 14905-14921.

Martin P., Tuazon E. C., Aschmann S. M., Arey J. and Atkinson R., 2002. Formation and Atmospheric Reactions of 4,5-Dihydro-2-methylfuran. Journal of Physical Chemistry A**,** 106, 11492-11501

Martinez R. D., Buitrago A. A., Howell N. W., Hearn C. H. G. and Joens J. A., 1992. The near UV absorption spectra of several aliphatic aldehydes and ketones at 300K. Atmospheric Environment, 26A, 785-792.

McLaren R., Singleton D. L., Lai J. Y. K., Khouw B., Singer E., Wu Z. and Niki H., 1996. Analysis of motor vehicle sources and their contribution to ambient hydrocarbon distributions at urban sites in Toronto during the Southern Oxidants Study. Atmospheric Environment, 30, 2219-2232.

McRae, G.J., Goodin, W.R., Seinfeld, J.H., 1982. Development of a second-generation mathematical model for urban air pollution-I. Model formulation. Atmospheric Environment, 16, 679-696.

Meller R., Raber W., Crowley J. N., Jenkin M. E. and Moortgat G. K., 1991. The UV-visible absorption spectrum of methylglyoxal. Journal of Photochemistry and Photobiology A: Chemistry, 62, 163-171.

Meller R. E. and Moortgat G. K., 2000. Temperature dependence of the absorption cross sections of formaldehyde between 223 and 323 K in the wavelength range 225 –375 nm. Journal of Geophysical Research, 105, 7089 –7101.

Meyrahn H., Pauly J., Scheneider W. and Warneck, P., 1986. Quantum Yields for the Photodissociation of Acetone in Air and an Estimate for the Life Time of Acetone in the Lower Troposphere. Journal of Atmospheric Chemistry, 4, 277-291.

Miyoshi A., Hatakeyama S. and Washida N., 1994. OH Radical-Initiated Photooxidation of Isoprene: An Estimate of Global CO Production, Journal of Geophysical Research, 99, 18779-18787.

Molina L. T. and Molina M. J., 1986. Absolute absorption cross sections of ozone in the 185 to 350 nm wavelength range. Journal of Geophysical Research, 91, 14501-14508.

Muthuramu K., Shepson P. B. and O'Brien J. M., 1993. Preparation, Analysis, and Atmospheric Production of Multifunctional Organic Nitrates. Environmental Science and Technology, 27, 1117-1124.

Neeb P. and Moortgat G. K., 1999. Formation of OH Radicals in the Gas-Phase Reaction of Propene, Isobutene, and Isoprene with O3: Yields and Mechanistic Implications. Journal of Physical Chemistry A, 103, 9003-9012.

Niki H., Maker P. D., Savage C. M. and Breitenbach L. P., 1981. An FTIR study of Mechanisms for the OH radical initiated oxidation of C2H4 in the presence of NO – detection of glycolaldehyde. Chemical Physics Letters, 80, 499-503.

Noziere B., Barnes I. and Becker K., 1999. Product study and mechanisms of the reactions of α-pinene and of pinonaldehyde with OH radicals. Journal of Geophysical Research, 104, 23645-23658.

Ntziachristos L. and Samaras Z., 2000. COPERT III, Computer programme to calculate emissions from road transport, Methodology and emission factors (Version 2.1). European Environment Agency.

Nunes T. V. 1996. Biogenic emissions of non-methane hydrocarbons. Contribution for the determination of VOC emission rates from forest ecosystems. (in Portuguese) Ph.D. Thesis, University of Aveiro, Portugal.

Nunes T. V. and Pio, C. A., 2001.Emission of volatile organic compounds from Portuguese eucalyptus forest. Chemosphere, 3, 239-248.

O'Brien J. M., Czuba E., Hastie D. R., Francisco J. S. and Shepson P. B., 1998. Determination of the Hydroxy Nitrate Yields from the Reaction of C_2-C_6 Alkenes with OH in the Presence of NO. Journal Physical Chemistry A, 102, 8903-8908.

Orlando J., Nozière B., Tyndall G., Orzechowska G., Paulson S. and Rudich Y., 2000: Product studies of the OH- and ozone-initiated oxidation of some monoterpenes. Journal of Geophysical Research, 105, 11561-11572.

Owen S., Boissard C., Street R. A., Duckham S. C., Csiky O. and Hewitt C. N., 1997. Screening of 18 Mediterranean plant species for volatile organic compound emissions. Atmospheric Environment, 31, 101–118.

Owen S. M., Boissard C. and Hewitt C. N., 2001. Volatile organic compounds (VOCs) emitted from 40 Mediterranean plant species: VOC speciation and extrapolation to habitat scale. Atmospheric Environment, 35, 5393–5409.

Paulson S. E. and J. H. Seinfeld 1992. Atmospheric Photooxidation of 1-Octene: OH, O3, and O(3P) reactions. Environmental Science and Technology, 26, 1165-1173.

Paulson S. E., Flagan R. C., Seinfeld J. H., 1992. Atmospheric photo-oxidation of isoprene: part I. the hydroxyl radical and ground state atomic oxygen reactions. International Journal of Chemical Kinetics, 24, 79-101.

Paulson S. E., Chung M., Sen A. D. and Orzechowska G., 1998. Measurement of OH Radical Formation from the Reaction of Ozone with Several Biogenic Alkenes. Journal of Geophysical Research, 103, 25533-25539.

Paulson S. E., Fenske J. D., Sen A. D. and Callahan T. W., 1999a. A Novel Small-Ratio Relative-Rate Technique for Measuring OH Formation Yields from the Reactions of O_3 with Alkenes in the Gas Phase, and Its Application to the Reactions of Ethene and Propene. Journal of Physical Chemistry A, 103, 2050 –2059.

Paulson S. E., Chung M. T. and Hasson A., 1999b. OH radical formation from the gas phase of ozone with terminal alkenes, and relationship between structure and mechanism. Journal of Physical Chemistry A, 103, 8125 –8138.

Peeters J., Boullart W. and Hoeymissen J. V., 1994, Proceedings of EUROTRAC Symposium 94, SPB Academic Publ., The Hague, The Netherlands, 110.

Peeters J., Vereecken L. and Fantechi G., 2001. The detailed mechanism of the OH-initiated atmospheric oxidation of α-pinene: a theoretical study Physical Chemistry Chemical Physics, 3, 5489-5504.

Pinho P. G., 2000. Modelling Biogenic Hydrocarbons Emissions Influence in Photochemical Pollution. Application to the Portuguese Coast. (in Portuguese). Master Thesis, University of Aveiro, Portugal

Pinho P. G., Pio C. A. and Jenkin M. E., 2005. Evaluation of isoprene degradation in the detailed tropospheric chemical mechanism, MCM v3, using environmental chamber data. Atmospheric Environment, 39, 1303-1322.

Pinho P. G., Pio C. A., Carter W. P. L. and Jenkin M. E., 2006. Evaluation of alkene degradation in the detailed tropospheric chemistry mechanism, MCM v3, using environmental chamber data. Journal of Atmospheric Chemistry, 55, 55-79.

Pio C. A., Nunes T. V. and Brito S., 1993. Volatile hydrocarbon emissions from common and native species of vegetation in Portugal, in General Assessment of Biogenic Emissions and Deposition of Nitrogen Compounds, Sulphur Compounds and Oxidants in Europe, CEC/BIATEX Workshop, CEC Air Pollution Rep. 47, E. Guyot SA, Brussels, pp. 291–298.

Pio C. A., Silva P. A., Cerqueira M. A. and Nunes T.V., 2005. Diurnal and seasonal emissions of volatile organic compounds from cork oak (Quercus suber) trees. Atmospheric Environment, 39, 1817–1827.

Plum I. C., Sanhueza E., Atkinson R., Carter W. P. L. and Pitts J. N. ,1983. OH radical rate constants and photolysis rates of α-dicarbonyls. Environmental Science and Technology, 17, 479-484.

Pokharel S. S, Bishop G. A. and Stedman D. H., 2002. An on-road motor vehicle emissions inventory for Denver: an efficient alternative to modelling. Atmospheric Environment, 36, 5177 –5184.

PORG, 1997. Ozone in the United Kingdom. Fourth report of the UK Photochemical Oxidants Review Group, Department of the Environment, Transport and the Regions, London. Published by Institute of Terrestrial Ecology, Bush Estate, Penicuik, Midlothian, EH26 0QB, UK. ISBN:0-870393-30-9, available at www.aeat.co.uk/netcen/airqual/reports/home.html.

Poschl U., von Kuhlmann R., Poisson N. and Crutzen P. J., 2000. Development and intercomparison of condensed isoprene oxidation mechanisms for global atmospheric modelling. Journal of Atmospheric Chemistry, 37, 29-52.

Raber W. H. and Moortgat G. K., 1996. In: Barker, J.(Ed.), Progress and Problems in Atmospheric Chemistry. World Scientific Publishing Company, Singapore, pp.318 –373.

RADICAL, 2002. Final report on the EU fourth framework project ‘evaluation of radical sources in atmospheric chemistry through chamber and laboratory studies, RADICAL ’.European Communities Report EUR 20254 EN, G. K. Moortgat (Coordinator), MPI Mainz, Germany.

Reimann S., Calanca P. and Hofer P., 2000. The anthropogenic contribution to isoprene concentrations in a rural atmosphere. Atmospheric Environment, 34, 109-115.

Reynolds S. D., Roth P. M. and Seinfeld J. H., 1973. Mathematical modeling of photochemical air pollution-I. Formulation of the model. Atmospheric Environment, 7, 1033-1061.

Rickard A. R., Johnson D., McGill C. D. and Marston G., 1999. OH Yields in the Gas-Phase Reactions of Ozone with Alkenes. Journal of Physical Chemistry A, 103, 7656-7664.

Roberts J. M. and Fajer, R. W., 1989. UV Absorption Cross Sections of Organic Nitrates of Potential Atmospheric Importance and Estimation of Atmospheric Lifetimes. Environmental Science and Technology, 23, 945-961.

Ruppert L., Becker K. H., Noziere B. and Spittler, M., 1999. Development of monoterpene oxidation mechanisms: results from laboratory and smog chamber studies. Borrell, P.M., Borrell, P.(Eds.), Transport and Chemical Transformation in the Troposphere. Proceedings of the EUROTRAC-2 Symposium '98.WIT press, Southampton, UK, pp. 63 –68.

Ruppert L. and Becker K. H., 2000. A product study of the OH radical-initiated oxidation of isoprene: formation of C-5-unsaturated diols. Atmospheric Environment, 34, 1529-1542

Sander S. P., Friedl R. R., DeMore W. B., Golden D. M., Kurylo M. J., Hampson R. F., Huie R. E., Moortgat G. K., Ravishankara A. R., Kolb C. E. and Molina M. J., 2000. Chemical Kinetics and Photochemical Data for Use in Stratospheric Modeling, Evaluation Number 13. JPL Publication 00-3, Jet Propulsion Laboratory, California Institute of Technology, Pasadena, CA.

Sander S. P., Friedl R. R., Golden D. M., Kurylo M. J., Huie R. E., Orkin V. L., Moortgat G. K., Ravishankara A. R., Kolb C. E, Molina M. J. and Finlayson-Pitts B. J., 2003. Chemical Kinetics and Photochemical Data for Use in Atmospheric Studies, evaluation number 14: NASA panel for data evaluation. JPL Publication 02-25, Jet Propulsion Laboratory, Pasadena.

Saunders S. M., Jenkin M. E., Derwent R. G. and Pilling M. J., 2003. Protocol for the development of the Master Chemical Mechanism, MCM v3, Part A: tropospheric degradation of non-aromatic volatile organic compounds. Atmospheric Chemistry and Physics, 3, 161-180.

Shepson P. B., Edney E. O., Kleindienst T. E., Pittman J. H., Namie G. R. and Cupitt L. T., 1985. The Production of Organic Nitrates from Hydroxyl and Nitrate Radical Reaction with Propylene. Environmental Science and Technology, 19, 849-854.

Siese M., Becker K. H., Brockmann K. J., Geiger H., Hofzumahaus A., Holland F., Mihelcic D. and Wirtz K., 2001.Direct measurement of OH radicals from ozonolysis of selected alkenes: a EUPHORE simulation chamber study. Environmental Science and Technology, 35, 4660-4667.

Singer B. C and Harley R. A., 2000. A fuel-based inventory of motor vehicle exhaust emissions in the Los Angeles area during summer 1997. Atmospheric Environment, 34, 1783-1795.

Simon V., Luchetta L. and Torres, L., 2001. Estimating the emission of volatile organic compounds (VOC) from the French forest ecosystem. Atmospheric Environment, 35, 115– 126.

Simpson D., Winiwater W., Börjesson G., Cinderby S., Ferreiro A., Guenther A., Hewitt C. N., Janson R., Khalil M. A. K., Owen S., Pierce T., Puxbaum H., Shearer M., Skiba U., Steinbrecher R., Tarrasón L. and Öquist M. G., 1999. Inventorying emissions from nature in Europe. Journal of Geophysical Research, 104, 8113-8152.

Smith G. D., Molina L. T. and Molina M., 2002. Measurement of radical quantum yields from formaldehyde photolysis between 269 and 339 nm. Journal of Physical Chemistry A, 106, 1233 –1240.

Sprengnether M., Demerjian K. L., Donahue N. M. and Anderson J.G., 2002, Product analysis of the OH oxidation of isoprene and 1,3-butadiene in the presence of NO, Journal of Geophysical Research, 107 (D15): 4269, doi:10.1029/2001JD000716.

Stockwell W. R., Middleton P., Chang J. S. and Tang X., 1990. The second generation regional acid deposition model chemical mechanism for regional air quality modeling. Journal of Geophysical Research, 95, 16343-16367.

Stroud C. A., Roberts J. M., Williams E. J., Hereid D., Parrish D. D., Angevine W., Fehsenfeld F. C., Wisthaler A., Hansel A., Martinez M., Harder H., Brune W. H., Alicke B., Stutz J. and White A. B., 2002 Nighttime isoprene trends at an urban forested site during the 1999 southern oxidant study, Journal of Geophysical Research, 107, (D16), 4291, doi:10.1029/2001JD000959.

Talukdar R. K., Burkholder J. B., Hunter M., Giles M. K. Roberts J. M. and Ravishankara A. R., 1997. Atmospheric fate of several alkyl nitrates Part 2 - UV absorption cross-sections and photodissociation quantum yields. Journal of the Chemical Society Faraday transactions, 16, 2797-2805.

Tingey D. T., Manning M., Grothaus L. C. and Burns W. F., 1980. Influence of light and temperature on monoterpene emission rates from slash pine. Plant Physiology, 65, 797-801.

Tingey D. T., Evans R. and Gumpertz M., 1981. Effects of environmental conditions on isoprene emission from live oak. Planta, 152, 565–570.

Transportation Research Board, 2000. Highway Capacity Manual. Transportation Research Board, National Academy of Science, Washington, D.C. ISBN 9991332944.

Utembe S. R., Jenkin M. E., Derwent R. G., Lewis A. C. Hopkins J. R. and Hamilton J. F., 2005. Modelling the ambient distribution of organic compounds during the August 2003 ozone episode in the southern UK. Faraday Discussions, 130, 1-16.

Vaghjiani G. L. and Ravishankara A. R., 1990. Photodissociation of H_2O_2 and CH_3OOH at 248 nm and 298 K: Quantum yields for OH, O(^3P) and H(^2S). Journal of Physical Chemistry, 92, 996-1003.

Vereecken L. and Peeters J., 2000. Theoretical Study of the Formation of Acetone in the OH-initiated Atmospheric Oxidation of α-Pinene. Journal of Physical Chemistry A, 104, 11140-11146.

Vestreng V., Breivik K., Adams M., Wagener A., Goodwin J., Rozovskkaya O. and Pacyna J. M., 2005, Inventory Review 2005, Emission Data reported to LRTAP Convention and NEC Directive, Initial review of HMs and POPs, Technical report MSC-W 1/2005, ISSN 0804-2446

Wängberg I., Barnes I. and Becker K. H., 1997. Product and mechanistic study of the reaction of NO_3 radicals with α-pinene. Environmental Science and Technology, 31, 2130 –2135.

Warneck P., 2001. Photodissociation of acetone in the troposphere:an algorithm for the quantum yield. Atmospheric Environment, 35, 5773 –5777.

Wayne R. P., Barnes I., Biggs P., Burrows J. P., Canosa-Mas C. E., Hjorth J., Le Bras G., Moortgat G. K., Perner D., Poulet G., Restelli G. and Sidebottom H. 1991. The Nitrate Radical. Physics, Chemistry and the Atmosphere. Atmospheric Environment, 25A, 1-203.

Whitehouse L. E., Tomlin A. S. and Pilling M. J., 2004a. Systematic reduction of complex tropospheric chemical mechanisms, Part I: sensitivity and time-scale analyses. Atmospheric Chemistry and Physics, 4, 2025-2056.

Whitehouse L. E., Tomlin A. S. and Pilling M. J., 2004b. Systematic reduction of complex tropospheric chemical mechanisms, Part II: lumping using a time-scale based approach. Atmospheric Chemistry and Physics, 4, 2057-2081.

Williams J., Roberts J. M., Fehsenfeld F. C., Bertman S. B., Buhr M. P., Goldan P. D., Hubler G., Kuster W. C., Ryerson T. B., Trainer M. and Young V., 1997. Regional ozone from biogenic hydrocarbons deduced from airborne measurements of PAN, PPN and MPAN. Geophysical Research Letters, 24, 1099-1102.

Winer A. M., Fitz D. R. and Miller P. R., 1983: Investigation of the role of natural hydrocarbons in photochemical smog formation in California. Contract No. AO-056-32, prepared for the California Air Resources Board, by the Statewide Air Pollution Research Center, Riverside, California, U.S.A

Winer A. M., Arey J., Atkinson, R., Aschmann, S. M., Long, W. D., Morrison, C. L. and Olszyk, D. M., 1992. Emission rates of organics from vegetation in California's central valley. Atmospheric Environment, 26A, 14, 2647-2659.

Winer A. M., Karlik J. and Arey J., 1998. Biogenic Hydrocarbon Inventories for California Essential Databases. Contract No. 95-309, State of California Air Resources Board, U.S.A.

Winterhalter R., Neeb P., Grossmann D., Kolloff A., Horie O. and Moortgat, G., 2000. Products and mechanism of the gas phase reaction of ozone with b pinene. Journal of Atmospheric Chemistry, 35, 165-197.

Wisthaler A., Jensen N. R., Winterhalter R., Lindinger W. and Hjorth J., 2001. Measurements of Acetone and other Gas Phase Product Yields from the OH-initiated Oxidation of Terpenes by Proton-Transfer-Reaction Mass Spectrometry (PTR-MS). Atmospheric Environment, 35, 6151-6191.

Yli-Tuomi T., Aarnio P., Pirjola L., Mäkelä T., Hillamo R. and Matti J., 2005. Emissions of fine particles, NO_x, and CO from on-road vehicles in Finland. Atmospheric Environment, 39, 6696-6706.

Yu J., Cocker III D. R., Griffin R. J., Flagan R. C. and Seinfeld, J. H.,1999. Gas-phase ozone oxidation of monoterpenes: gaseous and particulate products. Journal of Atmospheric Chemistry, 34, 207-258.

Zador J., Wagner V., Wirtz K. and Pilling M. J., 2005. Quantitative assessment of uncertainties for a model of tropospheric ethene oxidation using the European Photoreactor (EUPHORE). Atmospheric Environment, 39, 2805-2817.

Zhu L. and Ding, C. F., 1997. Temperature dependence of the near UV absorption spectra and photolysis products of ethyl nitrate. Chemical Physics Letters, 265, 177-184.

7 Appendix

7.1 Appendix I

The Photolysis reactions and parameters assigned as function of solar zenith angle (χ) are present in below tables.

Table 15: Photolysis reactions and parameters assigned as function of solar zenith angle (χ) calculated using Tropospheric Ultraviolet and Visible Radiation Model for clear sky conditions at an altitude of 0.5 km and the absorption cross sections and quantum yield presented in Table 12.

J (MCM FACSIMILE code)		$J=y_0+a\cos(\chi)+b\cos(\chi)^2+c\cos(\chi)^3$			
		y_0	a	b	c
J<1>	O3 = O1D	6.429E-07	-1.627E-05	7.387E-05	-2.385E-06
J<2>	O3 = O	-3.821E-06	1.254E-03	-1.011E-03	3.069E-04
J<3>	H2O2 = OH + OH	1.476E-08	1.210E-06	1.701E-05	-9.309E-06
J<4>	NO2 = NO + O	-1.128E-04	1.041E-02	8.811E-03	-9.050E-03
J<5>	NO3 = NO	-3.164E-04	6.633E-02	-6.004E-02	1.965E-02
J<6>	NO3 = NO2 + O	-3.409E-03	4.905E-01	-3.884E-01	1.045E-01
J<7>	HONO = OH + NO	-1.978E-05	1.992E-03	2.550E-03	-2.269E-03
J<8>	HNO3 = OH + NO2	7.186E-09	-1.669E-07	1.806E-06	-6.849E-07
J<11>	HCHO = CO + HO2 + HO2	1.073E-07	1.411E-08	8.151E-05	-4.267E-05
J<12>	HCHO = H2 + CO	-1.095E-07	2.107E-05	9.969E-05	-6.496E-05
J<13>	CH3CHO = CH3O2 + HO2 + CO	7.110E-08	-2.114E-06	1.490E-05	-5.364E-06
J<14>	C2H5CHO = C2H5O2 + HO2 + CO	1.745E-07	-4.333E-06	5.129E-05	-2.152E-05
J<15>	n-C3H7CHO = NC3H7O2 + CO + HO2	8.611E-08	-6.717E-08	4.969E-05	-2.576E-05
J<16>	n-C3H7CHO = CH3CHO + C2H4	4.416E-08	1.077E-07	2.937E-05	-1.514E-05
J<17>	i-C3H7CHO = i-C3H7O2 + HO2 + CO;	2.091E-07	-4.017E-07	1.399E-04	-7.368E-05
J<18>	CH_2=C(CH_3)CHO = CH3CO3 + HCHO + CO + HO2	-4.307E-08	5.503E-06	1.463E-05	-1.055E-05
J<19>	CH_2=C(CH_3)CHO = CH_2=C(CH_3)COO2 +HO2	-4.307E-08	5.503E-06	1.463E-05	-1.055E-05
J<21>	CH3C(O)CH3 = CH3CO3 + CH3O2	8.216E-09	-2.109E-07	1.482E-06	-3.728E-07
J<22>	CH3C(O)C2H5 = CH3CO3 + C2H5O2	4.537E-08	-1.207E-06	1.209E-05	-4.974E-06
J<23>	CH3C(O)CH=CH2 = C3H6 + CO	-7.435E-08	8.882E-06	2.298E-05	-1.666E-05
J<24>	CH3C(O)CH=CH2 = CH3CO3 + HCHO + CO + HO2	-7.435E-08	8.882E-06	2.298E-05	-1.666E-05
J<31>	$(CHO)_2$ = CO + CO + H2	-1.166E-06	1.100E-04	-3.039E-05	-1.744E-05
J<32>	$(CHO)_2$ = HCHO + CO	-1.725E-07	1.657E-05	-4.604E-06	-2.590E-06
J<33>	$(CHO)_2$ = CO + CO + HO2 + HO2	6.095E-08	8.611E-07	4.665E-05	-2.484E-05
J<34>	CH3C(O)CHO = CH3CO3 + CO + HO2	-2.444E-06	2.262E-04	-2.769E-05	-5.726E-05
J<35>	CH3C(O)C(O)CH3 = CH3CO + CH3CO	-3.801E-06	3.323E-04	1.810E-04	-2.242E-04
J<41>	CH3OOH = CH3O + OH	5.362E-09	1.361E-06	1.262E-05	-7.216E-06
J<51>	CH3NO3 = CH3O + NO2	1.025E-08	-2.414E-07	2.843E-06	-1.122E-06
J<52>	C2H5NO3 = C2H5O + NO2	1.510E-08	-3.954E-07	3.411E-06	-1.238E-06
J<53>	n-C3H7NO3 = NC3H7O + NO2	1.782E-08	-4.421E-07	4.484E-06	-1.716E-06
J<54>	IC3H7NO3 = IC3H7O + NO2	2.594E-08	-5.736E-07	7.460E-06	-3.102E-06
J<55>	t-C4H9NO3 = TC4H9O + NO2	4.940E-08	-6.660E-07	2.041E-05	-9.438E-06
J<56>	CH3C(O)CH2ONO2 = CH3C(O)CH2O + NO2	3.885E-08	-7.923E-07	1.343E-05	-5.972E-06
J<57>	CH3C(O)CH2ONO2 = CH3CO + HCHO + NO2	2.805E-08	-7.147E-07	6.006E-06	-2.068E-06

Table 16: Update photolysis reactions and parameters assigned as function of solar zenith angle (χ) calculated as a function of solar zenith angle determined using Tropospheric Ultraviolet and Visible Radiation Model for clear sky conditions at an altitude of 0.5 km and the absorption cross sections and quantum yield after the refinements obtained in chamber evaluation, Table 13.

J (MCM FACSIMILE code)		$J=y_0+a\cos(\chi)+b\cos(\chi)^2+c\cos(\chi)^3$			
		y_0	a	b	c
J<11>	HCHO = CO + HO2 + HO2	8.895E-08	2.836E-06	1.026E-04	-5.599E-05
J<12>	HCHO = H2 + CO	-9.124E-08	1.951E-05	9.823E-05	-6.318E-05
J<18>	$CH_2=C(CH_3)CHO$ = CH3CO3 + HCHO + CO + HO2	-4.855E-09	6.500E-07	1.788E-06	-1.291E-06
J<19>	$CH_2=C(CH_3)CHO$ = $CH_2=C(CH_3)COO2$ +HO2	-4.855E-09	6.500E-07	1.788E-06	-1.291E-06
J<21>	CH3C(O)CH3 = CH3CO3 + CH3O2	1,284E-08	-3,456E-07	2,010E-06	-4,390E-07
J<22>	CH3C(O)C2H5 = CH3CO3 + C2H5O2	2.188E-08	-5.928E-07	6.027E-06	-2.477E-06
J<23>	CH3C(O)CH=CH2 = C3H6 + CO	-1.655E-10	6.608E-07	5.203E-06	-3.079E-06
J<24>	CH3C(O)CH=CH2 = CH3CO3 + HCHO + CO + HO2	-1.655E-10	6.608E-07	5.203E-06	-3.079E-06

7.2 Appendix II

Isoprene and Monoterpenes Species Emission Potentials for standard conditions (Ts = 303 K and PAR = 1000 ($\mu mol.m^{-2}.s^{-1}$)) and species biomass densities ($g.m^{-2}$) are presented in below table.

Table 17: Isoprene and Monoterpenes Species Emission Potentials for standard conditions (Ts = 303 K and PAR = 1000 ($\mu mol.m^{-2}.s^{-1}$)) and species biomass densities ($g.m^{-2}$).

Species	Common Name	Isoprene ($\mu g.g^{-1}.h^{-1}$)	Emission factor Source	Monoterpenes ($\mu g.g^{-1}.h^{-1}$)	Emission factor Source	Density ($g.m^{-2}$)	Density Source
Castanea sativa	European chestnut	0.0	Pio et al., 1993	8.7	Pio et al., 1993	320	Simpson *et al.,* 1999
Citrus limon	Lemon	0.0	Pio et al., 1993	3.6	Winer *et al.,* 1992	300	Simpson *et al.,* 1999
Citrus sinensis	Orange	0.0	Pio et al., 1993	1.7	Winer *et al.,* 1992	300	Simpson *et al.,* 1999
Eucalyptus globulus	Blue gum	32.0	Nunes and Pio, 2001	1.7	Nunes and Pio, 2000[1]	300	Nunes, 1996
Malus Domestica	Apple tree	0.5	Guenther et al.,.1996	0.6	Guenther et al.,.1996	300	Simpson *et al.,* 1999
Myrtus communis	True Myrtle	25.0	Hansen *et al.,*1997	0.3	Owen *et al.,*1997	300	Simpson *et al.,* 1999
Olea europeia	Olive tree	0.0	Pio et al., 1993	0.36	Pio et al., 1993	200	Simpson *et al.,* 1999
Pinus Pinaster	Maritime pine	0.0	Pio et al., 1993	2.0	Pio et al., 2000; Nunes and Pio, 2000[1]	700	Nunes, 1996
Pinus Pinea	Umbrella pine	0.0	Pio et al., 1993	6.0	Owen *et al.,* 1997	700	Simpson *et al.,* 1999
Pinus nigra	Austrian black pine	13.2	Pio et al., 1993	0.0	Pio et al., 1993	700	Simpson *et al.,* 1999
Pinus sylvestris	Austrian black pine	0.0	Pio et al., 1993	3.4	Pio et al., 1993	700	Simpson *et al.,* 1999
Pinus radiata	Monterey pine	0.0	Pio et al., 1993	0.3	Pio et al., 1993	700	Simpson *et al.,* 1999
Pyrus communis	Pear tree	0.0	Pio et al., 1993	0.36	Pio et al., 1993	300	Simpson *et al.,* 1999
Platanus occidentalis	Plane	27.5	Evans *et al.* 1982[2]	0.0	Evans *et al.* 1982[2]	320	Simpson *et al.,* 1999
Populus alba	White poplar	25.0	Winer et al.,.1998	0.0	Pio et al.,.1993	320	Simpson *et al.,* 1999
Populus nigra	Lombardy Poplar	36.0	Winer et al.,.1998	0.0	Pio *et al.,* 1993	320	Simpson *et al.,* 1999
Populus tremula	European aspen	51.0	Hakola *et al.,* 1998	4.6	Hakola *et al.,* 1998	320	Simpson *et al.,* 1999
Prunus Avium	Cherry	0.0	Winer et al.,.1992	0.08	Winer et al.,.1992	300	Simpson *et al.,* 1999
Prunus Persica	Peach tree	0.0	Pio et al., 1993	0.3	Winer et al.,.1992	300	Simpson *et al.,* 1999
Quercus coccifera	Kermes oak	0.1	Hansen e Seufert, 1996[2]	18.7	Hansen e Seufert, 1996[2]	200	Simpson *et al.,* 1999
Quercus Ilex	Holm oak	0.0	Pio et al., 1993	22.0	Bertin *et al.,* 1997	500	Simpson *et al.,* 1999
Quercus pyrenaica	Pyrenees oak	59.0	Csiky e Seufert,1999[2]	0.3	Csiky e Seufert,1999[2]	320	Simpson *et al.,* 1999
Quercus robur	European oak	60.0	Steinbrecher et al., 1993[3]	0.2	Steinbrecher et al., 1993[3]	320	Simpson *et al.,* 1999
Quercus suber	Cork oak	0.0	Pio et al., 2005	25.0	Pio et al., 2005	111	Pio et al., 2005
Robinia pseudoacasia	Acácia branca	11.0	Winer *et al.,* 1983	0.0	Winer *et al.,* 1983	320	Simpson *et al.,* 1999
Salix Alba	White willow	28.0	Owen *et al.,* 2001	0.0	Owen *et al.,* 2001	150	Simpson *et al.,* 1999
Secale cereale	Rye	0.0	König et al.,.1995	0.08	König et al.,.1995	200	UNECE/EMEP 2003.
Ulex Europaeus	Gorse	1.5	Pio et al., 1993	0.4	Pio et al., 1993	200	Simpson *et al.,* 1999
Ulmus Campestris	Elm	0.0	Pio et al., 1993	1.65	Pio et al., 1993	320	Simpson *et al.,* 1999
Vitis vinifera	Grape	0.0	König *et al.,*1995	0.015	König *et al.,*1995	200	UNECE/EMEP 2003.

[1]cited in Simon *et al.,* 2001;
[2]cited in Kesselmeier and Staudt., 1999;
[3] cited in Simpson *et al.,* 1999.

Non Emitters of isoprene and monoterpenes

Species	Common Name	Source
Zea mays	Corn	König *et al.,*1995
Triticum aestivum	Wheat	König *et al.,*1995 Winer *et al.,*1992
Oriza sativa	Rice	Winer et al.,.1992
Fraxinus excelsior	Ash	Winer et al.,.1992

Ecosystems

Ecosystem	Isoprene (μg.g-1.h-1)	Emission factor Source	Monoterpenes (μg.g-1.h-1)	Emission factor Source	Density (g.m-2)	Density Source
Pasture	0.1	Simpson *et al.,* 1999	0.1	Simpson *et al.,* 1999	400	Simpson *et al.,* 1999
Grassland	0.1	Simpson *et al.,* 1999	0.1	Simpson *et al.,* 1999	400	Simpson *et al.,* 1999
Garrique	8.0	Simpson *et al.,* 1999	0.6	Simpson *et al.,* 1999	200	Simpson *et al.,* 1999
Maqui	8.0	Simpson *et al.,* 1999	0.65	Simpson *et al.,* 1999	400	Simpson *et al.,* 1999

7.3 Appendix III

Vehicle distribution by vehicle type and age, circulating in Portugal, at the end of year 2000 (see Figure 121)

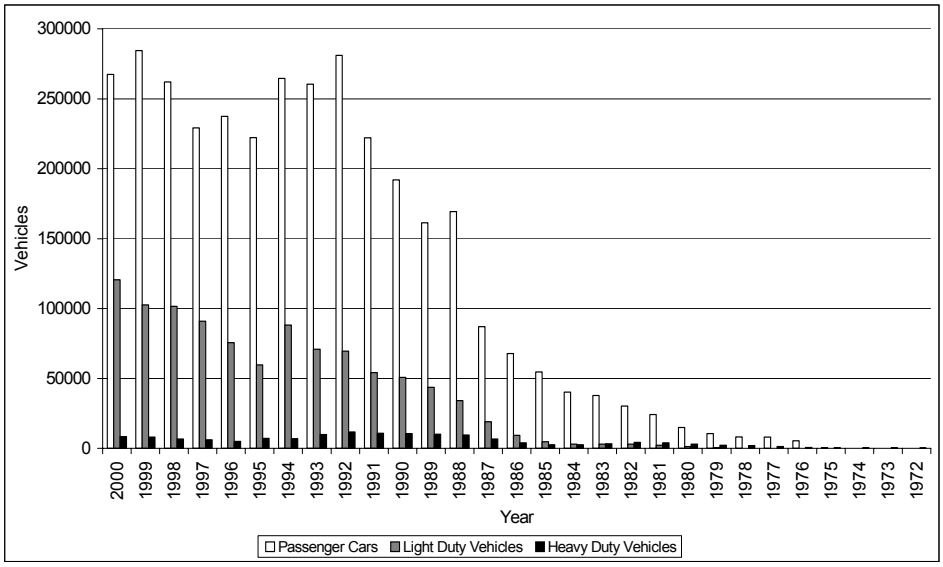

Figure 121: Vehicle distribution by vehicle type and age, circulating in Portugal, at the end of year 2000.

Emission factors (g pollutant).(dm^{-3} fuel) were calculated considering an average speed of 60 $km.h^{-1}$ (for heavy duty vehicles) and 70 $km.h^{-1}$ (for other vehicle types). Table 18 presents obtained emission factors for different vehicle types, expressed in (g pollutant).km^{-1}.$vehicle^{-1}$ and (g pollutant).(dm^{-3} fuel) considering the vehicle distribution circulating in Portugal at the end of year 2000.

Table 18: Hot emission factors for different vehicle types, in (g pollutant).km^{-1}.vehicle^{-1} and (g pollutant).(dm^{-3} fuel), considering the vehicle distribution by vehicle type circulating in Portugal at the end of year 2000.

	NOx	VOC	NOx	VOC
	(g pollutant).km^{-1}.vehicle^{-1}	(g pollutant).km^{-1}.vehicle^{-1}	(g pollutant).(dm^{-3} fuel)	(g pollutant).(dm^{-3} fuel)
Passenger Cars, Gasoline	0,93	0,34	16,53	6,00
Passenger Cars, diesel	0,48	0,04	9,44	0,88
Light duty vehicles, diesel <2.5	0,48	0,04	9,44	0,88
Light duty vehicles, diesel <3.5	0,94	0,10	12,87	1,41
heavy duty vehicles, diesel	5,61	0,92	24,20	3,99

The hot emission factors for different fuel type in (g pollutant).(dm^{-3} fuel) considering the vehicle distribution by vehicle type circulating in Portugal in the end of year 2000 and the percentages of fuel sales in the study domain (35% gasoline and 65% diesel) are present in Table 19.

Table 19: Hot emission factors for different fuel type in (g pollutant).(dm^{-3} fuel) considering the vehicle distribution by vehicle type circulating in Portugal in the end of year 2000 and the percentages of fuel sales in the study domain (35% gasoline and 65% diesel).

	NOx	VOC
	(g pollutant).(dm^{-3} fuel)	(g pollutant).(dm^{-3} fuel)
Emission factor for gasoline	16,53	6,00
Emission factor for diesel	13,84	1,75
Emission factor for fuel	14,78	3,25

The average emission factors, obtained considering the distribution by vehicle type circulating in Portugal by the end of year 2000, see Table 20.

Table 20: Hot emission factors for different vehicle types, in (g pollutant).(km^{-1}.vehicle^{-1}), considering the vehicle distribution in Portugal by the end of year 2000.

	Passenger Cars, Gasoline			**Light duty vehicles, diesel <2.5**		
		(g pollutant).(km^{-1}.vehicle^{-1})			(g pollutant).(km^{-1}.vehicle^{-1})	
Type of Road	Speed (km.h^{-1})	NO_x	VOC	Speed (km.h^{-1})	NO_x	VOC
Secondary road	70	0,93	0,34	70	0,48	0,04
Main road	90	1,13	0,28	90	0,53	0,04
Highway	120	1,57	0,33	120	0,84	0,05
	Light duty vehicles, diesel <3.5			**Heavy duty vehicles, diesel**		
		(g pollutant).(km^{-1}.vehicle^{-1})			(g pollutant).(km^{-1}.vehicle^{-1})	
Type of Road	Speed (km.h^{-1})	NO_x	VOC	Speed (km.h^{-1})	NO_x	VOC
Secondary road	70	0,94	0,10	50	6,20	1,08
Main road	90	1,10	0,10	80	4,92	0,72
Highway	120	1,88	0,13	100	4,70	0,59

Table 21 presents the NMVOC speciation considering motor vehicles emissions.

Table 21: Selected NMVOC speciation of motor vehicles emissions, used in PTM application.

Species	MCM v3.1 designation	NMVOC (% wt.)	Species	MCM v3.1 designation	NMVOC (% wt.)
ETHANE	C2H6	1,16	ETHANAL (ACETALDEHYDE)	CH3CHO	4,43
PROPANE	C3H8	0,29	ACROLEIN	ACR	2,31
N-BUTANE	NC4H10	1,69	BENZENECARBONAL (BENZALDEHYDE)	BENZAL	0,75
2-METHYL-PROPANE (I-BUTANE)	IC4H10	0,59	METHACROLEIN	MACR	0,54
PENTANE (N-PENTANE)	NC5H12	0,76	BUTANAL (BUTYRALDEHYDE)	C3H7CHO	0,59
2-METHYLBUTANE (1-PENTANE)	IC5H12	2,53	METHYLPROPANAL (I-BUTYRALDEHYDE)	IPRCHO	1,27
HEXANE (N-HEXANE)	NC6H14	0,54	PROPANAL (PROPRIONALDEHYDE)	C2H5CHO	1,17
HEPTANE (N-HEPTANE)	NC7H16	0,37	PENTANAL (VALERALDEHYDE)	C4H9CHO	0,28
OCTANE (N-OCTANE)	NC8H18	0,34	PROPANONE (ACETONE)	CH3COCH3	1,88
2-METHYLHEXANE	M2HEX	0,77	BUTANONE (METHYL ETHYL KETONE)	MEK	0,72
NONANE (N-NONANE)	NC9H20	0,44	METHYLBENZENE (TOLUENE)	TOLUENE	4,57
3-METHYLHEXANE	M3HEX	0,50	ETHYL BENZENE	EBENZ	1,18
DECANE (N-DECANE)	NC10H22	0,92	1,3-DIMETHYL BENZENE (M-XYLENE)	MXYL	1,27
HENDECANE (N-UNDECANE)	NC11H24	0,84	1,4-DIMETHYL BENZENE (P-XYLENE)	PXYL	1,27
DODECANE (N-DODECANE)	NC12H26	14,09	1,2-DIMETHYL BENZENE (O-XYLENE)	OXYL	1,27
CYCLOHEXANE	CHEX	0,86	1,2,3-TRIMETHYL BENZENE (HEMIMELLITENE)	TM123B	0,45
ETHENE (ETHYLENE)	C2H4	9,80	1,2,4-TRIMETHYL BENZENE (PSEUDOCUMENE)	TM124B	1,73
PROPENE (PROPYLENE)	C3H6	3,71	1,3,5-TRIMETHYL BENZENE (MESITELENE)	TM135B	0,70
1-BUTENE	BUT1ENE	0,24	ETHENYL BENZENE (STYRENE)	STYRENE	0,58
ISOBUTENE	MEPROPENE	1,83	BENZENE	BENZENE	3,32
CIS-2-BUTENE	CBUT2ENE	0,40	1-ETHYL 3-METHYL BENZENE (M-ETHYL TOLUENE)	METHTOL	0,39
TRANS-2-BUTENE	TBUT2ENE	0,40	1-ETHYL 2-METHYL BENZENE (O-ETHYL TOLUENE)	OETHTOL	0,39
1-3 BUTADIENE	C4H6	1,25	1-ETHYL 4-METHYL BENZENE (P-ETHYL TOLUENE)	PETHTOL	0,39
1-PENTENE	PENT1ENE	0,04	N-PROPYL BENZENE	PBENZ	0,39
CIS-2-PENTENE	CPENT2ENE	0,11	I-PROPYL BENZENE (CUMENE)	IPBENZ	0,39
1-HEXENE	HEX1ENE	0,04	1,3-DIMETHYL 5-ETHYL BENZENE	DIME35EB	0,75
ETHYNE (ACETYLENE)	C2H2	2,78	1,3-DIETHYL 5-METHYLBENZENE	DIET35TOL	11,15
METHANAL (FORMALDEHYDE)	HCHO	8,39			

Note: All alkanes C>13 were aggregated as the largest alkane treated (i.e., dodecane NC12H26) and all C13+ aromatics as the largest aromatic treated (i.e., 1,3-diethyl-5-methyl benzene DIET35TOL).

Figure 122 shows the hourly variation patterns, used in current PTM application.

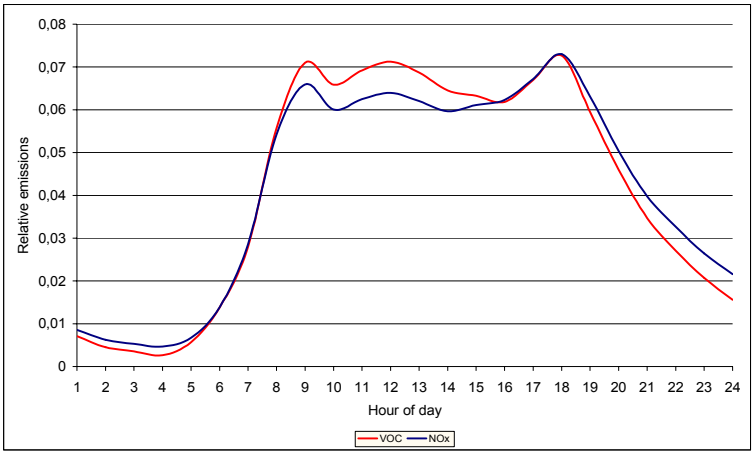

Figure 122: Relative NOx and VOC emissions of motor vehicles, with hour of day, used in PTM application.

7.4 Appendix IV

Portuguese emissions of NMVOC and NO_x in 2001 are presented in Figure 123 and Figure 124.

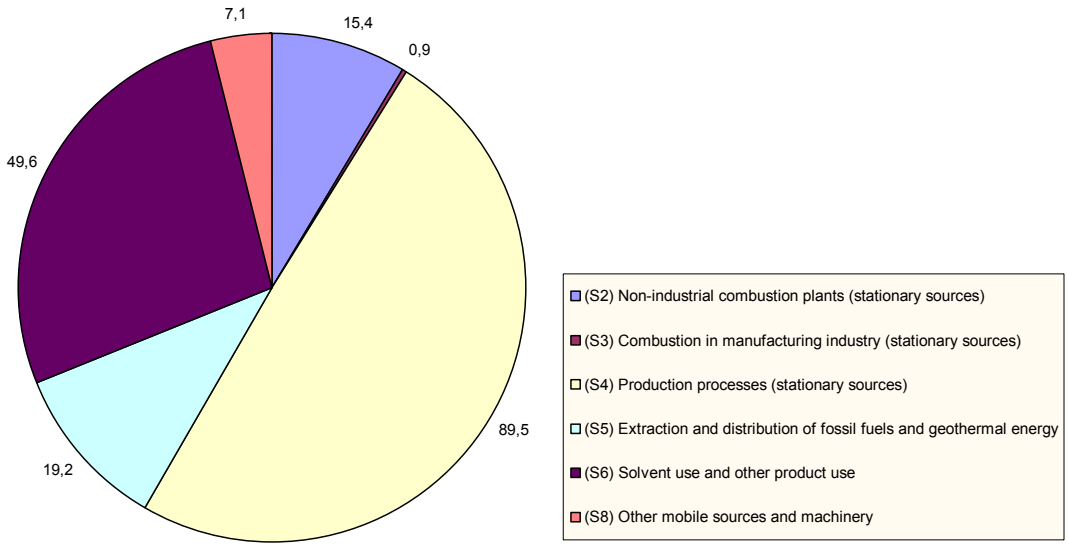

Figure 123: Portuguese emissions of NMVOC (kton.year^{-1}), SNAP sectors (2, 3, 4, 5, 6 and 8), for the year 2001.

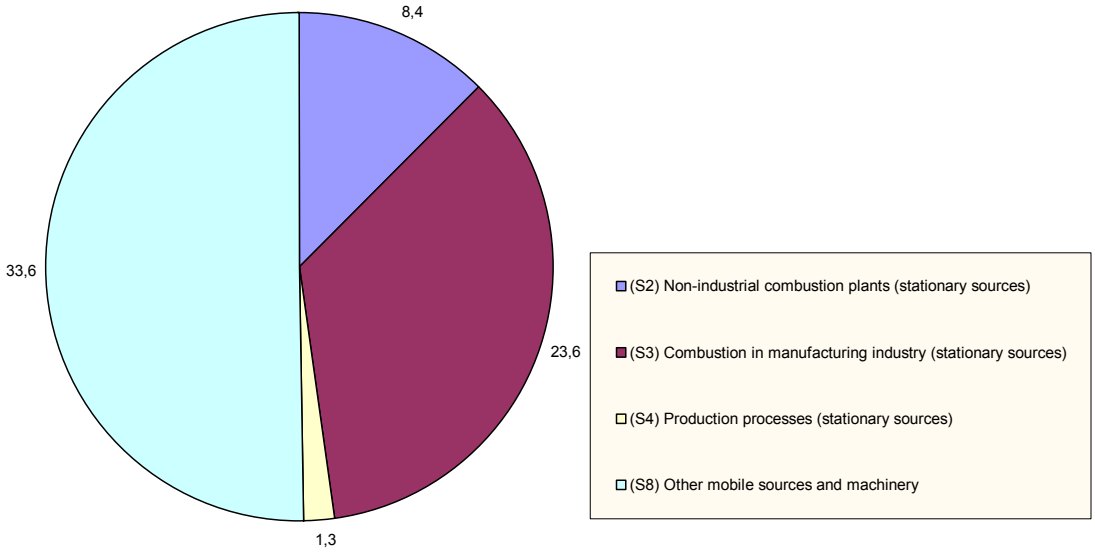

Figure 124: Portuguese emissions of NO_x (kton.year^{-1}), SNAP sectors (2, 3, 4, and 8), for the year 2001.

Point sources emission estimates were provided on CORINAIR inventory (EEA-ETC/AE-CORINAIR, 1996) and are present in Table 22.

Table 22: Annual emissions of NO_x and NMVOC (ton.year^{-1}) from point sources considered in study domain.

Point Source	NO_x (ton.year^{-1})	NMVOC (ton.year^{-1})
PVC resins	57	
Paper pulp	7	2
Paper pulp	1034	432
Nitric acid	450	

Table 23 presents speciation of the emitted anthropogenic NMVOC for the SNAP sectors (2, 3, 4, 5, 6 and 8) based on data from the UK NAEI (Jenkin *et al.,* 2000b).

Table 23: Speciation of the emitted anthropogenic NMVOC for the SNAP sectors (2, 3, 4, 5, 6 and 8) based on data from the UK NAEI (Jenkin *et al.,* 2000b).

		sector 2, 3, 4, 8	**sector 5**	**sector 6**
Species	**MCM v3.1 designation**	**NMVOC (% wt.)**	**NMVOC (% wt.)**	**NMVOC (% wt.)**
ETHANE	C2H6	4,09	6,47	0,00
PROPANE	C3H8	5,88	10,64	2,90
N-BUTANE	NC4H10	6,48	32,55	2,90
2-METHYL-PROPANE (I-BUTANE)	IC4H10	2,74	8,13	0,00
PENTANE (N-PENTANE)	NC5H12	4,73	10,55	3,62
2-METHYLBUTANE (1-PENTANE)	IC5H12	2,54	6,73	0,00
2,2-DIMETHYLPROPANE (NEO-PENTANE)	NEOP	1,37	0,24	0,00
HEXANE (N-HEXANE)	NC6H14	3,53	5,32	1,07
2-METHYLPENTANE	M2PE	0,63	0,81	0,10
3-METHYLPENTANE	M3PE	0,30	0,48	0,09
2,2-DIMETHYLBUTANE	M22C4	0,28	0,25	0,00
2,3-DIMETHYLBUTANE	M23C4	0,28	0,27	0,01
HEPTANE (N-HEPTANE)	NC7H16	1,36	6,05	0,10
2-METHYLHEXANE	M2HEX	0,47	0,59	0,00
3-METHYLHEXANE	M3HEX	0,46	0,59	0,11
OCTANE (N-OCTANE)	NC8H18	0,18	6,08	0,32
NONANE (N-NONANE)	NC9H20	0,02	0,01	2,44
DECANE (N-DECANE)	NC10H22	0,03	0,00	5,61
HENDECANE (N-UNDECANE)	NC11H24	0,02	0,00	4,37
DODECANE (N-DODECANE)	NC12H26	0,03	0,00	1,89
CYCLOHEXANE	CHEX	1,24	0,34	5,49
ETHENE (ETHYLENE)	C2H4	5,69	0,05	0,00
PROPENE (PROPYLENE)	C3H6	2,72	0,03	0,00
1-BUTENE	BUT1ENE	0,44	0,23	0,00
CIS-2-BUTENE	CBUT2ENE	0,30	0,33	0,00
TRANS-2-BUTENE	TBUT2ENE	0,30	0,36	0,00
2-METHYLPROPENE (1-BUTENE, BUTYLENE)	MEPROPENE	0,29	0,23	0,00
1-PENTENE	PENT1ENE	0,33	1,08	0,00
CIS-2-PENTENE	CPENT2ENE	0,00	0,19	0,00
TRANS-2-PENTENE	TPENT2ENE	0,00	0,36	0,00
2-METHYL-1-BUTENE	ME2BUT1ENE	0,00	0,00	0,00
3-METHYL-1-BUTENE	ME3BUT1ENE	0,01	0,00	0,00
2-METHYL-2-BUTENE	ME2BUT2ENE	0,01	0,00	0,00
1-HEXENE	HEX1ENE	0,26	0,20	0,06
CIS-2-HEXENE	CHEX2ENE	0,08	0,00	0,00
TRANS-2-HEXENE	THEX2ENE	0,08	0,00	0,00
1-3 BUTADIENE	C4H6	0,13	0,02	0,00
2-METHYL-1,3-BUTADIENE (ISOPRENE)	C5H8	0,00	0,02	0,00
ALPHA-PINENE	APINENE	0,03	0,00	0,06
ETHYNE (ACETYLENE)	C2H2	0,46	0,06	0,00
METHANAL (FORMALDEHYDE)	HCHO	2,29	0,00	0,00
ETHANAL (ACETALDEHYDE)	CH3CHO	0,22	0,00	0,00
PROPANAL (PROPRIONALDEHYDE)	C2H5CHO	0,05	0,00	0,00
BUTANAL (BUTYRALDEHYDE)	C3H7CHO	0,02	0,00	0,00
METHYLPROPANAL (I-BUTYRALDEHYDE)	IPRCHO	0,01	0,00	0,00
PENTANAL (VALERALDEHYDE)	C4H9CHO	0,00	0,00	0,00
GLYOXAL	GLYOX	0,01	0,00	0,00
METHYL GLYOXAL	MGLYOX	0,01	0,00	0,00
PROPANONE (ACETONE)	CH3COCH3	1,98	0,00	2,17
BUTANONE (METHYL ETHYL KETONE)	MEK	0,64	0,00	2,53
2-PENTANONE (METHYL N-PROPYL KETONE)	MPRK	0,00	0,00	0,00
3-METHYL 2-BUTANONE(METHYL I-PROPYL KETONE)	MIPK	0,00	0,00	0,00

3-PENTANONE (DIETHYL KETONE)	DIEK	0,01	0,00	0,06
2-HEXANONE (METHYL N-BUTYL KETONE)	HEX2ONE	0,00	0,00	0,09
3-HEXANONE (ETHYL N-PROPYL KETONE)	HEX3ONE	0,00	0,00	0,00
4-METHYL 2-PENTANONE (METHYL I-BUTYL KETONE)	MIBK	0,40	0,00	1,74
3,3-DIMETHYL 2-BUTANONE (METHYL T-BUTYL KETONE)	MTBK	0,00	0,00	0,00
CYCLOHEXANONE	CYHEXONE	0,09	0,00	0,29
METHANOL	CH3OH	1,78	0,00	0,73
ETHANOL	C2H5OH	21,79	0,00	10,93
1-PROPANOL (N-PROPANOL)	NPROPOL	0,40	0,00	1,92
2-PROPANOL (I-PROPANOL)	IPROPOL	0,77	0,00	2,07
1-BUTANOL (N-BUTANOL)	NBUTOL	0,34	0,00	1,73
2-BUTANOL (SEC-BUTANOL)	BUT2OL	0,24	0,00	0,62
2-METHYL-1-PROPANOL (I-BUTANOL)	IBUTOL	0,01	0,00	0,51
2-METHYL-2-PROPANOL (T-BUTANOL)	TBUTOL	0,22	0,00	0,06
3-PENTANOL	PECOH	0,00	0,00	0,00
3-METHYL-1-BUTANOL (I-PENTANOL, I-AMYL ALCOHOL)	ME3BUOL	0,00	0,00	0,00
2-METHYL-1-BUTANOL	IPEAOH	0,00	0,00	0,00
3-METHYL-2-BUTANOL	IPEBOH	0,00	0,00	0,01
2-METHYL-2-BUTANOL	IPECOH	0,00	0,00	0,00
4-HYDROXY-4-METHYL-2-PENTANONE (DIACETONE ALCOHOL)	MIBKAOH	0,00	0,00	0,44
CYCLOHEXANOL	CYHEXOL	0,09	0,00	0,06
ETHANE-1,2-DIOL (ETHYLENE GLYCOL)	ETHGLY	0,39	0,00	0,93
PROPANE-1,2-DIOL (PROPYLENE GLYCOL)	PROPGLY	0,00	0,00	0,02
DIMETHYL ETHER	CH3OCH3	0,00	0,00	0,18
DIETHYL ETHER	DIETETHER	0,23	0,00	0,02
DI I-PROPYL ETHER	DIIPRETHER	0,13	0,00	0,00
METHYL T-BUTYL ETHER	MTBE	0,00	0,00	0,00
ETHYL T-BUTYLETHER	ETBE	0,00	0,00	0,00
DIMETHOXY METHANE	DMM	0,00	0,00	0,00
DIMETHYL CARBONATE	DMC	0,00	0,00	0,00
2-METHOXY ETHANOL	MO2EOL	0,00	0,00	0,00
1-METHOXY 2-PROPANOL	PR2OHMOX	0,00	0,00	0,31
2-ETHOXY ETHANOL	EOX2EOL	0,00	0,00	0,60
2-BUTOXY ETHANOL	BUOX2ETOH	0,00	0,00	1,08
1-BUTOXY 2-PROPANOL	BOX2PROL	0,00	0,00	0,08
METHANOIC ACID	HCOOH	0,00	0,00	0,00
ETHANOIC ACID	CH3CO2H	0,60	0,00	0,08
PROPANOIC ACID	PROPACID	0,01	0,00	0,00
METHYL FORMATE	CH3OCHO	0,01	0,00	0,00
METHYL ACETATE	METHACET	2,86	0,00	0,00
ETHYL ACETATE	ETHACET	0,42	0,00	2,90
N-PROPYL ACETATE	NPROACET	0,01	0,00	0,32
I-PROPYL ACETATE	IPROACET	0,04	0,00	0,95
N-BUTYL ACETATE	NBUTACET	0,05	0,00	2,47
S-BUTYL ACETATE	SBUTACET	0,00	0,00	0,11
BENZENE	BENZENE	2,98	0,39	0,00
METHYLBENZENE (TOLUENE)	TOLUENE	2,16	0,19	6,91
1,2-DIMETHYL BENZENE (O-XYLENE)	OXYL	0,70	0,02	0,85
1,3-DIMETHYL BENZENE (M-XYLENE)	MXYL	0,70	0,06	3,34
1,4-DIMETHYL BENZENE (P-XYLENE)	PXYL	2,05	0,00	0,82
ETHYL BENZENE	EBENZ	0,20	0,02	1,25
1,2,3-TRIMETHYL BENZENE (HEMIMELLITENE)	TM123B	0,01	0,00	0,59
1,2,4-TRIMETHYL BENZENE (PSEUDOCUMENE)	TM124B	0,03	0,00	1,58
1,3,5-TRIMETHYL BENZENE (MESITELENE)	TM135B	0,02	0,00	0,61
1-ETHYL 2-METHYL BENZENE (O-ETHYL TOLUENE)	OETHTOL	0,01	0,00	0,42
1-ETHYL 3-METHYL BENZENE (M-ETHYL TOLUENE)	METHTOL	0,02	0,00	0,66
1-ETHYL 4-METHYL BENZENE (P-ETHYL TOLUENE)	PETHTOL	0,02	0,00	0,46
N-PROPYL BENZENE	PBENZ	0,03	0,00	0,38
I-PROPYL BENZENE (CUMENE)	IPBENZ	0,11	0,00	0,17
1,3-DIMETHYL 5-ETHYL BENZENE (3,5-DIMETHYL ETHYL BENZENE)	DIME35EB	0,09	0,07	2,90
1,3-DIETHYL 5-METHYLBENZENE (3,5-DIETHYL TOLUENE)	DIET35TOL	0,00	0,00	0,51
ETHENYL BENZENE (STYRENE)	STYRENE	1,21	0,00	0,28
BENZENECARBONAL (BENZALDEHYDE)	BENZAL	0,00	0,00	0,04
CHLOROMETHANE (METHYL CHLORIDE)	CH3CL	0,46	0,00	0,00
DICHLOROMETHANE (METHYLENE DICHLORIDE)	CH2CL2	2,51	0,00	2,13
TRICHLOROMETHANE (CHLOROFORM)	CHCL3	0,05	0,00	0,00
1,1,1-TRICHLOROETHANE (METHYL CHLOROFORM)	CH3CCL3	0,95	0,00	3,15
CIS-1,2-DICHLOROETHENE	CDICLETH	0,78	0,00	0,00
TRANS-1,2-DICHLOROETHENE	TDICLETH	0,05	0,00	0,00
TRI-CHLOROETHENE	TRICLETH	0,15	0,00	4,26
TETRA-CHLOROETHENE (PER-CHLOROETHYLENE)	TCE	0,33	0,00	1,52

The temporal variations applied to the emissions of NMVOC and NO_x were based on those estimated for the UK by Jenkin *et al.* (2000c), and are presented in Figure 125 and Figure 126.

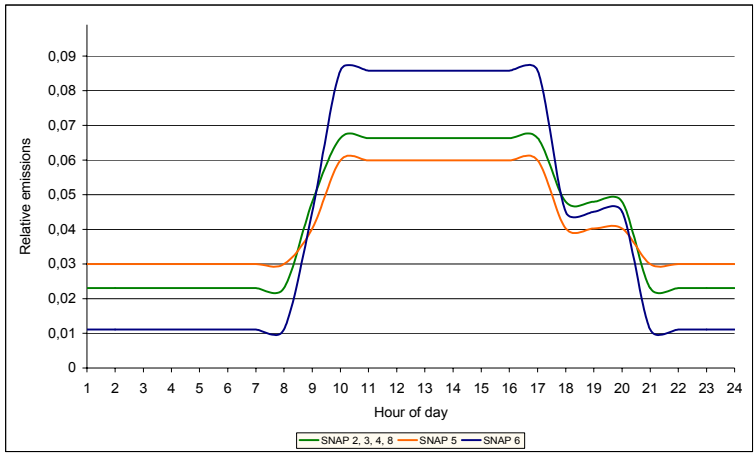

Figure 125: Relative NMVOC emissions for the SNAP sectors (2, 3, 4, 5, 6 and 8) based on data from the UK NAEI (Jenkin *et al.,* 2000c), with hour of day, used in PTM application.

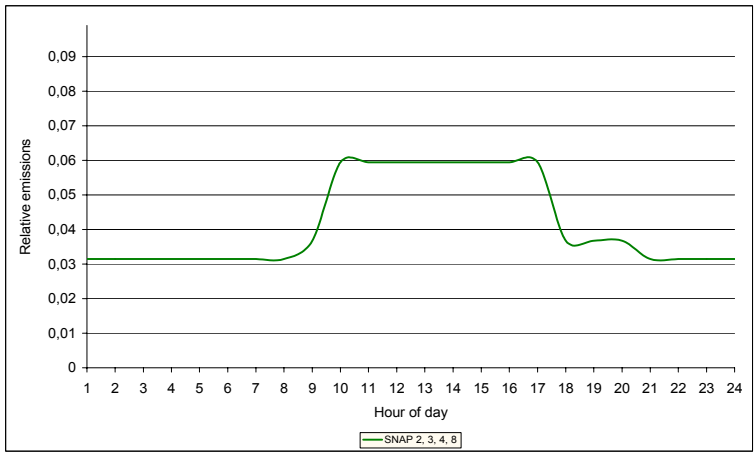

Figure 126: Relative NO_x emissions for the SNAP sectors (2, 3, 4, and 8) based on data from the UK NAEI (Jenkin *et al.,* 2000b), with hour of day, used in PTM application.